Optimal boundary traffic control and state estimation with disturbances

Lina Guan

UNIVERSITÉ GRENOBLE ALPES

THÈSE

pour obtenir le grade de

DOCTEUR DE L'UNIVERSITÉ DE GRENOBLE ALPES

Spécialité : **AUTOMATIQUE - PRODUCTIQUE**

Arrêté ministériel : 7 Juillet 2022

Présentée par
Lina GUAN

Thèse dirigée par **Christophe PRIEUR** et
codirigée par **Liguo ZHANG**

préparée au sein du
laboratoire Grenoble Image, Parole, Signal, Automatique (GIPSA-lab)
dans **Electronique, Electrotechnique, Automatique et Traitement du Signal (EEATS)**

Optimal Boundary Traffic Control and State Estimation with Disturbances

Thèse soutenue publiquement le **15 Septembre 2022**,
devant le jury composé de :

Paola GOATIN
INRIA Sophia Antipolis-Méditerranée (France), Rapporteur
Rafael VAZQUEZ
University of Sevilla (Seville, Spain), Rapporteur
Jean-Michel CORON
Université Pierre et Marie Curie (Paris, France), Examinateur
Ying TANG
Université de Lille (Lille, France), Examinateur
Emmanuel WITRANT
Université Grenoble Alpes (Grenoble, France), Président
Yuxian ZHANG
Shenyang University of Technology (Shenyang, China), Examinateur
Christophe PRIEUR
CNRS (Grenoble, France), Directeur de thèse
Liguo ZHANG
Beijing University of Technology (Beijing, China), Encadrant de thèse

Contents

List of Figures

List of Tables

Table of abbreviations and acronyms

PDEs	*Partial Differential Equations*
ODE	*Ordinary Differential Equation*
LWR	*Lighthill-Whitham-Richards*
PW	*Payne-Whitham*
ARZ	*Aw-Rascle-Zhang*
SG	*Speed Gradient*
Aw-Rascle	*Aw-Rascle*
CAVs	*Connected and Autonomous Vehicles*
HDV	*Human-Driven Vehicle*
iISS	*Integral Input-to-State Stable*
PI	*Proportional Integral*
LMIs	*Linear Matrix Inequalities*
SIRD	*susceptible-infected-recovered-dead*
LHS	*Latin Hypercube Sampling*

Chapter 1

Introduction

Context and history

Traffic congestion on urban road networks has increased substantially, since 1950 [Cav05]. Traffic congestion is characterized by slow speeds, longer trip times, and increased vehicular queuing. When vehicles are fully stopped for periods, this is known as a traffic jam [MAC12] [Dar90] or (informally) a traffic snarl-up [FHSA93]. Traffic congestion has several negative impacts: reduction of regional economic health, delays, more time to travel "just in case", increasing air pollution and carbon dioxide emissions, more frequent repairs and replacements of vehicles, road rage and reduced health of motorists, interfering with the passage of emergency vehicles, and a higher chance of collisions.

Traffic congestion resulting from traffic breakdown is an ubiquitous problem. Traffic breakdown usually arises from the combination of three ingredients: high traffic demand, bottlenecks, and disturbances caused by individual drivers (see [TK12]). High traffic demand, which is the inflow indicating the potential average traffic flow on the main road and exceeding the bottleneck capacity, such as during rush hours, causes the slow velocity of the traffic stream. A bottleneck is defined as a local reduction of the road capacity (see [TK12]). Most bottlenecks include flow-conserving bottlenecks and non-flow-conserving bottlenecks with additional sources and sinks, for example, on-ramp and off-ramp bottlenecks, or permanent and temporary types such as the blocking effect resulting from accidents or traffic lights. The interaction of controlled autonomous vehicles (as the moving bottlenecks) with the surrounding traffic and the possibility to reduce congestion effect caused by some fixed bottlenecks downstream are studied in [Goa+21]. On the basis of the Kerner–Klenov–Wolf (KKW) model of three-phase traffic flow theory, the traffic flow model of expressway ramp system under the accident conditions is proposed in [Zen+21], and the combined bottleneck effect of accidents on the traffic flow under the open boundary condition is simulated and analyzed. Considering the LWR model, the optimal location problem is analytically identified, formulated, and solved for variable speed limit application areas inside a lane drop bottleneck in [MJ20]. Traffic breakdown usually occurs, when there are disturbances caused by individual drivers, such as abrupt lane changes, braking maneuvers, or other unanticipated actions. The disturbances often lead to a platoon of vehicles following each other at small time gaps which eventually becomes the first propagating upstream traffic wave of a triggered stop-and-go state. Beyond the factors resulting in the traffic breakdown, high traffic demand is the most effective ingredient. The disturbances caused by bottlenecks or individual drivers can not grow and propagate on account of unconditional stability, if the traffic flux on the main road is low enough. However, in spite of the absolute stability, traffic breakdown will take place with inflow in excess of the capacity of bottlenecks. The local capacity reduction is the decisive attribute of characterizing the obstructing effect of a bottleneck. Furthermore, we can not predict the time and location of individual traffic breakdown due to the stochastic and single-vehicle natures of disturbances caused by individual drivers. In this manuscript, we investigate the traffic congestion problem on a main road with high traffic demand at the inlet and a bottleneck at the outlet.

Aiming to understand and develop an optimal transport network with efficient movement of vehicles and minimal traffic congestion problem, traffic flow is used to study the interactions between travelers (drivers and their vehicles) and infrastructure (highways, signage, and traffic control devices) in mathematics and transportation engineering. Attempts to produce a mathematical theory of traffic flow date back to the 1920s, when Frank Knight first produced an analysis of traffic equilibrium, which was refined into Wardrop's first and second principles of equilibrium in 1952. A point $x = x*$ in the state space is said to be an equilibrium point of a system if it has the property that whenever the state of the system starts at $x*$, it will remain at $x*$ for all future time. An equilibrium point is stable if all solutions of a system starting at nearby points stay nearby; otherwise, it is unstable. It is asymptotically stable if all solutions of a system starting at nearby points not only stay nearby, but also tend to the equilibrium point as time approaches infinity [KG02]. Nonetheless, even with the advent of significant computer processing power, to date, there has been no satisfactory general theory that can be consistently applied to real flow conditions. Current traffic models use a mixture of empirical and theoretical techniques. These models are then developed into traffic forecasts, and take account of proposed local or major changes, such as increased vehicle use, changes in land use, or changes in the mode of transport (with people moving from bus to train or car, for example), and to identify areas of congestion where the network needs to be adjusted. Nevertheless, calculations about congested networks are more complex and rely more on empirical studies and extrapolations from actual road counts. Because these are often urban or suburban in nature, other factors (such as road-user safety and environmental considerations) also influence the optimum conditions. There are common spatiotemporal empirical features of traffic congestion that are qualitatively the same for different highways in different countries, measured during years of traffic observations. Some of these common features of traffic congestion define the synchronized flow and wide moving jam traffic phases of congested traffic in Kerner's three-phase traffic theory of traffic flow (see also Traffic congestion reconstruction with Kerner's three-phase theory). In a free-flowing network, traffic flow theory refers to the traffic stream variables of speed, flow, and concentration. These relationships are mainly concerned with uninterrupted traffic flow, primarily found on freeways or expressways. In this manuscript, we study the congested traffic flow on a freeway. Freeways are defined as those facilities that afford uninterrupted flow of traffic, i.e., there is full access control. Control of access refers to public access rights from properties along the freeway; access to freeway facilities is allowed only through selected public roads, typically on- and off-ramps [Bla80]. Thus, freeways typically operate at higher speeds and higher capacities than urban arterial streets or local roadways [Ele14].

Traffic flow is generally constrained along a one-dimensional pathway. Vehicles following each other along a given travel lane will have parallel trajectories, and trajectories will cross when one vehicle passes another. There are three main variables to visualize a traffic stream: speed (v), density (ρ, the number of vehicles per unit of space), and flow (q, the number of vehicles per unit of time) [Ele14]. These fundamental traffic flow characteristics are related as follows:

$$flow = density \times speed.$$

Speed is the distance covered per unit of time. In practice, the average speed is measured by sampling vehicles in a given area over a period of time. In traffic flow, the two most important densities are critical density (ρ_c) and jam density (ρ_m). The maximum density achievable under free flow is critical density, while jam density is the maximum density achieved under congestion. Flow is the number of vehicles passing a reference point per unit of time. In addition to providing information on the speed, flow, and density of traffic streams, Fig. 1.1 may illustrate the propagation of congestion (shockwave) upstream from a traffic bottleneck. Congestion shockwave will vary in propagation length, depending upon the upstream traffic flow and density. However, shockwave will generally travel upstream at a rate of approximately 20 km/h. The triangular

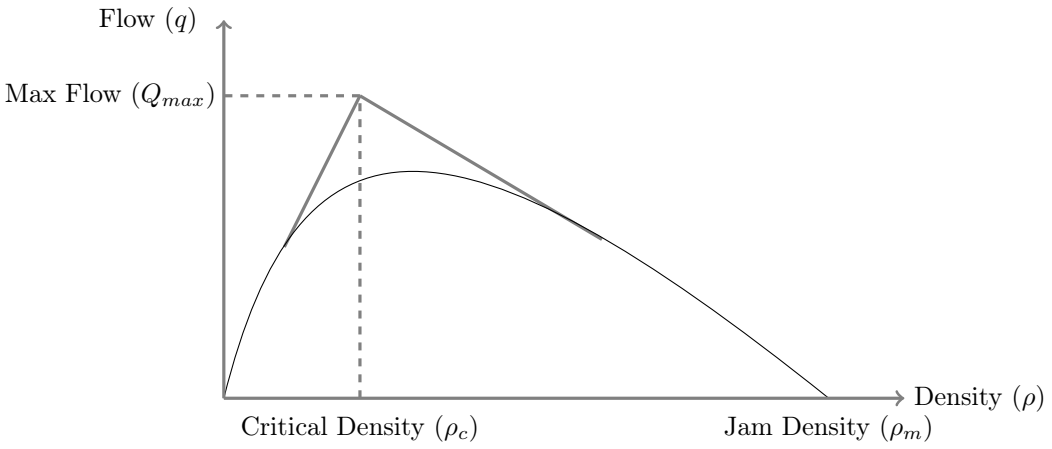

Figure 1.1: Flow Density relationship.

curve consists of the free flow side created by placing the free flow velocity vector of a roadway at the origin of the flow-density graph and the congested branch created by placing the vector of the shock wave speed at zero flow and jam density. The congested branch has a negative slope, which implies that the higher the density on the congested branch the lower the flow; therefore, even though there are more cars on the road, the number of cars passing a single point is less than if there were fewer cars on the road. The intersection of free flow and congested vectors is the apex of the curve and is considered as the capacity of the roadway, which is the traffic condition at which the maximum number of vehicles can pass by a point in a given time period. The flow and capacity at this point are the optimum flow and optimum density, respectively. The term "capacity" has been used to quantify the traffic-carrying ability of transportation facilities. The value of capacity is used when designing or rehabilitating highway facilities to determine their geometric design characteristics such as the desirable number of lanes, it is used to design the traffic signalization schemes of intersections and arterial streets, it is used in evaluating whether an existing facility can handle the traffic demand expected in the future, and it is also used in the operations and management of traffic control systems (ramp metering algorithms, congestion pricing algorithms, signal control optimization, incident management, etc.) [Ele14]. The first traffic stream model was developed by Greenshields [BD+35], who developed a linear speed–density relationship based on field data. Figure 1.2 provides a sketch of the Greenshields model, which consists of the flow–speed, flow–density, and speed–density relationships. There are three main ways to study traffic flow [KG18], corresponding to the three scales: *microscopic* scale, every vehicle is considered as an individual. An equation can be written for each, usually an ordinary differential equation (ODE); *macroscopic* scale, similar to models of fluid dynamics, it is considered useful to employ a system of partial differential equations, which balance laws for some gross quantities of interest; *mesoscopic* "kinetic" scale, intermediate possibility, following methods of statistical mechanics, can be computed using an integrodifferential equation such as the Boltzmann equation. Beyond three scales, macroscopic models typically described by partial differential equations (PDEs) are more suitable to study congested traffic and disturbances in the traffic flow.

There are many macroscopic models. The first order Lighthill-Whitham-Richards (LWR) model (see [LW55] and [Ric56]) represents density-velocity relation in equilibrium and fails to model stop-and-go traffic. The second-order Payne-Whitham (PW) model (see [Pay71] and [Whi99]) consists of momentum equation and conservation law, and it is a nonlinear second-order deviation from density-velocity equilibrium. The second order Aw-Rascle-Zhang (ARZ) model (see [AR00] and [Zha02]) is derived from the combination of these two models (LWR model

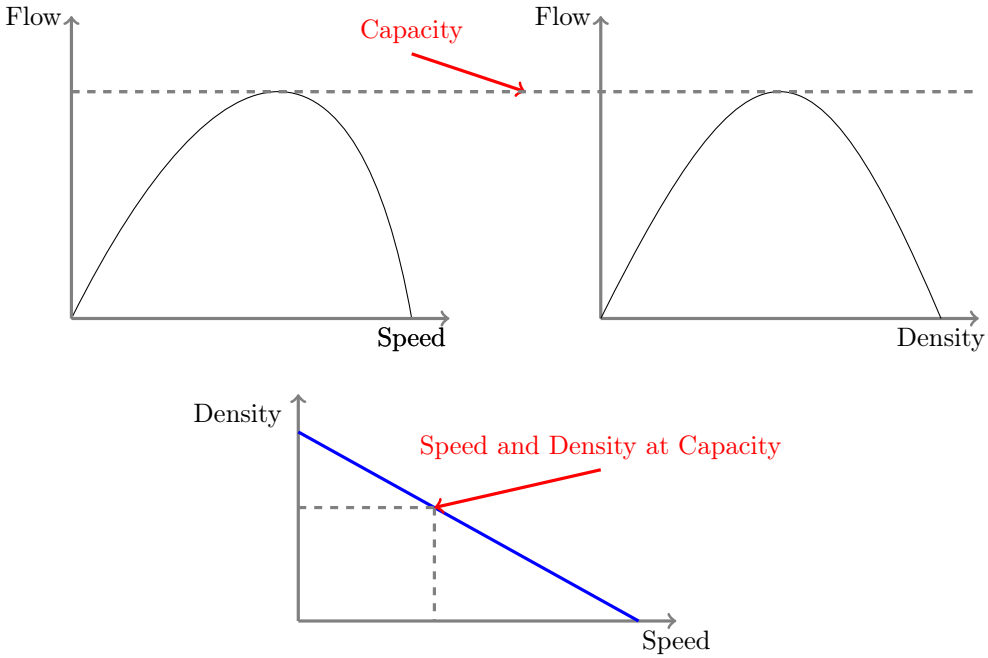

Figure 1.2: Flow, speed, density relationships: the Greenshields model.

and PW model) through suitable definition and coefficients. There are also some new models to solve some problems or to improve the model properties. A new car-following model is presented in [Tan+09]. The exact boundary controllability of a class of nonlocal conservation laws modeling traffic flow is studied in [Bay+21]. In [GK07], the authors propose a new continuum model with an additional anisotropic term that ensures the characteristic velocities can be less than or equal to the macroscopic flow speed. In [LBCG20], a new macroscopic traffic flow model is presented resulting from the physical realism of the boundedness of traffic acceleration. Except the single road models, there are some models for networks. A macroscopic traffic flow model is presented to deal with conservation laws on networks and coupled boundary conditions at the junctions with buffers of fixed arbitrary size and time-dependent split ratios in [LB+20]. A two-dimensional traffic dynamic model for large-scale traffic networks is introduced in [Mol+19]. In this manuscript, the ARZ traffic model of hyperbolic PDEs is used to estimate the disturbance rejection capacity and reject disturbances to stabilize the single lane traffic flow system. Computing the value of $\mathcal{L}_2$ gain from disturbance to output is a classical control method to measure the disturbance rejection capacity (see the recent survey [MP20]). For linear systems with $\mathcal{L}_2$ disturbances, the problems of disturbance tolerance and rejection are formulated and solved in [FLH04]. In [HLM02b] and [HLM02a], under conditions written with linear matrix inequalities, $\mathcal{L}_2$ gain is applied to characterize the ability to reject disturbance for linear systems in the presence of actuator saturation and disturbance as in Chapter 5 of [LL18] and Chapter 3 of [Tar+11].

The complex and nonlinear way of traffic behavior is dependent on the interactions of massive vehicles. Several equilibriums, frequent lane changes, overtaking, and platoon dispersion probably happen in congested traffic on account of the interplay between different types of vehicles and drivers [NL07]. Besides the homogeneous models as above, there are many macroscopic traffic flow models for heterogeneous traffic. Paper [FW15] studies a two-type vehicle heterogeneous traffic model to acquire overtaking and creeping traffic flows. In [MR17], the extended macroscopic N-type Aw-Rascle (AR) traffic model is used for heterogeneous traffic by using area occupancy. The concept of area occupancy is introduced for measuring heterogeneous traffic concentration

in [MR06] and [AD08]. In [MR21], a continuum multi-type traffic model is introduced on the basis of a three-dimensional flow–concentration surface. An n-population generalization of the Lighthill–Whitham-Richards traffic flow model is presented in [BGC03]. For the mixed traffic, some models have been presented. In [JW04], an extended speed gradient (SG) model is used to study the mixed traffic flow system. In [Liu+21], the data-driven optimal controller is designed for connected and autonomous vehicles (CAVs) in a mixed-traffic situation (specifically, including heterogeneous human-driven vehicles). The interaction between CAV and human-driven vehicle (HDV) dynamics is investigated, and a complete CAV control input and the feasible conditions of a platoon formation are presented in [MM22] (see also [Tay+21]). In [Gar+20], a model is proposed for mixed traffic composed of few CAVs in the bulk flow, relying on a multi-scale approach to couple a PDE describing the entire traffic flow and ODEs describing CAV trajectories. About the traffic networks, paper [TCL21] contributes to the boundary control design for multi-directional congested traffic evolving on large-scale urban networks represented by a continuum of two-dimensional planes, and in [AB22], a delay-robust stabilizing state feedback boundary control law is developed for an underactuated network of two subsystems of heterodirectional linear first-order $n + m$ hyperbolic PDEs systems. For the study of multi-type traffic system in this manuscript, we introduce the multi-type AR traffic flow hyperbolic model to design a controller for rejecting disturbances and stabilizing the system.

In order to stabilize hyperbolic systems of highway traffic, it is natural to use a proportional-integral (PI) boundary feedback control strategy on available control signals such as ramp metering or variable speed limits on a road, due to its actual superiority in attenuating disturbances in engineering. In control theory, the PI feedback control method is a fruitful paradigm for industrial and real-life applications for infinite-dimensional systems (see e.g., [ACL05]). Indeed, dissipative PI boundary conditions have been given for one-dimensional linear hyperbolic systems of balance laws in [DBC12]. Lyapunov stability of hyperbolic systems of conservation laws is achieved for boundary control law with integral action in [SM+08]. A PI controller only depending on one side measurable angular velocity is used to analyze the stability of the inhomogeneous drilling model in [TJ+20]. In [ZPQ19], a PI boundary feedback controller is designed to stabilize the oscillations of the traffic parameters on a freeway segment by using on-ramp metering and variable speed control. Paper [ZP17] proves the local stability of a positive hyperbolic system by designing a PI boundary feedback controller to stabilize the oscillations of the traffic parameters on a freeway by the Lyapunov method. For the stability of a cascaded network consisting of several 2×2 linear hyperbolic systems, PI output feedback controllers are designed to reject disturbance and regulate output to the desired points in [TAX18].

For the stability analysis in this manuscript, integral input-to-state stability (iISS) (a closely related notion of input-to-state stability (ISS), that is known as one of the central notions in the control theory of dynamical systems since the seminal paper [Son89]) is used to estimate the impact of the integral of the disturbances to the state norm [MI15a]. Indeed it allows for the description of the disturbance effect on the state of nonlinear finite-dimensional systems and provides some design methods of dynamical output feedback laws (see the survey [Son08]). For infinite-dimensional systems, the theory has been recently generalized in [KMZ21]. In this manuscript, we exploit such a notion (iISS) in a quasi-linear infinite-dimensional system with boundary control and perturbation. More precisely, by providing an iISS property, we design an observer of the homogeneous linearized traffic flow model that guarantees the accurate estimation of the traffic state under the condition that the initial estimation is not too far from the actual state.

In this research, we use the backstepping method to derive a boundary feedback controller to alleviate traffic congestion. The backstepping approach is the extension of Volterra integral transformations and can be used to systematically design controller and observers for linear PDEs. For the infinite-dimensional system, the controllers and observers can be derived directly and all

analysis can be done without discretization before implementation on a computer. The rationale behind the backstepping method in this manuscript is the following: through constructing an appropriate Volterra integral transformation, the original PDE system is mapped to an integral iISS target system. The original system inherits the stability property thanks to the invertibility of backstepping transformation. The kernels derived from the backstepping transformation are adopted as gains of the original system feedback controller.

The backstepping method for hyperbolic PDEs was initially introduced by [KS08], [Krs08] and [SCK10]. For the backstepping boundary control design of hyperbolic systems, there are some theoretical results obtained recently. The robust output regulation problem for boundary-controlled linear 2×2 hyperbolic systems is solved in [Deu17a]. By implementing the finite-time state feedback regulator with disturbance observers, the finite-time output regulation problem is solved in [Deu17b]. Two closely related state feedback adaptive control laws are designed for the stabilization of linear hyperbolic systems with constant but uncertain in-domain and boundary parameters in [AA18]. An output feedback control law is designed for a quasi-linear 2×2 system of first-order hyperbolic PDEs with actuation and measurement on only one end of the domain, and the local H^2 exponential stability of the closed-loop system is proved in [VKB12]. [Cor+13] uses a backstepping transformation to design a full-state feedback control law and derives H^2 exponential stability for a quasi-linear 2×2 system of first-order hyperbolic PDEs. An output feedback controller is designed for the underactuated cascade network of interconnected PDEs systems using backstepping in [Aur20]. Paper [BCH21] studies the sufficient conditions for local input-to-state stability in the sup norm of general quasi-linear hyperbolic systems with boundary input disturbances. [Vaz+19] uses the backstepping method to stabilize the low-frequency parts of a 2-D reaction-diffusion system with Neumann-type boundary conditions. In consideration of the limits of technology and cost, there have been works inspired by [VKC11], designing an observer-based output feedback control law for the linearized ARZ traffic flow model by using backstepping transformations (see also [YK19a]). On the basis of PDE backstepping, the solutions to stabilization of homodirectional and General heterodirectional linear coupled hyperbolic PDEs are yielded by both full-state and observer-based output feedback, and the trajectory tracking problems are solved in [Hu+16]. Bilateral control and observation problems for a class of viscous Hamilton–Jacobi PDEs are tackled by backstepping in [BLV19]. In [Yu+20], a boundary observer for the nonlinear ARZ traffic flow model is designed to the information of traffic states using the backstepping method. An observer-based output feedback control law is designed for the linearized ARZ traffic flow model by using backstepping transformations in [YK19b]. In [VK19], the problem of boundary control design and observation are dealt with for radially varying coefficients reaction-diffusion equation under revolution symmetry conditions on a sphere by the backstepping method. Paper [BYK21] uses the backstepping method to design an output feedback boundary control for the stop-and-go traffic problem of a linearized two-class AR traffic flow system.

Instead of solving an identification problem for the traffic flow, we solve this problem for a pandemic dynamic. Until now, COVID-19 has widely spread over the world and has resulted in huge pressure on hospital capacity and massive death of the population in the world. Quarantine and lockdown measures have effectively controlled the spread of the infection, in particular in China (see [Kuc+20]). Quarantine is a rather old technique to prevent the spread of diseases. It is used at the individual level to constrain the movement of the population and encourage them to stay at home. Lockdown measures reduce the pandemic transmission by increasing social distance and limiting the contacts and mobility of people, e.g. with the cancellation of public gatherings, the closure of public transportation, and the closure of borders. But longstanding lockdown results in inestimable financial costs, many job losses, and particularly psychological panic of people and social instability. As declared by some governments (see [Gos+20]), testing is crucial to exit lockdown, mitigate health harm and decrease economic expenses. In this manuscript, we consider

two classes of active detection. The first one is the short-range test: molecular or Polymerase Chain Reaction (PCR) test, which is used to detect whether one person has been infected in the past. The second test is the long-range test: serology or immunity test, which allows determining whether one person is immune to COVID-19 now. This test is used to identify the individuals that cannot be infected again.

There have been many papers that focus on estimating the effect of lockdown strategies on the spread of the pandemic (e.g. [BHM20] and [Roq+20]). In [Pra+20], the lockdown effect is estimated using stochastic approximation, expectation maximization, and estimation of basic reproductive numbers. In the last part of this manuscript, we aim at evaluating the dynamics of the pandemic after the lockdown by looking at the transport effect. For our research on COVID-19, we aim to evaluate the effect of lockdown within a given geographical scale in France, such as the largest cities, urban agglomerations, French departments, or one of the 13 Metropolitan Regions (to go from the finest geographical scale to the largest one). The estimations of effect are also considered in different age classes, such as early childhood, scholar childhood, working-class groups, or the elderly. Besides, we propose to understand the effect of partial lockdown or other confinement strategies depending on some geographical perimeters or some age groups (as the one that Lyon experienced very recently, see [Fra20]).

Contributions

The work presented in this manuscript lies in the domain of the control theory of traffic flow dynamics. To be more specific, the objective is to seek an optimal tuning of control law for alleviating the congested traffic and rejecting disturbances on a considered roadway with a bottleneck at the downstream boundary. In this framework, we investigate the optimization control problem of the homogeneous and heterogeneous traffic flow dynamics described by quasi-linear hyperbolic PDEs. Our main contributions are as follows:

- For sake of consequently strengthening the robustness of the homogeneous traffic dynamics, the first main contributions of our work are the design of a PI boundary feedback controller maximizing the disturbance rejection and the design of an observer-based output boundary control of traffic breakdown to remove or weaken the effect of high traffic demand, with the fastest convergence rate.

- This manuscript states a new result on the controller design by using the backstepping method for the linearized multi-type traffic flow hyperbolic system around a nonuniform equilibrium to reject disturbances and then alleviate the congested traffic. Firstly, this work presents the derivation of an extended multi-type AR traffic flow model in the characteristic form. Secondly, we prove the integral input-to-state stability (iISS) of a target system that has a source term of integral form and a proportional-integral (PI) boundary control for rejecting disturbances. Moreover, a controller implemented by ramp metering is designed to robustly stabilize the heterogeneous traffic system by applying the backstepping method to the multi-type vehicle traffic model.

- In the study of the COVID-19 epidemic, one contribution is that an extension of the typical SIRD pandemic model is presented for characterizing the regional spread of COVID-19 in France before and after the lockdown strategies. In order to estimate the effect of lockdown strategies and understand the evolution of the undetected compartments for each region in France, an optimization algorithm is used to solve the following identification problem: derive the optimal parameters for regions by fitting the extended model to real reported data during the lockdown. Based on regional model analysis before and after the lockdown, we present a network model to characterize the pandemic transmission between regions in France after the lockdown and evaluate the transport effect of the COVID-19 pandemic, when considering all age classes together. The most interesting point is the chosen exponential transmission rate (time-dependent) function β, in order to incorporate the complex effect of lockdown and unlock down strategies.

Structure

This manuscript is organized as follows:

In Chapter 2, we succeed to design a PI controller computed on the linearized ARZ traffic model. Computing the value of L^2 gain from disturbance to output, that is to measure the disturbance rejection capacity (see the recent survey [MP20]), yields numerically tractable conditions since convex conditions are derived for the PI controller design. Moreover, by means of numerical simulations, the stability of the quasi-linear ARZ model in a closed-loop with this controller is obtained.

In Chapter 3, the linearized ARZ traffic flow model with boundary disturbances is derived by making use of coordinate transformation and linearization around the equilibrium. Using backstepping transformation to map the linearized ARZ traffic flow model into an iISS target system, we obtain a full-state feedback controller. We use the backstepping method to derive an observer-based output feedback controller to alleviate the congested traffic resulting from traffic breakdown. Finally, the optimization problem is discussed and the results of numerical simulations are provided.

Chapter 4 presents the derivation of an extended multi-type AR traffic flow model in the characteristic form and proves the iISS of the target system which has a source term of integral form and a PI boundary control for rejecting disturbances. Moreover, a controller implemented by ramp metering is designed to robustly stabilize the heterogeneous traffic system by applying the backstepping method to the multi-type vehicle traffic model.

In Chapter 5, extending the control problem of the linearized multi-type traffic system in Chapter 4, we solve the problem of the stabilization for a multi-type traffic flow system of quasi-linear PDEs in the congested regime, with disturbances and actuation at the inlet boundary and capacity drop in the downstream boundary of a considered road segment. The controller which is designed for the linearized system by backstepping method is applied to locally stabilize the quasi-linear system around a nonuniform equilibrium. The iISS of the quasi-linear system is derived by making use of the Lyapunov method to analyze the iISS of the target system, which is mapped into the quasi-linear system by a backstepping transformation.

In Chapter 6, considering the context of pandemic dynamics, an extended model is derived from the classical pandemic SIRD model and the rationale behind the model is explained. We present the parameters optimization problem and estimate the effect of lockdown strategies. From the calibration of parameters for each region in France, we derive the pandemic start date of regions. A network model of pandemic transmission between regions is introduced and the network simulation is implemented. By using the same model as the pandemic network of regions in France, we simulate the pandemic network of all cities in France.

Some conclusions and perspectives end this manuscript.

So far, there are several papers published and reviewed as follows:

- Lina Guan, Liguo Zhang, and Christophe Prieur. "Optimal PI controller rejecting disturbance for ARZ traffic model". In: 59th IEEE Conference on Decision and Control (CDC). 2020, pp. 5665–5670;
- Lina Guan, Christophe Prieur, Liguo Zhang, Clémentine Prieur, Didier Georges, and Pascal

Bellemain. "Transport effect of COVID-19 pandemic in France". In: Annual Reviews in Control 50 (2020), pp. 394–408;

- Lina Guan, Liguo Zhang, and Christophe Prieur. "Optimal observer-based output feedback controller for traffic congestion with bottleneck". In: International Journal of Robust and Nonlinear Control 31 (15 2021), pp. 7087–7106;
- Lina Guan, Liguo Zhang, and Christophe Prieur. "Optimal Boundary ISS Controller for Heterogeneous and Congested Traffic". In: Automatica (2021), under review as a Regular Paper;
- Lina Guan, Liguo Zhang, and Christophe Prieur. "Stabilization of Heterogeneous quasi-linear Traffic Flow System with Disturbances". In: IEEE Transactions on Automatic Control (2022), under review;
- Lina Guan, Christophe Prieur, and Liguo Zhang. "State observation for Heterogeneous quasi-linear Traffic Flow System with Disturbances". In: Mathematics of Control, Signals, and Systems (2022), under review;

Notation

Let us conclude this chapter by providing the notation used in this manuscript. The set of positive real numbers is represented by $\mathbb{R}_{>0}$.

C^0 is the set of continuous functions, and C^1 is the set of continuously differentiable functions. A function belongs to the set C^2 if the first and second derivatives of the function both exist and are continuous. If the derivatives $f^{(n)}$ exist for all positive integers n, the function is smooth or equivalently, belongs to the set C^∞.

$\max(S)$ is the maximum value of all the elements in S if S is a set.

$\partial_t f$ and $\partial_x f$ respectively denote the partial derivatives of a function f with respect to the variables t and x. f' denotes the first derivative of a function f with respect to the variable x, and $\dot{f}$ denotes the first derivative of a function f with respect to the variable t.

For a function $\varphi = [\varphi_1, \dots, \varphi_n]^\top : [0, L] \times [0, +\infty) \to \mathbb{R}^n$, we define the following norms, the L^1-norm

$$\|\varphi\|_{L^1((0,L);\mathbb{R}^n)} = \int_0^L \left(|\varphi_1(\xi, t)| + \cdots + |\varphi_n(\xi, t)|\right) \mathrm{d}\xi,$$

the L^2-norm

$$\|\varphi\|_{L^2((0,L);\mathbb{R}^n)} = \left(\int_0^L (\varphi_1^2(\xi, t) + \cdots + \varphi_n^2(\xi, t)) \,\mathrm{d}\xi\right)^{\frac{1}{2}},$$

the L^∞-norm

$$\|\varphi\|_{L^\infty((0,L);\mathbb{R}^n)} = \max\left\{\|\varphi_1\|_{L^\infty((0,L);\mathbb{R})}, \dots, \|\varphi_n\|_{L^\infty((0,L);\mathbb{R})}\right\},$$

the H^1-norm

$$\|\varphi\|_{H^1((0,L);\mathbb{R}^n)} = \left(\int_0^L \left(\|\varphi\|^2_{L^2((0,L);\mathbb{R}^n)} + \|\varphi_x\|^2_{L^2((0,L);\mathbb{R}^n)}\right) \mathrm{d}x\right)^{\frac{1}{2}},$$

and the H^2-norm

$$\|\varphi\|_{H^2((0,L);\mathbb{R}^n)} = \left(\int_0^L \left(\|\varphi\|^2_{L^2((0,L);\mathbb{R}^n)} + \|\varphi_x\|^2_{L^2((0,L);\mathbb{R}^n)} + \|\varphi_{xx}\|^2_{L^2((0,L);\mathbb{R}^n)}\right) \mathrm{d}x\right)^{\frac{1}{2}}.$$

$\mathbb{R}^n$ denotes the set of real n-dimensional column vectors. $\mathbb{R}^{n\times l}$ denotes the set of real $n \times l$ matrices. $0_{n\times l}$ denotes the $n \times l$ zero matrix. I_n is a n-dimensional identity matrix. $\mathcal{D}_n$ denotes the set of n-dimensional diagonal matrix. $\mathcal{D}_n^+$ denotes the set of n-dimensional diagonal matrix in which the main diagonal entries are positive.

The n-dimensional column vector is represented as $M = \begin{bmatrix} M_1 & M_2 & \cdots & M_n \end{bmatrix}^\top$, where the argument M_i $(i = 1, 2, \dots, n)$ is a scalar or a column vector. The diagonal matrix is represented as $M = \mathrm{diag}\{d_1, d_2, \dots, d_n\}$ with the diagonal entry d_i $(i = 1, 2, \dots, n)$. The block diagonal matrix is represented as $M = \mathrm{diag}\{M_1, M_2, \dots, M_n\}$, and the block matrix is represented as $M = \begin{bmatrix} M_{11} & M_{12} & \cdots & M_{1n} \\ M_{21} & M_{22} & \cdots & M_{2n} \\ \vdots & \vdots & \ddots & \vdots \\ M_{n1} & M_{n2} & \cdots & M_{nn} \end{bmatrix}$, where the main diagonal argument M_i $(i = 1, 2, \dots, n)$ and the

argument M_{ij} $(i, j = 1, 2, \ldots, n)$ are matrices. $[M]_{i,j}$ denotes the entry of matrix M in the i-th row and the j-th column. $\{M_{ij}\}_{n_1 \leq i \leq n_2, l_1 \leq j \leq l_2}$ denotes a matrix consisting of the entries of matrix M in the rows from n_1-th to n_2-th and the columns from l_1-th to l_2-th.

M^{-1} denotes the inverse matrix of a square matrix M. $M^{\top}$ denotes the transpose of a matrix M. $\lambda(M)$ is the set of all the eigenvalues of a matrix M, and $|\lambda(M)|$ is the set of absolute values of all the eigenvalues if M is a square matrix.

The symbol $*$ stands for a symmetric block in a matrix.

Chapter 2

Control of homogeneous linearized traffic without bottleneck

Contents

A perturbed distributed parameter model is used, and a boundary control is designed to reject the perturbations. More precisely an optimal tuning PI feedback control law is computed to maximally reject the disturbances and stabilize the traffic in a congested regime. The disturbance applies at the boundary of the linearized ARZ model. Therefore the disturbance operator is unbounded, rendering the control problem very challenging. To analyze and design the optimal tuning PI controller for this infinite-dimensional system, the $\mathcal{L}_2$ gain is computed to estimate the disturbance rejection. Numerically tractable conditions are computed and written with linear matrix inequalities (LMIs). As a result, the estimation of an upper bound of the $\mathcal{L}_2$ gain, from the disturbance to the controlled output, can be formulated as an optimization problem with LMI constraints. The validity of this method is checked on simulations of the nonlinear ARZ model in a closed-loop with this optimal tuning PI controller.

This chapter has been published in [GZP20].

2.1 Linearized ARZ traffic flow model

The Aw-Rascle-Zhang model is a typically local second-order macroscopic traffic flow model composed of the following continuity and acceleration equations:

$$\partial_t \rho(x,t) + \partial_x(v(x,t)\rho(x,t)) = 0, \tag{2.1}$$

$$\partial_t v(x,t) + (v(x,t) - \rho(x,t)p'(\rho(x,t)))\,\partial_x v(x,t) = \frac{V_e(\rho(x,t)) - v(x,t)}{\tau}, \tag{2.2}$$

with an independent space variable x in $(0, L)$ on a road section of length L, and an independent time variable t in $[0, \infty)$. As the locally aggregated quantities, the traffic density $\rho(x,t)$ is defined as the number of vehicles per unit length at time t, and the mean speed $v(x,t)$ is the average speed of the vehicles passing the location x for a fixed time interval. With the maximal free flow speed

v_f and the maximum density ρ_m, the inequalities $0 < v \leq v_f$ and $0 < \rho \leq \rho_m$ hold. The speed adaptation time τ is a constant and corresponds to the inverse of agility. In the previous model, the equilibrium speed $V_e(\rho)$ is the speed-density relation given by Greenshield's model in [BD+35] as

$$V_e(\rho) = v_f \left(1 - \frac{\rho}{\rho_m}\right). \tag{2.3}$$

The speed adaptation term or relaxation term located on the right side of the equation (2.2) describes the mean acceleration of the vehicles in the local neighborhood for reaching the equilibrium speed.

The traffic pressure $p(\rho)$ is an increasing function of density defined as, with a positive constant γ,

$$p(\rho) = v_f - V_e(\rho) = v_f \left(\frac{\rho}{\rho_m}\right)^{\gamma}. \tag{2.4}$$

The constant γ represents the reflection of the driver to the increasing density and can be tuned to get the realistic traffic pressure $p(\rho)$. For simplicity of analysis, $\gamma = 1$ is chosen. By defining $\omega = v + \frac{v_f}{\rho_m}\rho$ as a new variable representing the traffic "friction" or drivers' property [FS13] and transporting with the vehicle velocity in the traffic flow, the fully nonlinear system (2.1)-(2.2) is changed into the following quasi-linear system, for all $x \in [0, L]$, $t \in [0, \infty)$,

$$\partial_t \omega(x,t) + v(x,t)\partial_x \omega(x,t) = \frac{v_f - \omega(x,t)}{\tau}, \tag{2.5}$$

$$\partial_t v(x,t) + (2v(x,t) - \omega(x,t))\partial_x v(x,t) = \frac{v_f - \omega(x,t)}{\tau}. \tag{2.6}$$

In (2.6), the propagation velocity $2v - \omega > 0$ stands for the weak interactions between the vehicles, the traffic wave propagates with the traffic flow (downstream) at this characteristic velocity in free traffic. Usually, the propagation velocity of the traffic wave is slightly less than the average free-flow vehicle speed in free traffic. Reversely, the characteristic velocity $2v - \omega < 0$ represents the traffic waves moving against the traffic flow (upstream) in congested traffic due to the reaction of the drivers to their respective leading vehicles. In this study, we take into account the control problem of perturbation in congested traffic situations.

Denote by $(\omega^*, v^*)^\top$ in $C^1([0, L]; \mathbb{R}^2)$ a equilibrium of the system (2.5)-(2.6) such that $2v^*(x) - \omega^*(x) < 0$ for all $x \in [0, L]$ on a stable and inhomogeneous road (with speed and density gradients). Note that it depends on the space variable x and the corresponding density is $\rho^* = \frac{\rho_m}{v_f}(\omega^* - v^*)$. The deviations from the system states $(\omega, v)^\top$ are defined as $\widetilde{\omega}^h = \omega - \omega^*, \widetilde{v}^h = v - v^*$, then the quasi-linear deviation system is obtained, for all $x \in [0, L]$, $t \in [0, \infty)$,

$$\partial_t \widetilde{\omega}^h(x,t) + \Lambda_1^h(\widetilde{\omega}^h, \widetilde{v}^h, x)\partial_x \widetilde{\omega}^h(x,t) + \widetilde{v}^h(x,t)\omega^{*\prime}(x) + \frac{\widetilde{\omega}^h(x,t)}{\tau} = 0, \tag{2.7}$$

$$\partial_t \widetilde{v}^h(x,t) + \Lambda_2^h(\widetilde{\omega}^h, \widetilde{v}^h, x)\partial_x \widetilde{v}^h(x,t) + \left(2\widetilde{v}^h(x,t) - \widetilde{\omega}^h(x,t)\right) v^{*\prime}(x) + \frac{\widetilde{\omega}^h(x,t)}{\tau} = 0, \tag{2.8}$$

with two characteristic velocities

$$\Lambda_1^h(\widetilde{\omega}^h, \widetilde{v}^h, x) = \widetilde{v}^h(x,t) + v^*(x),$$
$$\Lambda_2^h(\widetilde{\omega}^h, \widetilde{v}^h, x) = 2\widetilde{v}^h(x,t) - \widetilde{\omega}^h(x,t) + 2v^*(x) - \omega^*(x),$$

where $\Lambda_1^h(\widetilde{\omega}^h, \widetilde{v}^h, x) > 0$, $\Lambda_2^h(\widetilde{\omega}^h, \widetilde{v}^h, x) < 0$.

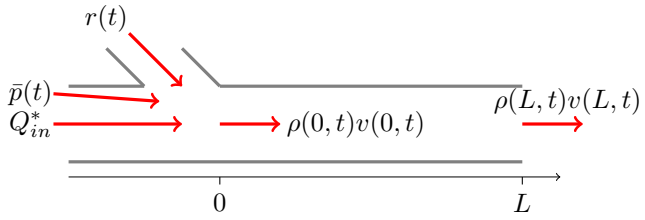

Figure 2.1: Traffic flow in a freeway segment.

An uniform equilibrium of the system (2.7)-(2.8) is considered in this chapter, define $\omega^* = v_f$ and select the constant v^* such that $2v^* - \omega^* < 0$, then the following linearized ARZ model can be derived, for all $x \in [0, L]$, $t \in [0, \infty)$,

$$\partial_t \begin{bmatrix} \widetilde{\omega}^h(x,t) \\ \widetilde{v}^h(x,t) \end{bmatrix} + \begin{bmatrix} \lambda_1^h & 0 \\ 0 & -\lambda_2^h \end{bmatrix} \partial_x \begin{bmatrix} \widetilde{\omega}^h(x,t) \\ \widetilde{v}^h(x,t) \end{bmatrix} = \begin{bmatrix} -\frac{1}{\tau} & 0 \\ -\frac{1}{\tau} & 0 \end{bmatrix} \begin{bmatrix} \widetilde{\omega}^h(x,t) \\ \widetilde{v}^h(x,t) \end{bmatrix}, \tag{2.9}$$

where the constant characteristic velocities $\lambda_1^h = v^*, -\lambda_2^h = 2v^* - \omega^*$. We want to maximize going through traffic at the inlet as in [PG06], then, according to the flow conservation at the inlet (see Figure 2.1), we have, for all $t \in [0, \infty)$,

$$Q_{in}^* + \bar{p}(t) + r(t) = \rho(0,t)v(0,t) \le Q_{max}, \tag{2.10}$$

where Q_{in}^* denotes the equilibrium inflow at the upstream boundary, $\bar{p} \to 0$ is the unknown disturbances of inflow serving as exogenous variable (externally given model input) depending on time t and satisfying $0 \le Q_{in}^* + \bar{p}(t) \le Q_{in}^{max}$ (Q_{in}^{max} is the flux limit of the incoming road), and $0 \le r \le Q_{rmp}^{max}$ (Q_{rmp}^{max} is the flux limit on the on-ramp) is on-ramp metering. Because of the capping strategy in [MAC12] for ramp metering, if the total flow $Q_{in}^* + \bar{p}(t) + r(t)$ exceeds the flow limit Q_{max} of the main road, it is capped to this value Q_{max} by the access traffic light, so a queue of n waiting vehicles forms at the on-ramp. As long as $0 < n \le n_{max}$, the ramp metering is active restricting the ramp flow to $r = \max(0, Q_{max} - (Q_{in}^* + \bar{p}(t)))$. The speed at the inlet $v(0,\cdot)$ and the density at the inlet $\rho(0,\cdot)$ satisfy $0 < v(0,\cdot) \le v_f$ and $0 < \rho(0,\cdot) \le \rho_m$.

A system can be precisely controlled by only tuning the proportional gain, but PI control strengthens the stability in the presence of disturbances. In control engineering, the PI controller is mainly used to improve the stability property of the controlled system. The following PI boundary feedback control law is introduced, for all $t \in [0, \infty)$,

$$r(t) = Q_{rmp}^* + k_{P1}(\rho(L,t) - \rho^*) + k_{I1} \int_0^t (\rho(L,\sigma) - \rho^*)\, \mathrm{d}\sigma, \tag{2.11}$$

$$v(L,t) = v^* + k_{P2}(v(0,t) - v^*) + k_{I2} \int_0^t (v(0,\sigma) - v^*)\, \mathrm{d}\sigma, \tag{2.12}$$

where $Q_{rmp}^* > 0$ denotes the equilibrium on-ramp flow at the segment boundary upstream, and it satisfies $Q_{in}^* + Q_{rmp}^* = \rho^* v^*$, here density ρ^* is given by $\rho^* = \frac{\rho_m}{v_f}(\omega^* - v^*)$. The inflow speed $v(0,\cdot)$ and the outflow $q(L,\cdot)$ are measurement outputs, so the outflow density $\rho(L,\cdot) = \frac{q(L,\cdot)}{v(L,\cdot)}$. The inlet on-ramp metering r and the outlet variable speed $0 < v(L,\cdot) \le v_f$ are boundary control inputs. The coefficients $k_{P1}, k_{I1}, k_{P2}, k_{I2}$ are proportional and integral tuning gains.

Let $\widetilde{\rho} = \rho - \rho^*$, then (2.11)-(2.12) can be rewritten as, for all $t \in [0, \infty)$,

$$r(t) = Q^*_{rmp} + k_{P1}\widetilde{\rho}(L,t) + k_{I1}\int_0^t \widetilde{\rho}(L,\sigma)\,\mathrm{d}\sigma, \tag{2.13}$$

$$\widetilde{v}^h(L,t) = k_{P2}\widetilde{v}^h(0,t) + k_{I2}\int_0^t \widetilde{v}^h(0,\sigma)\,\mathrm{d}\sigma. \tag{2.14}$$

Combining feedback control laws (2.13)-(2.14) with (2.10) and linearizing, the following boundary condition can be attained, for all $t \in [0, \infty)$,

$$\bar{p}(t) + k_{P1}\widetilde{\rho}(L,t) + k_{I1}\int_0^t \widetilde{\rho}(L,\sigma)\,\mathrm{d}\sigma = v^*\widetilde{\rho}(0,t) + \rho^*\widetilde{v}^h(0,t). \tag{2.15}$$

Getting rid of the high order terms, we deduce from (2.13) and (2.15), for all $t \in [0, \infty)$,

$$\begin{aligned}
\widetilde{\omega}^h(0,t) =& \widetilde{v}^h(0,t) + \frac{v_f}{\rho_m}\widetilde{\rho}(0,t)\\
=& \frac{v_f\bar{p}(t)}{\rho_m v^*} + \left(1 - \frac{v_f\rho^*}{\rho_m v^*}\right)\widetilde{v}^h(0,t) + \frac{v_f k_{P1}}{\rho_m v^*}\widetilde{\rho}(L,t) + \frac{v_f k_{I1}}{\rho_m v^*}\int_0^t \widetilde{\rho}(L,\sigma)\,\mathrm{d}\sigma\\
=& \frac{v_f\bar{p}(t)}{\rho_m v^*} + \frac{k_{P1}}{v^*}\widetilde{\omega}^h(L,t) + \frac{k_{I1}}{v^*}\int_0^t \widetilde{\omega}^h(L,\sigma)\,\mathrm{d}\sigma + \left(1 - \frac{v_f\rho^*}{\rho_m v^*} - \frac{k_{P1}k_{P2}}{v^*}\right)\widetilde{v}^h(0,t)\\
&- \left(\frac{k_{P1}k_{I2}}{v^*} + \frac{k_{I1}k_{P2}}{v^*}\right)\int_0^t \widetilde{v}^h(0,\sigma)\,\mathrm{d}\sigma.
\end{aligned} \tag{2.16}$$

Combining (2.14) and (2.16) together for the system (2.9), the following PI boundary feedback controller can be derived, for all $t \in [0, \infty)$,

$$\begin{bmatrix}\widetilde{\omega}^h(0,t)\\ \widetilde{v}^h(L,t)\end{bmatrix} = K_P^h\begin{bmatrix}\widetilde{\omega}^h(L,t)\\ \widetilde{v}^h(0,t)\end{bmatrix} + K_I^h\int_0^t \begin{bmatrix}\widetilde{\omega}^h(L,\sigma)\\ \widetilde{v}^h(0,\sigma)\end{bmatrix}\,\mathrm{d}\sigma + \theta(t), \tag{2.17}$$

where

$$K_P^h = \begin{bmatrix}\frac{k_{P1}}{v^*} & 1 - \frac{v_f\rho^*}{\rho_m v^*} - \frac{k_{P1}k_{P2}}{v^*}\\ 0 & k_{P2}\end{bmatrix}, \qquad K_I^h = \begin{bmatrix}\frac{k_{I1}}{v^*} & \frac{-k_{P1}k_{I2} - k_{I1}k_{P2}}{v^*}\\ 0 & k_{I2}\end{bmatrix}$$

are respectively proportional and integral tuning matrices, and $\theta(t) = \begin{bmatrix}\frac{v_f\bar{p}(t)}{\rho_m v^*} & 0\end{bmatrix}^\top$. is an external disturbance input vector. Assume the tuning parameters k_{I1} and k_{I2} are different from 0, so that the matrix K_I^h is invertible.

Letting $R(x,t) = (\widetilde{\omega}^h(x,t), \widetilde{v}^h(x,t))^\top$, for all t in $[0,\infty)$ and all x in $[0,L]$, system (2.9) and (2.17) can be rewritten as

$$\partial_t R(x,t) + \Lambda^h\partial_x R(x,t) = MR(x,t), \tag{2.18}$$

$$R_{in}(t) = K_P^h R_{out}(t) + K_I^h\int_0^t R_{out}(\sigma)\,\mathrm{d}\sigma + \theta(t), \tag{2.19}$$

where

$$\Lambda^h = \mathrm{diag}\{\lambda_1^h, -\lambda_2^h\}, \qquad M = \begin{bmatrix}-\frac{1}{\tau} & 0\\ -\frac{1}{\tau} & 0\end{bmatrix},$$
$$R_{in}(t) = (\widetilde{\omega}^h(0,t), \widetilde{v}^h(L,t))^\top, \qquad R_{out}(t) = (\widetilde{\omega}^h(L,t), \widetilde{v}^h(0,t))^\top.$$

The disturbance must be constrained by an upper limit of energy to avoid the boundlessness of the state and output. As in [TPSJ05], assume that the energy of time-varying disturbance vector θ is limited in L^2 space by a constant positive value δ^h such that

$$\|\theta(t)\|_{\mathcal{L}_2} + \|\dot{\theta}(t)\|_{\mathcal{L}_2} = \left(\int_0^t \theta^\top(\sigma)\theta(\sigma)d\sigma\right)^{\frac{1}{2}} + \left(\int_0^t \dot{\theta}^\top(\sigma)\dot{\theta}(\sigma)\,\mathrm{d}\sigma\right)^{\frac{1}{2}} \le \frac{1}{\sqrt{\delta^h}}, \quad \forall t \ge 0. \tag{2.20}$$

2.2 Finite-gain $\mathcal{L}_2$ stable and $\mathcal{L}_2$ gain

As stated in [KG02], the definition of finite-gain $\mathcal{L}_2$ stable and $\mathcal{L}_2$ gain are given as follows.

Definition 2.1
If there exist non-negative constants k and g such that

$$\|y\|_{\mathcal{L}_2} \leq k\|u\|_{\mathcal{L}_2} + g, \tag{2.21}$$

for all u in L^2 space, where u and y are respectively the system disturbance input and controlled output, and g is a function of the initial condition, then the system is said to be finite-gain $\mathcal{L}_2$ stable and has $\mathcal{L}_2$ gain less than or equal to k.

Let

$$X(t) = \int_0^t R_{out}(\sigma)\,\mathrm{d}\sigma + K_I^{(1)-1}\theta(t), \tag{2.22}$$

where t in $[0, \infty)$, then

$$\dot{X}(t) = R_{out}(t) + K_I^{(1)-1}\dot{\theta}(t), \tag{2.23}$$

and (2.19) is rewritten as

$$R_{in}(t) = K_P^h R_{out}(t) + K_I^h X(t). \tag{2.24}$$

Consider the initial conditions

$$R(x,0) = \begin{bmatrix}\widetilde{\omega}^h(x,0)\\ \widetilde{v}^h(x,0)\end{bmatrix} = R_0(x), \tag{2.25}$$

and

$$X(0) = K_I^{(1)-1}\theta(0) = K_I^{(1)-1}\theta_0, \tag{2.26}$$

where $R_0(x)$ in $L^2(0,L)$, x in $(0,L)$ and θ_0 in $\mathbb{R}^2$.

It is important to note the finite-gain $\mathcal{L}_2$ stability of the system and to compute the $\mathcal{L}_2$ gain from $(\theta, \dot{\theta})^\top$ to R_{in} or an upper bound of it. The following theorem presents the theoretical sufficient conditions for system (2.18), (2.23)-(2.24) to address this problem.

Theorem 2.1
Considering the system (2.18), (2.23)-(2.24), if there exist positive constants μ and η, a diagonal matrix P_1^h in $\mathbb{R}^{2\times 2}$, a symmetric matrix P_2^h in $\mathbb{R}^{2\times 2}$ and a matrix P_3^h in $\mathbb{R}^{2\times 2}$ such that for all x in $[0,L]$,

$$\Omega^h = \begin{bmatrix}\Omega_{11}^h & \Omega_{12}^h & \Omega_{13}^h & \Omega_{14}^h\\ * & \Omega_{22}^h & \Omega_{23}^h & O_2\\ * & * & \Omega_{33}^h & \Omega_{34}^h\\ * & * & * & \Omega_{44}^h\end{bmatrix} \geq 0, \tag{2.27}$$

where

$$
\begin{aligned}
\Omega_{11}^h &= \mu|\Lambda^h|\mathcal{P}_1^h(x) - M^\top\mathcal{P}_1^h(x) - \mathcal{P}_1^h(x)M,\\
\Omega_{12}^h &= \Omega_{14}^h = -P_3^h,\\
\Omega_{13}^h &= -M^\top P_3^h,\\
\Omega_{22}^h &= -\frac{1}{L}\left(e^{\mu L}K_P^{(1)\top}|\Lambda^h|P_1^hK_P^h - |\Lambda^h|P_1^h + \frac{1}{\eta}K_P^{(1)\top}K_P^h\right),\\
\Omega_{23}^h &= -\frac{1}{L}\left(e^{\mu L}K_P^{(1)\top}|\Lambda^h|P_1^hK_I^h + K_P^{(1)\top}|\Lambda^h|P_3^h - |\Lambda^h|P_3^h + \frac{1}{\eta}K_P^{(1)\top}K_I^h\right) - P_2^h,\\
\Omega_{33}^h &= -\frac{1}{L}\left(e^{\mu L}K_I^{(1)\top}|\Lambda^h|P_1^hK_I^h + K_I^{(1)\top}|\Lambda^h|P_3^h + P_3^{(1)\top}|\Lambda^h|K_I^h + \frac{1}{\eta}K_I^{(1)\top}K_I^h\right),\\
\Omega_{34}^h &= -P_2^h,\\
\Omega_{44}^h &= \frac{1}{L}I_2,
\end{aligned}
$$

with $|\Lambda^h| = \mathrm{diag}\{\lambda_1^h, \lambda_2^h\}$, $\mathcal{P}_1^h(x) = P_1^h\mathrm{diag}\{e^{\mu(L-x)}, e^{\mu x}\}$, *null matrix* O_2 *and identity matrix* I_2 *are in* $\mathbb{R}^{2\times 2}$, *and*

$$
\begin{bmatrix} P_1^h & P_3^h \\ * & P_2^h \end{bmatrix} \geq 0, \tag{2.28}
$$

then for all initial conditions (2.25) and (2.26), and $\theta(t)$ *satisfying (2.20), the system (2.18), (2.23)-(2.24) is finite-gain* $\mathcal{L}_2$ *stable and the* $\mathcal{L}_2$ *gain from* $(\theta, \dot{\theta})^\top$ *to* R_{in} *is less than or equal to* $\sqrt{\eta m}$ *for a positive constant* m *depending only on* K_I^h.

Proof. The following candidate Lyapunov function is defined, for all $x \in [0, L]$, $t \in [0, \infty)$,

$$
\begin{aligned}
V^h(R(x,t), X(t)) &= \int_0^L \begin{bmatrix} R(x,t) \\ X(t) \end{bmatrix}^\top \begin{bmatrix} \mathcal{P}_1^h(x) & P_3^h \\ * & P_2^h \end{bmatrix} \begin{bmatrix} R(x,t) \\ X(t) \end{bmatrix} \mathrm{d}x\\
&= \int_0^L R^\top(x,t)\mathcal{P}_1^h(x)R(x,t)\,\mathrm{d}x + \int_0^L \left(R^\top(x,t)P_3^hX(t) + X^\top(t)P_3^{(1)\top}R(x,t)\right)\mathrm{d}x\\
&\quad + LX^\top(t)P_2^hX(t).
\end{aligned} \tag{2.29}
$$

One can observe that from

$$
\lambda_{\min}\cdot\|(R,X)^\top\|_{\mathcal{L}_2}^2 \leq V^h(R,X) \leq \lambda_{\max}\cdot\|(R,X)^\top\|_{\mathcal{L}_2}^2 \tag{2.30}
$$

with $\lambda_{\min}$ (the minimal eigenvalue of matrix $\begin{bmatrix} P_1^h & P_3^h \\ * & P_2^h \end{bmatrix}$) and $\lambda_{\max}$ (the maximal eigenvalue of matrix $\begin{bmatrix} e^{\mu L}P_1^h & P_3^h \\ * & P_2^h \end{bmatrix}$), the positive semi-definiteness of V^h is guaranteed by (2.28).

The time derivative of V^h along the solutions to system (2.18), (2.23)-(2.24) is written as follows, for all $t \in [0, \infty)$,

$$
\dot{V^h} = \dot{V_1^h} + \dot{V_2^h} + \dot{V_3^h}, \tag{2.31}
$$

with

$$\dot{V}_1^h = \int_0^L \left((\partial_t R(x,t))^\top \mathcal{P}_1^h(x) R(x,t) + R^\top(x,t)\mathcal{P}_1^h(x)\partial_t R(x,t)\right) \mathrm{d}x, \tag{2.32}$$

$$\dot{V}_2^h = \int_0^L \left((\partial_t R(x,t))^\top P_3^h X(t) + R^\top(x,t)P_3^h \dot{X}(t) + \dot{X}^\top(t)P_3^{(1)\top} R(x,t) + X^\top(t)P_3^{(1)\top}\partial_t R(x,t)\right) \mathrm{d}x, \tag{2.33}$$

$$\dot{V}_3^h = L\dot{X}^\top(t)P_2^h X(t) + LX^\top(t)P_2^h \dot{X}(t). \tag{2.34}$$

Using (2.18) and performing an integration by parts in (2.32), the following result is achieved, for all $t \in [0,\infty)$,

$$\begin{aligned}\dot{V}_1^h =& -R^\top(x,t)\Lambda^h\mathcal{P}_1^h(x)R(x,t)\Big|_0^L + \int_0^L R^\top(x,t)\left(\Lambda^h\mathcal{P}_1^{(1)\prime}(x) + M^\top\mathcal{P}_1^h(x) + \mathcal{P}_1^h(x)M\right)R(x,t)\,\mathrm{d}x\\ =& R^\top(0,t)\Lambda^h\mathcal{P}_1^h(0)R(0,t) - R^\top(L,t)\Lambda^h\mathcal{P}_1^h(L)R(L,t)\\ &+ \int_0^L R^\top(x,t)\left(-\mu|\Lambda^h|\mathcal{P}_1^h(x) + M^\top\mathcal{P}_1^h(x) + \mathcal{P}_1^h(x)M\right)R(x,t)\,\mathrm{d}x.\end{aligned} \tag{2.35}$$

Previous equation (2.35) can be rewritten as, for all $t \in [0,\infty)$,

$$\begin{aligned}\dot{V}_1^h =& R_{out}^\top(t)\left(e^{\mu L}K_P^{(1)\top}|\Lambda^h|P_1^hK_P^h - |\Lambda^h|P_1^h\right)R_{out}(t) + e^{\mu L}R_{out}^\top(t)K_P^{(1)\top}|\Lambda^h|P_1^hK_I^hX(t)\\ &+ e^{\mu L}X^\top(t)K_I^{(1)\top}|\Lambda^h|P_1^hK_P^hR_{out}(t) + e^{\mu L}X^\top(t)K_I^{(1)\top}|\Lambda^h|P_1^hK_I^hX(t)\\ &+ \int_0^L R^\top(x,t)\left(-\mu|\Lambda^h|\mathcal{P}_1^h(x) + M^\top\mathcal{P}_1^h(x) + \mathcal{P}_1(x)M\right)R(x,t)\,\mathrm{d}x.\end{aligned} \tag{2.36}$$

From (2.18) and (2.23), the following result can be derived from (2.33) by using an integration by parts, for all $t \in [0,\infty)$,

$$\begin{aligned}\dot{V}_2^h =& \left(-R^\top(x,t)\Lambda^hP_3^hX(t) - X^\top(t)P_3^{(1)\top}\Lambda^hR(x,t)\right)\Big|_0^L\\ &+ \int_0^L \Big(R^\top(x,t)P_3^hR_{out}(t) + R^\top(x,t)P_3^h(K_I^{(1)-1}\dot{\theta}(t))\\ &+ (K_I^{(1)-1}\dot{\theta}(t))^\top P_3^{(1)\top}R(x,t) + R_{out}^\top(t)P_3^{(1)\top}R(x,t)\\ &+ R^\top(x,t)M^\top P_3^hX(t) + X^\top(t)P_3^{(1)\top}MR(x,t)\Big)\,\mathrm{d}x\\ =& \left(R^\top(0,t) - R^\top(L,t)\right)\Lambda^hP_3^hX(t) + X^\top(t)P_3^{(1)\top}\Lambda^h\left(R(0,t) - R(L,t)\right)\\ &+ \int_0^L \Big(R^\top(x,t)P_3^hR_{out}(t) + R^\top(x,t)P_3^h(K_I^{(1)-1}\dot{\theta}(t)) + R_{out}^\top(t)P_3^{(1)\top}R(x,t)\\ &+ (K_I^{(1)-1}\dot{\theta}(t))^\top P_3^{(1)\top}R(x,t) + R^\top(x,t)M^\top P_3^hX(t) + X^\top(t)P_3^{(1)\top}MR(x,t)\Big)\,\mathrm{d}x.\end{aligned} \tag{2.37}$$

Previous equation (2.37) can be rewritten as, for all $t \in [0,\infty)$,

$$\begin{aligned}\dot{V}_2^h =& \left(K_P^hR_{out}(t) + K_I^hX(t)\right)^\top|\Lambda^h|P_3^hX(t) - R_{out}^\top(t)|\Lambda^h|P_3^hX(t)\\ &+ X^\top(t)P_3^{(1)\top}|\Lambda^h|(K_P^hR_{out}(t) + K_I^hX(t)) - X^\top(t)P_3^{(1)\top}|\Lambda^h|R_{out}(t)\\ &+ \int_0^L \Big(R^\top(x,t)P_3^hR_{out}(t) + R_{out}^\top(t)P_3^{(1)\top}R(x,t) + R^\top(x,t)M^\top P_3^hX(t) + X^\top(t)P_3^{(1)\top}MR(x,t)\\ &+ R^\top(x,t)P_3^h(K_I^{(1)-1}\dot{\theta}(t)) + (K_I^{(1)-1}\dot{\theta}(t))^\top P_3^{(1)\top}R(x,t)\Big)\,\mathrm{d}x.\end{aligned} \tag{2.38}$$

From (2.23), for all $t \in [0, \infty)$, we can convert (2.34) into

$$\dot{V_3^h} = LR_{out}^\top(t)P_2^hX(t) + L(K_I^{(1)-1}\dot{\theta}(t))^\top P_2^hX(t) + LX^\top(t)P_2^hR_{out}(t) + LX^\top(t)P_2^h(K_I^{(1)-1}\dot{\theta}(t)). \tag{2.39}$$

Then from (2.36), (2.38) and (2.39), the following result can be derived, for all $t \in [0, \infty)$,

$$\begin{aligned} &\dot{V^h} + \frac{1}{\eta}R_{in}^\top(t)R_{in}(t) - \theta^\top(t)\theta(t) - \dot{\theta}^\top(t)(K_I^{(1)-1})^\top K_I^{(1)-1}\dot{\theta}(t) \\ &\leq -\int_0^L \begin{bmatrix} R(x,t) \\ R_{out}(t) \\ X(t) \\ K_I^{(1)-1}\dot{\theta}(t) \end{bmatrix}^\top \Omega^h \begin{bmatrix} R(x,t) \\ R_{out}(t) \\ X(t) \\ K_I^{(1)-1}\dot{\theta}(t) \end{bmatrix} \mathrm{d}x, \end{aligned} \tag{2.40}$$

where Ω^h satisfies (2.27). Thus, for any θ satisfying (2.20), for all $t \in [0, \infty)$,

$$\dot{V^h} \leq -\frac{1}{\eta}R_{in}^\top(t)R_{in}(t) + \theta^\top(t)\theta(t) + \dot{\theta}^\top(t)(K_I^{(1)-1})^\top K_I^{(1)-1}\dot{\theta}(t). \tag{2.41}$$

By integrating the both sides of the previous inequality (2.41) over the interval $[0, t]$, one can derive that, for all $x \in [0, L]$, $t \in [0, \infty)$,

$$\begin{aligned} &\int_0^t \dot{V^h}(R(x,\sigma), X(\sigma))\,\mathrm{d}\sigma \\ &\leq -\frac{1}{\eta}\int_0^t R_{in}^\top(\sigma)R_{in}(\sigma)\,\mathrm{d}\sigma + m\int_0^t \theta^\top(\sigma)\theta(\sigma)\,\mathrm{d}\sigma + m\int_0^t \dot{\theta}^\top(\sigma)\dot{\theta}(\sigma)\,\mathrm{d}\sigma, \end{aligned} \tag{2.42}$$

where $m = \max\{1, \lambda_{\max}((K_I^{(1)-1})^\top K_I^{(1)-1})\}$. Then from $V^h(R, X) \geq 0$, for all $x \in [0, L]$, $t \in [0, \infty)$,

$$\int_0^t R_{in}^\top(\sigma)R_{in}(\sigma)\,\mathrm{d}\sigma \leq \eta V^h(R_0(x), X(0)) + \eta m\int_0^t \theta^\top(\sigma)\theta(\sigma)\,\mathrm{d}\sigma + \eta m\int_0^t \dot{\theta}^\top(\sigma)\dot{\theta}(\sigma)\,\mathrm{d}\sigma. \tag{2.43}$$

Using the inequality $\alpha^2 + \beta^2 \leq (\alpha + \beta)^2$ for non-negative numbers α and β and taking the square roots, one obtain that from (2.20), for all $x \in [0, L]$,

$$\|R_{in}\|_{\mathcal{L}_2} \leq \sqrt{\eta V^h(R_0(x), X(0))} + \sqrt{\eta m}(\|\theta\|_{\mathcal{L}_2} + \|\dot{\theta}\|_{\mathcal{L}_2}) \leq \sqrt{\eta V^h(R_0(x), X(0))} + \sqrt{\frac{\eta m}{\delta^h}}, \tag{2.44}$$

where the bias term $\sqrt{\eta V^h(R_0(x), X(0))} \leq \sqrt{\eta\lambda_{\max}}\|(R_0(x), X(0))^\top\|_{\mathcal{L}_2}$ depends on the coefficients η, $\lambda_{\max}$ (depends on μ, see (2.30)), the initial conditions $R_0(x)$, and $X(0)$. Therefore the coefficients η and μ determine the attractive domain of the closed-loop system with respect to the initial state. Note that from (2.20) and (2.44), if $R_0(x) = 0$, $x \in [0, L]$, and $\theta_0 = 0$,

$$\|R_{in}\|_{\mathcal{L}_2} \leq \sqrt{\eta m}(\|\theta\|_{\mathcal{L}_2} + \|\dot{\theta}\|_{\mathcal{L}_2}) \leq \sqrt{\frac{\eta m}{\delta^h}}. \tag{2.45}$$

Therefore, the system (2.18), (2.23)-(2.24) is finite-gain $\mathcal{L}_2$ stable and has $\mathcal{L}_2$ gain which is less than or equal to $\sqrt{\eta m}$. □

2.3 Numerical studies

2.3.1 Optimization

The smaller value of the $\mathcal{L}_2$ gain, the stronger the capacity of disturbance rejection is. In order to maximize the capacity of rejecting disturbance, based on Theorem 2.1, the following optimization

problem is considered to estimate $\mathcal{L}_2$ gain,

$$\min_{P_1^h,\, P_2^h,\, P_3^h,\, \mu} \eta$$
$$\text{subject to relations (2.27) and (2.28).} \tag{2.46}$$

2.3.2 Simulations

In order to seek the optimal values of parameter matrices K_P^h, K_I^h through the numerical simulation of optimization problem, we consider a road segment with parameters $\rho_m = 213.3\,\text{veh./km}$, $v_f = 160\,\text{km/h}$, $L = 1\,\text{km}$, and $\tau = 60\,\text{s}$. The initial conditions are, for all $x \in [0, L]$,

$$\rho(x,0) = \rho^* + 0.8 \sin 4\pi x,$$
$$v(x,0) = v^* + 1.8 \cos 4\pi x,$$

where the equilibrium $(\rho^*, v^*)^\top = (120, 70)^\top$ satisfies the ARZ equations (2.1)-(2.2). With given $\delta^h = 0.6$ in (2.20), the disturbance $\bar{p}(t)$ is given as Figure 2.2.

During solving the optimization problem (2.46), given μ on the domain $(0, 0.02]$ with a step size 0.001, we search the minimal value ($\eta_{\min}$) of η satisfying (for a discretized version of x with a step size $\frac{L}{30}$) the linear matrix inequalities (2.27)-(2.28) for each discrete quantity of μ by using the "yalmip" package on Matlab. The used function "optimize" which is common for solving optimization problems on Matlab consists of the chosen solver "sdpt3" (tried several solvers, only this one can compute), the constraints (2.27)-(2.28), and the objective η. We derive the curve of $\eta_{\min}$ with respect to the coefficient μ on the domain $(0, 0.02]$ in Figure 2.3. For the minimum value of $\eta_{\min}(= 1.002)$, $\mu = 0.003$ should be selected from Figure 2.3. Moreover, we solve the optimization problem by computing the best tuning parameters $k_{P1}, k_{P2}, k_{I1}, k_{I2}$, and we get $k_{P1} = -20$, $k_{P2} = -0.1$, $k_{I1} = -2$, $k_{I2} = -0.2$, and $m = 1337.4$. So the corresponding parameter matrices K_P^h and K_I^h of the PI boundary controller in (2.17) are

$$K_P^h = \begin{bmatrix} -0.2857 & -0.3143 \\ 0 & -0.1 \end{bmatrix}, \qquad K_I^h = \begin{bmatrix} -0.0286 & -0.06 \\ 0 & -0.2 \end{bmatrix}.$$

Under the minimum value of $\mathcal{L}_2$ gain η $(= 1.002)$, the state $(\widetilde{\omega}^h, \widetilde{v}^h)^\top$ of the linearized ARZ traffic system (2.18) converges to the zero equilibrium in Figure 2.4. That is, the optimal values of the parameters satisfying the conditions of Theorem 2.1 guarantee the stability of the linearized ARZ traffic system (2.18). We observe in Figure 2.5 that the state $(\rho, v)^\top$ of the nonlinear ARZ system (2.1)-(2.2) exponentially converges to the equilibrium $(\rho^*, v^*)^\top$. The obtained optimal values of the parameters for the linearized system (2.18) locally stabilize the nonlinear system (2.1)-(2.2).

2.4 Conclusion

In this chapter, the ARZ model has been introduced and an optimal tuning PI boundary controller has been computed for the homogeneous linearized traffic model without bottleneck. The conditions for finite-gain $\mathcal{L}_2$ stability and the computation of the $\mathcal{L}_2$ gain were given for the linearized ARZ system to reject disturbances. Moreover, numerical simulation emphasized the interest of this controller for the nonlinear model.

In the next chapter, we consider the bottleneck case and we solve an observation problem.

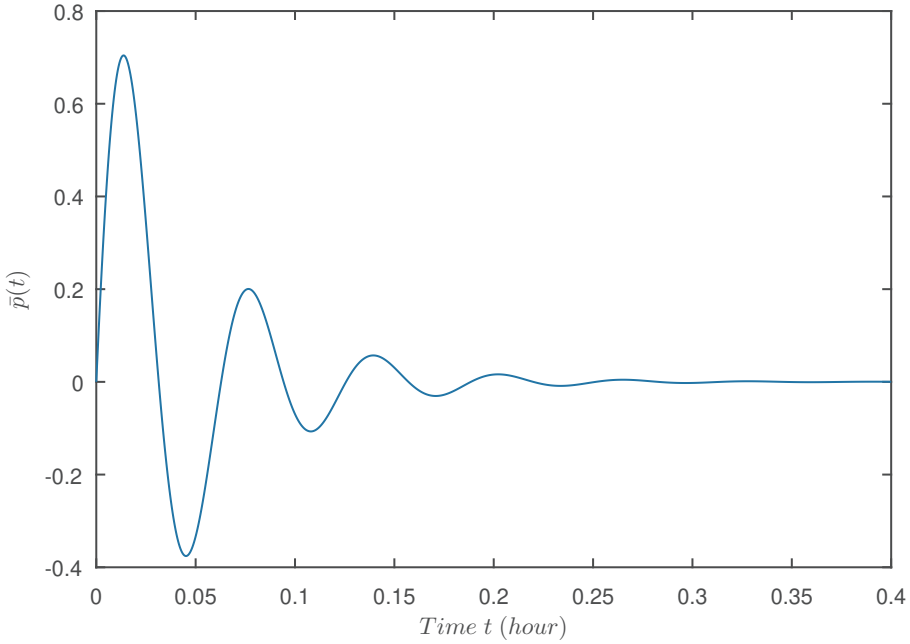

Figure 2.2: Disturbance $\bar{p}(t)$.

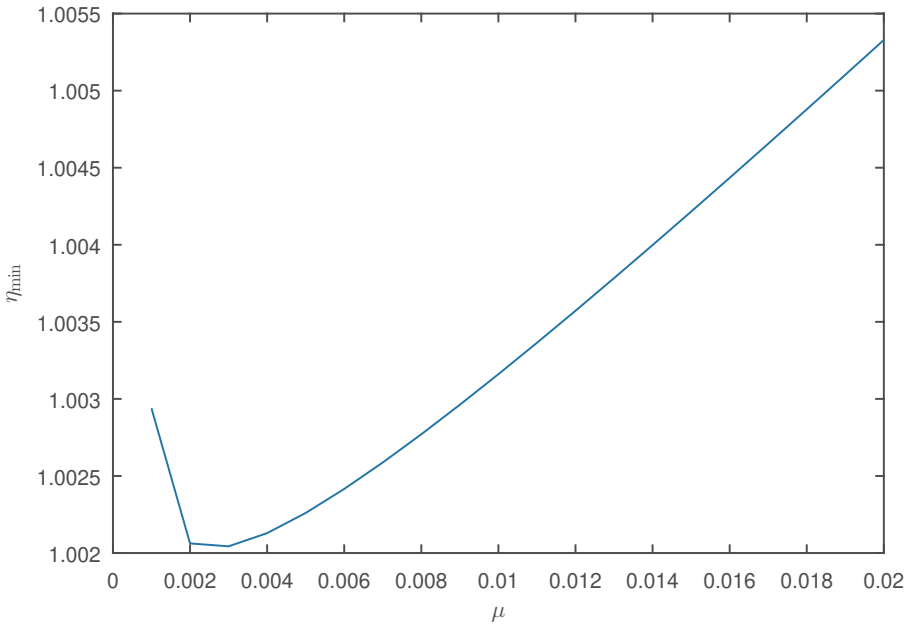

Figure 2.3: The curve of $\eta_{\min}$ with respect to the coefficient μ on the domain $(0, 0.02]$.

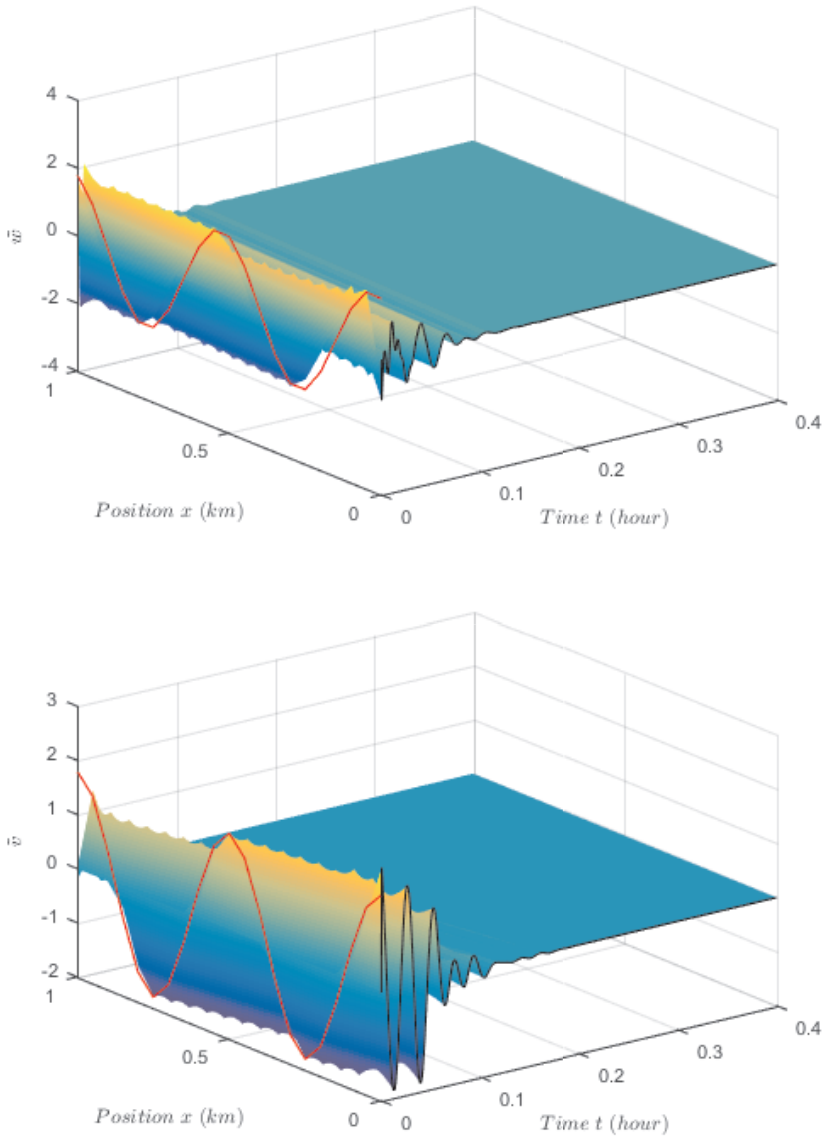

Figure 2.4: Evolutions of state variables of the linearized ARZ traffic system $(\widetilde{\omega}^h, \widetilde{v}^h)^\top$ in (2.18) with respect to spatial variable x and time variable t.

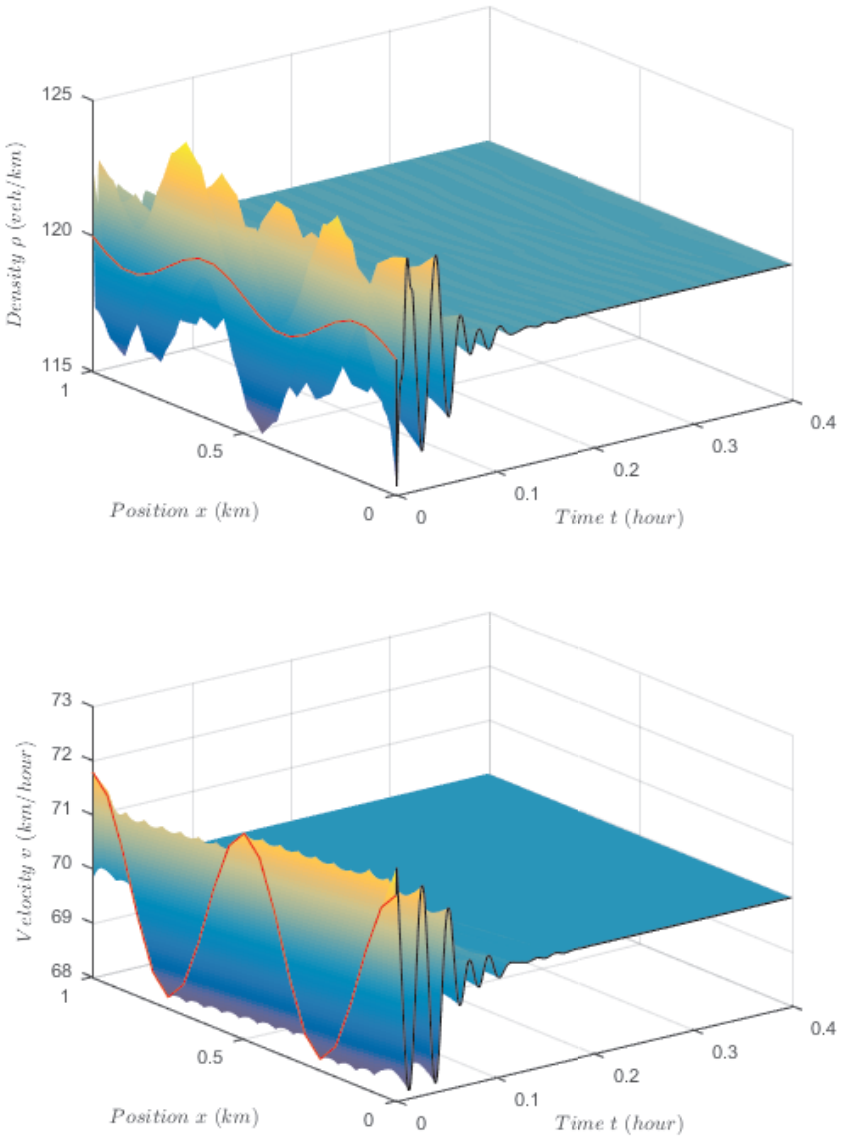

Figure 2.5: Evolutions of state variables of nonlinear ARZ system $(\rho, v)^\top$ in (2.1)-(2.2) with respect to spatial variable x and time variable t.

Chapter 3

Observer-based output feedback control of homogeneous linearized traffic with bottleneck

Contents

This chapter designs an optimal tuning observer-based output feedback control for traffic breakdown to alleviate the congested traffic using the backstepping method and optimization. The linearized Aw-Rascle-Zhang model is used to represent the congested traffic dynamics resulting from traffic breakdown. Based on the factors leading to traffic breakdown, we take into account the boundary conditions consisting of a boundary with a constant density and a speed drop at the upstream inlet of a bottleneck, and a boundary with a disturbance of inflow (high traffic demand) at the inlet of the road segment under consideration. To alleviate the congested traffic, a dynamic feedback controller is designed at the upstream boundary. By using the backstepping approach, an observer-based output feedback controller is computed to guarantee the integral input-to-state stability of the closed-loop system. By establishing an optimization problem and solving it, the optimal value of the considered class controller is obtained. The performance of the output feedback controller is also validated by numerical simulations.

This chapter has been published in [GZP21b].

3.1 Traffic flow system and control problem

3.1.1 Coordinate transformation and linearization around equilibrium

In this section, we perform a change of variables and linearize the model (2.7)-(2.8) around the nonuniform equilibrium. Define the coordinate transformation

$$\epsilon_1 = \psi_1(x)\widetilde{\omega}^h, \tag{3.1}$$
$$\epsilon_2 = \psi_2(x)\widetilde{v}^h, \tag{3.2}$$

with

$$\psi_1(x) = \exp\left(\int_0^x \frac{1}{\tau v^*(s)}\,\mathrm{d}s\right),$$
$$\psi_2(x) = \exp\left(\int_0^x v^{*\prime}(s)\cdot\frac{2}{2v^*(s)-\omega^*(s)}\,\mathrm{d}s\right),$$

for all x in $(0, L)$, then the system (2.7)-(2.8) is rewritten as follows, for all $x \in [0, L]$, $t \in [0, \infty)$,

$$\partial_t\epsilon_1(x,t) + \Lambda_1^h(\epsilon_1,\epsilon_2,x)\partial_x\epsilon_1(x,t) + c_1(x)\epsilon_2(x,t) - \frac{\psi_2^{-1}(x)}{\tau v^*(x)}\epsilon_1(x,t)\epsilon_2(x,t) = 0, \tag{3.3}$$
$$\begin{aligned}\partial_t\epsilon_2(x,t) + \Lambda_2^h(\epsilon_1,\epsilon_2,x)\partial_x\epsilon_2(x,t) + c_2(x)\epsilon_1(x,t)\\ + v^{*\prime}(x)\cdot\frac{2\epsilon_2(x,t)}{2v^*(x)-\omega^*(x)}\left(2\psi_2^{-1}(x)\epsilon_2(x,t) - \psi_1^{-1}(x)\epsilon_1(x,t)\right) = 0,\end{aligned} \tag{3.4}$$

with

$$\begin{aligned}&\Lambda_1^h(\epsilon_1,\epsilon_2,x) = \psi_2^{-1}(x)\epsilon_2 + v^*(x),\\ &\Lambda_2^h(\epsilon_1,\epsilon_2,x) = 2\psi_2^{-1}(x)\epsilon_2 - \psi_1^{-1}(x)\epsilon_1 + 2v^*(x) - \omega^*(x),\\ &c_1(x) = \omega^{*\prime}(x)\psi_1(x)\psi_2^{-1}(x),\\ &c_2(x) = \left(\frac{1}{\tau} - v^{*\prime}(x)\right)\psi_1^{-1}(x)\psi_2(x).\end{aligned}$$

From the linearization of the quasi-linear equation (3.3)-(3.4), we can derive, for all $x \in [0, L]$, $t \in [0, \infty)$,

$$\partial_t\epsilon_1(x,t) + \lambda_1^h(x)\partial_x\epsilon_1(x,t) + c_1(x)\epsilon_2(x,t) = 0, \tag{3.5}$$
$$\partial_t\epsilon_2(x,t) - \lambda_2^h(x)\partial_x\epsilon_2(x,t) + c_2(x)\epsilon_1(x,t) = 0, \tag{3.6}$$

with $\lambda_1^h = v^* > 0$, $\lambda_2^h = \omega^* - 2v^* > 0$.

3.1.2 Problem statement

As described in [MAC12], beyond the deterministic factors causing traffic breakdown, high traffic demand is the most effective ingredient. The disturbances caused by bottlenecks or individual drivers can not grow and propagate on account of unconditional stability if the traffic load is low enough. However, in spite of the absolute stability, traffic breakdown will take place with inflow in excess of the capacity of bottlenecks on the considered road segment. The local capacity reduction is the decisive attribute in characterizing the obstructing effect of a bottleneck. Furthermore, we

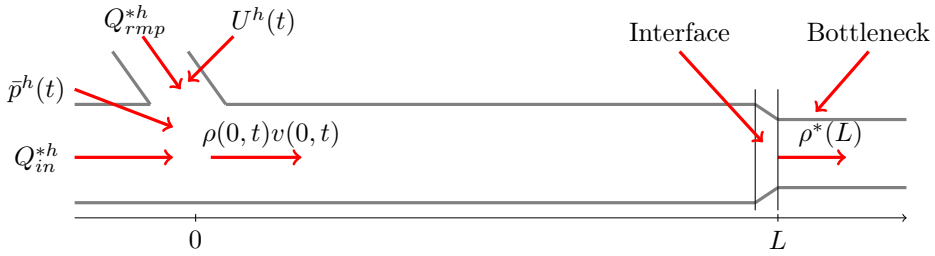

Figure 3.1: Traffic flow on a road segment with an downstream on-ramp bottleneck.

can not predict the time and location of individual traffic breakdown due to the stochastic and single-vehicle nature of disturbances caused by individual drivers.

In order to increase the efficiency and stability of traffic flow, we solve the control problem (in an optimal way that is introduced late precisely) of high traffic demand by ramp metering in the presence of a bottleneck and disturbances on the road. Considering a road segment with a constant density at the inlet of the bottleneck, the diagram of the control model is illustrated in Figure 3.1. To be more specific, the boundary condition at $x = L$ is, for all $t \geq 0$,

$$\rho(L,t) = \rho^*(L). \tag{3.7}$$

As described in [PG06], the interface at the bottleneck plays a key role in the analysis of the boundary condition at the inlet of a bottleneck. It is a buffer zone for velocity drop (the velocity in the interface is continuously decreasing from the left boundary of interface to $x = L$). The value of the velocity limit $v(L,\cdot)$ is derived from the constant density $\rho^*(L)$ and the measurement of the flux $q(L,\cdot)$ at the inlet of a bottleneck.

We want to maximize going through traffic at the inlet as in [PG06], so on the basis of the conservation of vehicle flows, the boundary condition with disturbances caused by high traffic demand at the upstream inlet $x = 0$ can be derived, for all $t \in [0,\infty)$,

$$Q^{*h}_{in} + Q^{*h}_{rmp} + U^h(t) + \bar{p}^h(t) = \rho(0,t)v(0,t) \leq Q^h_{max}, \tag{3.8}$$

where Q^{*h}_{rmp}, Q^{*h}_{in} and $\bar{p}^h$ are same as in Chapter 2, and the control is defined as $U^h(t)$ and would depend only on t. The total inflow at the inlet consisting of the total inflow at the ramp $0 \leq Q^{*h}_{rmp} + U^h(t) \leq Q^{max}_{1h}$ (Q^{max}_{1h} is the flux limit of the incoming road) and the total inflow at the inlet $0 \leq Q^{*h}_{in} + \bar{p}^h(t) \leq Q^{max}_{2h}$ (Q^{max}_{2h} is the flux limit on the on-ramp) is limited to Q^h_{max}, and the referenced inflow satisfies $Q^{*h}_{in} + Q^{*h}_{rmp} = \rho^*(0)v^*(0)$. Because of the capping strategy in [MAC12] for ramp metering, if the total flow $Q^{*h}_{in} + Q^{*h}_{rmp} + U^h(t) + \bar{p}^h(t)$ exceeds the flow limit Q^h_{max}, it is capped to this value Q^h_{max} by the access traffic light, so a queue of n_h waiting vehicles forms at the on-ramp. As long as $0 < n_h \leq n^h_{max}$ (n^h_{max} is the limit number of vehicles at the on-ramp), the ramp metering is active restricting the ramp flow to $Q^{*h}_{rmp} + U^h(t) = \max(0, Q^h_{max} - (Q^{*h}_{in} + \bar{p}^h(t)))$. The speed at the inlet $v(0,\cdot)$ and the density at the inlet $\rho(0,\cdot)$ satisfy $0 < v(0,\cdot) \leq v_f$ and $0 < \rho(0,\cdot) \leq \rho_m$. The difference between the measured speed at the inlet $v(0,t)$ and the corresponding equilibrium $v^*(0) \geq 0$ acts as the model output, i.e., for all $t \in [0,\infty)$,

$$y^h(t) = v(0,t) - v^*(0), \tag{3.9}$$

and the control law U^h is implemented by the on-ramp metering at the upstream boundary of the main road. Ramp metering temporarily reduces the traffic throughput and delays to increase it to prevent a traffic breakdown and the associated capacity drop. We compute the optimal gains of controller U^h depending on the output y^h only, so that the system states converge to the

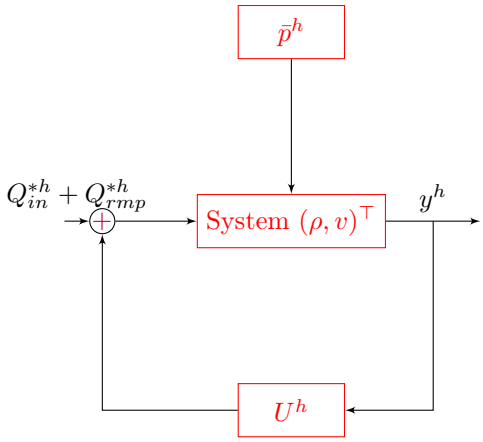

Figure 3.2: Block diagram of closed-loop control system

equilibrium at the fastest speed, up to a constant depending on the size of the disturbance $\bar{p}^h$. See the block diagram of the closed-loop control system in Figure 3.2.

Therefore, from (3.7) and (3.1)-(3.2), the boundary condition at $x = L$ may be achieved as, for all $t \geq 0$,

$$\epsilon_2(L,t) = \frac{1}{\kappa}\epsilon_1(L,t), \tag{3.10}$$

with $\kappa = \psi_1(L)\psi_2^{-1}(L)$. The following linearized boundary condition at $x = 0$ is derived from (3.8), for all $t \in [0,\infty)$,

$$\epsilon_1(0,t) = q_1\epsilon_2(0,t) + q_2\left(U^h(t) + \bar{p}^h(t)\right), \tag{3.11}$$

with $q_1 = \frac{2v^*(0)-\omega^*(0)}{v^*(0)}$, $q_2 = \frac{v_f}{\rho_m v^*(0)}$.

We reformulate the previous control problem as follows. We seek the optimal parameters of an observer-based output feedback control law upstream of a considerate road section in order to remove or weaken the effect of high traffic demand and stabilize the linearized ARZ traffic flow model. Inspired by [VKC11], [Cor+13], but using different backstepping transformations due to different boundary conditions, we can design a new observer-based output feedback control law. Firstly, we derive a full-state feedback control law with kernels from the backstepping transformation mapping the original system to an integral Input-to-State Stable (iISS) target system. Roughly speaking, a system is said to be iISS if there is an estimation of the impact of the integral of the input (in our case, the disturbance $\bar{p}^h$) to the state, and to prove that this input-to-state map is stable. An observer is designed to observe the states of the linearized ARZ traffic flow system. The precise observation to the states of the original system is guaranteed by the analytic expressions of injection gains which are obtained by the backstepping transformation mapping the error system (derived by subtracting the state-observer system from the original system) to the same target system. Finally, the optimal parameters of the observer-based output feedback controller are derived by solving the optimization problem with the objective function, defined as the highest rate of exponential convergence.

3.2 Full-state feedback controller

The main results of this chapter are the iISS of a target system with PI boundary conditions and the design of a full-state feedback controller through backstepping transformation.

3.2.1 Target system

Firstly, we introduce a target system, for all $x \in [0, L]$, $t \in [0, \infty)$,

$$\partial_t \alpha(x,t) + \lambda_1^h(x)\partial_x \alpha(x,t) = 0, \tag{3.12}$$

$$\partial_t \beta(x,t) - \lambda_2^h(x)\partial_x \beta(x,t) = 0, \tag{3.13}$$

$$\alpha(0,t) = q_1 \beta(0,t) + k_i^h \eta(t), \tag{3.14}$$

$$\beta(L,t) = \frac{1}{\kappa}\alpha(L,t), \tag{3.15}$$

where $k_i^h \in \mathbb{R} \setminus \{0\}$ is an integral tuning parameter, and

$$\eta(t) = \int_0^t (\beta(0,s) - \alpha(0,s))\, \mathrm{d}s + \frac{1}{k_i^h} q_2 \bar{p}^h(t). \tag{3.16}$$

According to the following theorem, the target system (3.12)-(3.16) is integral input-to-state stable for L^2-norm.

Theorem 3.1
Assume there exist positive constants μ, θ, p_1, p_2, p_4, q_3, q_4 and constant p_3 such that for all x in $[0, L]$,

$$M_1 = \begin{bmatrix} M_1^{11} & M_1^{12} & M_1^{13} \\ * & M_1^{22} & M_1^{23} \\ * & * & M_1^{33} \end{bmatrix} \geq 0 \tag{3.17}$$

with

$$\begin{aligned}
M_1^{11} &= p_1 e^{-\mu L} - \frac{p_2}{\kappa^2} e^{\mu L}, \\
M_1^{12} &= 0, \\
M_1^{13} &= -\frac{p_3}{2\kappa} e^{\frac{\mu}{2}L}, \\
M_1^{22} &= -p_1 q_1^2 + p_2 - \frac{3q_4 L}{2}|p_3|(1-q_1)^2, \\
M_1^{23} &= -p_1 q_1 k_i^h + \frac{p_3}{2} - \frac{1}{2} p_4 L(1-q_1), \\
M_1^{33} &= -p_1 k_i^h k_i^h - \frac{3q_4 L}{2}|p_3| k_i^h k_i^h + (1-m)L\left(p_4 k_i^h - \frac{q_3}{2}\left|\frac{1}{k_i^h}\right| q_2 p_4\right),
\end{aligned}$$

$$\begin{bmatrix} \frac{p_2}{\lambda_2^h(x)} & \frac{p_3}{2\lambda_2^h(x)} \\ \frac{p_3}{2\lambda_2^h(x)} & \frac{p_4}{2} \end{bmatrix} > 0, \tag{3.18}$$

$$m\left(k_i^h - \frac{q_3}{2}\left|\frac{1}{k_i^h}\right| q_2\right) > \frac{\theta}{2}, \tag{3.19}$$

$$\mu > \frac{\theta}{\lambda_1^h(x)}, \tag{3.20}$$

and

$$\begin{bmatrix} \mu p_2 - \frac{|p_3|}{2q_4\lambda_2^h(x)^2} - \frac{\theta p_2}{\lambda_2^h(x)} & \frac{\mu p_3}{4} - \frac{\theta p_3}{2\lambda_2^h(x)} \\ \frac{\mu p_3}{4} - \frac{\theta p_3}{2\lambda_2^h(x)} & m\left(p_4 k_i^h - \frac{q_3}{2}\left|\frac{1}{k_i^h}\right| q_2 p_4\right) - \frac{\theta p_4}{2} \end{bmatrix} > 0. \tag{3.21}$$

Then there exists positive constants Ω_1, b_1 such that, for any $z_0 = (\alpha(\cdot,0), \beta(\cdot,0), \eta(0))^\top$ in $L^2((0,L);\mathbb{R}^3)$, and for any $\bar{p}^h$ such that $\dot{\bar{p}}^h \in C^0[0,\infty)$, the solution $z = (\alpha, \beta, \eta)^\top$ to the system (3.12)-(3.16) satisfies, for all $t \geq 0$,

$$\|z(\cdot,t)\|_{L^2}^2 \leq \Omega_1 e^{-\theta t}\|z_0\|_{L^2}^2 + b_1 \int_0^t \dot{\bar{p}}^2(s)\,\mathrm{d}s. \tag{3.22}$$

Remark 3.1
Some observations follow

- *From the inequality condition (3.19) in Theorem 3.1, it follows that the parameters m and k_i^h have the identical sign, i.e., $mk_i^h > 0$.*
- *Note that the first term at the right-hand side of inequality (3.22) is continuous, decreasing with respect to t and converging to zero as t goes to infinity. Since $b_1 > 0$, the second term is increasing and tends to the L^2 norm of $\dot{\bar{p}}^h$. That is, the integral input-to-state stability of system (3.12)-(3.16) holds, by following the terminology of [DEY00] and [MI15b].*

Proof. The following candidate Lyapunov function is proposed for the purpose of analyzing the stability of the homogeneous system (3.12)-(3.16),

$$W^h = \int_0^L \begin{bmatrix} \alpha(x,\cdot) \\ \beta(x,\cdot) \\ \eta(\cdot) \end{bmatrix}^\top P(x) \begin{bmatrix} \alpha(x,\cdot) \\ \beta(x,\cdot) \\ \eta(\cdot) \end{bmatrix} \mathrm{d}x = W_1^h + W_2^h + W_3^h + W_4^h, \tag{3.23}$$

with

$$P(x) = \begin{bmatrix} \frac{p_1}{\lambda_1^h(x)}e^{-\mu x} & 0 & 0 \\ * & \frac{p_2}{\lambda_2^h(x)}e^{\mu x} & \frac{p_3}{2\lambda_2^h(x)}e^{\frac{\mu x}{2}} \\ * & * & \frac{p_4}{2} \end{bmatrix}, \quad \text{for all } x \in [0,L],$$

where

$$W_1^h = p_1 \int_0^L \frac{e^{-\mu x}}{\lambda_1^h(x)}\alpha^2(x,\cdot)\,\mathrm{d}x, \tag{3.24}$$

$$W_2^h = p_2 \int_0^L \frac{e^{\mu x}}{\lambda_2^h(x)}\beta^2(x,\cdot)\,\mathrm{d}x, \tag{3.25}$$

$$W_3^h = p_3\eta(\cdot) \int_0^L \frac{e^{\frac{\mu x}{2}}}{\lambda_2^h(x)}\beta(x,\cdot)\,\mathrm{d}x, \tag{3.26}$$

$$W_4^h = \frac{p_4 L}{2}\eta^2(\cdot). \tag{3.27}$$

Taking account of inequality (3.18) with $p_1 > 0, \lambda_1^h(x) > 0$, for all $x \in [0,L]$, the following inequality holds for all x in $[0,L]$,

$$\begin{bmatrix} \frac{p_1}{\lambda_1^h(x)}e^{-\mu x} & 0 \\ * & \left(\frac{p_2}{\lambda_2^h(x)} - \frac{p_3^2 p_4^{-1}}{2\lambda_2^h(x)^2}\right)e^{\mu x} \end{bmatrix} > 0. \tag{3.28}$$

Using Schur complement with $p_4 > 0$, $P(x)$ is symmetric positive definite for all x in $[0, L]$. Therefore,

$$\begin{aligned}
&\lambda_{\min} \cdot \left(\int_0^L \left(\alpha^2(x,\cdot) + \beta^2(x,\cdot) \right) \mathrm{d}x + L\eta^2(\cdot) \right) \\
&\leq W^h \\
&\leq \lambda_{\max} \cdot \left(\int_0^L \left(\alpha^2(x,\cdot) + \beta^2(x,\cdot) \right) \mathrm{d}x + L\eta^2(\cdot) \right),
\end{aligned} \tag{3.29}$$

where $\lambda_{\min} = \min_{x\in[0,L]} \lambda(P(x)), \lambda_{\max} = \max_{x\in[0,L]} \lambda(P(x))$. In the previous equation, $\lambda(P(x))$ is the eigenvalue of $P(x)$ and $\lambda_{\min} > 0, \lambda_{\max} > 0$. From (3.16), one can derive, for all $t \in [0, \infty)$, $\dot{\eta}(t) = \beta(0,t) - \alpha(0,t) + \frac{1}{k_i^h} q_2 \dot{d}(t)$. The time derivatives of (3.24)-(3.27) along the solutions to the system (3.12)-(3.16) are computed using integration by parts in (3.24)-(3.26), Young's inequality in (3.26), for all $t \geq 0$,

$$\begin{aligned}
\dot{W}_1^h &= 2p_1 \int_0^L \frac{e^{-\mu x}}{\lambda_1^h(x)} \alpha(x,t) \partial_t \alpha(x,t) \, \mathrm{d}x \\
&= -p_1 \alpha^2(x,t) e^{-\mu x} \big|_0^L - \mu p_1 \int_0^L \alpha^2(x,t) e^{-\mu x} \, \mathrm{d}x \\
&= p_1 \left(q_1 \beta(0,t) + k_i^h \eta(t) \right)^2 - p_1 e^{-\mu L} \alpha^2(L,t) - \mu p_1 \int_0^L \alpha^2(x,t) e^{-\mu x} \, \mathrm{d}x,
\end{aligned} \tag{3.30}$$

$$\begin{aligned}
\dot{W}_2^h &= 2p_2 \int_0^L \frac{e^{\mu x}}{\lambda_2^h(x)} \beta(x,t) \partial_t \beta(x,t) \, \mathrm{d}x \\
&= p_2 \beta^2(x,t) e^{\mu x} \big|_0^L - \mu p_2 \int_0^L \beta^2(x,t) e^{\mu x} \, \mathrm{d}x \\
&= \frac{p_2}{\kappa^2} e^{\mu L} \alpha^2(L,t) - p_2 \beta^2(0,t) - \mu p_2 \int_0^L \beta^2(x,t) e^{\mu x} \, \mathrm{d}x,
\end{aligned} \tag{3.31}$$

$$\begin{aligned}
\dot{W}_3^h &= p_3 \dot{\eta}(t) \int_0^L \frac{e^{\frac{\mu x}{2}}}{\lambda_2^h(x)} \beta(x,t) \, \mathrm{d}x + p_3 \eta(t) \int_0^L \frac{e^{\frac{\mu x}{2}}}{\lambda_2^h(x)} \partial_t \beta(x,t) \, \mathrm{d}x \\
&= p_3 \left(\beta(0,t) - \alpha(0,t) + \frac{1}{k_i^h} q_2 \dot{\bar{p}}^h(t) \right) \int_0^L \frac{e^{\frac{\mu x}{2}}}{\lambda_2^h(x)} \beta(x,t) \, \mathrm{d}x + p_3 \eta(t) \beta(x,t) e^{\frac{\mu x}{2}} \Big|_0^L \\
&\quad - \frac{\mu}{2} p_3 \eta(t) \int_0^L \beta(x,t) e^{\frac{\mu x}{2}} \, \mathrm{d}x \\
&\leq \frac{q_4 L}{2} |p_3| \left((1-q_1)\beta(0,t) - k_i^h \eta(t) + \frac{1}{k_i^h} q_2 \dot{\bar{p}}^h(t) \right)^2 + \frac{1}{2q_4} |p_3| \int_0^L \frac{e^{\mu x}}{\lambda_2^h(x)^2} \beta^2(x,t) \, \mathrm{d}x \\
&\quad + p_3 \frac{e^{\frac{\mu L}{2}}}{\kappa} \eta(t) \alpha(L,t) - p_3 \eta(t) \beta(0,t) - \frac{\mu}{2} p_3 \eta(t) \int_0^L \beta(x,t) e^{\frac{\mu x}{2}} \, \mathrm{d}x, \\
&\leq \frac{3q_4 L}{2} |p_3| \left((1-q_1)^2 \beta^2(0,t) + k_i^h k_i^h \eta^2(t) + \frac{1}{k_i^h k_i^h} q_2^2 \dot{\bar{p}}^{h2}(t) \right) + \frac{1}{2q_4} |p_3| \int_0^L \frac{e^{\mu x}}{\lambda_2^h(x)^2} \beta^2(x,t) \, \mathrm{d}x \\
&\quad + p_3 \frac{e^{\frac{\mu L}{2}}}{\kappa} \eta(t) \alpha(L,t) - p_3 \eta(t) \beta(0,t) - \frac{\mu}{2} p_3 \eta(t) \int_0^L \beta(x,t) e^{\frac{\mu x}{2}} \, \mathrm{d}x,
\end{aligned} \tag{3.32}$$

$$\begin{aligned}
\dot{W}_4^h &= (1-q_1) p_4 L \eta(t) \beta(0,t) - k_i^h p_4 L \eta^2(t) + \frac{1}{k_i^h} q_2 p_4 L \eta(t) \dot{\bar{p}}^h(t) \\
&\leq (1-q_1) p_4 L \eta(t) \beta(0,t) - k_i^h p_4 L \eta^2(t) + \frac{q_3}{2} \left| \frac{1}{k_i^h} \right| q_2 p_4 L \eta^2(t) + \frac{1}{2q_3} \left| \frac{1}{k_i^h} \right| q_2 p_4 L \dot{\bar{p}}^{h2}(t).
\end{aligned} \tag{3.33}$$

Using (3.30)-(3.33), for all $t \geq 0$,

$$\dot{W}^h \leq -\theta W^h - \begin{bmatrix} \alpha(L,\cdot) \\ \beta(0,\cdot) \\ \eta(\cdot) \end{bmatrix}^\top M_1 \begin{bmatrix} \alpha(L,\cdot) \\ \beta(0,\cdot) \\ \eta(\cdot) \end{bmatrix} - \int_0^L \begin{bmatrix} \alpha(x,\cdot) \\ \beta(x,\cdot) \\ \eta(\cdot) \end{bmatrix}^\top M^{(1)}(x) \begin{bmatrix} \alpha(x,\cdot) \\ \beta(x,\cdot) \\ \eta(\cdot) \end{bmatrix} \mathrm{d}x + \left(\frac{3q_4 L}{2} |p_3| k_i^{(2)-2} q_2^2 + \frac{1}{2q_3} \left| \frac{1}{k_i^h} \right| q_2 p_4 L \right) \dot{\bar{p}}^{h2}(\cdot), \tag{3.34}$$

where M_1 is given by (3.17) and for all $x \in [0, L]$,

$$M^{(1)}(x) = \begin{bmatrix} A(x) & B^\top(x) \\ B(x) & C \end{bmatrix}, \tag{3.35}$$

with

$$A(x) = \begin{bmatrix} \left(\mu p_1 - \frac{\theta p_1}{\lambda_1^h(x)} \right) e^{-\mu x} & 0 \\ 0 & \left(\mu p_2 - \frac{|p_3|}{2q_4 \lambda_2^h(x)^2} - \frac{\theta p_2}{\lambda_2^h(x)} \right) e^{\mu x} \end{bmatrix},$$

$$B(x) = \begin{bmatrix} 0 & \left(\frac{\mu p_3}{4} - \frac{\theta p_3}{2\lambda_2^h(x)} \right) e^{\frac{\mu x}{2}} \end{bmatrix},$$

$$C = m \left(p_4 k_i^h - \frac{q_3}{2} \left| \frac{1}{k_i^h} \right| q_2 p_4 \right) - \frac{\theta p_4}{2}.$$

Therefore, using the Schur complement of C in $M^{(1)}(x)$ and (3.19), for all x in $[0, L]$, $M^{(1)}(x) > 0$ holds if and only if

$$A(x) - B^\top(x) C^{-1} B(x) = \begin{bmatrix} M^{11}(x) & M^{12}(x) \\ * & M^{22}(x) \end{bmatrix} > 0 \tag{3.36}$$

with

$$\begin{aligned} M^{11}(x) &= \left(\mu - \frac{\theta}{\lambda_1^h(x)} \right) p_1 e^{-\mu x}, \\ M^{12}(x) &= 0, \\ M^{22}(x) &= \left(\mu p_2 - \frac{|p_3|}{2q_4 \lambda_2^h(x)^2} - \frac{\theta p_2}{\lambda_2^h(x)} \right) e^{\mu x} \\ &\quad - \left(m(p_4 k_i^h - \frac{q_3}{2} |\frac{1}{k_i^h}| q_2 p_4) - \frac{\theta p_4}{2} \right)^{-1} \left(\frac{\mu p_3}{4} - \frac{\theta p_3}{2\lambda_2^h(x)} \right)^2 e^{\mu x}. \end{aligned}$$

Inequality (3.36) holds if and only if the conditions (3.19)-(3.21) are satisfied. Thus using (3.17), if $M^{(1)}(x) > 0$, for all $x \in [0, L]$, holds,

$$\dot{W}^h \leq -\theta W^h + a_1 \dot{\bar{p}}^{h2}(\cdot), \tag{3.37}$$

with $a_1 = \frac{3q_4 L}{2} |p_3| k_i^{(2)-2} q_2^2 + \frac{1}{2q_3} |\frac{1}{k_i^h}| q_2 p_4 L > 0$, and thus along the solutions to the system (3.12)-(3.16), for all $t \in [0, \infty)$,

$$W^h \leq e^{-\theta t} W^h(z_0) + a_1 e^{-\theta t} \int_0^t \dot{\bar{p}}^{h2}(s) e^{\theta s} \, \mathrm{d}s \leq e^{-\theta t} W^h(z_0) + a_1 \int_0^t \dot{\bar{p}}^{h2}(s) \, \mathrm{d}s. \tag{3.38}$$

Combining this relation with (3.29), there exists positive constants $\Omega_1 \geq \frac{\lambda_{\max}}{\lambda_{min}}, b_1 \geq \frac{a_1}{\lambda_{\min}}$ such

that, for all $t \in [0, \infty)$,

$$\begin{aligned}
&\int_0^L \left(\alpha^2(x,t) + \beta^2(x,t)\right) \mathrm{d}x + L\eta^2(t) \\
&\leq \frac{1}{\lambda_{\min}} W^h \\
&\leq \frac{1}{\lambda_{\min}} \left(e^{-\theta t} W^h(z_0) + a_1 \int_0^t \dot{\bar{p}}^{h2}(s)\, \mathrm{d}s \right) \\
&\leq \frac{1}{\lambda_{\min}} \left(e^{-\theta t} \cdot \lambda_{\max} \cdot \left(\int_0^L \left(\alpha^2(x,0) + \beta^2(x,0)\right) \mathrm{d}x + L\eta^2(0) \right) + a_1 \int_0^t \dot{\bar{p}}^{h2}(s)\, \mathrm{d}s \right) \\
&\leq \Omega_1 e^{-\theta t} \left(\int_0^L \left(\alpha^2(x,0) + \beta^2(x,0)\right) \mathrm{d}x + L\eta^2(0) \right) + b_1 \int_0^t \dot{\bar{p}}^{h2}(s)\, \mathrm{d}s, \qquad (3.39)
\end{aligned}$$

completing the proof of Theorem 3.1. □

3.2.2 Backstepping transformation and control law

In this section, a backstepping transformation is introduced to map the original system (3.5)-(3.6) into the target system (3.12)-(3.16). Consequently, we obtain the kernels in the introduced transformation by the kernel equations and the control law stabilizing the original system (3.5)-(3.6) by the mathematical expression involving these kernels.

As in [Cor+13], consider the backstepping transformation, for all $x \in [0, L]$, $t \in [0, \infty)$,

$$\alpha(x,t) = \epsilon_1(x,t) - \int_x^L G^{11}(x,\xi)\epsilon_1(\xi,t)\, \mathrm{d}\xi - \int_x^L G^{12}(x,\xi)\epsilon_2(\xi,t)\, \mathrm{d}\xi, \qquad (3.40)$$

$$\beta(x,t) = \epsilon_2(x,t) - \int_x^L G^{21}(x,\xi)\epsilon_1(\xi,t)\, \mathrm{d}\xi - \int_x^L G^{22}(x,\xi)\epsilon_2(\xi,t)\, \mathrm{d}\xi, \qquad (3.41)$$

where $G^{11}(x,\xi), G^{12}(x,\xi), G^{21}(x,\xi)$ and $G^{22}(x,\xi)$ in $L^2((0,L)^2;\mathbb{R})$ are kernels in the triangular domain $\mathbb{T}_1 = \left\{(x,\xi) \in \mathbb{R}^2 | \, 0 \leq x \leq \xi \leq L\right\}$.

Take time derivative and spatial derivative on the backstepping transformation (3.40) and (3.41), and substitute them into the target system (3.12)-(3.16) to get the following equations and boundary conditions of the kernels G^{11}, G^{12}, G^{21} and G^{22} from the original system (3.5)-(3.6) in the triangular domain $\mathbb{T}_1$. The kernels G^{11}, G^{12}, G^{21} and G^{22} should satisfy the following kernel equations, for $(x,\xi) \in \mathbb{T}_1$,

$$\lambda_1^h(x)\partial_x G^{11}(x,\xi) + \lambda_1^h(\xi)\partial_\xi G^{11}(x,\xi) = -\lambda_1^{h\prime}(\xi) G^{11}(x,\xi) + c_2(\xi) G^{12}(x,\xi), \qquad (3.42)$$

$$\lambda_1^h(x)\partial_x G^{12}(x,\xi) - \lambda_2^h(\xi)\partial_\xi G^{12}(x,\xi) = \lambda_2^{h\prime}(\xi) G^{12}(x,\xi) + c_1(\xi) G^{11}(x,\xi), \qquad (3.43)$$

$$\lambda_2^h(x)\partial_x G^{21}(x,\xi) - \lambda_1^h(\xi)\partial_\xi G^{21}(x,\xi) = \lambda_1^{h\prime}(\xi) G^{21}(x,\xi) - c_2(\xi) G^{22}(x,\xi), \qquad (3.44)$$

$$\lambda_2^h(x)\partial_x G^{22}(x,\xi) + \lambda_2^h(\xi)\partial_\xi G^{22}(x,\xi) = -\lambda_2^{h\prime}(\xi) G^{22}(x,\xi) - c_1(\xi) G^{21}(x,\xi), \qquad (3.45)$$

and the boundary conditions

$$G^{11}(x,L) = \frac{\lambda_2^h(L)}{\kappa\lambda_1^h(L)} G^{12}(x,L), \tag{3.46}$$

$$G^{12}(x,x) = \frac{c_1(x)}{\lambda_1^h(x)+\lambda_2^h(x)}, \tag{3.47}$$

$$G^{21}(x,x) = -\frac{c_2(x)}{\lambda_1^h(x)+\lambda_2^h(x)}, \tag{3.48}$$

$$G^{22}(x,L) = \frac{\kappa\lambda_1^h(L)}{\lambda_2^h(L)} G^{21}(x,L). \tag{3.49}$$

The well-posedness of the kernel equations (3.42)-(3.49) and the boundedness of kernel variables follow from a coordinate change $(x,\xi) \mapsto (L-\xi, L-x)$ and an application of Theorem A.1 in [Cor+13] in the triangular domain $\mathbb{T}_2 = \left\{(L-\xi, L-x) \in \mathbb{R}^2 | \, 0 \le L-\xi \le L-x \le L\right\}$. Therefore, for system (3.5)-(3.6), the following control law can be deduced, for all $t \in [0,\infty)$,

$$\begin{aligned} U^h(t) = {} & \frac{k_i^h}{q_2}\int_0^t \left(\epsilon_2(0,s) - \epsilon_1(0,s)\right) \mathrm{d}s \\ & + \frac{k_i^h}{q_2}\int_0^t\int_0^L \Big(\left(G^{11}(0,\xi) - G^{21}(0,\xi)\right)\epsilon_1(\xi,s) + \left(G^{12}(0,\xi) - G^{22}(0,\xi)\right)\epsilon_2(\xi,s)\Big)\,\mathrm{d}\xi\,\mathrm{d}s \\ & + \frac{1}{q_2}\int_0^L \Big(\left(G^{11}(0,\xi) - q_1 G^{21}(0,\xi)\right)\epsilon_1(\xi,t) + \left(G^{12}(0,\xi) - q_1 G^{22}(0,\xi)\right)\epsilon_2(\xi,t)\Big)\,\mathrm{d}\xi. \end{aligned} \tag{3.50}$$

Under the assumptions in the Theorem 3.1, the target system (3.12)-(3.16) is integral input-to-state stable. Thus, using the invertibility of backstepping transformation, the original system (3.5)-(3.6) is iISS in the L^2-norm with the control law (3.50).

Obviously, from (3.50), the practical implementation of the feedback control law needs the knowledge of the full state $(\epsilon_1, \epsilon_2)^\top$ over the whole spatial domain $[0, L]$. From (3.9), the output under coordinate transformation is, for all $t \in [0,\infty)$,

$$y^h(t) = \epsilon_2(0,t). \tag{3.51}$$

In the next section, the knowledge of the full state $(\epsilon_1, \epsilon_2)^\top$ in the control law U^h can be provided by a boundary state observer that uses the output y^h in (3.51) with a boundary measurement of $v(0,\cdot)$ only. The kernels $G^{11}(0,\xi), G^{12}(0,\xi), G^{21}(0,\xi)$ and $G^{22}(0,\xi)$, $\xi \in (0,L)$ can be derived by solving the kernel equations (3.42)-(3.49). Through choosing an appropriate value of k_i^h, the iISS of original system (3.5)-(3.6) is guaranteed with the control law (3.50).

3.3 Observer design and output feedback controller

From (3.9), we note that the output y^h can be obtained by the measurement of inlet speed $v(0,\cdot)$ of the considered road segment. In order to observe the state $(\epsilon_1, \epsilon_2)^\top$, a boundary observer is designed as in [VKC11] by constructing the system with the output injection terms: for all

$x \in [0, L]$, $t \in [0, \infty)$,

$$\partial_t \hat{\epsilon}_1(x,t) + \lambda_1^h(x)\partial_x \hat{\epsilon}_1(x,t) + c_1(x)\hat{\epsilon}_2(x,t) = r(x)\left(y^h(t) - \hat{\epsilon}_2(0,t)\right), \tag{3.52}$$

$$\partial_t \hat{\epsilon}_2(x,t) - \lambda_2^h(x)\hat{\partial}_x \epsilon_2(x,t) + c_2(x)\hat{\epsilon}_1(x,t) = s(x)\left(y^h(t) - \hat{\epsilon}_2(0,t)\right), \tag{3.53}$$

$$\hat{\epsilon}_1(0,t) = q_1\hat{\epsilon}_2(0,t) - L_i\int_0^t \left(y^h(\tau) - \hat{\epsilon}_2(0,\tau)\right)\mathrm{d}\tau + q_2 U^h(t), \tag{3.54}$$

$$\hat{\epsilon}_2(L,t) = \frac{1}{\kappa}\hat{\epsilon}_1(L,t). \tag{3.55}$$

In the previous equations, $\hat{\epsilon}_1$ and $\hat{\epsilon}_2$ are the observation of the state variables ϵ_1 and ϵ_2, the terms r and s are the output injection gains, and $L_i \in \mathbb{R}\setminus\{0\}$ is an integral tuning parameter. To reject perturbation to guarantee the convergence of the observed state to the real state, an integral term is added to a boundary condition of the observer. We design the boundary conditions of the observer system (3.52)-(3.55) such that the mathematical expression of injection gains r and s are as simple as possible.

The objective is to use the backstepping transformation to find r and s such that $(\hat{\epsilon}_1, \hat{\epsilon}_2)^\top$ converges to $(\epsilon_1, \epsilon_2)^\top$. The error system can be obtained by subtracting the observer system (3.52)-(3.55) from the original system (3.5)-(3.6) and (3.10), (3.11), for all $x \in [0, L]$, $t \in [0, \infty)$,

$$\partial_t \widetilde{\epsilon}_1(x,t) + \lambda_1^h(x)\partial_x \widetilde{\epsilon}_1(x,t) + c_1(x)\widetilde{\epsilon}_2(x,t) = -r(x)\widetilde{\epsilon}_2(0,t), \tag{3.56}$$

$$\partial_t \widetilde{\epsilon}_2(x,t) - \lambda_2^h(x)\partial_x \widetilde{\epsilon}_2(x,t) + c_2(x)\widetilde{\epsilon}_1(x,t) = -s(x)\widetilde{\epsilon}_2(0,t), \tag{3.57}$$

$$\widetilde{\epsilon}_1(0,t) = q_1\widetilde{\epsilon}_2(0,t) + L_i\int_0^t \widetilde{\epsilon}_2(0,\tau)\,\mathrm{d}\tau + q_2\bar{p}^h(t), \tag{3.58}$$

$$\widetilde{\epsilon}_2(L,t) = \frac{1}{\kappa}\widetilde{\epsilon}_1(L,t), \tag{3.59}$$

where $\widetilde{\epsilon}_1(x,t) = \epsilon_1(x,t) - \hat{\epsilon}_1(x,t)$, and $\widetilde{\epsilon}_2(x,t) = \epsilon_2(x,t) - \hat{\epsilon}_2(x,t)$.

In order to guarantee the iISS of the error system (3.56)-(3.59), the target system (3.12)-(3.16) is mapped into the error system by using the backstepping transformation, for all $x \in [0, L]$, $t \in [0, \infty)$,

$$\widetilde{\epsilon}_1(x,t) = \alpha(x,t) + \int_0^x F^{11}(x,\xi)\alpha(\xi,t)\,\mathrm{d}\xi + \int_0^x F^{12}(x,\xi)\beta(\xi,t)\,\mathrm{d}\xi, \tag{3.60}$$

$$\widetilde{\epsilon}_2(x,t) = \beta(x,t) + \int_0^x F^{21}(x,\xi)\alpha(\xi,t)\,\mathrm{d}\xi + \int_0^x F^{22}(x,\xi)\beta(\xi,t)\,\mathrm{d}\xi, \tag{3.61}$$

where the functions $F^{ij}(x,\xi)$ in $L^2((0,L)^2;\mathbb{R})$, $i,j = 1,2$ have to be determined in the triangular domain $\mathbb{T} = \left\{(x,\xi) \in \mathbb{R}^2 \middle| \, 0 \le \xi \le x \le L\right\}$.

Differentiating the transformation (3.60) and (3.61) with respect to t and x, substituting the results into the error system (3.56)-(3.59) and using the equations of the target system (3.12)-(3.16), the following kernel equations and boundary conditions of the kernels F^{11}, F^{12}, F^{21} and F^{22} can be derived in the triangular domain $\mathbb{T}$, for $(x,\xi) \in \mathbb{T}$,

$$\lambda_1^h(x)\partial_x F^{11}(x,\xi) + \lambda_1^h(\xi)\partial_\xi F^{11}(x,\xi) = -\lambda_1^h(\xi)' F^{11}(x,\xi) - c_1(x)F^{21}(x,\xi), \tag{3.62}$$

$$\lambda_1^h(x)\partial_x F^{12}(x,\xi) - \lambda_2^h(\xi)\partial_\xi F^{12}(x,\xi) = \lambda_2^h(\xi)' F^{12}(x,\xi) - c_1(x)F^{22}(x,\xi), \tag{3.63}$$

$$\lambda_2^h(x)\partial_x F^{21}(x,\xi) - \lambda_1^h(\xi)\partial_\xi F^{21}(x,\xi) = \lambda_1^h(\xi)' F^{21}(x,\xi) + c_2(x)F^{11}(x,\xi), \tag{3.64}$$

$$\lambda_2^h(x)\partial_x F^{22}(x,\xi) + \lambda_2^h(\xi)\partial_\xi F^{22}(x,\xi) = -\lambda_2^h(\xi)' F^{22}(x,\xi) + c_2(x)F^{12}(x,\xi), \tag{3.65}$$

with the boundary conditions

$$F^{11}(L,\xi) = \kappa F^{21}(L,\xi), \tag{3.66}$$

$$F^{12}(x,x) = -\frac{c_1(x)}{\lambda_1^h(x)+\lambda_2^h(x)}, \tag{3.67}$$

$$F^{21}(x,x) = \frac{c_2(x)}{\lambda_1^h(x)+\lambda_2^h(x)}, \tag{3.68}$$

$$F^{22}(L,\xi) = \frac{1}{\kappa}F^{12}(L,\xi). \tag{3.69}$$

The injection gains are, for all x in $[0,L]$,

$$r(x) = \lambda_2^h(0)F^{12}(x,0) - \left(1-\frac{L_i}{k_i^h}\right)\lambda_1^h(0)F^{11}(x,0), \tag{3.70}$$

$$s(x) = \lambda_2^h(0)F^{22}(x,0) - \left(1-\frac{L_i}{k_i^h}\right)\lambda_1^h(0)F^{21}(x,0), \tag{3.71}$$

where the kernels $F^{11}(x,0), F^{12}(x,0), F^{21}(x,0)$ and $F^{22}(x,0)$ are the solutions to the kernel equations (3.62)-(3.69). The well-posedness of the solutions to kernel equations (3.62)-(3.69) is guaranteed by the Theorem A.1 in [Cor+13] in the triangular domain $\mathbb{T}_2$ following a coordinate change $(x,\xi)\mapsto(L-\xi,L-x)$.

Based on the reversibility of the backstepping transformation, it is straightforward to prove the iISS of the error system (3.56)-(3.59) in the L^2 sense through studying the stability of the target system (3.12)-(3.16). To be more specific the following result proves, under appropriate assumptions, that adding an exponentially decreasing function of the initial condition, and the integral of the disturbance $\bar{p}^h$ provides an overbound of the L^2-norm of the state. See (3.73) below. This is a way to describe the impact of the integral of the disturbance $\bar{p}^h$ on the state. To derive such result, let for all $t\in[0,\infty)$,

$$\widetilde{\eta}(t) = \int_0^t \widetilde{\epsilon}_2(0,\tau)\,\mathrm{d}\tau + L_i^{-1}q_2\bar{p}^h(t). \tag{3.72}$$

Theorem 3.2
Under the assumptions of Theorem 3.1, consider the system (3.56)-(3.59), and the functions r and s respectively determined by (3.70) and (3.71), where $F^{11}(x,0), F^{12}(x,0), F^{21}(x,0)$ and $F^{22}(x,0)$ ($x\in[0,L]$) are obtained from (3.62)-(3.69), the equilibrium $\widetilde{\epsilon}_1\equiv\widetilde{\epsilon}_2\equiv 0$ is iISS in the L^2 sense, that is there exists positive constants Ω_2, b_2 such that, for any $(\widetilde{\epsilon}_1(\cdot,0),\widetilde{\epsilon}_2(\cdot,0))^\top$ in $L^2((0,L);\mathbb{R}^2)$, and for any $\bar{p}^h$ such that $\dot{\bar{p}}^h\in L^2[0,\infty)$, the solution $(\widetilde{\epsilon}_1,\widetilde{\epsilon}_2,\widetilde{\eta})^\top$ to the system (3.56)-(3.59) and (3.72) satisfies

$$\begin{aligned}&\int_0^L \left(\widetilde{\epsilon}_1^2(x,t)+\widetilde{\epsilon}_2^2(x,t)\right)\,\mathrm{d}x + L\widetilde{\eta}^2(t)\\ &\le \Omega_2 e^{-\theta t}\left(\int_0^L \left(\widetilde{\epsilon}_1^2(x,0)+\widetilde{\epsilon}_2^2(x,0)\right)\,\mathrm{d}x + L\widetilde{\eta}^2(0)\right) + b_2\int_0^t \dot{\bar{p}}^{h2}(s)\,\mathrm{d}s,\end{aligned} \tag{3.73}$$

for all $t\ge 0$.

Since the transformation (3.60)-(3.61) is invertible, the dynamical behavior of (3.56)-(3.59) is the same as the behavior of the target system (3.12)-(3.16). Under the assumptions of Theorem 3.1, the target system (3.12)-(3.16) is integral input-to-state stable in the L^2 sense. Thus the iISS of (3.56)-(3.59) is obtained from the invertibility and linearity of the backstepping transformation, in other words, (3.73) holds.

Moreover, on the basis of Theorem 3.2, as time t goes on, without disturbance $\bar{p}^h$, the state components $\hat{\epsilon}_1$ and $\hat{\epsilon}_2$ of the solutions to the observer (3.52)-(3.55) go to the real values ϵ_1 and ϵ_2. Therefore, the following observer-based output feedback controller is proposed by combining the full state feedback law (3.50) with the observer (3.52)-(3.55), for all $t \in [0, \infty)$,

$$\begin{aligned} U^h(t) = & \frac{k_i^h}{q_2} \int_0^t \left(y^h(s) - \hat{\epsilon}_1(0,s) \right) \mathrm{d}s \\ & + \frac{k_i^h}{q_2} \int_0^t \int_0^L \Big(\left(G^{11}(0,\xi) - G^{21}(0,\xi) \right) \hat{\epsilon}_1(\xi,s) + \left(G^{12}(0,\xi) - G^{22}(0,\xi) \right) \hat{\epsilon}_2(\xi,s) \Big) \mathrm{d}\xi \, \mathrm{d}s \\ & + \frac{1}{q_2} \int_0^L \Big(\left(G^{11}(0,\xi) - q_1 G^{21}(0,\xi) \right) \hat{\epsilon}_1(\xi,t) + \left(G^{12}(0,\xi) - q_1 G^{22}(0,\xi) \right) \hat{\epsilon}_2(\xi,t) \Big) \mathrm{d}\xi, \end{aligned} \tag{3.74}$$

where $\hat{\epsilon}_1$ and $\hat{\epsilon}_2$ are computed from (3.52)-(3.55), the kernels $G^{11}(0,\xi), G^{12}(0,\xi), G^{21}(0,\xi)$ and $G^{22}(0,\xi)$, $\xi \in (0, L)$ are computed from the kernel equations (3.42)-(3.49).
Combining Theorem 3.1 and Theorem 3.2, the following result can be derived, when closing the loop with the output feedback controller (3.74). The separation principle is used to prove the iISS of this closed-loop system.

Theorem 3.3
Under the assumptions of Theorem 3.1, for any $(\epsilon_1(\cdot,0), \epsilon_2(\cdot,0), \widetilde{\epsilon}_1(\cdot,0), \widetilde{\epsilon}_2(\cdot,0))^\top$ *in* $L^2((0,L);\mathbb{R}^4)$ *in* $\mathbb{R}$*, the observer-based output feedback controller (3.74) makes the equilibrium of the system (3.5)-(3.6) and (3.10), (3.11) and the error system (3.56)-(3.59) iISS in the* L^2 *sense, that is there exists positive constants* Ω_3, b_3 *such that along the solution to (3.5)-(3.6), for any* $\bar{p}^h$ *such that* $\dot{\bar{p}}^h \in L^2[0,\infty)$*, it holds, for all* t *in* $[0,\infty)$*,*

$$\begin{aligned} & \int_0^L \left(\epsilon_1^2(x,t) + \epsilon_2^2(x,t) \right) \mathrm{d}x + L\eta^2(t) + \int_0^L \left(\widetilde{\epsilon}_1^2(x,t) + \widetilde{\epsilon}_2^2(x,t) \right) \mathrm{d}x + L\widetilde{\eta}^2(t) \\ & \leq \Omega_3 e^{-\theta t} \left(\int_0^L \left(\epsilon_1^2(x,0) + \epsilon_2^2(x,0) \right) \mathrm{d}x + L\eta^2(0) + \int_0^L \left(\widetilde{\epsilon}_1^2(x,0) + \widetilde{\epsilon}_2^2(x,0) \right) \mathrm{d}x + L\widetilde{\eta}^2(0) \right) \\ & \quad + b_3 \int_0^t \dot{\bar{p}}^{h2}(s) \, \mathrm{d}s. \end{aligned} \tag{3.75}$$

Proof. The following candidate Lyapunov function is proposed, for all $x \in [0, L]$, $t \in [0, \infty)$,

$$W = W_1 + W_2, \tag{3.76}$$

where

$$W_1 = \int_0^L \begin{bmatrix} \epsilon_1(x,t) \\ \epsilon_2(x,t) \\ \eta(t) \end{bmatrix}^\top P_1(x) \begin{bmatrix} \epsilon_1(x,t) \\ \epsilon_2(x,t) \\ \eta(t) \end{bmatrix} \mathrm{d}x, \tag{3.77}$$

$$W_2 = \int_0^L \begin{bmatrix} \widetilde{\epsilon}_1(x,t) \\ \widetilde{\epsilon}_2(x,t) \\ \widetilde{\eta}(t) \end{bmatrix}^\top P_2(x) \begin{bmatrix} \widetilde{\epsilon}_1(x,t) \\ \widetilde{\epsilon}_2(x,t) \\ \widetilde{\eta}(t) \end{bmatrix} \mathrm{d}x, \tag{3.78}$$

with

$$P_j(x) = \begin{bmatrix} \frac{p_{j1}}{\lambda_1^h(x)} e^{-\mu x} & 0 & 0 \\ * & \frac{p_{j2}}{\lambda_2^h(x)} e^{\mu x} & \frac{p_{j3}}{2\lambda_2^h(x)} e^{\frac{\mu x}{2}} \\ * & * & \frac{p_{j4}}{2} \end{bmatrix}, \quad j = 1, 2, \quad \text{for all } x \in (0, L).$$

From Theorem 3.1 and the invertibility and linearity of the backstepping transformation, for the system (3.5)-(3.6) and (3.10), (3.11), there exist positive constants $p_{11}, p_{12}, p_{14}, C, a_1, b$ and a constant p_{13} such that for all $t \in [0, \infty)$,

$$\dot{W}_1 \leq -\theta W_1 + a_1 \dot{\bar{p}}^{h2}, \tag{3.79}$$

and

$$\begin{aligned} &\int_0^L \left(\epsilon_1^2(x,t) + \epsilon_2^2(x,t)\right) \mathrm{d}x + L\eta^2(t) \\ &\leq Ce^{-\theta t}\left(\int_0^L \left(\epsilon_1^2(x,0) + \epsilon_2^2(x,0)\right) \mathrm{d}x + L\eta^2(0)\right) + b\int_0^t \dot{\bar{p}}^{h2}(s)\,\mathrm{d}s. \end{aligned} \tag{3.80}$$

From Theorem 3.2, the iISS of the error system (3.56)-(3.59) guarantees exact observation of the state ϵ_1 and ϵ_2 of the system (3.5)-(3.6) under the assumptions of Theorem 3.1, i.e., there exist positive constants $p_{21}, p_{22}, p_{24}, a_2$ and a constant p_{23} such that

$$\dot{W}_2 \leq -\theta W_2 + a_2 \dot{\bar{p}}^{h2}. \tag{3.81}$$

and (3.73) hold.

According to the separation principle, and the inequalities (3.79)-(3.81), the Lyapunov function W for the output feedback closed-loop system consisting of the original system (3.5)-(3.6) and (3.10), (3.11) and the error system (3.56)-(3.59) satisfies

$$\dot{W} = \dot{W}_1 + \dot{W}_2 \leq -\theta W + (a_1 + a_2)\dot{\bar{p}}^{h2}, \tag{3.82}$$

Then for $\Omega_3 \geq \max\{\Omega_2, C\}, b_3 = b + b_2$, one can derive the following result from (3.73) and (3.80), for all $t \in [0, \infty)$,

$$\begin{aligned} &\int_0^L \left(\epsilon_1^2(x,t) + \epsilon_2^2(x,t)\right) \mathrm{d}x + L\eta^2(t) + \int_0^L \left(\widetilde{\epsilon}_1^2(x,t) + \widetilde{\epsilon}_2^2(x,t)\right) \mathrm{d}x + L\widetilde{\eta}^2(t) \\ &\leq \Omega_3 e^{-\theta t}\left(\int_0^L \left(\epsilon_1^2(x,0) + \epsilon_2^2(x,0)\right) \mathrm{d}x + L\eta^2(0) + \int_0^L \left(\widetilde{\epsilon}_1^2(x,0) + \widetilde{\epsilon}_2^2(x,0)\right) \mathrm{d}x + L\widetilde{\eta}^2(0)\right) \\ &\quad + b_3 \int_0^t \dot{\bar{p}}^{h2}(s)\,\mathrm{d}s. \end{aligned} \tag{3.83}$$

Therefore, it is proved that with the control law (3.74), the equilibrium $\epsilon_1 \equiv \epsilon_2 \equiv 0$ of the system (3.5)-(3.6) and (3.10), (3.11) is iISS in the L^2 sense. □

3.4 Optimal tuning controller and numerical studies

3.4.1 Optimal tuning controller

In order to seek the optimal tuning control law U^h in (3.74), the following optimization problem for the maximal θ can be considered to derive the optimal value of k_i^h:

$$\begin{aligned} &\max\ \theta \\ &\text{subject to}\, \mu, \theta, p_1, p_2, p_4, q_3, q_4 > 0, \text{and (3.17)-(3.21) for all } x \in [0, L]. \end{aligned} \tag{3.84}$$

Checking the constraints above requires dealing with the matrix inequalities that are not directly numerically tackled due to the products between unknown parameters. The parameters k_i^h, μ, θ, m can be given through line search methods, and the other variables p_1, p_2, p_3, p_4 can be derived by solving LMIs. We discretize the spatial variable x on the domain $[0, L]$ to solve finite LMIs.

Remark 3.2
The parameters k_i^h, μ and θ have effects on the iISS of the target system (3.12)-(3.16) in terms of the matrix inequalities. The parameter k_i^h serves as the integral tuning parameter at the boundary $x = 0$ of the target system (3.12)-(3.16), and it is the key parameter to determine the iISS property in the L^2 sense. The positive constant μ is involved in the exponent or power of the exponential terms of the Lyapunov function that is proposed to analyze the stability of the target system (3.12)-(3.16). It has also an effect on the condition number of the matrix M_1 in (3.17). The parameter θ is the exponential rate of convergence of the target system (3.12)-(3.16), the error system (3.56)-(3.59) and the closed-loop system (3.5)-(3.6). The higher θ is, the faster the closed-loop system (3.5)-(3.6) converges. Selecting the fitting parameters k_i^h, μ, and θ is done by three independent line searches and three different loops.

3.4.2 Simulations

In order to illustrate the performance of the proposed controller (3.74) in stabilizing the system (3.5)-(3.6) around the equilibrium, numerical simulations are done in this section. Given $\bar{p}^h, \omega^*, v^*$, compute controller for the linearized system (3.5)-(3.6) and simulate the nonlinear model. For simulations, we illustrate by rush hour the traffic demand $\bar{p}^h$ serving as an exogenous variable for the traffic flow model that varies on time scales.

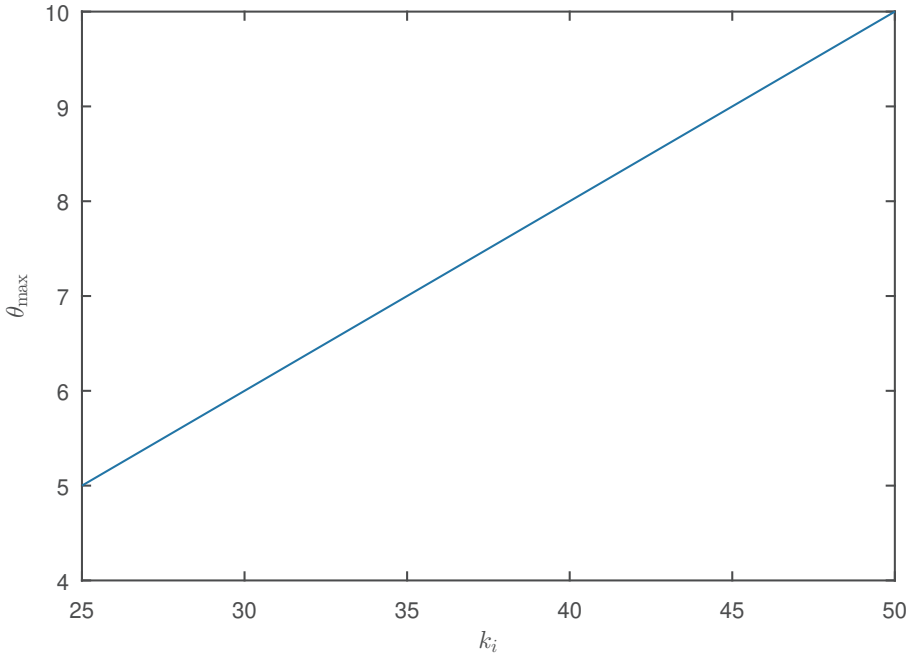

Figure 3.3: The curve of maximal θ with respect to the coefficient k_i^h on the domain $[25, 50]$.

For numerical simulations, the traffic parameters of a local road section under consideration are chosen as in [ZPQ19]: $L = 1\,\text{km}$, $v_f = 150\,\text{km/h}$, $\rho_m = 200\,\text{veh./km}$, $\tau = 60\,\text{s}$, $\bar{p}^h(t) = 420e^{-10t}\,\text{(veh./h)}$, $t \in [0, \infty)$. The update for each time step is computed in a two-stage Lax–Wendroff scheme (LeVeque, 1992). More details on applying the scheme to AR-type traffic models can be found in Yu, Gan, Bayen, and Krstic (2020). The equilibrium is chosen as $\rho^*(x) = 120 - 0.5x\,\text{(veh./km)}$, $v^*(x) = 70 - 0.5x\,\text{(km/h)}$, $x \in [0, L]$ which leads to the characteristic speeds $\lambda_1^h = 70 - 0.5x$, and $\lambda_2^h = 20 + 0.125x$, $x \in [0, L]$, then $q_1 = -0.2857$, $q_2 = 0.0107$, $q_3 = 1$,

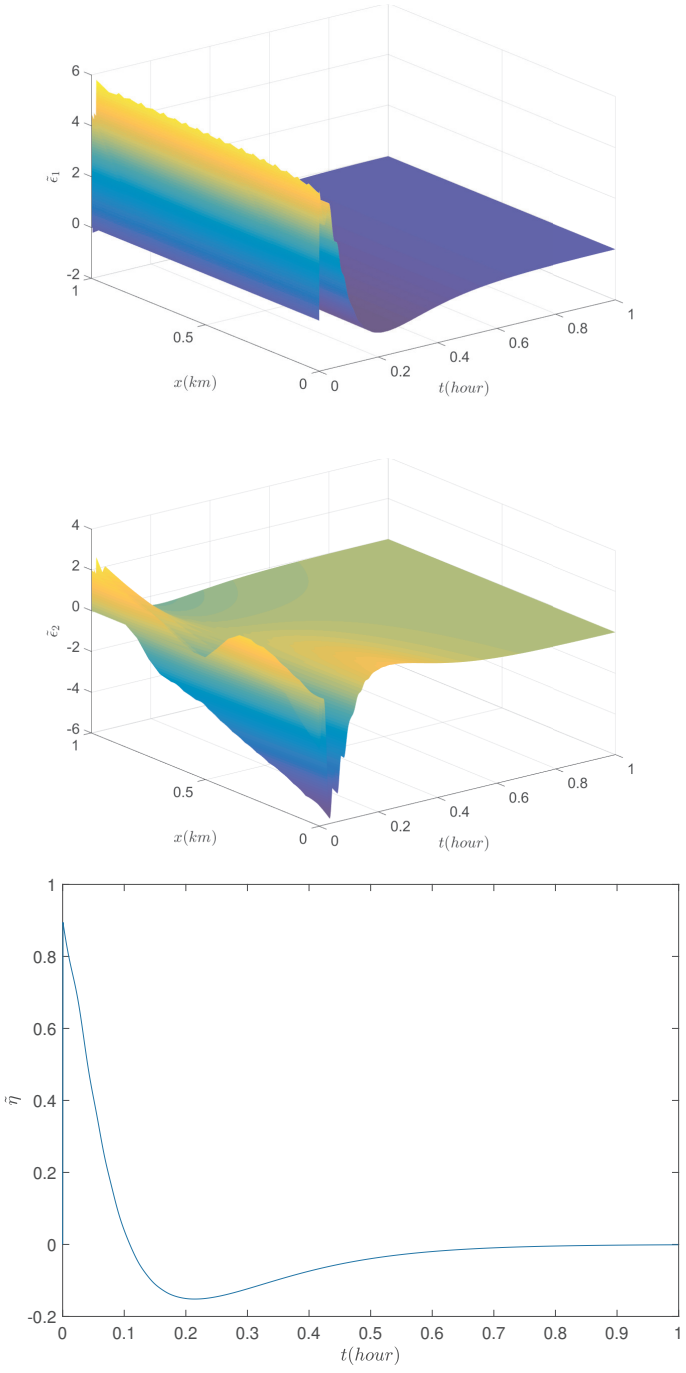

Figure 3.4: Evolutions of state variables of error system $(\widetilde{\epsilon}_1, \widetilde{\epsilon}_2, \widetilde{\eta})^\top$ in (3.56)-(3.59) with respect to spatial variable x and time variable t.

$q_4 = 1$, $\kappa = 2.2487$. The initial conditions are defined as, for all $x \in [0, L]$,

$$\rho(x, 0) = \rho^*(x) + 0.5 \sin 4\pi x,$$
$$v(x, 0) = v^*(x) + 1.8 \cos 4\pi x.$$

During solving the optimization problem (3.84), given k_i^h on the domain $[25, 50]$ with a step length

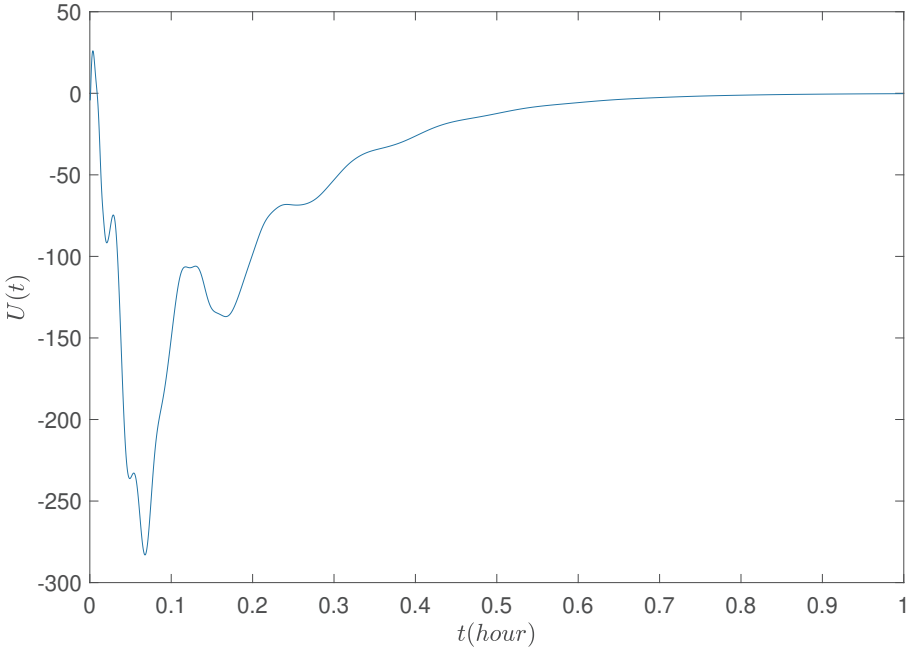

Figure 3.5: Observer-based output feedback controller $U^h(t)$.

1, we search the maximal value ($\theta_{\max}$) of θ satisfying (for all discrete quality of x with a step size $\frac{L}{20}$) the linear matrix inequalities (3.17)-(3.21) for each discrete quantity of k_i^h by using the "yalmip" programme on Matlab. The used function "optimize" which is common for solving optimization problems on Matlab consists of the chosen solver "sdpt3", the constraints (3.17)-(3.21), and the objective θ. We derive the curve of maximal θ with respect to the coefficient k_i^h on the domain $[25, 50]$ in Figure 3.3. It is checked in this figure that the larger k_i^h is, the larger is $\theta_{\max}$ given by (3.84). This figure can be used to compute the best performance, given an amplitude constraint on k_i^h. Choosing the control gain $k_i^h = 35$ in (3.50) and (3.74), $\mu = 0.6$, and $m = 0.1$, we get $\theta = 7, p_1 = 10.6524, p_2 = 15.966, p_3 = 0.0059, p_4 = 564.0186$, so that (3.17)-(3.21) hold. The integral tuning parameter is set $L_i = 5$ in (3.59), and using the method described and the code attached in Appendix F.2 of [AA19], the values of kernels $G^{11}, G^{12}, G^{21}, G^{22}$ are derived from numerical computation of the kernel equations (3.42)-(3.49) and the values of $F^{11}, F^{12}, F^{21}, F^{22}$ are obtained from the numerical computation of (3.62)-(3.69). Different from the previous research giving the explicit formula of backstepping transformations that can be used to deduce the explicit solutions of kernels, the numerical solutions of kernels in the general formation of backstepping transformations can be derived using [AA19].

The iISS of the error system (3.56)-(3.59) can be seen in Figure 3.4. The evolution of the output feedback controller U^h given by (3.74) is given in Figure 3.5. From Figure 3.5, we notice that the value of control input U^h could be negative and converge to zero because the physical control input $Q_{rmp}^{*h}+U^h$ locally stabilizes the system and is "close" to the equilibrium control input Q_{rmp}^{*h}. Thus the physical control input satisfies the positive constraint. In Figure 3.6, the state of the closed-loop system (2.1)-(2.2) with the output feedback control converges to zero equilibrium. This numerical result is consistent with Theorem 3.3. By comparing Figure 3.6 and Figure 3.7, it is obvious that the observer maintains the exponential convergence performance of the closed-loop system (2.1)-(2.2), and it is also capable of observing the full states of the system only by one boundary measurement as described earlier. Figure 3.8 gives the numerical simulations of the nonlinear ARZ traffic model in a closed-loop with the controller that is computed with the linearized model. It is obvious that the designed observer-based output feedback controller for

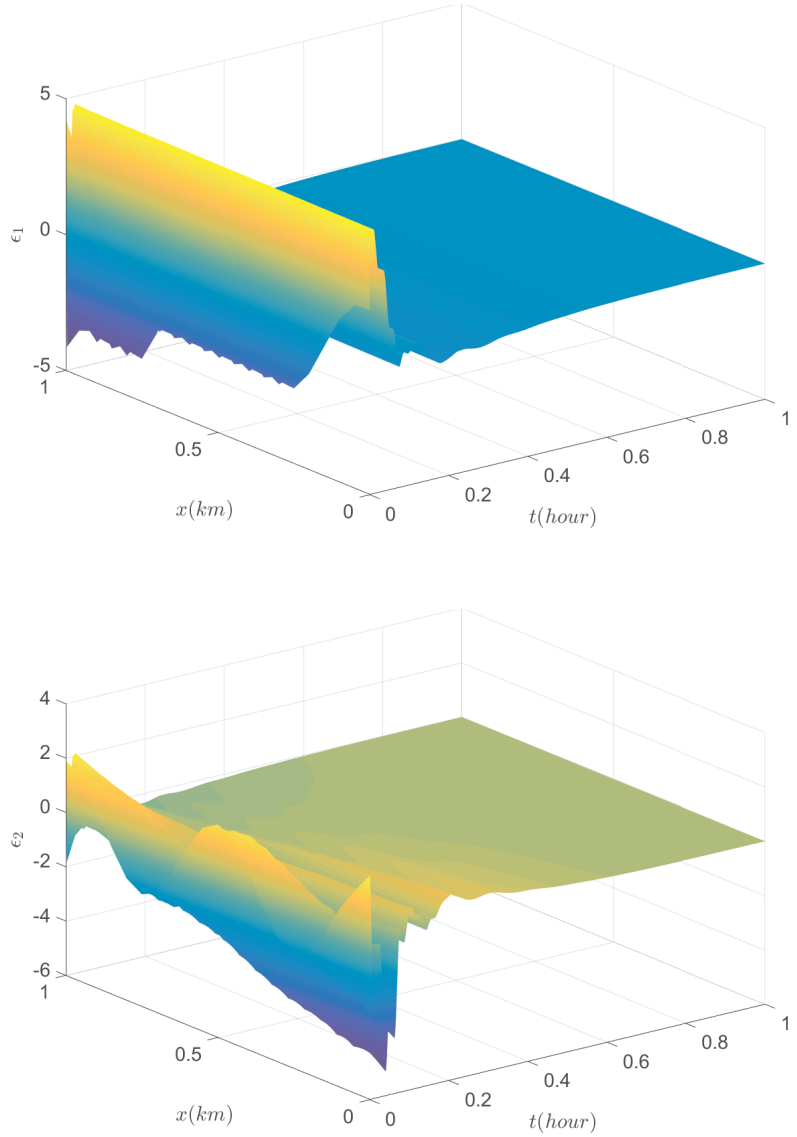

Figure 3.6: Evolutions of state variables of original system $(\epsilon_1, \epsilon_2)^\top$ in (3.5)-(3.6) with respect to spatial variable x and time variable t.

the linearized ARZ traffic system stabilizes the nonlinear system in the same way. Moreover, comparing the convergence speeds in open loop (nearly 0.4 hours in Figure 3.9) and in closed-loop with the optimal tuning controller (nearly 0.2 hours in Figure 3.8), we check that the system (2.1)-(2.2) converges to the equilibrium with the fastest speed using the designed optimal tuning controller.

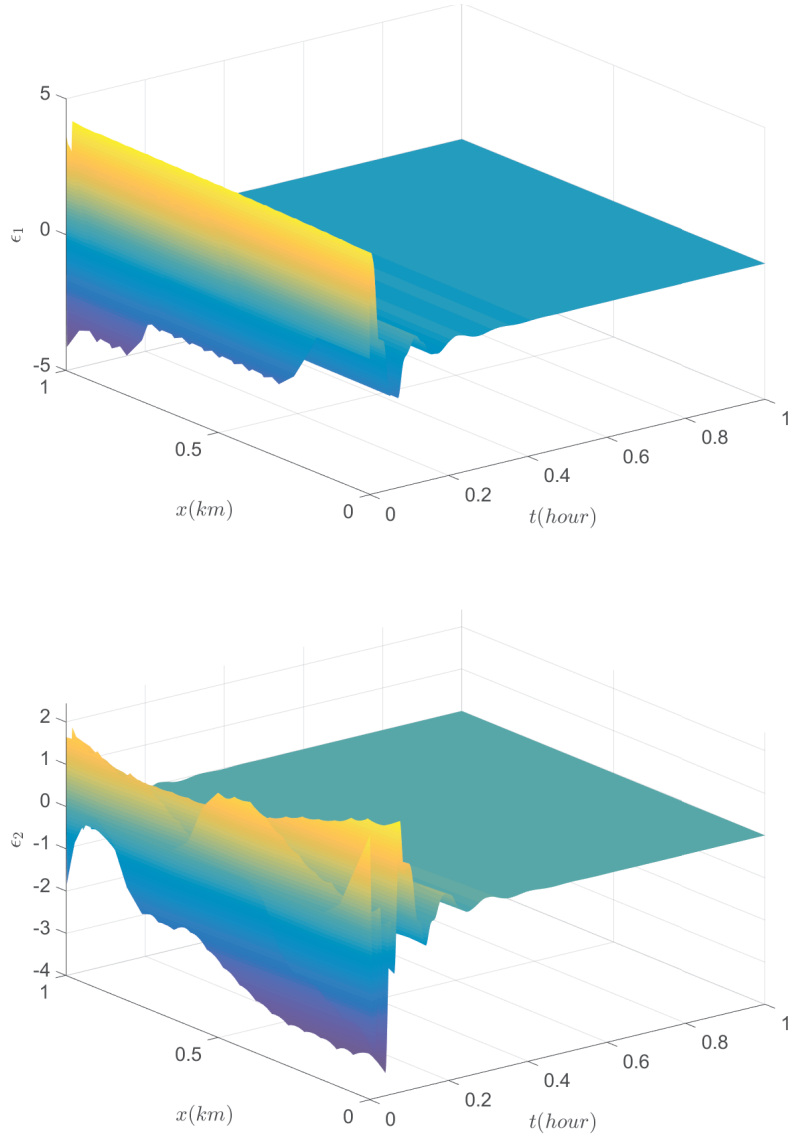

Figure 3.7: Evolutions of state variables of original system $(\epsilon_1, \epsilon_2)^\top$ in (3.5)-(3.6) with respect to spatial variable x and time variable t.

3.5 Conclusion

The stabilization of the homogeneous linearized Aw-Rascle-Zhang (ARZ) congestion traffic flow model with an unknown perturbation at the upstream boundary and a bottleneck at the downstream boundary was considered in this chapter. A full-state feedback controller was designed to stabilize the linear part of the nonlinear ARZ model. By designing an exponentially convergent observer that only needs to measure the upstream boundary state, an output state feedback controller and the iISS were achieved. Only the upstream inlet vehicle velocity was measured for the design of the control law and the unpredicted perturbation was rejected by designing proper injection gains for the observer.

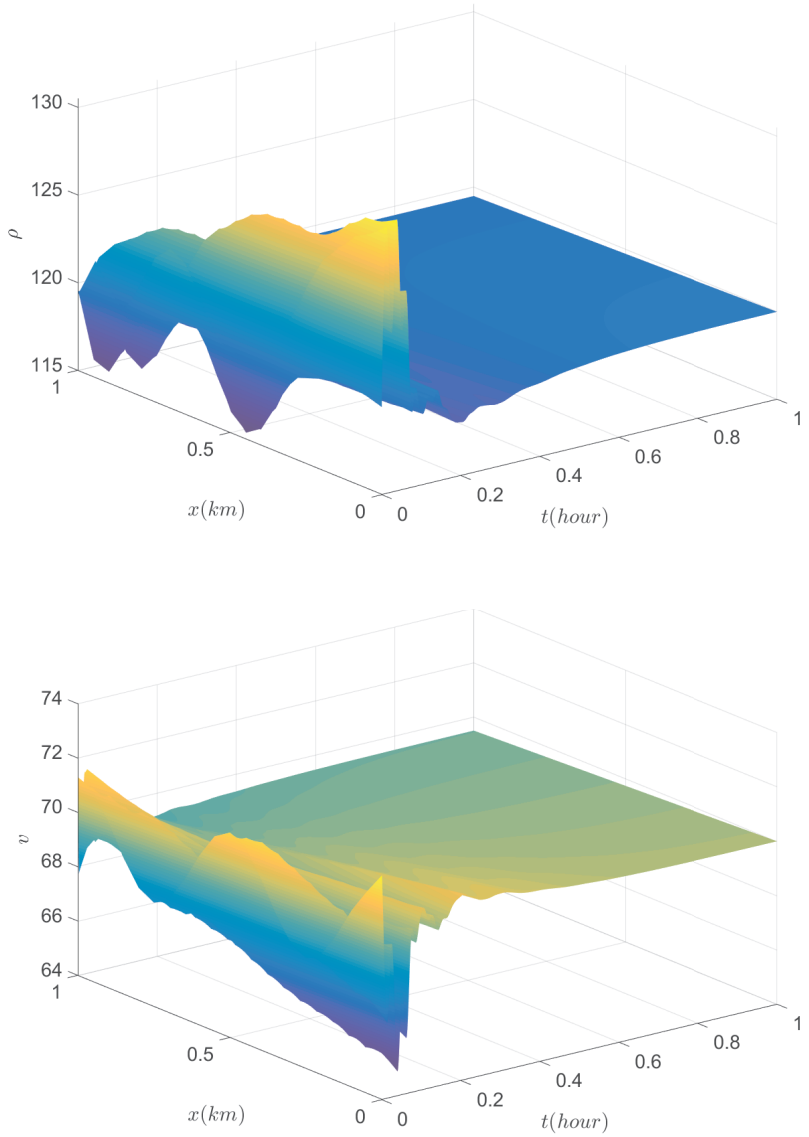

Figure 3.8: Spatial and time evolutions of state variables of plant system $(\rho, v)^\top$ in (2.1)-(2.2) in closed-loop with the optimal tuning controller computed for the linearized model (3.5)-(3.6).

In the next chapter, we design a controller to reject disturbance for the heterogeneous linearized traffic flow system with a bottleneck at the outlet boundary.

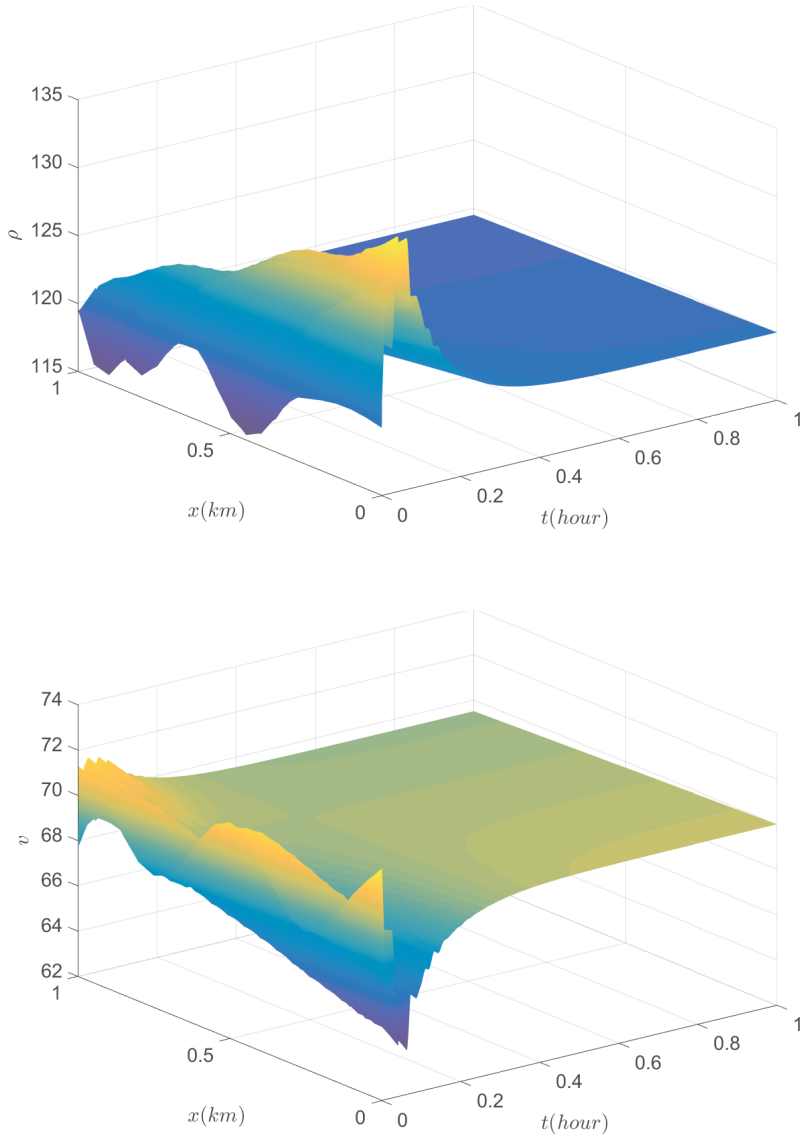

Figure 3.9: Spatial and time evolutions of state variables of plant system $(\rho, v)^\top$ in (2.1)-(2.2) in open loop.

Chapter 4

Control of heterogeneous linearized traffic with bottleneck

Contents

This chapter studies an optimal tuning boundary control law for a heterogeneous traffic flow model with disturbances to alleviate the congested traffic. The macroscopic first-order N-class Aw-Rascle traffic model consists of $2N$ hyperbolic partial differential equations. The vehicle size and the driver's behavior characterize the type of vehicle. There are m positive characteristic velocities and $2N - m$ negative characteristic velocities in the congested traffic after linearizing the model equations around the equilibrium depending on the spatial variable. By using the backstepping method, a controller implemented by a ramp metering at the inlet boundary is designed for rejecting the disturbances to stabilize the $2N \times 2N$ heterogeneous traffic system. The developed controller written as a proportional integral control is derived from mapping the original system to a target system with a proportional integral boundary control rejecting the disturbances. The integral input-to-state stability of the target system is proved by using the Lyapunov method.

This chapter has been submitted for publication in [GZP21a].

4.1 Traffic flow system and control problem

In this section, the multi-type AR traffic flow model and the interpretation of crucial parameters are presented. The preparations for designing the controller are also done including the transformations of states and the linearization around a nonuniform equilibrium. On the basis of the control problem to be solved, the corresponding boundary conditions are derived.

4.1.1 Multi-type AR traffic flow model

Extending the homogeneous traffic model in (2.1)-(2.2), we investigate the multi-type AR traffic flow model in [MR17] that describes the dynamics of heterogeneous traffic consisting of N vehicle types on a road segment with the length L,

$$\partial_t \rho_i(x,t) + \partial_x\Big(\rho_i(x,t)v_i(x,t)\Big) = 0, \tag{4.1}$$

$$\partial_t\Big(v_i(x,t) + p_i(Ao(\rho))\Big) + v_i(x,t)\partial_x\Big(v_i(x,t) + p_i(Ao(\rho))\Big) = \frac{V_{e,i}(Ao) - v_i(x,t)}{\tau_i}, \tag{4.2}$$

with the independent space variable $x \in (0, L)$ and the independent time variable $t \in [0, \infty)$, where i is the index of vehicle type with $i = 1, 2, \ldots, N$, $\rho_i(x,t)$ and $v_i(x,t)$ are respectively the density and velocity of vehicle type i. Additionally, the density $\rho_i(x,t)$ is defined as the number of vehicles passing the road section per unit length, and the velocity $v_i(x,t)$ is defined as the average speed of vehicles passing location x in unit time. The relaxation time τ_i of vehicle type i is subject to the driving behavior, the variable $Ao(\rho)$ is the area occupancy, the area occupancy $Ao(\rho)$ is formulated as

$$Ao(\rho) = \frac{a^\top \rho}{W}, \tag{4.3}$$

where $a = (a_1, a_2, \ldots, a_N)^\top$ (a_i is the occupied surface per vehicle for type i), $\rho = (\rho_1, \rho_2, \ldots, \rho_N)^\top$, and W is the width of the road segment. Area occupancy $Ao(\rho)$ describes the percentage of road space that is occupied by all the vehicle classes on the considered road section. In the physical sense, $0 < Ao(\rho) \leq 1$.

For the heterogeneous traffic, the traffic pressure function $p_i(Ao(\rho))$ of vehicle type i is an increasing function of the area occupancy $Ao(\rho)$ as follows (see [BYK21]),

$$p_i(Ao(\rho)) = v_i^M \left(\frac{Ao(\rho)}{Ao_i^M}\right)^{\gamma_i}, \quad i = 1, 2, \ldots, N, \tag{4.4}$$

where the free-flow velocity v_i^M and the maximum area occupancy $0 < Ao_i^M \leq 1$ of vehicle type i respectively describe the maximal velocity in the free regime and the maximum percentage of occupied surface in the congested regime, if there is only vehicle class i on the road. With the free flow speed v_i^M and the maximal density ρ_i^M, $0 < v_i \leq v_i^M$, $0 < \rho_i \leq \rho_i^M$ hold. As described in the paper [BYK21], the constant $\gamma_i > 1$ is the pressure exponent of the vehicle type i that can be tuned to get realistic traffic pressure $p_i(Ao(\rho))$.

The equilibrium speed-Ao relationship of vehicle class $i\,(= 1, 2, \ldots, N)$ is given by Greenshield's model in [BD+35] as

$$V_{e,i}(Ao(\rho)) = v_i^M - p_i(Ao(\rho)) = v_i^M \left(1 - \left(\frac{Ao(\rho)}{Ao_i^M}\right)^{\gamma_i}\right). \tag{4.5}$$

There is a negative connection from the decreasing function $V_{e,i}(Ao(\rho))$ describing the desired velocity of the drivers to the crowded degree.

4.1.2 Linearization of multi-type AR traffic flow model

Inspired by the case "2 vehicle classes" in [BYK21], the multi-type AR traffic model (4.1)-(4.2) is linearized around a nonuniform equilibrium

$$u^* = (\rho_1^*, v_1^*, \rho_2^*, v_2^*, \ldots, \rho_N^*, v_N^*)^\top \in C^1([0, L]; \mathbb{R}^{2N}),$$

where ρ_i^*, v_i^* satisfy, for $i = 1, 2, \dots, N$,

$$v_i^* \rho_i^{*\prime} + \rho_i^* v_i^{*\prime} = 0, \tag{4.6}$$

$$v_i^* v_i^{*\prime} + v_i^* p_i' = \frac{V_{e,i}(Ao(\rho^*)) - v_i^*}{\tau_i}, \tag{4.7}$$

with $\rho^* = (\rho_1^*, \rho_2^*, \dots, \rho_N^*)^\top$. From (4.6), note that $\rho_i^* v_i^* = d_i$ with the given constant d_i and the given value for $\rho_i^*(0), i = 1, 2 \dots, N$. Assume that there exists a physical case $\rho_i^* > 0, v_i^* > 0$, for all $x \in [0, L]$ satisfying the above equations (4.6)-(4.7) as in [BC17] for a class of physical 2×2 hyperbolic systems.

Denoting $\widetilde{u}^e = (\widetilde{\rho}_1, \widetilde{v}_1, \widetilde{\rho}_2, \widetilde{v}_2, \dots, \widetilde{\rho}_N, \widetilde{v}_N)^\top \in H^1([0, L] \times [0, \infty); \mathbb{R}^{2N})$ with $\widetilde{\rho}_i = \rho_i - \rho_i^*, \widetilde{v}_i = v_i - v_i^*$, $i = 1, 2, \dots, N$, the system (4.1)-(4.2) is transformed to the following equation, for all $x \in [0, L]$, $t \in [0, \infty)$,

$$A(\widetilde{u}^e)\partial_t \widetilde{u}^e(x,t) + B(\widetilde{u}^e)\partial_x \widetilde{u}^e(x,t) + C(\widetilde{u}^e)\widetilde{u}^e(x,t) = 0, \tag{4.8}$$

where, for $i, j = 1, 2, \dots, N$,

$$A(\widetilde{u}^e) = \begin{bmatrix} A_{11}(\widetilde{u}^e) & A_{12}(\widetilde{u}^e) & \cdots & A_{1N}(\widetilde{u}^e) \\ A_{21}(\widetilde{u}^e) & A_{22}(\widetilde{u}^e) & \cdots & A_{2N}(\widetilde{u}^e) \\ \vdots & \vdots & \ddots & \vdots \\ A_{N1}(\widetilde{u}^e) & A_{N2}(\widetilde{u}^e) & \cdots & A_{NN}(\widetilde{u}^e) \end{bmatrix},$$

with

$$A_{ij}(\widetilde{u}^e) = \begin{cases} \begin{bmatrix} 1 & 0 \\ \delta_{ii}(\rho) & 1 \end{bmatrix}, & \text{if } j = i, \\ \begin{bmatrix} 0 & 0 \\ \delta_{ij}(\rho) & 0 \end{bmatrix}, & \text{if } j \neq i, \end{cases}$$

$$B(\widetilde{u}^e) = \begin{bmatrix} B_{11}(\widetilde{u}^e) & B_{12}(\widetilde{u}^e) & \cdots & B_{1N}(\widetilde{u}^e) \\ B_{21}(\widetilde{u}^e) & B_{22}(\widetilde{u}^e) & \cdots & B_{2N}(\widetilde{u}^e) \\ \vdots & \vdots & \ddots & \vdots \\ B_{N1}(\widetilde{u}^e) & B_{N2}(\widetilde{u}^e) & \cdots & B_{NN}(\widetilde{u}^e) \end{bmatrix},$$

with

$$B_{ij}(\widetilde{u}^e) = \begin{cases} \begin{bmatrix} \widetilde{v}_i + v_i^* & \widetilde{\rho}_i + \rho_i^* \\ (\widetilde{v}_i + v_i^*)\delta_{ii}(\rho) & \widetilde{v}_i + v_i^* \end{bmatrix}, & \text{if } j = i, \\ \begin{bmatrix} 0 & 0 \\ (\widetilde{v}_i + v_i^*)\delta_{ij}(\rho) & 0 \end{bmatrix}, & \text{if } j \neq i, \end{cases}$$

and

$$C(\widetilde{u}^e) = \begin{bmatrix} C_{11}(\widetilde{u}^e) & C_{12}(\widetilde{u}^e) & \cdots & C_{1N}(\widetilde{u}^e) \\ C_{21}(\widetilde{u}^e) & C_{22}(\widetilde{u}^e) & \cdots & C_{2N}(\widetilde{u}^e) \\ \vdots & \vdots & \ddots & \vdots \\ C_{N1}(\widetilde{u}^e) & C_{N2}(\widetilde{u}^e) & \cdots & C_{NN}(\widetilde{u}^e) \end{bmatrix},$$

with

$$C_{ij}(\widetilde{u}^e)=\begin{cases}\begin{bmatrix} v_i^{*\prime} & \rho_i^{*\prime} \\ \frac{1}{\tau_i}\delta_{ii}(\rho)+v_i^*\sigma_{ii}(\rho)\rho_i^{*\prime} & \frac{1}{\tau_i}+v_i^{*\prime}+\sum_{k=1}^N\delta_{ik}(\rho)\rho_k^{*\prime}\end{bmatrix}, & \text{if } j=i,\\ \begin{bmatrix} 0 & 0 \\ \frac{1}{\tau_i}\delta_{ij}(\rho)+v_i^*\sigma_{ij}(\rho)\rho_j^{*\prime} & 0\end{bmatrix}, & \text{if } j\neq i.\end{cases}$$

Therein, for $i,j,k=1,2,\ldots,N$,

$$\begin{aligned}\delta_{ij}(\rho)&=\partial_{\rho_j}p_i\left(Ao(\rho)\right)=\frac{v_i^M\gamma_i a_j}{Ao_i^M W}\left(\frac{Ao(\rho)}{Ao_i^M}\right)^{\gamma_i-1},\\ \delta_{ij}(\rho^*)&=\partial_{\rho_j}p_i\left(Ao(\rho^*)\right)=\frac{v_i^M\gamma_i a_j}{Ao_i^M W}\left(\frac{Ao(\rho^*)}{Ao_i^M}\right)^{\gamma_i-1},\\ \sigma_{ikj}(\rho^*)&=\partial_{\rho_k}\delta_{ij}(\rho^*)=\frac{v_i^M\gamma_i(\gamma_i-1)a_k a_j}{(Ao_i^M W)^2}\left(\frac{Ao(\rho^*)}{Ao_i^M}\right)^{\gamma_i-2}.\end{aligned}$$

Because of the invertibility of $A(\widetilde{u}^e)$, i.e., $|A(\widetilde{u}^e)|\neq 0$, we transform and linearize the system (4.8) around the nonuniform equilibrium u^*, then for all $t\in[0,\infty)$, $x\in(0,L)$, the linearized system is derived with $\rho^*=(\rho_1^*,\rho_2^*,\ldots,\rho_N^*)^\top$ as follows, for all $x\in[0,L]$, $t\in[0,\infty)$,

$$\partial_t\widetilde{u}^e(x,t)+F(u^*)\partial_x\widetilde{u}^e(x,t)=G(u^*)\widetilde{u}^e(x,t), \tag{4.9}$$

where, for $i,j=1,2,\ldots,N$,

$$F(u^*)=\begin{bmatrix}F_{11}(u^*) & F_{12}(u^*) & \cdots & F_{1N}(u^*)\\ F_{21}(u^*) & F_{22}(u^*) & \cdots & F_{2N}(u^*)\\ \vdots & \vdots & \ddots & \vdots\\ F_{N1}(u^*) & F_{N2}(u^*) & \cdots & F_{NN}(u^*)\end{bmatrix},$$

with

$$F_{ij}(u^*)=\begin{cases}\begin{bmatrix} v_i^* & \rho_i^* \\ 0 & v_i^*-\rho_i^*\delta_{ii}(\rho^*)\end{bmatrix}, & \text{if } j=i,\\ \begin{bmatrix} 0 & 0 \\ (v_i^*-v_j^*)\delta_{ij}(\rho^*) & -\rho_j^*\delta_{ij}(\rho^*)\end{bmatrix}, & \text{if } j\neq i,\end{cases}$$

and

$$G(u^*)=\begin{bmatrix}G_{11}(u^*) & G_{12}(u^*) & \cdots & G_{1N}(u^*)\\ G_{21}(u^*) & G_{22}(u^*) & \cdots & G_{2N}(u^*)\\ \vdots & \vdots & \ddots & \vdots\\ G_{N1}(u^*) & G_{N2}(u^*) & \cdots & G_{NN}(u^*)\end{bmatrix},$$

with

$$G_{ij}(u^*)=\begin{cases}\begin{bmatrix} v_i^{*\prime} & \rho_i^{*\prime} \\ \frac{1}{\tau_i}\delta_{ii}(\rho^*)+v_i^*\sigma_{ii}(\rho^*)\rho_i^{*\prime}-\delta_{ii}(\rho^*)v_i^{*\prime} & \frac{1}{\tau_i}+v_i^{*\prime}+\sum_{k=1,k\neq i}^N\delta_{ik}(\rho^*)\rho_k^{*\prime}\end{bmatrix}, & \text{if } j=i,\\ \begin{bmatrix} 0 & 0 \\ \frac{1}{\tau_i}\delta_{ij}(\rho^*)+v_i^*\sigma_{ij}(\rho^*)\rho_j^{*\prime}-\delta_{ij}(\rho^*)v_j^{*\prime} & -\delta_{ij}(\rho^*)\rho_j^{*\prime}\end{bmatrix}, & \text{if } j\neq i.\end{cases}$$

Inspired by [Zha+06], the characteristic polynomial P_{2N} (characteristic variable λ) in this chapter is analyzed as follows,

$$\begin{aligned}
&P_{2N}(\lambda) = |\lambda I_{2N} - F(u^*)| \\
&= (\lambda-\phi_1)(\lambda-\phi_2)\cdots(\lambda-\phi_{2N-1})(\lambda-\phi_{2N}) \\
&\times\left(1+\left(\frac{1}{\lambda-\phi_1}-\frac{1}{\lambda-\phi_2}\right)\cdots\left(\frac{1}{\lambda-\phi_{2N-1}}-\frac{1}{\lambda-\phi_{2N}}\right)\right. \\
&\left.(\phi_1-\phi_3)(\phi_3-\phi_5)\cdots(\phi_{2N-3}-\phi_{2N-1})(\phi_{2N-1}-\phi_1)\right),
\end{aligned} \tag{4.10}$$

with $\phi_1 = v_1^*$, $\phi_2 = v_1^* - \rho_1^*\delta_{11}(\rho^*)$, $\phi_3 = v_2^*$, $\phi_4 = v_2^* - \rho_2^*\delta_{22}(\rho^*)$, ..., $\phi_{2N-1} = v_N^*$, $\phi_{2N} = v_N^* - \rho_N^*\delta_{NN}(\rho^*)$. Assume that $\phi_1 > \phi_2 > \phi_3 > \phi_4 > \cdots > \phi_{2N-1} > \phi_{2N}$, then

$$P_{2N}(\phi_i) < 0, \quad i = 1, 2, \ldots, 2N, \tag{4.11}$$

$$P_{2N}(\phi_1 + \phi_3 + \cdots + \phi_{2N-1}) > 0, \tag{4.12}$$

and there is a constant a_i, $i = 1, 2, 3, \ldots, N-1$, on the domain $\phi_{2i} > a_i > \phi_{2i+1}$ such that

$$P_{2N}(a_i) > 0. \tag{4.13}$$

By using the intermediate value theorem, (4.11), (4.12), (4.13) imply that the polynomial $P_{2N}(\lambda)$ has $2N-1$ distinct positive eigenvalues λ_1, λ_2, λ_3, λ_4, ..., λ_{2N-1} such that

$$\begin{aligned}
&\phi_1 + \phi_3 + \cdots + \phi_{2N-1} > \lambda_1 > \phi_1 > \phi_2 > \lambda_2 > a_1 > \lambda_3 > \phi_3 > \phi_4 > \lambda_4 > a_2 > \lambda_5 > \phi_5 \\
&> \cdots > \lambda_{2N-3} > \phi_{2N-3} > \phi_{2N-2} > \lambda_{2N-2} > a_{N-1} > \lambda_{2N-1} > \phi_{2N-1} > 0.
\end{aligned} \tag{4.14}$$

From (4.10), note that if $\lambda < \min\{2\phi_3 - \phi_1, 2\phi_5 - \phi_3, \ldots, 2\phi_{2N-1} - \phi_{2N-3}, 2\phi_{2N} - \phi_{2N-1}\}$, then it holds

$$P_{2N}(\lambda) > 0. \tag{4.15}$$

Therefore, if $\phi_{2N} < 0$, there is a negative eigenvalue $-\lambda_{2N}$ on the domain $0 > \phi_{2N} > -\lambda_{2N} > \min\{2\phi_3 - \phi_1, 2\phi_5 - \phi_3, \ldots, 2\phi_{2N-1} - \phi_{2N-3}, 2\phi_{2N} - \phi_{2N-1}\}$; if $\phi_{2N} > 0$, there is a negative eigenvalue $-\lambda_{2N}$ on the domain $0 > -\lambda_{2N} > \min\{2\phi_3 - \phi_1, 2\phi_5 - \phi_3, \ldots, 2\phi_{2N-1} - \phi_{2N-3}, 2\phi_{2N} - \phi_{2N-1}\}$ under the following conditions

$$\begin{aligned}
P_{2N}(0) =& \phi_1\phi_2\cdots\phi_{2N-1}\phi_{2N} + (\phi_1-\phi_2)(\phi_3-\phi_4) \\
&\cdots(\phi_{2N-1}-\phi_{2N})(\phi_1-\phi_3)(\phi_3-\phi_5) \\
&\cdots(\phi_{2N-3}-\phi_{2N-1})(\phi_{2N-1}-\phi_1) < 0.
\end{aligned} \tag{4.16}$$

By the analysis of (4.15), we note that under the condition (4.16), there is not less than one negative eigenvalue (congested traffic), if $0 > \min\{2\phi_3 - \phi_1, 2\phi_5 - \phi_3, \ldots, 2\phi_{2N-1} - \phi_{2N-3}, 2\phi_{2N} - \phi_{2N-1}\}$. If $0 < \min\{2\phi_3 - \phi_1, 2\phi_5 - \phi_3, \ldots, 2\phi_{2N-1} - \phi_{2N-3}, 2\phi_{2N} - \phi_{2N-1}\}$, all the eigenvalues are positive (free traffic). The analysis of eigenvalues in this chapter is the generalization of the case $N = 2$ in [BYK21].

The hyperbolicity of the system (4.9) is clearly discussed as above, i.e., for all $u^* \in C^1([0, L]; \mathbb{R}^{2N})$, the matrix $F(u^*)$ has $2N$ real distinct eigenvalues different to zero. Given $2N$ eigenvalues

$$\lambda_1^e > \lambda_2^e > \cdots > \lambda_m^e > 0 > -\lambda_{m+1}^e > \cdots > -\lambda_{2N}^e, \tag{4.17}$$

of $F(u^*)$, $\lambda_i^e \in C^1([0,L];\mathbb{R}_{>0})$, $i=1,\dots,2N$, that does not depend on t, and assuming that the congestion mode is kept along the trajectory, we denote by m the number of positive eigenvalues. We get that $2N-m$ is the number of waves against the traffic flow (upstream) in the congested traffic due to the reaction of the drivers to their respective leading vehicles, and due to the high value of $Ao(\rho)$. In order to alleviate the traffic congestion, we thus compute the $2N-m$ boundary conditions reducing $\|Ao(\rho)\|_{L^\infty((0,L);\mathbb{R})}$. Due to (4.3), it's done by controlling the sum of the states. Because of $\|Ao(\rho)\|_{L^\infty} \leq C\|Ao(\rho)\|_{H^1}$ with a positive constant C, we will study the scenarios $2N-m \geq 1$ in the H^1 sense in this chapter. The two-type vehicle case is investigated in the paper [BYK21], where $m=3$, $N=2$. With an invertible transformation matrix $T \in C^1([0,L];\mathbb{R}^{2N\times 2N})$ whose columns are the corresponding right eigenvectors of $2N$ eigenvalues, by using the transformation $\omega = T^{-1}\widetilde{u} \in H^1([0,L]\times[0,+\infty);\mathbb{R}^{2N})$, the linearized system (4.9) is rewritten as, for all $x\in(0,L)$, $t\in[0,+\infty)$,

$$\partial_t\omega(x,t) + \Lambda^e(x)\partial_x\omega(x,t) = M^e(x)\omega(x,t), \tag{4.18}$$

where

$$\begin{aligned}
&\Lambda^e = \mathrm{diag}\{\Lambda^+, -\Lambda^-\} \in C^1([0,L];\mathcal{D}_{2N}),\\
&\Lambda^+ = \mathrm{diag}\{\lambda_1^e, \lambda_2^e, \dots, \lambda_m^e\} \in C^1([0,L];\mathcal{D}_m^+),\\
&\Lambda^- = \mathrm{diag}\{\lambda_{m+1}^e, \lambda_{m+2}^e, \dots, \lambda_{2N}^e\} \in C^1([0,L];\mathcal{D}_{2N-m}^+),\\
&M^e = T^{-1}G(u^*)T \in C^1([0,L];\mathbb{R}^{2N\times 2N}).
\end{aligned}$$

Then, the following definitions are given for the subsequent analysis and investigation,

$$\begin{aligned}
&|\Lambda^e| = \mathrm{diag}\left\{\Lambda^+, \Lambda^-\right\} \in C^1([0,L];\mathcal{D}_{2N}^+),\\
&\Lambda^{e\prime} = \mathrm{diag}\left\{\lambda_1^{e\prime}, \dots, \lambda_m^{e\prime}, -\lambda_{m+1}^{e\prime}, \dots, -\lambda_{2N}^{e\prime}\right\} \in C^0([0,L];\mathcal{D}_{2N}),\\
&(\Lambda^+)' = \mathrm{diag}\{\lambda_1^{e\prime}, \lambda_2^{e\prime}, \dots, \lambda_m^{e\prime}\} \in C^0([0,L];\mathcal{D}_m^+),\\
&(\Lambda^-)' = \mathrm{diag}\{\lambda_{m+1}^{e\prime}, \lambda_{m+2}^{e\prime}, \dots, \lambda_{2N}^{e\prime}\} \in C^0([0,L];\mathcal{D}_{2N-m}^+),
\end{aligned}$$

where $\lambda_i^{e\prime}$ $(i=1,2,\dots,2N)$ is the derivative of λ_i^e with respect to the spatial variable x.

4.1.3 Problem statement

The control problem is motivated by alleviating the congestion on a road segment with the disturbances at the inlet boundary and the flow restriction at the downstream boundary. For example, the occurrence of traffic congestion is attributed to the excess capacity of a bottleneck at the downstream outlet and the high traffic demand (modeled as the disturbances) at the upstream inlet of the considered road section.

In order to alleviate the traffic congestion, we design a boundary control law to reject disturbances for an investigated road segment, on which a ramp metering is installed at the inlet $x=0$ and a constant density is kept at the outlet $x=L$,

$$\rho_i(L,t) = \rho_i^*(L), \quad \forall t\in[0,+\infty), \tag{4.19}$$

for $i=1,2,\dots,N$. As described in Chapter 3, the constant equilibrium density $\rho_i^*(L)$ at the outlet for each vehicle class i is guaranteed by the measurement of flux at the outlet of the considered road section and the implementation of the speed limit signs in the interface. The diagram of the control model is illustrated in Figure 4.1.

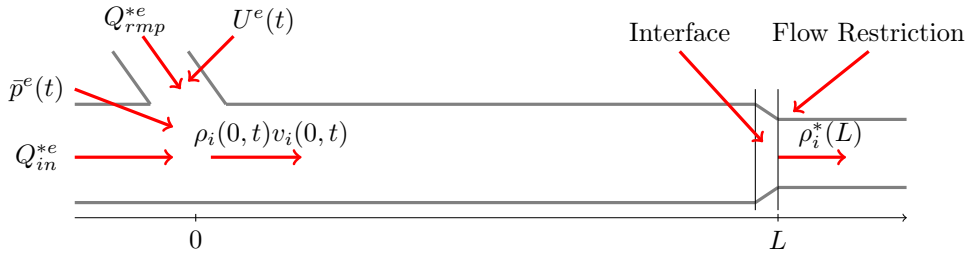

Figure 4.1: Multi-type vehicles traffic on a road with disturbances and flow restriction.

We can derive the following equation based on the flow conservation at the upstream inlet $x = 0$, for all $t \in [0, \infty)$,

$$Q^{*e}_{in} + \bar{p}^e(t) + Q^{*e}_{rmp} + \Theta U^e(t) = \begin{bmatrix} \rho_1(0,t)v_1(0,t) \\ \rho_2(0,t)v_2(0,t) \\ \vdots \\ \rho_N(0,t)v_N(0,t) \end{bmatrix}, \tag{4.20}$$

where $Q^{*e}_{in} \in \mathbb{R}^N$ is a vector whose entries are the constant inflow of each vehicle class, and $\bar{p}^e \in \mathbb{C}^1([0,\infty);\mathbb{R}^N)$ is a vector whose entries are the unknown disturbances of flow rate of each vehicle class and serves as an exogenous variable depending on the time variable t. The actuation signal vector $U^e \in \mathbb{C}^0([0,\infty);\mathbb{R}^{2N-m})$ with a coefficient matrix $\Theta \in \mathbb{R}^{N\times 2N-m}(\mathbb{R})$ is implemented by the on-ramp metering at the upstream boundary of the considered road segment. The matrix Θ is the control matrix describing the impact of the control input to the flow of each vehicle class. We want to maximize going through traffic at the inlet as in [PG06], then the total inflow at the inlet consisting of the total inflow at the ramp $0 \le \begin{bmatrix} 1 & 1 & \dots & 1 \end{bmatrix} (Q^{*e}_{rmp} + U^e(t)) \le Q^{max}_{1e}$ (Q^{max}_{1e} is the flux limit of the incoming road) and the total inflow at the inlet $0 \le \begin{bmatrix} 1 & 1 & \dots & 1 \end{bmatrix} (Q^{*e}_{in} + \bar{p}^e(t)) \le Q^{max}_{2e}$ (Q^{max}_{2e} is the flux limit on the on-ramp) is limited to the maximum flow $Q^e_{max} \ge \begin{bmatrix} 1 & 1 & \dots & 1 \end{bmatrix} (Q^{*e}_{in} + \bar{p}^e(t) + Q^{*e}_{rmp} + \Theta U^e(t)) \ge 0$, and $0 < v_i(0,\cdot) \le v^M_i$, $0 < Ao(\rho(0,\cdot)) \le \max\{Ao^M_1, Ao^M_2, \dots, Ao^M_N\}$. From (4.6), the nominal on-ramp flux rate $Q^{*e}_{rmp} \in \mathbb{R}^N$ satisfies the relation

$$Q^{*e}_{in} + Q^{*e}_{rmp} = \begin{bmatrix} \rho^*_1(0)v^*_1(0) \\ \rho^*_2(0)v^*_2(0) \\ \vdots \\ \rho^*_N(0)v^*_N(0) \end{bmatrix} = \begin{bmatrix} \rho^*_1(L)v^*_1(L) \\ \rho^*_2(L)v^*_2(L) \\ \vdots \\ \rho^*_N(L)v^*_N(L) \end{bmatrix} = \begin{bmatrix} d_1 \\ d_2 \\ \vdots \\ d_N \end{bmatrix}. \tag{4.21}$$

The equation (4.21) represents the sum of the inflow Q^{*e}_{in} and the referenced input on-ramp flux rate Q^{*e}_{rmp}, as the referenced input, is equivalent to the equilibrium flow at the inlet and outlet boundaries of the considered road segment as in [BC11]. Then, (4.20) shows that the control input is implemented to reject the disturbances $\bar{p}^e$. From the physical control input $Q^{*e}_{rmp} + \Theta U^e(t) = Q^{*e}_{rmp}\left(1 + \frac{\Theta U^e(t)}{Q^{*e}_{rmp}}\right)$, we note that because of $Q^{*e}_{rmp} + \Theta U^e(t)$ fluctuating around Q^{*e}_{rmp}, $0 < 1 + \frac{\Theta U^e(t)}{Q^{*e}_{rmp}} < 2$ is around 1, so the control of the multiplicity $1 + \frac{\Theta U^e(t)}{Q^{*e}_{rmp}}$ is more precise for data processing in the engineering application, see the block diagram of the closed-loop control system in Figure 3.2.

From the boundary condition at $x = L$, by combining control laws (4.20) with (4.21) and linearizing, the boundary conditions are derived, for all $t \ge 0$,

$$A_1 \widetilde{u}^e(0,t) = \bar{p}^e(t) + \Theta U^e(t), \tag{4.22}$$

$$B_1 \widetilde{u}^e(L,t) = 0, \tag{4.23}$$

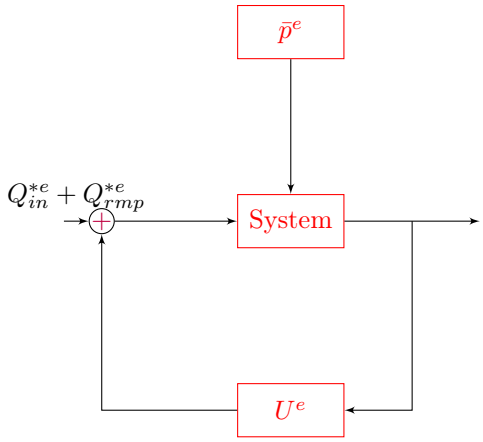

Figure 4.2: Block diagram of closed-loop control system

with

$$A_1 = \text{diag}\{[v_1^*(0), \rho_1^*(0)], \ldots, [v_N^*(0), \rho_N^*(0)]\} \in \mathbb{R}^{N\times 2N},$$
$$B_1 = \text{diag}\{\begin{bmatrix}1 & 0\\ 0 & 0\end{bmatrix}, \ldots, \begin{bmatrix}1 & 0\\ 0 & 0\end{bmatrix}\} \in \mathbb{R}^{2N\times 2N}.$$

For the sake of alleviating the congested traffic and preventing the capacity drop, a controller is designed by using the backstepping approach in this chapter. In the next subsection, a Riemann coordinate transformation of the state $\widetilde{\omega}^e$ is dealt to make the development and analysis of the controller easier.

4.1.4 Riemann coordinates transformation

By the transformation

$$R = \begin{bmatrix}R^+\\ R^-\end{bmatrix} = \Psi(x)\widetilde{\omega}^e, \quad x \in [0, L], \tag{4.24}$$

with $\Psi(x) = \text{diag}\left\{\Psi^+(x), \Psi^-(x)\right\}$,

$$\Psi^+(x) = \text{diag}\left\{e^{-\int_0^x \frac{[M(s)]_{1,1}}{\lambda_1^e(s)}\,\mathrm{d}s}, e^{-\int_0^x \frac{[M(s)]_{2,2}}{\lambda_2^e(s)}\,\mathrm{d}s}, \ldots, e^{-\int_0^x \frac{[M(s)]_{m,m}}{\lambda_m^e(s)}\,\mathrm{d}s}\right\},$$
$$\Psi^-(x) = \text{diag}\left\{e^{\int_0^x \frac{[M(s)]_{m+1,m+1}}{\lambda_{m+1}^e(s)}\,\mathrm{d}s}, e^{\int_0^x \frac{[M(s)]_{m+2,m+2}}{\lambda_{m+2}^e(s)}\,\mathrm{d}s}, \ldots, e^{\int_0^x \frac{[M(s)]_{2N,2N}}{\lambda_{2N}^e(s)}\,\mathrm{d}s}\right\},$$

from $\widetilde{\omega}^e$ to the new variable R with $R^+ : [0, L] \times [0, \infty) \to \mathbb{R}^m$, $R^- : [0, L] \times [0, \infty) \to \mathbb{R}^{2N-m}$, we can derive the following system with a simpler source term in which all the diagonal entries of the coefficient matrix are zero, for all $x \in [0, L]$, $t \in [0, \infty)$,

$$\partial_t R(x, t) + \Lambda^e(x)\partial_x R(x, t) = \Sigma(x)R(x, t), \tag{4.25}$$
$$R_{in}(t) = K_P^e R_{out}(t) + \Gamma_0(\bar{p}^e(t) + \Theta U^e(t)), \tag{4.26}$$

where

$$\Sigma = \begin{bmatrix} \Sigma^{++} & \Sigma^{+-} \\ \Sigma^{-+} & \Sigma^{--} \end{bmatrix} \in C^1([0,L];\mathbb{R}^{2N\times 2N}),$$
$$R_{in} = \begin{bmatrix} R^+(0,\cdot) \\ R^-(L,\cdot) \end{bmatrix} \in L^\infty([0,+\infty);\mathbb{R}^{2N}),$$
$$R_{out} = \begin{bmatrix} R^+(L,\cdot) \\ R^-(0,\cdot) \end{bmatrix} \in L^\infty([0,+\infty);\mathbb{R}^{2N}),$$
$$K_P^e = \begin{bmatrix} 0_{m\times m} & \Gamma_1 \\ \Gamma_3 & 0_{2N-m\times 2N-m} \end{bmatrix} \in \mathbb{R}^{2N\times 2N},$$
$$\Gamma_0 = \begin{bmatrix} \Gamma_2 \\ 0_{2N-m\times N} \end{bmatrix} \in \mathbb{R}^{2N\times N},$$

with

$$\Sigma^{++} = \{\epsilon_{ij}\}_{1\le i,j\le m} \in C^1([0,L];\mathbb{R}^{m\times m}),$$
$$\Sigma^{+-} = \{\epsilon_{ij}\}_{1\le i\le m, m+1\le j\le 2N} \in C^1([0,L];\mathbb{R}^{m\times 2N-m}),$$
$$\Sigma^{-+} = \{\epsilon_{ij}\}_{m+1\le i\le 2N, 1\le j\le m} \in C^1([0,L];\mathbb{R}^{2N-m\times m}),$$
$$\Sigma^{--} = \{\epsilon_{ij}\}_{m+1\le i\le 2N, m+1\le j\le 2N} \in C^1([0,L];\mathbb{R}^{2N-m\times 2N-m}),$$

and $\epsilon_{ij} \in C^1([0,L])$,

$$\epsilon_{ij} = \begin{cases} 0, & \text{if } j = i, \\ [\Psi]_{i,i}\cdot[M]_{i,j}\cdot[\Psi]_{j,j}^{-1}, & \text{if } j \neq i. \end{cases}$$

There are matrices $\Upsilon_1 \in \mathbb{R}^{m\times N}(\mathbb{R})$ and $\Upsilon_2 \in \mathbb{R}^{2N-m\times N}(\mathbb{R})$ such that $\Upsilon_1 A_1 T^+(0) \in \mathbb{R}^{m\times m}(\mathbb{R})$ and $\Upsilon_2 A_2 T^-(L) \in \mathbb{R}^{2N-m\times 2N-m}(\mathbb{R})$ are invertible, we obtain

$$\Gamma_1 = -(\Upsilon_1 A_1 T^+(0))^{-1}\Upsilon_1 A_1 T^-(0), \qquad \Gamma_2 = (\Upsilon_1 A_1 T^+(0))^{-1}\Upsilon_1,$$
$$\Gamma_3 = -\Psi^-(L)(\Upsilon_2 A_2 T^-(L))^{-1}\Upsilon_2 A_2 T^+(L)(\Psi^+(L))^{-1},$$

with $A_2 = \operatorname{diag}\{[1,0],\dots,[1,0]\} \in \mathbb{R}^{N\times 2N}$,

$$T^+(0) = \left\{T_{ij}^0\right\}_{1\le i\le 2N, 1\le j\le m} \in \mathbb{R}^{2N\times m},$$
$$T^-(0) = \left\{T_{ij}^0\right\}_{1\le i\le 2N, m+1\le j\le 2N} \in \mathbb{R}^{2N\times 2N-m},$$
$$T^+(L) = \left\{T_{ij}^L\right\}_{1\le i\le 2N, 1\le j\le m} \in \mathbb{R}^{2N\times m},$$
$$T^-(L) = \left\{T_{ij}^L\right\}_{1\le i\le 2N, m+1\le j\le 2N} \in \mathbb{R}^{2N\times 2N-m},$$

and

$$T_{ij}^0 = [T(0)]_{i,j}, \quad T_{ij}^L = [T(L)]_{i,j}.$$

Since the transformation (4.24) is invertible, the linearized system in density and velocity has the same stability property as the system (4.25)-(4.26).

4.2 Controller design

4.2.1 Target system

Consider the backstepping transformations, for all $x \in [0, L]$, $t \in [0, \infty)$,

$$Z^+(x,t) = R^+(x,t), \tag{4.27}$$

$$Z^-(x,t) = R^-(x,t) - \int_x^L G^1(x,\xi)R^+(\xi,t)\,\mathrm{d}\xi - \int_x^L G^2(x,\xi)R^-(\xi,t)\,\mathrm{d}\xi, \tag{4.28}$$

where G^1, G^2 are piecewise differentiable kernels defined on the triangular domain $\mathbb{T} = \{(x,\xi) \in \mathbb{R}^2 | \, 0 \le x \le \xi \le L\}$, that will be defined in Section 4.2.2.

In many papers, the proportional controllers are computed, but in this manuscript, since there are some perturbation, integral action is needed and thus PI control laws are designed. Inspired by [Hu+16], the following target system is introduced, for all $x \in (0, L)$, $t \in [0, +\infty)$,

$$\partial_t Z(x,t) + \Lambda^e(x)\partial_x Z(x,t) = \Sigma_1(x)Z(x,t) + \int_x^L C_1(x,\xi)Z(\xi,t)\,\mathrm{d}\xi + k_1(x)Z_{out}(t), \tag{4.29}$$

$$\dot{X}(t) = K_I^e Z_{out}(t) + \Gamma_0 \dot{\bar{p}}^e(t), \tag{4.30}$$

$$Z_{in}(t) = K_P^e Z_{out}(t) + X(t), \tag{4.31}$$

$$X(t) = K_I^e \int_0^t Z_{out}(\sigma)\,\mathrm{d}\sigma + \Gamma_0 \bar{p}^e(t), \tag{4.32}$$

where

$$Z(x,t) = \begin{bmatrix} Z^+(x,t) \\ Z^-(x,t) \end{bmatrix}, \quad \Sigma_1(x) = \begin{bmatrix} \Sigma^{++}(x) & \Sigma^{+-}(x) \\ 0 & 0 \end{bmatrix},$$

$$k_1 = \begin{bmatrix} 0_{m\times m} & 0_{m\times 2N-m} \\ K_1 & 0_{2N-m\times 2N-m} \end{bmatrix} \in C^1([0,L];\mathbb{R}^{2N\times 2N}),$$

$$Z_{in}(t) = \begin{bmatrix} Z^+(0,t) \\ Z^-(L,t) \end{bmatrix}, \quad Z_{out}(t) = \begin{bmatrix} Z^+(L,t) \\ Z^-(0,t) \end{bmatrix},$$

$$C_1(x,\xi) = \begin{bmatrix} C^+(x,\xi) & C^-(x,\xi) \\ 0 & 0 \end{bmatrix}, \quad K_I^e = \begin{bmatrix} K_{I11}^e & K_{I12}^e \\ 0_{(2N-m)\times m} & 0_{(2N-m)\times(2N-m)} \end{bmatrix},$$

with $K_I^{11} \in \mathbb{R}^{m\times m}, K_I^{12} \in \mathbb{R}^{m\times 2N-m}$. Here k_1 is a strictly upper triangular matrix, and C^+, C^- are given as the solutions to the Volterra integral equations, for all (x,ξ) in $\mathbb{T}$,

$$C^+(x,\xi) = \Sigma^{+-}(x)G^1(x,\xi) + \int_x^\xi C^-(x,s)G^1(s,\xi)\,\mathrm{d}s, \tag{4.33}$$

$$C^-(x,\xi) = \Sigma^{+-}(x)G^2(x,\xi) + \int_x^\xi C^-(x,s)G^2(s,\xi)\,\mathrm{d}s. \tag{4.34}$$

The system (4.29)-(4.32) is considered under the initial conditions,

$$Z(\cdot,0) = Z_0(\cdot) = \begin{bmatrix} Z_0^+(\cdot) \\ Z_0^-(\cdot) \end{bmatrix}, \tag{4.35}$$

$$X(0) = X_0 = \Gamma_0 \bar{p}^e(0) \in \mathbb{R}^{2N}. \tag{4.36}$$

The exponential stability for the H^1-norm of target system (4.29)-(4.32) is as follows.

Theorem 4.1
The equilibrium $Z(x,t) \equiv \mathbf{0}$ of the system (4.29)-(4.32) is integral input-to-state stable for the H^1-norm if there exist positive constants α, q_1, q_2, q_3, q_4, diagonal positive-definite matrices $P_1, P_4 \in \mathbb{R}^{2N\times 2N}$, a symmetric positive-definite matrix $P_2 \in \mathbb{R}^{2N\times 2N}$ and a matrix $P_3 \in \mathbb{R}^{2N\times 2N}$ such that the following matrix inequalities hold, for all $x \in [0, L]$,

(i)

$$\Omega^e(x) = \begin{bmatrix} \Omega^e_{11}(x) & \Omega^e_{12}(x) & \Omega^e_{13}(x) & \Omega^e_{14} \\ * & \Omega^e_{22} & \Omega^e_{23}(x) & \Omega^e_{24} \\ * & * & \Omega^e_{33} & \Omega^e_{34} \\ * & * & * & \Omega^e_{44}(x) \end{bmatrix} \geq 0, \tag{4.37}$$

where

$$\Omega^e_{11}(x) = -\Lambda^{e\prime}(x)P_1 - \alpha P_1 - \left(\Sigma_1^\top(x)P_1 + P_1\Sigma_1(x) + q_1 L\nu_1^2 I_{2N} + \left(\frac{L}{q_1} + \frac{L}{q_2}\right) C_1^\top(0,x)C_1(0,x)\right),$$
$$\Omega^e_{12}(x) = -P_3K_I^e - P_1k_1(x),$$
$$\Omega^e_{13}(x) = -\Lambda^{e\prime}(x)P_3 - \alpha P_3 - \Sigma_1^\top(x)P_3,$$
$$\Omega^e_{14} = 0,$$
$$\Omega^e_{22} = \frac{1}{L}E_2P_1 - \frac{1}{L}K_P^{e\top}E_1P_1K_P^e - \frac{1}{L}K_I^{e\top}E_1P_4K_I^e,$$
$$\Omega^e_{23}(x) = -\frac{1}{L}K_P^{e\top}E_1P_1 - \frac{1}{L}\left(K_P^{e\top}M_1 + M_2\right) - K_I^{e\top}P_2 - k_1^\top(x)P_3,$$
$$\Omega^e_{24} = -\frac{1}{L}K_I^{e\top}E_1P_4K_P^e,$$
$$\Omega^e_{33} = -\frac{1}{L}E_1P_1 - \frac{1}{L}\left(M_1 + M_1^\top\right) - \alpha P_3 - q_2L\nu_2^2 I_{2N},$$
$$\Omega^e_{34} = 0,$$
$$\Omega^e_{44}(x) = \frac{1}{L}E_2P_4 - \frac{1}{L}K_P^{e\top}E_1P_4K_P^e - \frac{1}{q_4}k_1^\top(x)k_1(x),$$

with

$$M_1 = \begin{bmatrix} \Lambda^+(0)P_3^{++} & \Lambda^+(0)P_3^{+-} \\ -\Lambda^-(L)P_3^{-+} & -\Lambda^-(L)P_3^{--} \end{bmatrix}, \qquad M_2 = \begin{bmatrix} -\Lambda^+(L)P_3^{++} & -\Lambda^+(L)P_3^{+-} \\ \Lambda^-(0)P_3^{-+} & \Lambda^-(0)P_3^{--} \end{bmatrix},$$

$$P_3^{++} = \{P_3\}_{1\leq i,j\leq m}, \qquad P_3^{+-} = \{P_3\}_{1\leq i\leq m, m+1\leq j\leq 2N},$$
$$P_3^{-+} = \{P_3\}_{m+1\leq i\leq 2N, 1\leq j\leq m}, \qquad P_3^{--} = \{P_3\}_{m+1\leq i\leq 2N, m+1\leq j\leq 2N},$$
$$E_1 = \operatorname{diag}\{\Lambda^+(0), \Lambda^-(L)\}, \qquad E_2 = \operatorname{diag}\{\Lambda^+(L), \Lambda^-(0)\},$$
$$\nu_1 = \max\left(\lambda(P_1)\right), \qquad \nu_2 = \max\left(|\lambda(P_3)|\right),$$

(ii)

$$M^e(x) = \left(-\Lambda^{e\prime}(x) - \alpha I_{2N}\right)P_4 - \left(\Sigma_1^\top(x)P_4 + P_4\Sigma_1(x) + (q_3L + q_4)\nu_3^2 I_{2N} + \frac{L}{q_3}C_1^\top(0,x)C_1(0,x)\right) \geq 0, \tag{4.38}$$

with $\nu_3 = \max\left(\lambda(P_4)\right)$.

In other words, there exist positive constants b_1, c_1 such that, for every $Z_0 \in H^1((0,L);\mathbb{R}^{2N})$, $X_0 \in \mathbb{R}^{2N}$, and for any $\bar{p}^e$ such that $\dot{\bar{p}}^e \in C^0[0,\infty)$, the solution $Z \in C^0([0,\infty);H^1((0,L);\mathbb{R}^{2N})$,

$X \in C^0([0,\infty);\mathbb{R}^{2N})$ to the Cauchy problem (4.29)-(4.32), (4.35)-(4.36) is defined on $[0,\infty)\times[0,L]$ and satisfies

$$\|Z(\cdot,t)\|_{H^1}^2 + |X(t)|^2 \le c_1 e^{-\alpha t}\left(\|Z_0\|_{H^1}^2 + |X_0|^2\right) + b_1 \int_0^t \dot{\bar{p}}^{e\top}(s)\dot{\bar{p}}^e(s)\,\mathrm{d}s, \quad \forall t \in [0,\infty). \tag{4.39}$$

Proof. The following H^1 Lyapunov function candidate is introduced for the stability analysis of the heterogeneous system (4.29)-(4.32), for all $x \in [0,L]$, $t \in [0,\infty)$,

$$V^e\left(Z(x,t), X(t), Z_t(x,t)\right) = V_1^e + V_2^e + V_3^e + V_4^e, \tag{4.40}$$

where

$$V_1^e = \int_0^L Z^\top(x,\cdot)\mathcal{P}_1(x)Z(x,\cdot)\,\mathrm{d}x, \tag{4.41}$$

$$V_2^e = \int_0^L \left(Z^\top(x,\cdot)\mathcal{P}_3(x)X(\cdot) + X^\top(\cdot)\mathcal{P}_3^\top(x)Z(x,\cdot)\right)\mathrm{d}x, \tag{4.42}$$

$$V_3^e = LX^\top(\cdot)P_2X(\cdot), \tag{4.43}$$

$$V_4^e = \int_0^L Z_t^\top(x,\cdot)\mathcal{P}_4(x)Z_t(x,\cdot)\,\mathrm{d}x, \tag{4.44}$$

and

$$\mathcal{P}_1(x) \triangleq P_1\mathrm{diag}\left\{e^{-\mu x}I_m, e^{\mu x}I_{2N-m}\right\},$$

$$\mathcal{P}_3(x) \triangleq P_3\mathrm{diag}\left\{e^{-\frac{\mu}{2}x}I_m, e^{\frac{\mu}{2}x}I_{2N-m}\right\},$$

$$\mathcal{P}_4(x) \triangleq P_4\mathrm{diag}\left\{e^{-\mu x}I_m, e^{\mu x}I_{2N-m}\right\},$$

where, by definition, the notation Z_t must be understood as, for all $x \in [0,L]$, $t \in [0,\infty)$,

$$\partial_t Z(x,t) \triangleq -\Lambda^e(x)\partial_x Z(x,t) + \Sigma_1(x)Z(x,t) + \int_x^L C_1(x,\xi)Z(\xi,t)\,\mathrm{d}\xi + k_1(x)Z_{out}(t).$$

Under the definition of V^e and straightforward observations, there exists a positive real constant β such that, for every Z, we can obtain the following inequality,

$$\begin{aligned}&\frac{1}{\beta}\int_0^L \left(\|Z(x,\cdot)\|_{L^2}^2 + |X(\cdot)|^2 + \|\partial_x Z(x,\cdot)\|_{L^2}^2\right)\mathrm{d}x\\ &\le V^e \le \beta\int_0^L \left(\|Z(x,\cdot)\|_{L^2}^2 + |X(\cdot)|^2 + \|\partial_x Z(x,\cdot)\|_{L^2}^2\right)\mathrm{d}x.\end{aligned} \tag{4.45}$$

By time differentiation of (4.29) and (4.31), Z_t can be shown to satisfy the following equations, for all $x \in [0,L]$, $t \in [0,\infty)$,

$$\partial_{tt}Z(x,t) = -\Lambda^e(x)\partial_{tx}Z(x,t) + \Sigma_1(x)\partial_t Z(x,t) + \int_x^L C_1(x,\xi)\partial_t Z(\xi,t)\,\mathrm{d}\xi + k_1(x)\dot{Z}_{out}(\cdot), \tag{4.46}$$

$$\dot{Z}_{in}(t) = K_P^e\dot{Z}_{out}(t) + \dot{X}(t). \tag{4.47}$$

Taking time derivative of V_1^e along the solutions to (4.29)-(4.32) and using integration by parts,

the following result is achieved, for all $t \in [0, \infty)$,

$$\begin{aligned}\dot{V}_1^{\,e} \leq & Z_{out}^{\top}(t)\left(K_P^{e\top}\bar{E}_1 P_1 K_P^e - e^{-\mu L}\bar{E}_2 P_1\right) Z_{out}(t) + Z_{out}^{\top}(t) K_P^{e\top}\bar{E}_1 P_1 X(t) \\ & + X^{\top}(t) P_1 \bar{E}_1 K_P^e Z_{out}(t) + X^{\top}(t)\bar{E}_1 P_1 X(t) \\ & + \int_0^L Z^{\top}(x,t)\left(\Lambda^{e\prime}(x)\mathcal{P}_1(x) - \mu|\Lambda^e(x)|\mathcal{P}_1(x)\right) Z(x,t)\,\mathrm{d}x. \\ & + \int_0^L \Bigg(\left(\Sigma_1(x)Z(x,t) + \int_x^L C_1(x,\xi)Z(\xi,t)\,\mathrm{d}\xi + k_1(x)Z_{out}(\cdot)\right)^{\top} \mathcal{P}_1(x)Z(x,t) \\ & + Z^{\top}(x,t)\mathcal{P}_1(x)\left(\Sigma_1(x)Z(x,t) + \int_x^L C_1(x,\xi)Z(\xi,t)\,\mathrm{d}\xi + k_1(x)Z_{out}(\cdot)\right)\Bigg)\mathrm{d}x, \end{aligned} \tag{4.48}$$

with

$$\bar{E}_1 = \mathrm{diag}\left\{\Lambda^+(0), e^{\mu L}\Lambda^-(L)\right\}, \qquad \bar{E}_2 = \mathrm{diag}\left\{\Lambda^+(L), e^{\mu L}\Lambda^-(0)\right\}.$$

By taking time derivative of V_2^e along the solutions to (4.29)-(4.32) and using integration by parts, we get for all $t \in [0, \infty)$,

$$\begin{aligned}\dot{V}_2^{\,e} \leq & Z_{out}^{\top}(t)\left(K_P^{e\top}\bar{M}_1 + \bar{M}_2\right) X(t) + X^{\top}(t)\bar{M}_1 X(t) + X^{\top}(t)\left(\bar{M}_1^{\top}K_P^e + \bar{M}_2^{\top}\right) Z_{out}(t) \\ & + X^{\top}(t)\bar{M}_1^{\top}X(t) + \int_0^L Z^{\top}(x,t)\left(\Lambda^{e\prime}(x)\mathcal{P}_3(x) - \frac{\mu}{2}|\Lambda^e(x)|\mathcal{P}_3(x)\right) X(t)\,\mathrm{d}x \\ & + \int_0^L X^{\top}(t)\left(-\frac{\mu}{2}\mathcal{P}_3^{\top}(x)|\Lambda^e(x)| + \mathcal{P}_3^{\top}(x)\Lambda^{e\prime}(x)\right) Z(x,t)\,\mathrm{d}x \\ & + \int_0^L \left(Z^{\top}(x,t)\mathcal{P}_3(x)K_I^e Z_{out}(t) + Z_{out}^{\top}(t)K_I^{e\top}\mathcal{P}_3^{\top}(x)Z(x,t)\right)\mathrm{d}x \\ & + \kappa_1\int_0^L Z^{\top}(x,t)\mathcal{P}_3(x)\Gamma_0\left(Z^{\top}(x,t)\mathcal{P}_3(x)\Gamma_0\right)^{\top}\mathrm{d}x + \frac{L}{\kappa_1}\dot{\tilde{p}}^{e\top}(t)\dot{\tilde{p}}^e(t) \\ & + \int_0^L \Bigg(\left(\Sigma_1(x)Z(x,t) + \int_x^L C_1(x,\xi)Z(\xi,t)\,\mathrm{d}\xi + k_1(x)Z_{out}(\cdot)\right)^{\top} \mathcal{P}_3(x)X(t) \\ & + X^{\top}(t)\mathcal{P}_3^{\top}(x)\left(\Sigma_1(x)Z(x,t) + \int_x^L C_1(x,\xi)Z(\xi,t)\,\mathrm{d}\xi + k_1(x)Z_{out}(\cdot)\right)\Bigg)\mathrm{d}x, \end{aligned} \tag{4.49}$$

with a positive constant κ_1 and

$$\bar{M}_1 = \begin{bmatrix} \Lambda^+(0)P_3^{++} & \Lambda^+(0)P_3^{+-} \\ -e^{-\frac{\mu}{2}L}\Lambda^-(L)P_3^{-+} & -e^{\frac{\mu}{2}L}\Lambda^-(L)P_3^{--} \end{bmatrix},$$
$$\bar{M}_2 = \begin{bmatrix} -e^{-\frac{\mu}{2}L}\Lambda^+(L)P_3^{++} & -e^{\frac{\mu}{2}L}\Lambda^+(L)P_3^{+-} \\ \Lambda^-(0)P_3^{-+} & \Lambda^-(0)P_3^{--} \end{bmatrix}.$$

By taking time derivative of V_3^e along the solutions to (4.30), we can derive the following result with a positive constant κ_2, for all $t \in [0, \infty)$,

$$\begin{aligned}\dot{V}_3^{\,e} \leq & LZ_{out}^{\top}(t)K_I^{e\top}P_2 X(t) + LX^{\top}(t)P_2 K_I^e Z_{out}(t) \\ & + L\kappa_2 X^{\top}(t)P_2\Gamma_0\left(X^{\top}(t)P_2\Gamma_0\right)^{\top} + \frac{L}{\kappa_2}\dot{\tilde{p}}^{e\top}(t)\dot{\tilde{p}}^e(t). \end{aligned} \tag{4.50}$$

Taking time derivative of V_4^e along the solutions to (4.29)-(4.32), (4.46) and using integration by

parts, we get for all $t \in [0,\infty)$,

$$\begin{aligned}
\dot{V}_4^{\,e} \leq\ & \dot{Z}_{out}^\top(t)\left(K_P^{e\top}\bar{E}_1P_4K_P^e - e^{-\mu L}\bar{E}_2P_4\right)\dot{Z}_{out}(t) + \dot{Z}_{out}^\top(t)K_P^{e\top}P_4\bar{E}_1K_I^eZ_{out}(t)\\
&+ Z_{out}^\top(t)K_I^{e\top}\bar{E}_1P_4K_P^e\dot{Z}_{out}(t) + Z_{out}^\top(t)K_I^{e\top}\bar{E}_1P_4K_I^eZ_{out}(t) + \frac{1}{\kappa_3}\dot{\bar{p}}^{e\top}(t)\dot{\bar{p}}^e(t)\\
&+ \kappa_3\dot{Z}_{out}^\top(t)K_P^{e\top}\bar{E}_1P_4\Gamma_0\left(K_P^{e\top}\bar{E}_1P_4\Gamma_0\right)^\top\dot{Z}_{out}(t)\\
&+ \kappa_4Z_{out}^\top(t)K_I^{e\top}\bar{E}_1P_4\Gamma_0\left(K_I^{e\top}\bar{E}_1P_4\Gamma_0\right)^\top Z_{out}(t) + \frac{1}{\kappa_4}\dot{\bar{p}}^{e\top}(t)\dot{\bar{p}}^e(t)\\
&+ \dot{\bar{p}}^e(t)^\top\Gamma_0^\top\bar{E}_1P_4\Gamma_0\dot{\bar{p}}^e(t) + \int_0^L \partial_tZ^\top(x,t)\left(\Lambda^{e\prime}(x)\mathcal{P}_4(x) - \mu|\Lambda^e(x)|\mathcal{P}_4(x)\right)\partial_tZ(x,t)\,\mathrm{d}x\\
&+ \int_0^L\Bigg(\left(\Sigma_1(x)\partial_tZ(x,t) + \int_x^L C_1(x,\xi)\partial_tZ(\xi,t)\,\mathrm{d}\xi + k_1(x)\dot{Z}_{out}(\cdot)\right)^\top\mathcal{P}_4(x)\partial_tZ(x,t)\\
&+ \partial_tZ^\top(x,t)\mathcal{P}_4(x)\left(\Sigma_1(x)\partial_tZ(x,t) + \int_x^L C_1(x,\xi)\partial_tZ(\xi,t)\,\mathrm{d}\xi + k_1(x)\dot{Z}_{out}(\cdot)\right)\Bigg)\,\mathrm{d}x, \quad (4.51)
\end{aligned}$$

with positive constants κ_3 and κ_4.

The three rightmost integrals in (4.48), (4.49) and (4.51) are considered individually, for all $t \in [0,\infty)$,

$$\begin{aligned}
&\int_0^L\Bigg(\Big(\Sigma_1(x)Z(x,t) + \int_x^L C_1(x,\xi)Z(\xi,t)\,\mathrm{d}\xi + k_1(x)Z_{out}(\cdot)\Big)^\top\mathcal{P}_1(x)Z(x,t)\\
&\quad + Z^\top(x,t)\mathcal{P}_1(x)\Big(\Sigma_1(x)Z(x,t) + \int_x^L C_1(x,\xi)Z(\xi,t)\,\mathrm{d}\xi + k_1(x)Z_{out}(\cdot)\Big)\Bigg)\,\mathrm{d}x\\
&\leq \int_0^L\Big(\left(\Sigma_1(x)Z(x,t) + k_1(x)Z_{out}(\cdot)\right)^\top\mathcal{P}_1(x)Z(x,t) + Z^\top(x,t)\mathcal{P}_1(x)\left(\Sigma_1(x)Z(x,t) + k_1(x)Z_{out}(\cdot)\right)\Big)\,\mathrm{d}x\\
&\quad + q_1Le^{2\mu L}\nu_1^2\int_0^L Z^\top(x,t)Z(x,t)\,\mathrm{d}x + \frac{L}{q_1}\int_0^L\left(C_1(0,x)Z(x,t)\right)^\top\left(C_1(0,x)Z(x,t)\right)\mathrm{d}x. \quad (4.52)
\end{aligned}$$

Similarly, we derive the inequalities for the other two integrals, for all $t \in [0,\infty)$,

$$\begin{aligned}
&\int_0^L\Bigg(\left(\Sigma_1(x)Z(x,t) + \int_x^L C_1(x,\xi)Z(\xi,t)\,\mathrm{d}\xi + k_1(x)Z_{out}(\cdot)\right)^\top\mathcal{P}_3(x)X(t)\\
&+ X^\top(t)\mathcal{P}_3^\top(x)\left(\Sigma_1(x)Z(x,t) + \int_x^L C_1(x,\xi)Z(\xi,t)\,\mathrm{d}\xi + k_1(x)Z_{out}(\cdot)\right)\Bigg)\,\mathrm{d}x\\
&\leq \int_0^L\Big(\left(\Sigma_1(x)Z(x,t) + k_1(x)Z_{out}(\cdot)\right)^\top\mathcal{P}_3(x)X(t) + X^\top(t)\mathcal{P}_3^\top(x)\left(\Sigma_1(x)Z(x,t) + k_1(x)Z_{out}(\cdot)\right)\Big)\,\mathrm{d}x\\
&\quad + q_2Le^{\mu L}\nu_2^2\int_0^L X^\top(t)X(t)\,\mathrm{d}x + \frac{L}{q_2}\int_0^L\left(C_1(0,x)Z(x,t)\right)^\top\left(C_1(0,x)Z(x,t)\right)\mathrm{d}x, \quad (4.53)
\end{aligned}$$

$$
\begin{aligned}
&\int_0^L \Bigg(\left(\Sigma_1(x)\partial_t Z(x,t) + \int_x^L C_1(x,\xi)\partial_t Z(\xi,t)\,\mathrm{d}\xi + k_1(x)\dot{Z}_{out}(\cdot) \right)^\top \mathcal{P}_4(x)\partial_t Z(x,t) \\
&+ \partial_t Z^\top(x,t)\mathcal{P}_4(x) \left(\Sigma_1(x)\partial_t Z(x,t) + \int_x^L C_1(x,\xi)\partial_t Z(\xi,t)\,\mathrm{d}\xi + k_1(x)\dot{Z}_{out}(\cdot) \right) \Bigg)\,\mathrm{d}x \\
&\leq \int_0^L \Big((\Sigma_1(x)\partial_t Z(x,t) + k_1(x)\dot{Z}_{out}(\cdot))^\top \mathcal{P}_4(x)\partial_t Z(x,t) + \partial_t Z^\top(x,t)\mathcal{P}_4(x)(\Sigma_1(x)\partial_t Z(x,t) + k_1(x)\dot{Z}_{out}(\cdot)) \Big)\,\mathrm{d}x \\
&\quad + q_3 L e^{2\mu L}\nu_3^2 \int_0^L \partial_t Z^\top(x,t)\partial_t Z(x,t)\,\mathrm{d}x + \frac{L}{q_3}\int_0^L (C_1(0,x)\partial_t Z(x,t))^\top (C_1(0,x)\partial_t Z(x,t))\,\mathrm{d}x \\
&\leq \int_0^L \Big((\Sigma_1(x)Z_t(x,\cdot))^\top \mathcal{P}_4(x) Z_t(x,\cdot) + Z_t^\top(x,\cdot)\mathcal{P}_4(x)\Sigma_1(x)Z_t(x,\cdot) \Big)\,\mathrm{d}x \\
&+ (q_3 L + q_4)e^{2\mu L}\nu_3^2 \int_0^L Z_t^\top(x,\cdot)Z_t(x,\cdot)\,\mathrm{d}x + \frac{L}{q_3}\int_0^L (C_1(0,x)Z_t(x,\cdot))^\top (C_1(0,x)Z_t(x,\cdot))\,\mathrm{d}x \\
&+ \frac{1}{q_4}\int_0^L (k_1(x)\dot{Z}_{out}(\cdot))^\top (k_1(x)\dot{Z}_{out}(\cdot))\,\mathrm{d}x. \qquad (4.54)
\end{aligned}
$$

Using (4.48)-(4.54), there exists a constant $\alpha > 0$ such that, for all $t \in [0,\infty)$,

$$
\begin{aligned}
\dot{V}^e &= \dot{V_1}^e + \dot{V_2}^e + \dot{V_3}^e + \dot{V_4}^e \\
&\leq -\alpha V^e - \int_0^L \begin{bmatrix} Z(x,\cdot) \\ Z_{out}(\cdot) \\ X(\cdot) \\ \dot{Z}_{out}(\cdot) \end{bmatrix}^\top \bar{\Omega}^e(x) \begin{bmatrix} Z(x,\cdot) \\ Z_{out}(\cdot) \\ X(\cdot) \\ \dot{Z}_{out}(\cdot) \end{bmatrix} \mathrm{d}x - \int_0^L \partial_t Z^\top(x,t)\bar{M}^e(x)\partial_t Z(x,t)\,\mathrm{d}x \\
&\quad + \dot{\bar{p}}^{e\top}(t)\left[\left(\frac{L}{\kappa_1} + \frac{L}{\kappa_2} + \frac{1}{\kappa_3} + \frac{1}{\kappa_4} \right) I_{2N} + \Gamma_0^\top \bar{E}_1 P_4 \Gamma_0 \right] \dot{\bar{p}}^e(t), \qquad (4.55)
\end{aligned}
$$

where, for all $x \in [0, L]$,

$$
\bar{\Omega}^e(x) = \begin{bmatrix} \bar{\Omega}^e_{11}(x) & \bar{\Omega}^e_{12}(x) & \bar{\Omega}^e_{13}(x) & \bar{\Omega}^e_{14} \\ * & \bar{\Omega}^e_{22} & \bar{\Omega}^e_{23}(x) & \bar{\Omega}^e_{24} \\ * & * & \bar{\Omega}^e_{33} & \bar{\Omega}^e_{34} \\ * & * & * & \bar{\Omega}^e_{44}(x) \end{bmatrix} \qquad (4.56)
$$

with

$$\begin{aligned}
\bar{\Omega}^e_{11}(x) &= \mu|\Lambda^e(x)|\mathcal{P}_1(x) - \Lambda^{e\prime}(x)\mathcal{P}_1(x) - \alpha\mathcal{P}_1(x) - \kappa_1\mathcal{P}_3(x)\Gamma_0(\mathcal{P}_3(x)\Gamma_0)^\top \\
&\quad - \left(\Sigma_1^\top(x)\mathcal{P}_1(x) + \mathcal{P}_1(x)\Sigma_1(x) + q_1 L e^{2\mu L}\nu_1^2 I_{2N} + \left(\frac{L}{q_1} + \frac{L}{q_2}\right) C_1^\top(0,x)C_1(0,x)\right), \\
\bar{\Omega}^e_{12}(x) &= -\mathcal{P}_3(x)K_I^e - \mathcal{P}_1(x)k_1(x), \\
\bar{\Omega}^e_{13}(x) &= \frac{\mu}{2}|\Lambda^e(x)|\mathcal{P}_3(x) - \Lambda^{e\prime}(x)\mathcal{P}_3(x) - \alpha\mathcal{P}_3(x) - \Sigma_1^\top(x)\mathcal{P}_3(x), \\
\bar{\Omega}^e_{14} &= 0, \\
\bar{\Omega}^e_{22} &= \frac{e^{-\mu L}}{L}\bar{E}_2P_1 - \frac{1}{L}K_P^{e\top}\bar{E}_1P_1K_P^e - \frac{1}{L}K_I^{e\top}\bar{E}_1P_4K_I^e - \frac{\kappa_4}{L}K_I^{e\top}\bar{E}_1P_4\Gamma_0(K_I^{e\top}\bar{E}_1P_4\Gamma_0)^\top, \\
\bar{\Omega}^e_{23}(x) &= -\frac{1}{L}K_P^{e\top}\bar{E}_1P_1 - \frac{1}{L}\left(K_P^{e\top}\bar{M}_1 + \bar{M}_2\right) - K_I^{e\top}P_2 - k_1^\top(x)\mathcal{P}_3(x), \\
\bar{\Omega}^e_{24} &= -\frac{1}{L}K_I^{e\top}\bar{E}_1P_4K_P^e, \\
\bar{\Omega}^e_{33} &= -\frac{1}{L}\bar{E}_1P_1 - \frac{1}{L}\left(\bar{M}_1 + \bar{M}_1^\top\right) - \kappa_2P_2\Gamma_0(P_2\Gamma_0)^\top - \alpha P_2 - q_2 L e^{\mu L}\nu_2^2 I_{2N}, \\
\bar{\Omega}^e_{34} &= 0, \\
\bar{\Omega}^e_{44}(x) &= \frac{e^{-\mu L}}{L}\bar{E}_2P_4 - \frac{1}{L}K_P^{e\top}\bar{E}_1P_4K_P^e - \frac{\kappa_3}{L}K_P^{e\top}\bar{E}_1P_4\Gamma_0\left(K_P^{e\top}\bar{E}_1P_4\Gamma_0\right)^\top - \frac{1}{q_4}k_1^\top(x)k_1(x),
\end{aligned}$$

and

$$\begin{aligned}
\bar{M}^e(x) =& \left(-\Lambda^{e\prime}(x) + \mu|\Lambda^e(x)| - \alpha I_{2N}\right)\mathcal{P}_4(x) \\
&- \Big(\Sigma_1^\top(x)\mathcal{P}_4(x) + \mathcal{P}_4(x)\Sigma_1(x) + (q_3L + q_4)e^{2\mu L}\nu_3^2 I_{2N} + \frac{L}{q_3}C_1^\top(0,x)C_1(0,x)\Big). \quad (4.57)
\end{aligned}$$

Under the conditions (4.37), (4.38), $\exists\,\mu,\kappa_1,\kappa_2,\kappa_3,\kappa_4 > 0$ small enough, such that $\bar{\Omega}^e(x) \geq 0$ and $\bar{M}^e(x) \geq 0$, for all $x \in [0,L]$, thus for all $t \in [0,\infty)$,

$$\dot{V}^e \leq -\alpha V^e + \alpha_1 \dot{\tilde{p}}^{e\top}(t)\dot{\tilde{p}}^e(t), \quad (4.58)$$

with $\alpha_1 = \max\left(\lambda\left(\left(\frac{L}{\kappa_1} + \frac{L}{\kappa_2} + \frac{1}{\kappa_3} + \frac{1}{\kappa_4}\right)I_{2N} + \Gamma_0^\top P_4\bar{E}_1\Gamma_0\right)\right)$. Thus along the solutions to the system (4.29)-(4.32), for all $t \in [0,\infty)$,

$$V^e \leq V^e(0)e^{-\alpha t} + \alpha_1\int_0^t \dot{\tilde{p}}^{e\top}(s)\dot{\tilde{p}}^e(s)\,\mathrm{d}s. \quad (4.59)$$

Combining this relation with (4.45), there exist positive constants $c_1 = \beta^2$, $b_1 = \beta\alpha_1$ such that, for all $t \in [0,\infty)$,

$$\begin{aligned}
&\int_0^L \left(\|Z(x,t)\|_{L^2}^2 + |X(t)|^2 + \|Z_x(x,t)\|_{L^2}^2\right)\mathrm{d}x \\
&\leq c_1 e^{-\alpha t}\left(\int_0^L \left(\|Z_0(x)\|_{L^2}^2 + |X_0|^2 + \|\partial_x Z(x,0)\|_{L^2}^2\right)\mathrm{d}x\right) + b_1\int_0^t \dot{\tilde{p}}^{e\top}(s)\dot{\tilde{p}}^e(s)\,\mathrm{d}s, \quad (4.60)
\end{aligned}$$

completing the proof of Theorem 4.1. □

Based on the invertibility of backstepping transformation, it can be shown that the H^1 norm of the system (4.29)-(4.32) is equivalent to the H^1 norm of the system (4.25)-(4.26). Thus, the exponential stability of the H^1 norm of the system (4.29)-(4.32) implies the corresponding one for the H^1 norm of the system (4.25)-(4.26).

4.2.2 Control law

Take time derivative and spatial derivative on (4.27) and (4.28), and substitute them into (4.29)-(4.32) to get the following equations of the kernels G^1 and G^2, for all $(x,\xi)\in\mathbb{T}$,

$$\Lambda^-(x)\partial_x G^1(x,\xi)-\partial_\xi G^1(x,\xi)\Lambda^+(\xi)=G^1(x,\xi)\left((\Lambda^+)'(\xi)+\Sigma^{++}(\xi)\right)+G^2(x,\xi)\Sigma^{-+}(\xi), \quad (4.61)$$
$$\Lambda^-(x)\partial_x G^2(x,\xi)+\partial_\xi G^2(x,\xi)\Lambda^-(\xi)=G^2(x,\xi)\left(-(\Lambda^-)'(\xi)+\Sigma^{--}(\xi)\right)+G^1(x,\xi)\Sigma^{+-}(\xi), \quad (4.62)$$

with the boundary conditions

$$G^1(x,x)\Lambda^+(x)+\Lambda^-(x)G^1(x,x)=\Sigma^{-+}(x), \quad (4.63)$$
$$G^2(x,x)\Lambda^-(x)-\Lambda^-(x)G^2(x,x)=-\Sigma^{--}(x), \quad (4.64)$$
$$G^1(x,L)\Lambda^+(L)-G^2(x,L)\Lambda^-(L)\Gamma_3=K_1(x). \quad (4.65)$$

These equations are under-determined, and to ensure well-posedness, the additional boundary conditions are added,

$$G^2_{ij}(0,\xi)=g^2_{ij}(\xi), \quad 1\le j<i\le 2N-m, \quad (4.66)$$

for some arbitrary functions $g^2_{ij}, 1\le j<i\le 2N-m$.

There is a matrix $\overline{\Theta}\in\mathbb{R}^{2N-m\times m}$ such that $\overline{\Theta}\Gamma_2\Theta$ is invertible, then we deduce, from (4.26), (4.27), (4.28), (4.31), (4.32), the following controller defined as, for all $t\in[0,\infty)$,

$$\begin{aligned}U^e(t)=&(\overline{\Theta}\Gamma_2\Theta)^{-1}\overline{\Theta}\int_0^t\left(K^e_{I11}R^+(L,\sigma)+K^e_{I12}R^-(0,\sigma)\right)\mathrm{d}\sigma\\&-(\overline{\Theta}\Gamma_2\Theta)^{-1}\overline{\Theta}K^e_{I12}\int_0^t\int_0^L\left(G^1(0,\xi)R^+(\xi,\sigma)+G^2(0,\xi)R^-(\xi,\sigma)\right)\mathrm{d}\xi\,\mathrm{d}\sigma\\&-(\overline{\Theta}\Gamma_2\Theta)^{-1}\overline{\Theta}\Gamma_1\int_0^L\left(G^1(0,\xi)R^+(\xi,t)+G^2(0,\xi)R^-(\xi,t)\right)\mathrm{d}\xi. \quad (4.67)\end{aligned}$$

Due to the dependence of U on the parameter Γ_2 and the inclusion of the parameter Γ_2 in the coefficient matrix Γ_0, Γ_0 has an effect on U, and thus has an impact on the iISS of the system (4.25)-(4.26). Under the assumptions of Theorem 4.1, the target system (4.29)-(4.32) is integral input-to-state stable. Thus, using the invertibility of backstepping transformation, the original system (4.25), (4.26) is integral input-to-state stable in the H^1-norm with the control law (4.67).

4.3 Conclusion

The robust control problem was studied to stabilize the heterogeneous linearized AR traffic flow system with a bottleneck at the outlet boundary. A controller was designed to reject disturbance by using backstepping.

Inspired by [Cor+13], the $\mathbf{H}^2$ locally iISS is studied for the heterogeneous quasi-linear AR traffic flow system in the next chapter.

Chapter 5

Control of heterogeneous quasi-linear traffic with bottleneck

Contents

In this chapter, we investigate the problem of boundary stabilization for a heterogeneous $2N \times 2N$ quasilinear traffic flow system with disturbances in the congested regime. The H^2 integral input-to-state stability of a multi-type traffic flow system described by $2N \times 2N$ first-order quasilinear hyperbolic partial differential equations is obtained in a closed loop with a boundary controller. The control input at the inlet boundary of the considered road section is designed for the linearized system by using the backstepping method. Making use of the backstepping transformation, the H^2 integral input-to-state stability of the quasilinear system is derived by mapping the transformed quasilinear system into an H^2 integral input-to-state stable target system for which a strict Lyapunov function is constructed.

This chapter has been submitted for publication in [GZP22].

5.1 Multi-type quasi-linear hyperbolic traffic flow system and problem statement

5.1.1 Multi-type quasi-linear traffic model

The introduced multi-type traffic flow model (4.8) that represents the dynamics of a heterogeneous traffic on a road segment with road length L and the number of vehicle types N is rewritten as the following quasi-linear form, for all $x \in [0, L]$, $t \in [0, \infty)$,

$$\partial_t \widetilde{u}^e(x,t) + \widetilde{F}(\widetilde{u}^e, u^*)\partial_x \widetilde{u}^e(x,t) = \widetilde{G}(\widetilde{u}^e, u^*)\widetilde{u}^e(x,t), \tag{5.1}$$

where

$$\widetilde{F}(\widetilde{u}^e, u^*) = \begin{bmatrix} \widetilde{F}_{11}(\widetilde{u}^e, u^*) & \widetilde{F}_{12}(\widetilde{u}^e, u^*) & \cdots & \widetilde{F}_{1N}(\widetilde{u}^e, u^*) \\ \widetilde{F}_{21}(\widetilde{u}^e, u^*) & \widetilde{F}_{22}(\widetilde{u}^e, u^*) & \cdots & \widetilde{F}_{2N}(\widetilde{u}^e, u^*) \\ \vdots & \vdots & \ddots & \vdots \\ \widetilde{F}_{N1}(\widetilde{u}^e, u^*) & \widetilde{F}_{N2}(\widetilde{u}^e, u^*) & \cdots & \widetilde{F}_{NN}(\widetilde{u}^e, u^*) \end{bmatrix},$$

with for $i, j = 1, 2, \cdots, N$,

$$\widetilde{F}_{ij}(\widetilde{u}, u^*) = \begin{cases} \begin{bmatrix} \widetilde{v}_i + v_i^* & \widetilde{\rho}_i + \rho_i^* \\ 0 & \widetilde{v}_i + v_i^* - (\widetilde{\rho}_i + \rho_i^*)\delta_{ii}(\rho) \end{bmatrix}, & \text{if } j = i, \\ \begin{bmatrix} 0 & 0 \\ ((\widetilde{v}_i + v_i^*) - (\widetilde{v}_j + v_j^*))\delta_{ij}(\rho) & -(\widetilde{\rho}_j + \rho_j^*)\delta_{ij}(\rho) \end{bmatrix}, & \text{if } j \neq i, \end{cases}$$

and

$$\widetilde{G}(\widetilde{u}^e, u^*) = \begin{bmatrix} \widetilde{G}_{11}(\widetilde{u}^e, u^*) & \widetilde{G}_{12}(\widetilde{u}^e, u^*) & \cdots & \widetilde{G}_{1N}(\widetilde{u}^e, u^*) \\ \widetilde{G}_{21}(\widetilde{u}^e, u^*) & \widetilde{G}_{22}(\widetilde{u}^e, u^*) & \cdots & \widetilde{G}_{2N}(\widetilde{u}^e, u^*) \\ \vdots & \vdots & \ddots & \vdots \\ \widetilde{G}_{N1}(\widetilde{u}^e, u^*) & \widetilde{G}_{N2}(\widetilde{u}^e, u^*) & \cdots & \widetilde{G}_{NN}(\widetilde{u}^e, u^*) \end{bmatrix},$$

with for $i, j = 1, 2, \ldots, N$, $\widetilde{G}_{ij}$ is defined as

$$\widetilde{G}_{ij}(\widetilde{u}^e, u^*) = \begin{cases} \begin{bmatrix} v_i^{*\prime} & \rho_i^{*\prime} \\ \frac{1}{\tau_i}\delta_{ii}(\rho^*) + v_i^* \sum_{k=1}^N \sigma_{iki}(\rho^*)\rho_k^{*\prime} - \delta_{ii}(\rho)v_i^{*\prime} & \frac{1}{\tau_i} + v_i^{*\prime} + \sum_{k=1, k\neq i}^N \delta_{ik}(\rho^*)\rho_k^{*\prime} \end{bmatrix}, & \text{if } j = i, \\ \begin{bmatrix} 0 & 0 \\ \frac{1}{\tau_i}\delta_{ij}(\rho^*) + v_i^* \sum_{k=1}^N \sigma_{ikj}(\rho^*)\rho_k^{*\prime} - \delta_{ij}(\rho)v_j^{*\prime} & -\delta_{ij}(\rho)\rho_j^{*\prime} \end{bmatrix}, & \text{if } j \neq i, \end{cases}$$

The hyperbolicity of the system (5.1) exists around zero equilibrium on the basis of the discussion in Chapter 4, because for all $u^* \in C^2([0, L]; \mathbb{R}^{2N})$, as $\widetilde{u} \to 0$, $F(\widetilde{u}, u^*) \to F(0, u^*)$ which has $2N$ real distinct nonzero eigenvalues $\lambda_1 > \lambda_2 > \cdots > \lambda_m > 0 > -\lambda_{m+1} > \cdots > -\lambda_{2N}$ ($\lambda_i \in C^2([0, L]; \mathbb{R}_{>0})$, $i = 1, \ldots, 2N$, with the number of positive eigenvalues m ($0 \leq m < 2N$)). We will study the scenarios $2N - m \geq 1$ in the H^2 sense in this chapter.

5.1.2 Problem statement

The motivation of control is to alleviate the congested traffic on a road segment, with disturbances at the inlet boundary, in the presence of constant density and velocity drop in the downstream boundary. The diagram of the control model is presented in Figure 4.1. The problem is equivalent to computing the boundary control U^e in the space H^2 such that system (5.1) converges to zero equilibrium, with the following boundary conditions, for all $t \in [0, \infty)$,

$$A_1 \widetilde{u}^e(0, t) = \bar{p}^e(t) + \Theta U^e(t) - \Pi_{NL}(\widetilde{u}^e(0, t)), \tag{5.2}$$

$$B_1 \widetilde{u}^e(L, t) = 0, \tag{5.3}$$

where

$$\Pi_{NL}(\widetilde{u}^e(0, t)) = \left[\widetilde{\rho}_1(0, t)\widetilde{v}_1(0, t), \ldots, \widetilde{\rho}_N(0, t)\widetilde{v}_N(0, t)\right]^\top \in C^2([0, \infty); \mathbb{R}^N).$$

The well-posedness of the closed-loop system (5.1), (5.2)-(5.3) in the H^2 space holds under a necessary condition that the initial conditions $\widetilde{u}^e(\cdot,0)=\widetilde{u}_0^e(\cdot)\in H^2([0,L];\mathbb{R}^{2N})$ satisfy the following second-order compatibility conditions,

$$A_1\widetilde{u}_0^e(0)=\bar{p}^e(0)+\Theta U^e(0)-\Pi_{NL}(\widetilde{u}_0^e(0)), \tag{5.4}$$
$$B_1\widetilde{u}_0^e(L)=0, \tag{5.5}$$
$$\begin{aligned}&A_1\left(-\widetilde{F}(\widetilde{u}_0^e(0),u^*(0))\widetilde{u}_0^{e\prime}(0)+\widetilde{G}(\widetilde{u}_0^e(0),u^*(0))\widetilde{u}_0^e(0)\right)\\&=\dot{\bar{p}}^e(0)+\Theta\dot{U}^e(0)-\left.\frac{\mathrm{d}\Pi_{NL}}{\mathrm{d}\widetilde{u}^e}\right|_{t=0}\left(-\widetilde{F}(\widetilde{u}_0^e(0),u^*(0))\widetilde{u}_0^{e\prime}(0)+\widetilde{G}(\widetilde{u}_0^e(0),u^*(0))\widetilde{u}_0^e(0)\right),\end{aligned} \tag{5.6}$$
$$B_1\widetilde{F}(\widetilde{u}_0^e(L),u^*(L))\widetilde{u}_0^{e\prime}(L)=B_1\widetilde{G}(\widetilde{u}_0^e(L),u^*(L))\widetilde{u}_0^e(L). \tag{5.7}$$

In the compatibility conditions, (5.5) and (5.7) naturally derived from the physical meaning, but (5.4) and (5.6) are artificially derived from the designed feedback control law and they rigorously require the specific values of the initial conditions. Keeping the effect of stabilization of the control law, a modification of the control law is done in the boundary conditions (5.2)-(5.3), so that there is no requirement of any specific values on the initial conditions. More precisely, inspired by [Cor+13], the modified boundary conditions extend the controller as follows: for all $t\in[0,\infty)$,

$$A_1\widetilde{u}^e(0,t)=\bar{p}^e(t)+\Theta U^e(t)+w_1(t)+w_2(t)-\Pi_{NL}(\widetilde{u}^e(0,t)), \tag{5.8}$$
$$B_1\widetilde{u}^e(L,t)=0, \tag{5.9}$$

where $w_1,w_2\in C^1([0,\infty);\mathbb{R}^N)$ are the solutions of the following system:

$$\dot{w}_1=-d_1w_1,\qquad \dot{w}_2=-d_2w_2, \tag{5.10}$$

with the positive constants d_1,d_2 ($d_1\neq d_2$). Under the modification of the control law, we can obtain the following compatibility conditions,

$$A_1\widetilde{u}_0^e(0)=\bar{p}^e(0)+\Theta U^e(0)+w_1(0)+w_2(0)-\Pi_{NL}(\widetilde{u}_0^e(0)), \tag{5.11}$$
$$B_1\widetilde{u}_0^e(L)=0, \tag{5.12}$$
$$\begin{aligned}&A_1\left(-\widetilde{F}(\widetilde{u}_0^e(0),u^*(0))\widetilde{u}_0^{e\prime}(0)+\widetilde{G}(\widetilde{u}_0^e(0),u^*(0))\widetilde{u}_0^e(0)\right)\\&=\dot{\bar{p}}^e(0)+\Theta\dot{U}^e(0)+(-d_1w_1(0)-d_2w_2(0))-\left.\frac{\mathrm{d}\Pi_{NL}}{\mathrm{d}\widetilde{u}^e}\right|_{t=0}\\&\times\left(-\widetilde{F}(\widetilde{u}_0^e(0),u^*(0))\widetilde{u}_0^{e\prime}(0)+\widetilde{G}(\widetilde{u}_0^e(0),u^*(0))\widetilde{u}_0^e(0)\right),\end{aligned} \tag{5.13}$$
$$B_1\widetilde{F}(\widetilde{u}_0^e(L),u^*(L))\widetilde{u}_0^{e\prime}(L)=B_1\widetilde{G}(\widetilde{u}_0^e(L),u^*(L))\widetilde{u}_0^e(L). \tag{5.14}$$

For the purpose of eliminating the compatibility conditions (5.4) and (5.6), the following initial conditions of w_1, w_2 are selected,

$$w_1(0)+w_2(0)=g_1(\widetilde{u}_0^e), \tag{5.15}$$
$$-(d_1w_1(0)+d_2w_2(0))=g_2(\widetilde{u}_0^e), \tag{5.16}$$

with

$$g_1(\widetilde{u}_0^e)=A_1\widetilde{u}_0^e(0)-\bar{p}^e(0)-\Theta U^e(0)+\Pi_{NL}(\widetilde{u}_0^e(0)), \tag{5.17}$$
$$\begin{aligned}g_2(\widetilde{u}_0^e)&=A_1\left(-\widetilde{F}(\widetilde{u}_0^e(0),u^*(0))\widetilde{u}_0^{e\prime}(0)+\widetilde{G}(\widetilde{u}_0^e(0),u^*(0))\widetilde{u}_0^e(0)\right)\\&-\dot{\bar{p}}^e(0)-\Theta\dot{U}^e(0)+\left.\frac{\mathrm{d}\Pi_{NL}}{\mathrm{d}\widetilde{u}^e}\right|_{t=0}\left(-\widetilde{F}(\widetilde{u}_0^e(0),u^*(0))\widetilde{u}_0^{e\prime}(0)+\widetilde{G}(\widetilde{u}_0^e(0),u^*(0))\widetilde{u}_0^e(0)\right).\end{aligned} \tag{5.18}$$

Select

$$w_1(0) = -\frac{g_2(\widetilde{u}_0^e) + d_2 g_1(\widetilde{u}_0^e)}{d_1 - d_2}, \tag{5.19}$$

$$w_2(0) = \frac{d_1 g_1(\widetilde{u}_0^e) + g_2(\widetilde{u}_0^e)}{d_1 - d_2}, \tag{5.20}$$

to verify the compatibility conditions (5.4) and (5.6).

5.1.3 State transformations

For deriving the form of characteristic values of the quasi-linear system (5.1), (5.8)-(5.9), (5.10) and making the analysis easier (the main diagonal elements in the matrix of source term are all zero), we handle a transformation for the state $\widetilde{u}^e$. Defining an invertible transformation $\bar{R}(x,t) = \Phi(x)\widetilde{u}^e(x,t)$, $\Phi(x) = \Psi(x)T^{-1}(x)$ with $x \in [0,L]$, $t \in [0,\infty)$, from $\widetilde{u}^e$ to the new variables $\bar{R} = (\bar{R}^+, \bar{R}^-)^\top : [0,L]\times[0,\infty) \to \mathbb{R}^{2N}$ with $\bar{R}^+ : [0,L]\times[0,\infty) \to \mathbb{R}^m$, $\bar{R}^- : [0,L]\times[0,\infty) \to \mathbb{R}^{2N-m}$, $\bar{R}_{in}(t) = (\bar{R}^+(0,t), \bar{R}^-(L,t))^\top$, $\bar{R}_{out}(t) = (\bar{R}^+(L,t), \bar{R}^-(0,t))^\top$, the system (5.1), (5.8)-(5.9), (5.10) is mapped into the following simplified system, for all $x \in [0,L]$, $t \in [0,\infty)$,

$$\partial_t \bar{R}(x,t) + \Lambda^e(x)\partial_x \bar{R}(x,t) - \Sigma(x)\bar{R}(x,t) + \Lambda_{NL}(\bar{R},x)\partial_x \bar{R}(x,t) = \Sigma_{NL}(\bar{R},x)\bar{R}(x,t), \tag{5.21}$$

$$\bar{R}_{in}(t) = K_P^e \bar{R}_{out}(t) + \Gamma_0\Big(\bar{p}^e(t) + \Theta U^e(t)\Big) + \Gamma_0(w_1(t) + w_2(t)) - \Gamma_0 \Pi_{NL}(\Phi^{-1}(0)\bar{R}(0,t)), \tag{5.22}$$

where

$$\Lambda^e(x) = \bar{\Lambda}^e(0,x), \qquad \Sigma(x) = \bar{\Sigma}(0,x),$$
$$\Lambda_{NL}(\bar{R},x) = \bar{\Lambda}^e(\bar{R},x) - \Lambda^e(x), \qquad \Sigma_{NL}(\bar{R},x) = \bar{\Sigma}(\bar{R},x) - \Sigma(x),$$

with

$$\bar{\Lambda}^e(\bar{R},x) = \Phi(x)\widetilde{F}\left(\Phi^{-1}(x)\bar{R}, u^*\right)\Phi^{-1}(x),$$
$$\bar{\Sigma}(\bar{R},x) = \Phi(x)\widetilde{G}\left(\Phi^{-1}(x)\bar{R}, u^*\right)\Phi^{-1}(x) - \Phi(x)\widetilde{F}\left(\Phi^{-1}(x)\bar{R}, u^*\right)\Phi^{-1}(x)',$$

the main diagonal elements of matrix $\Sigma \in C^2([0,L];\mathbb{R}^{2N\times 2N}(\mathbb{R}))$ are zeros. The well-posedness of the system (5.21)-(5.22) in the H^2 space is under a necessary condition that the initial condition $\bar{R}(\cdot,0) = \bar{R}_0(\cdot) \in H^2([0,L];\mathbb{R}^{2N})$ satisfies the following second-order compatibility condition,

$$\bar{R}_{in}(0) = K_P^e \bar{R}_{out}(0) + \Gamma_0\left(\bar{p}^e(0) + \Theta U^e(0)\right) + \Gamma_0(w_1(0) + w_2(0)) - \Gamma_0\Pi_{NL}(\Phi^{-1}(0)\bar{R}_0(0)), \tag{5.23}$$

$$\begin{aligned}
&\left([M_i^1]_{1\le i\le m}, [M_j^2]_{m+1\le j\le 2N}\right)^\top \\
=&K_P^e\left([M_i^2]_{1\le i\le m}, [M_j^1]_{m+1\le j\le 2N}\right)^\top + \Gamma_0\left(\dot{\bar{p}}^e(0) + \Theta\dot{U}^e(0)\right) \\
&+ \Gamma_0(-d_1 w_1(0) - d_2 w_2(0)) - \Gamma_0 \frac{\mathrm{d}\Pi_{NL}}{\mathrm{d}\widetilde{u}^e}(\Phi^{-1}(0))\Big|_{t=0} \\
&\times \Phi^{-1}(0)\Big(-\left(\Lambda^e(0) + \Lambda_{NL}(\bar{R}_0(0),0)\right)\bar{R}_0'(0) + \left(\Sigma(0) + \Sigma_{NL}(\bar{R}_0(0),0)\right)\bar{R}_0(0)\Big),
\end{aligned} \tag{5.24}$$

with

$$M^1 = -\left(\Lambda^e(0) + \Lambda_{NL}(\bar{R}_0(0),0)\right)\bar{R}_0'(0) + \left(\Sigma(0) + \Sigma_{NL}(\bar{R}_0(0),0)\right)\bar{R}_0(0),$$
$$M^2 = -\left(\Lambda^e(L) + \Lambda_{NL}(\bar{R}_0(L),L)\right)\bar{R}_0'(L) + \left(\Sigma(L) + \Sigma_{NL}(\bar{R}_0(L),L)\right)\bar{R}_0(L).$$

Since for $x \in [0,L]$, $\Lambda_{NL}(0,x) = 0$, $\Sigma_{NL}(0,x) = 0$ and $\Pi_{NL}(0) = \frac{\mathrm{d}\Pi_{NL}}{\mathrm{d}\widetilde{u}^e}(0) = 0$, then 0 is a equilibrium of the quasi-linear system (5.21)-(5.22). For the sake of conveniently analyzing the applicability of the designed controller for the linearized system, the quasi-linear system (5.21)-(5.22) is written as the linear part plus the nonlinear terms, done in the next section.

5.2 Local iISS of quasi-linear model

Inspired by [Cor+13], the problem of local H^2 iISS of the first-order hyperbolic quasi-linear system (4.8) is studied in this section. We will show that the controller derived for the linearized system by using the backstepping method locally stabilizes this quasi-linear system.

Concerning the linearized system (4.25), (4.26), the designed control law U^e is derived by using the following backstepping transformation, for all $x \in [0, L]$, $t \in [0, \infty)$,

$$Z(x,t) = R(x,t) - \int_x^L K(x,\xi)R(\xi,t)\,\mathrm{d}\xi = \mathcal{K}[R], \tag{5.25}$$

where $K(x,\xi) = \begin{bmatrix} 0 & 0 \\ G^1(x,\xi) & G^2(x,\xi) \end{bmatrix}$, with piecewise differentiable G^1 and G^2 defined on the domain $\mathbb{T} = \{(x,\xi) \in \mathbb{R}^2 | \, 0 \le x \le \xi \le L\}$ as in Chapter 4.

The corresponding iISS target system is, for all $x \in [0, L]$, $t \in [0, \infty)$,

$$\partial_t Z(x,t) + \Lambda^e(x)\partial_x Z(x,t) = \Sigma_1(x)Z(x,t) + \int_x^L C_1(x,\xi)Z(\xi,t)\,\mathrm{d}\xi + k_1(x)Z_{out}(t), \tag{5.26}$$

$$Z_{in}(t) = K_P^e Z_{out}(t) + K_I^e \int_0^t Z_{out}(\sigma)\,\mathrm{d}\sigma + \Gamma_0 \bar{p}^e(t), \tag{5.27}$$

where $Z = (Z^+, Z^-)^\top$, with $Z^+ : [0, L] \times [0, \infty) \to \mathbb{R}^m$, $Z^- : [0, L] \times [0, \infty) \to \mathbb{R}^{2N-m}$, $Z_{in}(t) = (Z^+(0,t), Z^-(L,t))^\top$, $Z_{out}(t) = (Z^+(L,t), Z^-(0,t))^\top$, the matrices Σ_1, C_1 and K_I^e are given as in Chapter 4. The controller for the linearized system (4.25), (4.26) is derived as follows, for all $t \in (0, \infty)$,

$$\begin{aligned} U^e(R) = {} & (\overline{\Theta}\Gamma_2\Theta)^{-1}\overline{\Theta} \int_0^t \left(KI_{11}^e R^+(L,\sigma) + KI_{12}^e R^-(0,\sigma)\right)\,\mathrm{d}\sigma \\ & - (\overline{\Theta}\Gamma_2\Theta)^{-1}\overline{\Theta}KI_{12}^e \int_0^t \int_0^L \left[G^1(0,\xi)R^+(\xi,\sigma) + G^2(0,\xi)R^-(\xi,\sigma)\right]\mathrm{d}\xi\,\mathrm{d}\sigma \\ & - (\overline{\Theta}\Gamma_2\Theta)^{-1}\overline{\Theta}\Gamma_1 \int_0^L \left[G^1(0,\xi)R^+(\xi,t) + G^2(0,\xi)R^-(\xi,t)\right]\mathrm{d}\xi, \end{aligned} \tag{5.28}$$

where the coefficient matrices Γ_1, Γ_2 are given, and the matrix $\overline{\Theta}$ is in $\mathbb{R}^{2N-m\times m}$ and such that $\overline{\Theta}\Gamma_2\Theta$ is invertible. So the controller in terms of the original variable $\widetilde{u}^e$ in (5.8) is, for all $t \in (0, \infty)$,

$$\begin{aligned} U^e(t) = {} & (\overline{\Theta}\Gamma_2\Theta)^{-1}\overline{\Theta} \int_0^t \left(\begin{bmatrix} KI_{11}^e & 0 \end{bmatrix}\Phi(L)\widetilde{u}^e(L,\sigma) + \begin{bmatrix} 0 & KI_{12}^e \end{bmatrix}\Phi(0)\widetilde{u}^e(0,\sigma)\right)\mathrm{d}\sigma \\ & - (\overline{\Theta}\Gamma_2\Theta)^{-1}\overline{\Theta}KI_{12}^e \int_0^t \int_0^L \begin{bmatrix} G^1(0,\xi) & G^2(0,\xi) \end{bmatrix}\Phi(\xi)\widetilde{u}^e(\xi,\sigma)\,\mathrm{d}\xi\,\mathrm{d}\sigma \\ & - (\overline{\Theta}\Gamma_2\Theta)^{-1}\overline{\Theta}\Gamma_1 \int_0^L \begin{bmatrix} G^1(0,\xi) & G^2(0,\xi) \end{bmatrix}\Phi(\xi)\widetilde{u}^e(\xi,t)\,\mathrm{d}\xi. \end{aligned} \tag{5.29}$$

The formula of control law U^e in (5.28) for the linearized system (4.25), (4.26) is derived by using backstepping method and the proof of iISS of the corresponding target system (5.26)-(5.27) is obtained in Chapter 4. In this chapter, we derive the iISS of the quasi-linear system (5.1), (5.8)-(5.9), (5.10) with the state feedback law (5.29) as follows:

Theorem 5.1
Considering the system (5.1), (5.10) with the extended boundary conditions (5.8)-(5.9), the initial

conditions $\widetilde{u}_0^e \in H^2([0,L];\mathbb{R}^{2N})$, $w_1(0), w_2(0) \in \mathbb{R}^N$ *verifying (5.19)-(5.20), and the control law (5.29). Then, for every* $\alpha > 0$, *there exist positive constants* δ, c, b *such that, for any* $\bar{p}^e$ *satisfying* $\dot{\bar{p}}^e \in C^1[0,\infty)$, $\ddot{\bar{p}}^e \in C^0[0,\infty)$, *if* $\|\widetilde{u}_0^e\|_{H^2} \leq \delta$, *it holds that for all* $t \in [0,\infty)$,

$$\begin{aligned}&\|\widetilde{u}^e(\cdot,t)\|_{H^2}^2 + |w_1(t)|^2 + |w_2(t)|^2\\ &\leq ce^{-\alpha t}\big(\|\widetilde{u}_0^e\|_{H^2}^2 + |w_1(0)|^2 + |w_2(0)|^2\big) + b\int_0^t (|\dot{\bar{p}}^e(s)|^2 + |\ddot{\bar{p}}^e(s)|^2)\,\mathrm{d}s. \end{aligned} \tag{5.30}$$

Proof. As a result of the invertible transformation $\Phi(x)$, $x \in [0,L]$, the system (5.1), (5.8)-(5.9), (5.10) has the same dynamical behavior as the system (5.21)-(5.22). Therefore, in order to prove the iISS of the quasi-linear system (5.1), (5.8)-(5.9), (5.10), we firstly prove the iISS of the quasi-linear system (5.21)-(5.22) after applying the control law U^e in (5.28), which is designed for the linearized system (4.25), (4.26). The quasi-linear system (5.21)-(5.22) is mapped into a target system $\bar{Z}$ by using the direct transformation $\bar{Z} = \mathcal{K}[\bar{R}]$ and the inverse transformation $\bar{R} = \mathcal{L}[\bar{Z}]$ with $C^2(\mathbb{T})$ kernel functions. Differentiating twice with respect to x in these transformations, it is shown that the H^2 norm of $\bar{Z}$ is equivalent to the H^2 norm of $\bar{R}$. So local iISS of the system (5.21)-(5.22) is the same as the local iISS of the target system. The equations of the target system $\bar{Z}$ is, for all $x \in [0,L]$, $t \in [0,\infty)$,

$$\begin{aligned}&\partial_t \bar{Z}(x,t) + \Lambda^e(x)\partial_x \bar{Z}(x,t) = \Sigma_1(x)\bar{Z}(x,t)\\ &\qquad + \int_x^L C_1(x,\xi)\bar{Z}(\xi,t)\,\mathrm{d}\xi + k_1(x)\bar{Z}_{out}(t) + F_3[\bar{Z},\partial_x\bar{Z}] + F_4[\bar{Z},\bar{Z}_{out}],\end{aligned} \tag{5.31}$$

$$\bar{Z}_{in}(t) = K_P^e \bar{Z}_{out}(t) + \bar{X}(t) + \Gamma_0(w_1(t) + w_2(t)), \tag{5.32}$$

$$\bar{X}(t) = K_I^e \int_0^t \bar{Z}_{out}(\sigma)\,\mathrm{d}\sigma + \Gamma_0\Big(\bar{p}^e(t) - \bar{\Pi}_{NL}(\bar{Z}(0,t))\Big), \tag{5.33}$$

where

$$\begin{aligned}&F_3[\bar{Z},\partial_x\bar{Z}] = -\mathcal{K}[\big(\Lambda^e(x) + F_1[\bar{Z}]\big)\,\partial_x\bar{Z}] + \Lambda^e(x)\partial_x\bar{Z},\\ &F_4[\bar{Z},\bar{Z}_{out}] = -\mathcal{K}_{12}[\bar{Z},\bar{Z}_{out}] - \mathcal{K}[\big(\Lambda^e(x) + F_1[\bar{Z}]\big)\,\mathcal{K}_1[\mathcal{L}[\bar{Z}]] + \Sigma(x)\mathcal{L}[\bar{Z}] + F_2[\bar{Z}]\mathcal{L}[\bar{Z}]],\\ &\bar{\Pi}_{NL}(\bar{Z}(0,t)) = \Pi_{NL}(\Phi^{-1}(0)\bar{R}(0,t)),\\ &\mathcal{K}_{12}[\bar{Z},\bar{Z}_{out}] = \Sigma_1(x)\bar{Z}(x,t) + \int_x^L C_1(x,\xi)\bar{Z}(\xi,t)\,\mathrm{d}\xi + k_1(x)\bar{Z}_{out}(t),\\ &\mathcal{K}_1[\bar{Z}] = \int_x^L \partial_x K(x,\xi)\bar{Z}(\xi,t)\,\mathrm{d}\xi - K(x,x)\bar{Z}(x,t),\\ &F_1[\bar{Z}] = \Lambda_{NL}(\mathcal{L}[\bar{Z}],x),\\ &F_2[\bar{Z}] = \Sigma_{NL}(\mathcal{L}[\bar{Z}],x),\end{aligned}$$

with $\bar{Z} = (\bar{Z}^+,\bar{Z}^-)^\top$, $\bar{Z}^+ : [0,L]\times[0,\infty) \to \mathbb{R}^m$, $\bar{Z}^- : [0,L]\times[0,\infty) \to \mathbb{R}^{2N-m}$, $\bar{Z}_{in}(t) = (\bar{Z}^+(0,t), \bar{Z}^-(L,t))^\top$, $\bar{Z}_{out}(t) = (\bar{Z}^+(L,t), \bar{Z}^-(0,t))^\top$. Next, the local stability of the system (5.31)-(5.33) in the space H^2 is analyzed by using the Lyapunov approach. It includes analyzing the growth of $\|\bar{Z}\|_{L^2}$, $\|\eta\|_{L^2}$ and $\|\zeta\|_{L^2}$ (by definition $\eta = \partial_t\bar{Z}$ and $\zeta = \partial_{tt}\bar{Z}$). Remark that in order to directly use the iISS analysis results of the target system (4.46)-(4.47) in Chapter 4, the equations of $\bar{Z}$ and η are written as the same structure as the equations of the target system

(4.46)-(4.47). From system (5.31)-(5.33), we derive, for all $x \in [0, L]$, $t \in [0, \infty)$,

$$\begin{aligned}
&\partial_t \eta(x,t) = -\Lambda^e(x)\partial_x \eta(x,t) + \Sigma_1(x)\eta(x,t) \\
&+ \int_x^L C_1(x,\xi)\eta(\xi,t)\,\mathrm{d}\xi + k_1(x)\dot{\bar{Z}}_{out}(t) + F_5[\bar{Z}, \partial_x\eta] + F_6[\bar{Z}, \eta, \partial_x\bar{Z}, \dot{\bar{Z}}_{out}], \qquad (5.34)\\
&\eta_{in}(t) = K_P^e \eta_{out}(t) + \dot{\bar{X}}(t) + \Gamma_0(-d_1 w_1(t) - d_2 w_2(t)), \qquad (5.35)\\
&\dot{\bar{X}}(t) = K_I^e \bar{Z}_{out}(t) + \Gamma_0\Big(\dot{\bar{p}}^e(t) - \frac{\mathrm{d}\Pi_{NL}}{\mathrm{d}\bar{Z}}(\bar{Z}(0,t))\eta(0,t)\Big), \qquad (5.36)
\end{aligned}$$

where

$$\begin{aligned}
&F_5[\bar{Z}, \partial_x\eta] = \mathcal{K}[(\Lambda^e(x) + F_1[\bar{Z}])\partial_x\eta] + \Lambda^e(x)\partial_x\eta,\\
&F_6[\bar{Z}, \eta, \partial_x\bar{Z}, \dot{\bar{Z}}_{out}] = \mathcal{K}[\big(\Lambda^e(x) + F_1[\bar{Z}]\big)\,\mathcal{K}_1[\mathcal{L}[\eta]] - \Sigma(x)\mathcal{L}[\eta]\\
&- F_2[\bar{Z}]\mathcal{L}[\eta] + F_{12}[\eta](\partial_x\bar{Z} + \mathcal{K}_1[\mathcal{L}[\bar{Z}]]) - F_{22}[\eta]\mathcal{L}[\bar{Z}]] - \mathcal{K}_{12}[\eta, \dot{\bar{Z}}_{out}],\\
&F_{12}[\eta] = \dot{F}_1[\bar{Z}],\\
&F_{22}[\eta] = \dot{F}_2[\bar{Z}].
\end{aligned}$$

The following Lyapunov function candidate is introduced for the stability analysis of system (5.31)-(5.33), for all $x \in [0, L]$, $t \in [0, \infty)$, $\bar{V}^e\left(\bar{Z}(x,t), \bar{X}(t), \eta(x,t), \zeta(x,t)\right) = \bar{V}_1^e + \bar{V}_2^e + \bar{V}_3^e$, where

$$\begin{aligned}
\bar{V}_1^e = \int_0^L &\Big(\bar{Z}^\top(x,\cdot)\bar{\mathcal{P}}_{11}(x)\bar{Z}(x,\cdot) + \bar{Z}^\top(x,\cdot)\bar{\mathcal{P}}_{12}(x)\bar{X}(\cdot)\\
&+ \bar{X}^\top(\cdot)\bar{\mathcal{P}}_{12}^\top(x)\bar{Z}(x,\cdot) + \bar{X}^\top(\cdot)\bar{P}_{22}\bar{X}(\cdot)\Big)\,\mathrm{d}x, \qquad (5.37)\\
\bar{V}_2^e = \int_0^L &\eta^\top(x,\cdot)\bar{\mathcal{P}}_3(x)\eta(x,\cdot)\,\mathrm{d}x, \qquad (5.38)\\
\bar{V}_3^e = \int_0^L &\zeta^\top(x,\cdot)\bar{\mathcal{P}}_4[\bar{Z}](x)\zeta(x,\cdot)\,\mathrm{d}x, \qquad (5.39)
\end{aligned}$$

with

$$\bar{\mathcal{P}}_{11}(x) \triangleq \bar{P}_{11}\mathrm{diag}\left\{e^{-\mu x}I_m, e^{\mu x}I_{2N-m}\right\},$$

$$\bar{\mathcal{P}}_{12}(x) \triangleq \bar{P}_{12}\mathrm{diag}\left\{e^{-\frac{\mu}{2}x}I_m, e^{\frac{\mu}{2}x}I_{2N-m}\right\},$$

$$\bar{\mathcal{P}}_3(x) \triangleq \bar{P}_3\mathrm{diag}\left\{e^{-\mu x}I_m, e^{\mu x}I_{2N-m}\right\},$$

$\bar{\mathcal{P}}_4[\bar{Z}](x)$ is defined in [Cor+13, Lemma 5.2], $\bar{P}_{11}$, $\bar{P}_3$ are $2N \times 2N$ diagonal positive-definite matrices, $\bar{P}_{22}$ is a $2N \times 2N$ symmetric positive-definite matrix, and $\bar{P}_{12}$ is a $2N \times 2N$ matrix.

Take the time derivative of $\bar{V}_1^e$ along the solutions to (5.31)-(5.33), use integration by parts, and define $\dot{\bar{V}}_1^e = \dot{\bar{V}}_{1L}^e + \dot{\bar{V}}_{1NL}^e$, where $\dot{\bar{V}}_{1L}^e$ is the time derivative of $\bar{V}_1^e$ along the linear target system

(5.26)-(5.27), computed as follows

$$
\begin{aligned}
\dot{\bar{V}}^e_{1L} &= -\bar{Z}^\top(x,t)\Lambda^e(x)\bar{\mathcal{P}}_{11}(x)\bar{Z}(x,t)\Big|_0^L + \int_0^L \bar{Z}^\top(x,t)\left(\Lambda^e(x)\bar{\mathcal{P}}_{11}(x)\right)_x \bar{Z}(x,t)\,\mathrm{d}x \\
&- \left(\bar{Z}^\top(x,t)\Lambda^e(x)\bar{\mathcal{P}}_{12}(x)\bar{X}(t) + \bar{X}^\top(t)\bar{\mathcal{P}}_{12}^\top(x)\Lambda^e(x)\bar{Z}(x,t)\right)\Big|_0^L \\
&+ \int_0^L \left(\bar{Z}^\top(x,t)\left(\Lambda^e(x)\bar{\mathcal{P}}_{12}(x)\right)_x \bar{X}(t) + \bar{X}^\top(t)\left(\bar{\mathcal{P}}_{12}^\top(x)\Lambda^e(x)\right)_x \bar{Z}(x,t)\right)\mathrm{d}x \\
&+ \int_0^L \Big(\Big(\Sigma_1(x)\bar{Z}(x,t) + \int_x^L C_1(x,\xi)\bar{Z}(\xi,t)\,\mathrm{d}\xi + k_1(x)\bar{Z}_{out}(t)\Big)^\top(\bar{\mathcal{P}}_{11}(x)\bar{Z}(x,t) + \bar{\mathcal{P}}_{12}(x)\bar{X}(t)) \\
&+ (\bar{Z}^\top(x,t)\bar{\mathcal{P}}_{11}(x) + \bar{X}^\top(t)\bar{\mathcal{P}}_{12}^\top(x))\Big(\Sigma_1(x)\bar{Z}(x,t) + \int_x^L C_1(x,\xi)\bar{Z}(\xi,t)\,\mathrm{d}\xi + k_1(x)\bar{Z}_{out}(t)\Big)\Big)\,\mathrm{d}x \\
&+ \int_0^L \Big((\bar{Z}^\top(x,t)\bar{\mathcal{P}}_{12}(x) + \bar{X}^\top(t)\bar{P}_{22})\Big(K_I^e\bar{Z}_{out}(t) + \Gamma_0\dot{\bar{p}}^e(t)(t)\Big) \\
&+ \Big(K_I^e\bar{Z}_{out}(t) + \Gamma_0\dot{\bar{p}}^e(t)(t)\Big)^\top(\bar{\mathcal{P}}_{12}^\top(x)\bar{Z}(x,t) + \bar{P}_{22}\bar{X}(t))\Big)\,\mathrm{d}x, \qquad (5.40)
\end{aligned}
$$

and where $\dot{\bar{V}}^e_{1NL}$ is defined as:

$$
\begin{aligned}
\dot{\bar{V}}^e_{1NL} &= \int_0^L \Big(\Big(F_3[\bar{Z},\partial_x\bar{Z}] + F_4[\bar{Z},\bar{Z}_{out}]\Big)^\top\bar{\mathcal{P}}_{11}(x)\bar{Z}(x,t) + \bar{Z}^\top(x,t)\bar{\mathcal{P}}_{11}(x)\Big(F_3[\bar{Z},\partial_x\bar{Z}] + F_4[\bar{Z},\bar{Z}_{out}]\Big)\Big)\,\mathrm{d}x \\
&+ \int_0^L \Big(\bar{Z}^\top(x,t)\bar{\mathcal{P}}_{12}(x)\Big(-\Gamma_0\frac{\mathrm{d}\Pi_{NL}}{\mathrm{d}\bar{Z}}(\bar{Z}(0,t))\eta(0,t)\Big) + \Big(-\Gamma_0\frac{\mathrm{d}\Pi_{NL}}{\mathrm{d}\bar{Z}}(\bar{Z}(0,t))\eta(0,t)\Big)^\top\bar{\mathcal{P}}_{12}^\top(x)\bar{Z}(x,t) \\
&+ \Big(F_3[\bar{Z},\partial_x\bar{Z}] + F_4[\bar{Z},\bar{Z}_{out}]\Big)^\top\bar{\mathcal{P}}_{12}(x)\bar{X}(t) + \bar{X}^\top(t)\bar{\mathcal{P}}_{12}^\top(x)\Big(F_3[\bar{Z},\partial_x\bar{Z}] + F_4[\bar{Z},\bar{Z}_{out}]\Big)\Big)\,\mathrm{d}x \\
&+ L\Big(-\Gamma_0\frac{\mathrm{d}\Pi_{NL}}{\mathrm{d}\bar{Z}}(\bar{Z}(0,t))\eta(0,t)\Big)^\top\bar{P}_{22}\bar{X}(t) + L\bar{X}^\top(t)\bar{P}_{22}\Big(-\Gamma_0\frac{\mathrm{d}\Pi_{NL}}{\mathrm{d}\bar{Z}}(\bar{Z}(0,t))\eta(0,t)\Big). \qquad (5.41)
\end{aligned}
$$

Take the time derivative of $\bar{V}_2^e$ along the solutions to (5.31)-(5.33), use integration by parts, and define $\dot{\bar{V}}_2^e = \dot{\bar{V}}_{2L}^e + \dot{\bar{V}}_{2NL}^e$, where $\dot{\bar{V}}_{2L}^e$ is the time derivative of $\bar{V}_2^e$ along the linear target system (5.26)-(5.27), for all $t \in [0,\infty)$,

$$
\begin{aligned}
\dot{\bar{V}}^e_{2L} &= -\eta^\top(x,t)\Lambda^e(x)\bar{\mathcal{P}}_3(x)\eta(x,t)\Big|_0^L + \int_0^L \eta^\top(x,t)\left(\Lambda^e(x)\bar{\mathcal{P}}_3(x)\right)_x \eta(x,t)\,\mathrm{d}x \\
&+ \int_0^L \Big(\Big(\Sigma_1(x)\eta(x,t) + \int_x^L C_1(x,\xi)\eta(\xi,t)\,\mathrm{d}\xi + k_1(x)\dot{\bar{Z}}_{out}(t)\Big)^\top\bar{\mathcal{P}}_3(x)\eta(x,t) \\
&+ \eta^\top(x,t)\bar{\mathcal{P}}_3(x)\Big(\Sigma_1(x)\eta(x,t) + \int_x^L C_1(x,\xi)\eta(\xi,t)\,\mathrm{d}\xi + k_1(x)\dot{\bar{Z}}_{out}(t)\Big)\Big)\,\mathrm{d}x, \qquad (5.42)
\end{aligned}
$$

and where $\dot{\bar{V}}^e_{2NL}$ is defined as: for all $t \in [0,\infty)$,

$$\begin{aligned}
\dot{\bar{V}}^e_{2NL} &= (K^e_P \dot{\bar{Z}}_{out}(t))^\top \bar{E}_1 \bar{P}_3 \Big(-\Gamma_0 \frac{\mathrm{d}\Pi_{NL}}{\mathrm{d}\bar{Z}}(\bar{Z}(0,t))\eta(0,t)\Big) \\
&+ \Big(-\Gamma_0 \frac{\mathrm{d}\Pi_{NL}}{\mathrm{d}\bar{Z}}(\bar{Z}(0,t))\eta(0,t)\Big)^\top \bar{P}_3 \bar{E}_1 (K^e_P \dot{\bar{Z}}_{out}(t)) \\
&+ \Big(K^e_I \bar{Z}_{out}(t) + \Gamma_0 \Big(\dot{\bar{p}}^e(t)(t) - \frac{\mathrm{d}\Pi_{NL}}{\mathrm{d}\bar{Z}}(\bar{Z}(0,t))\eta(0,t)\Big) - \Gamma_0(d_1 w_1(t) + d_2 w_2(t))\Big)^\top \\
&\bar{E}_1 \bar{P}_3 \Big(-\Gamma_0 \frac{\mathrm{d}\Pi_{NL}}{\mathrm{d}\bar{Z}}(\bar{Z}(0,t))\eta(0,t)\Big) \\
&+ \Big(-\Gamma_0 \frac{\mathrm{d}\Pi_{NL}}{\mathrm{d}\bar{Z}}(\bar{Z}(0,t))\eta(0,t)\Big)^\top \bar{E}_1 \bar{P}_3 \Big(K^e_I \bar{Z}_{out}(t) + \Gamma_0 \Big(\dot{\bar{p}}^e(t)(t) - \frac{\mathrm{d}\Pi_{NL}}{\mathrm{d}\bar{Z}}(\bar{Z}(0,t))\eta(0,t)\Big) \\
&- \Gamma_0(d_1 w_1(t) + d_2 w_2(t))\Big) \\
&+ \Big(-\Gamma_0 \frac{\mathrm{d}\Pi_{NL}}{\mathrm{d}\bar{Z}}(\bar{Z}(0,t))\eta(0,t)\Big)^\top \bar{E}_1 \bar{P}_3 \Big(-\Gamma_0 \frac{\mathrm{d}\Pi_{NL}}{\mathrm{d}\bar{Z}}(\bar{Z}(0,t))\eta(0,t)\Big) \\
&+ \int_0^L \Big(\Big(F_5[\bar{Z}, \partial_x \eta] + F_6[\bar{Z}, \eta, \partial_x \bar{Z}, \dot{\bar{Z}}_{out}]\Big)^\top \bar{\mathcal{P}}_3(x)\eta(x,t) \\
&+ \eta^\top(x,t)\bar{\mathcal{P}}_3(x)\Big(F_5[\bar{Z}, \partial_x \eta] + F_6[\bar{Z}, \eta, \partial_x \bar{Z}, \dot{\bar{Z}}_{out}]\Big)\Big)\,\mathrm{d}x. \qquad (5.43)
\end{aligned}$$

Since the term $\dot{\bar{V}}^e_{1L} + \dot{\bar{V}}^e_{2L}$ is analyzed in Theorem 4.1, which is for the iISS of the linear target system (5.26)-(5.27), there exist positive constants c_1, b_1, a_1, a_2, a_3, such that

$$\begin{aligned}
\dot{\bar{V}}^e_{1L} + \dot{\bar{V}}^e_{2L} \le & -c_1(\bar{V}^e_1 + \bar{V}^e_2) + b_1|\dot{\bar{p}}^e|^2 + a_1(|w_1|^2 + |w_2|^2) \\
& + a_2\|\bar{Z}\|_\infty(\bar{V}^e_1 + \bar{V}^e_2). \qquad (5.44)
\end{aligned}$$

Now analyze the remaining items $\dot{\bar{V}}^e_{1NL}$ and $\dot{\bar{V}}^e_{2NL}$. There exist positive constants k_1, k_2, k_3, k_4, k_5, k_6, k_7 such that for all $t \in [0,\infty)$,

$$\begin{aligned}
\dot{\bar{V}}^e_{1NL} &\le k_1 \int_0^L \big(\big|F_3[\bar{Z}, \partial_x \bar{Z}]\big| + \big|F_4[\bar{Z}, \bar{Z}_{out}]\big|\big)\,\big|\bar{Z}\big|\,\mathrm{d}x \\
&+ k_2 \int_0^L \Big(\big|\bar{Z}\big| \Big|\Gamma_0 \frac{\mathrm{d}\Pi_{NL}}{\mathrm{d}\bar{Z}}(\bar{Z}(0,t))\eta(0,t)\Big| + \big(\big|F_3[\bar{Z}, \partial_x \bar{Z}]\big| + \big|F_4[\bar{Z}, \bar{Z}_{out}]\big|\big)\,\big|\bar{X}(t)\big|\Big)\,\mathrm{d}x \\
&+ k_3 \Big|\Gamma_0 \frac{\mathrm{d}\Pi_{NL}}{\mathrm{d}\bar{Z}}(\bar{Z}(0,t))\eta(0,t)\Big|\,\big|\bar{X}(t)\big|,
\end{aligned}$$

$$\begin{aligned}
\dot{\bar{V}}^e_{2NL} &\le k_4 \big|\dot{\bar{Z}}_{out}(t)\big| \Big|\Gamma_0 \frac{\mathrm{d}\Pi_{NL}}{\mathrm{d}\bar{Z}}(\bar{Z}(0,t))\eta(0,t)\Big| \\
&+ k_5 \Big(\big|K^e_I \bar{Z}_{out}(t) + \Gamma_0 \dot{\bar{p}}^e(t)(t)\big| + \Big|\Gamma_0 \frac{\mathrm{d}\Pi_{NL}}{\mathrm{d}\bar{Z}}(\bar{Z}(0,t))\eta(0,t)\Big| \\
&+ |\Gamma_0(d_1 w_1(t) + d_2 w_2(t))|\Big) \Big|\Gamma_0 \frac{\mathrm{d}\Pi_{NL}}{\mathrm{d}\bar{Z}}(\bar{Z}(0,t))\eta(0,t)\Big| \\
&+ k_6 \Big|\Gamma_0 \frac{\mathrm{d}\Pi_{NL}}{\mathrm{d}\bar{Z}}(\bar{Z}(0,t))\eta(0,t)\Big|^2 \\
&+ k_7 \int_0^L \Big(\big|F_5[\bar{Z}, \partial_x \eta]\big| + \Big|F_6[\bar{Z}, \eta, \partial_x \bar{Z}, \dot{\bar{Z}}_{out}]\Big|\Big)\,|\eta|\,\mathrm{d}x.
\end{aligned}$$

Applying [Cor+13, Lemma B.2], there exists $\delta_1 > 0$, and positive constants k_8, k_9, k_{10}, h_1, h_2, h_3, h_4 such that for all $\bar{Z}$ satisfying $\|\bar{Z}\|_\infty \leq \delta_1$, it holds for all $t \in [0,\infty)$, $\left|\Gamma_0 \bar{\Pi}_{NL}(\bar{Z}(0,t))\right| \leq k_8|\bar{Z}(0,t)|$, $\|\bar{Z}\|_{L^2}^2 + \left|\bar{X}(t)\right|^2 \leq k_9 \bar{V}_1^e$, $\|\eta\|_{L^2}^2 \leq k_{10}\bar{V}_2^e$, and

$$
\begin{aligned}
&\int_0^L \left(\left|F_3[\bar{Z},\partial_x\bar{Z}]\right| + \left|F_4[\bar{Z},\bar{Z}_{out}]\right|\right)\left|\bar{Z}\right| \,\mathrm{d}x \leq h_1 k_9(\|\bar{Z}\|_\infty + \|\eta\|_\infty)\bar{V}_1^e,\\
&\int_0^L \left|\bar{Z}\right|\left|\Gamma_0 \frac{\mathrm{d}\Pi_{NL}}{\mathrm{d}\bar{Z}}(\bar{Z}(0,t))\eta(0,t)\right| \,\mathrm{d}x \leq h_2(k_9\|\bar{Z}\|_\infty \bar{V}_1^e + k_{10}\|\eta\|_\infty \bar{V}_2^e),\\
&\int_0^L \left(\left|F_3[\bar{Z},\partial_x\bar{Z}]\right| + \left|F_4[\bar{Z},\bar{Z}_{out}]\right|\right)\left|\bar{X}(t)\right| \,\mathrm{d}x \leq h_3 k_9(\|\bar{Z}\|_\infty + \|\eta\|_\infty)\bar{V}_1^e,\\
&\left|\Gamma_0 \frac{\mathrm{d}\Pi_{NL}}{\mathrm{d}\bar{Z}}(\bar{Z}(0,t))\eta(0,t)\right|\left|\bar{X}(t)\right| \leq h_4(k_9\|\bar{Z}\|_\infty \bar{V}_1^e + k_{10}\|\eta\|_\infty \bar{V}_2^e).
\end{aligned}
$$

We deduce, for all $\bar{Z}$ satisfying $\|\bar{Z}\|_\infty \leq \delta_1$,

$$
\dot{\bar{V}}_{1NL}^e \leq (h_1+h_3)k_9(\|\bar{Z}\|_\infty + \|\eta\|_\infty)\bar{V}_1^e + (h_2+h_4)(k_9\|\bar{Z}\|_\infty \bar{V}_1^e + k_{10}\|\eta\|_\infty \bar{V}_2^e). \tag{5.45}
$$

Applying [Cor+13, Lemma B.3], there exist positive constants $\delta_2 \leq \delta_1$, h_5, h_6, h_7, h_8, h_9, h_{10}, h_{11} such that for all $\bar{Z}$ satisfying $\|\bar{Z}\|_\infty + \|\eta\|_\infty \leq \delta_2$, $\|\zeta\|_{L^2} \leq k_{11}\bar{V}_3^{e\,1/2}$, $k_{11} > 0$, it holds for all $t \in [0,\infty)$,

$$
\begin{aligned}
&\left|\dot{\bar{Z}}_{out}(t)\right|\left|\Gamma_0 \frac{\mathrm{d}\Pi_{NL}}{\mathrm{d}\bar{Z}}(\bar{Z}(0,t))\eta(0,t)\right| \leq h_5\|\eta\|_\infty(\bar{V}_2^e + \bar{V}_3^e),\\
&\Bigg(\left|K_I^e \bar{Z}_{out}(t) + \Gamma_0 \dot{\bar{p}}^e(t)(t)\right| + \left|\Gamma_0 \frac{\mathrm{d}\Pi_{NL}}{\mathrm{d}\bar{Z}}(\bar{Z}(0,t))\eta(0,t)\right|\\
&+ \left|\Gamma_0(d_1 w_1(t) + d_2 w_2(t))\right|\Bigg)\left|\Gamma_0 \frac{\mathrm{d}\Pi_{NL}}{\mathrm{d}\bar{Z}}(\bar{Z}(0,t))\eta(0,t)\right|\\
&\leq h_6\|\bar{Z}\|_\infty \bar{V}_2^e + h_6\|\bar{Z}\|_\infty(\bar{V}_1^e + \bar{V}_2^e) + h_7\left|\dot{\bar{p}}^e(t)(t)\right|^2 + h_8(|w_1|^2 + |w_2|^2),\\
&\left|\Gamma_0 \frac{\mathrm{d}\Pi_{NL}}{\mathrm{d}\bar{Z}}(\bar{Z}(0,t))\eta(0,t)\right|^2 \leq h_9\|\bar{Z}\|_\infty \bar{V}_2^e,\\
&\int_0^L \Big(\left|F_5[\bar{Z},\partial_x\eta]\right| + \left|F_6[\bar{Z},\eta,\partial_x\bar{Z},\dot{\bar{Z}}_{out}]\right|\Big)\left|\eta\right| \,\mathrm{d}x\\
&\leq h_{10}\|\bar{Z}\|_\infty(\bar{V}_2^e + \bar{V}_3^e) + h_{11}\|\bar{Z}\|_\infty \bar{V}_2^e\left(\|\bar{Z}\|_\infty + \|\eta\|_\infty + 1\right),
\end{aligned}
$$

and therefore

$$
\begin{aligned}
\dot{\bar{V}}_{2NL}^e &\leq k_4 h_5\|\eta\|_\infty(\bar{V}_2^e + \bar{V}_3^e)\\
&+ (k_4h_5 + k_5h_6 + k_6h_9 + k_7h_{10} + k_7h_{11})\|\bar{Z}\|_\infty \bar{V}_2^e\\
&+ k_5\Big(h_6\|\bar{Z}\|_\infty(\bar{V}_1^e + \bar{V}_2^e) + h_7\left|\dot{\bar{p}}^e(t)(t)\right|^2 + h_8(|w_1|^2 + |w_2|^2)\Big)\\
&+ k_7h_{10}\|\bar{Z}\|_\infty \bar{V}_3^e + k_7h_{11}\bar{V}_2^e\left(\|\bar{Z}\|_\infty + \|\eta\|_\infty\right).
\end{aligned} \tag{5.46}
$$

Taking the time derivative in (5.34), we obtain the following equation for ζ, for all $x \in [0,L]$, $t \in [0,\infty)$,

$$
\partial_t\zeta(x,t) = -(\Lambda^e(x) - F_1[\bar{Z}])\partial_x\zeta(x,t) + F_7[\bar{Z},\zeta,\partial_x\zeta] + F_8[\bar{Z},\eta,\zeta,\partial_x\bar{Z},\partial_x\eta] + +k_1(x)\zeta_{out}(\cdot), \tag{5.47}
$$

$$
\zeta_{in}(t) = K_P^e\zeta_{out}(t) + \ddot{\bar{X}}(t) + \Gamma_0(d_1^2 w_1(t) + d_2^2 w_2(t)), \tag{5.48}
$$

$$
\ddot{\bar{X}}(t) = K_I^e\dot{\bar{Z}}_{out}(t) + \Gamma_0\Big(\ddot{\bar{p}}^e(t) - \frac{\mathrm{d}^2\Pi_{NL}}{\mathrm{d}\bar{Z}^2}(\bar{Z}(0,t))\eta^2(0,t) - \frac{\mathrm{d}\Pi_{NL}}{\mathrm{d}\bar{Z}}(\bar{Z}(0,t))\zeta(0,t)\Big), \tag{5.49}
$$

where

$$
\begin{aligned}
&F_7[\bar{Z},\zeta,\partial_x\zeta] = -\mathcal{K}[(\Lambda^e(x)+F_1[\bar{Z}])(\partial_x\zeta+\mathcal{K}_1[\mathcal{L}[\zeta]])] + (\Lambda^e(x)+F_1[\bar{Z}])(\partial_x\zeta+\mathcal{K}_1[\mathcal{L}[\zeta]]),\\
&F_8[\bar{Z},\eta,\zeta,\partial_x\bar{Z},\partial_x\eta] = -(\Lambda^e(x)+F_1[\bar{Z}])\mathcal{K}_1[\mathcal{L}[\zeta]] + \mathcal{K}[(\Sigma(x)+F_2[\bar{Z}])\mathcal{L}[\zeta]\\
&\qquad\qquad - 2F_{12}[\bar{Z}](\partial_x\eta+\mathcal{K}_1[\mathcal{L}[\eta]]) + 2F_{22}[\bar{Z}]\mathcal{L}[\eta] + F_{23}\mathcal{L}[\bar{Z}] - F_{13}(\partial_x\bar{Z}+\mathcal{K}_1[\mathcal{L}[\bar{Z}]])],\\
&F_{13}[\bar{Z},\eta,\zeta] = \ddot{F}_1[\bar{Z}],\\
&F_{23}[\bar{Z},\eta,\zeta] = \ddot{F}_2[\bar{Z}].
\end{aligned}
$$

Take the time derivative of $\bar{V}_3^e$ along the solutions to (5.31)-(5.33), apply [Cor+13, Lemma 5.2], and define $\dot{\bar{V}}_3^e = \dot{\bar{V}}_{3L}^e + \dot{\bar{V}}_{3NL}^e$, where $\dot{\bar{V}}_{3L}^e$ is the time derivative of $\bar{V}_{3L}^e$ along the linear target system (5.26)-(5.27), for all $t\in[0,\infty)$,

$$
\begin{aligned}
\dot{\bar{V}}_{3L}^e &= -\zeta^\top(x,t)\Big(\bar{\mathcal{P}}_4[\bar{Z}](x)(\Lambda^e(x)+F_1[\bar{Z}])\Big)\zeta(x,t)\Big|_0^L\\
&+\int_0^L \zeta^\top(x,t)\Big(\bar{\mathcal{P}}_4[\bar{Z}](x)(\Lambda^e(x)+F_1[\bar{Z}])\Big)_x\zeta(x,t)\,\mathrm{d}x + \int_0^L \zeta^\top(x,\cdot)\left(\bar{\mathcal{P}}_4[\bar{Z}](x)\right)_t\zeta(x,\cdot),
\end{aligned}
$$

and

$$
\begin{aligned}
\dot{\bar{V}}_{3NL}^e = \int_0^L \Bigg(&\Big(F_7[\bar{Z},\zeta,\partial_x\zeta]+F_8[\bar{Z},\eta,\zeta,\partial_x\bar{Z},\partial_x\eta]+k_1(x)\zeta_{out}(\cdot)\Big)^\top\bar{\mathcal{P}}_4[\bar{Z}](x)\zeta(x,t)\\
&+\zeta^\top(x,t)\bar{\mathcal{P}}_4[\bar{Z}](x)\Big(F_7[\bar{Z},\zeta,\partial_x\zeta]+F_8[\bar{Z},\eta,\zeta,\partial_x\bar{Z},\partial_x\eta]+k_1(x)\zeta_{out}(\cdot)\Big)\Bigg)\,\mathrm{d}x.
\end{aligned}
$$

According to [Cor+13, Proposition 5.4], there exist positive constants c_2, h_{12}, h_{13}, h_{14}, h_{15}, h_{16}, h_{17}, h_{18}, h_{19}, h_{20} such that for all $t\in[0,\infty)$,

$$
\begin{aligned}
&-\zeta^\top(x,t)\Big(\bar{\mathcal{P}}_4[\bar{Z}](x)(\Lambda^e(x)+F_1[\bar{Z}])\Big)\zeta(x,t)\Big|_0^L\\
&\le h_{12}\|\zeta\|_\infty(\bar{V}_1^e+\bar{V}_2^e+\bar{V}_3^e)+h_{13}(|w_1|^2+|w_2|^2)+h_{14}\|\eta\|_\infty(\bar{V}_2^e+\bar{V}_3^e)+h_{15}|\ddot{d}|^2+h_{16}\|\zeta\|_\infty\bar{V}_2^e\bar{V}_2^e,\\
&\int_0^L\zeta^\top(x,t)\Big(\bar{\mathcal{P}}_4[\bar{Z}](x)\left(\Lambda^e(x)+F_1[\bar{Z}]\right)\Big)_x\zeta(x,t)\,\mathrm{d}x \le -c_2\bar{V}_3^e + h_{17}(\|\bar{Z}\|_\infty+\|\eta\|_\infty)\bar{V}_3^e,\\
&\int_0^L\zeta^\top(x,\cdot)\left(\bar{\mathcal{P}}_4[\bar{Z}](x)\right)_t\zeta(x,\cdot)\,\mathrm{d}x \le h_{18}\bar{V}_3^e\|\eta\|_\infty,\\
&\int_0^L\zeta^\top(x,t)\bar{\mathcal{P}}_4[\bar{Z}](x)\Big(F_7[\bar{Z},\zeta,\partial_x\zeta]+F_8[\bar{Z},\eta,\zeta,\partial_x\bar{Z},\partial_x\eta]++k_1(x)\zeta_{out}(\cdot)\Big)\,\mathrm{d}x\\
&\le h_{19}\bar{V}_2^e\|\zeta\|_\infty\left(\|\bar{Z}\|_\infty+\|\eta\|_\infty\right)+h_{20}\left(\|\eta\|_\infty\bar{V}_3^e+\|\zeta\|_\infty\bar{V}_2^e+\|\bar{Z}\|_\infty\bar{V}_3^e\right).
\end{aligned}
$$

Therefore there exist positive constants $\delta_3\le\delta_2$, c_3 and c_4 satisfying $c_3+c_4<c_2$ such that, for all $\bar{Z}$ satisfying $\|\bar{Z}\|_\infty+\|\eta\|_\infty+\|\zeta\|_\infty\le\delta_3$, it holds

$$
\dot{\bar{V}}_{3L}^e \le (-c_2+c_3)(\bar{V}_1^e+\bar{V}_2^e+\bar{V}_3^e)+h_{15}|\ddot{\bar{p}}^e|^2+h_{13}(|w_1|^2+|w_2|^2), \tag{5.50}
$$

$$
\dot{\bar{V}}_{3NL}^e \le c_4(\bar{V}_1^e+\bar{V}_2^e+\bar{V}_3^e). \tag{5.51}
$$

Combining (5.50), (5.51) with (5.44), (5.45), (5.46), and letting $c=c_3+c_4-c_2-c_1$ and $a=a_1+k_5h_8+h_{13}$, we get, for all $\|\bar{Z}\|_\infty+\|\eta\|_\infty+\|\zeta\|_\infty\le\delta_2$,

$$
\dot{\bar{V}}^e \le -c\bar{V}^e+(b_1+k_5h_7)|\dot{\bar{p}}^e|^2+h_{15}|\ddot{\bar{p}}^e|^2+a(|w_1|^2+|w_2|^2). \tag{5.52}
$$

By defining $\bar{W}^e=\bar{V}^e+\frac{b_4}{2}(\frac{|w_1|^2}{d_1}+\frac{|w_2|^2}{d_2})$, we derive

$$
\dot{\bar{W}}^e \le -c\bar{V}^e+(b_1+k_5h_7)|\dot{\bar{p}}^e(t)|^2+h_{15}|\ddot{\bar{p}}^e(t)|^2+(a-b_4)(|w_1|^2+|w_2|^2).
$$

Choosing $a < b_4$, for some positive constant c_5, we obtain

$$\dot{\bar{W}}^e \leq -c_5 \bar{W}^e + (b_1 + k_5 h_7)|\dot{\bar{p}}^e|^2 + h_{15}|\ddot{\bar{p}}^e|^2. \tag{5.53}$$

For sufficiently small $\bar{W}^e(0)$, $\bar{W}^e$ exponentially converge to zero. If $\|\bar{Z}\|_{L^2} + \|\eta\|_{L^2} + \|\zeta\|_{L^2}$ is sufficiently small, $\bar{V}^e$ is equivalent to the H^2 norm of $\bar{Z}$. We deduce (5.30) by a standard application of the comparison lemma. This concludes the proof of Theorem 5.1. □

Furthermore, under the assumption of Theorem 5.1, we deduce that the quasilinear plant system (4.1)-(4.2) is locally iISS around the nonuniform equilibrium u^* in the H^2 space.

Remark 5.1
The used methods in this paper can be extended to a general quasilinear hyperbolic system (5.1) with general coefficients.

5.3 Conclusion

The problem of robust boundary stabilization of a heterogeneous quasi-linear traffic flow system with a bottleneck was solved by actuation at the inlet boundary of the considered road segment. The applicability of the control law, which was designed for the corresponding linearized system by using the backstepping method in Chapter 4, has been proven for the local iISS of the heterogeneous quasi-linear traffic system.

In the next chapter, we extend this result to design an observer and combine them to obtain an observer-based output feedback controller for the heterogeneous quasi-linear traffic flow system with a bottleneck.

Chapter 6

Parameter identification: analysis of COVID

Contents

In this chapter, a parameter identification problem is solved for a distributed parameter system. This problem is not motivated by a traffic control application but rather by the analysis of COVID dynamics. More precisely, an extension of the classical pandemic SIRD model is considered for the regional spread of COVID-19 in France under lockdown strategies. This compartment model divides the infected and the recovered individuals into undetected and detected compartments respectively. By fitting the extended model to the real detected data during the lockdown, an optimization algorithm is used to derive the optimal parameters, the initial condition, and the epidemics start date of regions in France. Considering all the age classes together, a network model of the pandemic transport between regions in France is presented based on the regional extended model and is simulated to reveal the transport effect of the COVID-19 pandemic after lockdown. Using the measured values of displacement of people between cities, the pandemic network of all cities in France is simulated by using the same model and method as the pandemic network of regions. Finally, a discussion on an integrodifferential equation is given and a new model for the network pandemic model of each age class is provided.

This chapter has been published in [Gua+20].

6.1 Pandemic model

In this chapter, the scenario we consider is a large safe population into which a low level of infectious agents is introduced and a closed population with neither birth, natural death, nor migration. There is one basic model of modeling pandemic transmission which is well known as the susceptible-infected-recovered-dead (SIRD) model in [BCC12]. This mathematical compartmental

model is described as follows,

$$\dot{S}(t) = -\beta S(t)I(t), \tag{6.1}$$
$$\dot{I}(t) = \beta S(t)I(t) - (\alpha + \delta)I(t), \tag{6.2}$$
$$\dot{R}(t) = \delta I(t), \tag{6.3}$$
$$\dot{D}(t) = \alpha I(t) \tag{6.4}$$

where $S(t)$ is the number of susceptible people at time t, $I(t)$ is the number of infected people at time t, $R(t)$ is the number of recovered people at time t, $D(t)$ is the number of deaths due to pandemic until time t, with constant parameters: β is transmission rate per infected, δ is the removal or recovery rate, α is the disease mortality rate. The compartment variables $S(t), I(t), R(t), D(t)$ satisfy $S(t)+I(t)+R(t)+D(t) = N$ at any time instant t, here N is the total number of population of the considered area.

From the differential equations (6.1)-(6.4), it is obvious that at any time instant t, the total rate $\beta I(t)$ of transmission from the entire susceptible compartment to infected compartment is proportional to the infected I; the infected individuals recover at a constant rate δ; the infected go to death compartment at a constant rate α.

In fact, except for the detected well-known data, some undetected data cannot be measured but are significantly important for the analysis of the evolution of COVID-19 in France under lockdown policy. Moreover, they are useful to provide efficient social policies, such as optimal management of limited healthcare resources, the ideal decision of the duration and level of lockdown or re-lockdown, and so on.

Inspired by [Cha+20], the basic SIRD model is extended to a more sophisticated compartmental model which includes several features of the recent COVID-19 outbreak, with flexibility with respect to lockdown and test strategies. More sophisticated models could be considered, however it is important that the model we consider can be calibrated with the available data for French regions.

On the basis of the $SIDUHR^{+/-}$ model in [Cha+20], this model additionally considers that the infected undetected individuals I^- and the infected detected individuals I^+ get sicker and then go to intensive care U, and the hospitalized individuals H die (D) before attaining intensive care U. In our model, the short-term tests transfer the positive individuals from compartment I^- to compartment I^+. The detection using antibody tests allows transferring individuals from compartment R^- to compartment R^+. The presence of antibodies indicates that one person has recovered from the pandemic and is immune. The flow diagram of this model is sketched out in Figure 6.1.
The evolution of each compartments is modelled by the following equations,

$$\dot{S}(t) = -\beta(t)S(t)I^-(t), \tag{6.5}$$
$$\dot{I}^-(t) = \beta(t)S(t)I^-(t) - \lambda_1^{(4)}I^-(t) - (\gamma_{IR} + \gamma_{IH} + \gamma_{IU})I^-(t), \tag{6.6}$$
$$\dot{I}^+(t) = \lambda_1^{(4)}I^-(t) - (\gamma_{IR} + \gamma_{IH} + \gamma_{IU})I^+(t), \tag{6.7}$$
$$\dot{R}^-(t) = \gamma_{IR}I^-(t) - \lambda_2^{(4)}R^-(t), \tag{6.8}$$
$$\dot{R}^+(t) = \gamma_{IR}I^+(t) + \lambda_2^{(4)}R^-(t) + \gamma_{HR}H(t) + \gamma_{UR}U(t), \tag{6.9}$$
$$\dot{H}(t) = \gamma_{IH}(I^-(t) + I^+(t)) - (\gamma_{HR} + \gamma_{HU} + \gamma_{HD})H(t), \tag{6.10}$$
$$\dot{U}(t) = \gamma_{IU}(I^-(t) + I^+(t)) + \gamma_{HU}H(t) - (\gamma_{UR} + \gamma_{UD})U(t), \tag{6.11}$$
$$\dot{D}(t) = \gamma_{UD}U(t) + \gamma_{HD}H(t), \tag{6.12}$$

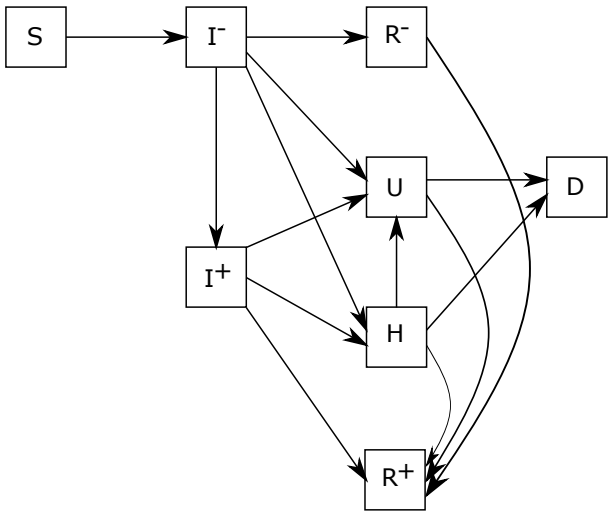

Figure 6.1: Compartments and flow of pandemic model.

with

$$S(t) + I^-(t) + I^+(t) + R^-(t) + R^+(t) + H(t) + U(t) + D(t) = N,$$

and initial conditions

$$S(t_0) = N, \tag{6.13}$$

$$I^-(t_0) = I_0^- > 0, \tag{6.14}$$

$$I^+(t_0) = R^-(t_0) = R^+(t_0) = H(t_0) = U(t_0) = D(t_0) = 0, \tag{6.15}$$

where $S(t)$ is the number of susceptible individuals at time t, $I^-(t)$ is the number of infected undetected individuals at time t, $I^+(t)$ is the number of infected detected individuals at time t, $R^-(t)$ is the number of recovered undetected individuals at time t, $R^+(t)$ is the number of recovered detected individuals at time t, $H(t)$ is the number of hospitalized individuals at time t, $U(t)$ is the number of individuals hospitalized in an intensive care unit at time t, $D(t)$ is the cumulative number of dead individuals from the hospital or intensive care at time t.

During the incubation period (time taken from infection to symptom exhibition) but after the latent period (time from infection to infectiousness, this is the so-called exposed period), the infected individuals can transmit the epidemic without any symptoms. Unfortunately, we do not have any data on the exposed population, making it hard to identify the number of infected individuals. Therefore we incorporate this class of infected individuals into the undetected infected compartment I^-.

The number of exposed individuals who travel internationally is neglected in this chapter, since (at the time of the writing) only a few people travel internationally. We do not consider here deaths from nursing homes for example, as in [Vei+20, Chapter 6], where a slight difference is considered at the French national scale. The main reason for that is the lack of data. Indeed, daily data on the total reported cases are unavailable in France on the regional scale. The initial conditions (6.13)-(6.15) mean that infected people I_0^- are introduced into a population consisting of susceptible individuals $S(t_0)$ at time instant t_0. Both I_0^- and t_0 are two unknown parameters that need to be identified.

Two types of tests are taken into account in this model, one is a class of virological tests like nasal ones that can detect new infectious cases from compartment I^-. The rate of these tests is

denoted by $\lambda_1^{(4)}$; another method is a class of serological tests that detect the individuals infected and sequentially recovered from compartment R^- applying blood or saliva samples, the rate of these tests (for example, blood test) is denoted by $\lambda_2^{(4)}$. This second type of test was not proposed in France until very recently, thus we consider in this work that $\lambda_2^{(4)} = 0$.

Remark 6.1
The second type of test is an antibody test that uses serological immunoassays to detect viral-specific antibodies: Immunoglobin M (IgM) and G (IgG). The antibodies IgM that suggests infection have a half-life of around five days, and they usually appear within five to seven days of infection and peak at around 21 days. The antibodies IgG that indicates recovery and immunity can be detected around 10 to 14 days after infection. The immunity test allows verifying if one person is immune to the epidemic. The identified immune person could obtain an immunity certificate to have normal social activities and then be allowed to travel between regions thus impacting our model. Consequently, the level of social interactions is raised, and then the social economy is recovered.

The other parameters in equation (6.5)-(6.12) are defined as follows:

- γ_{IR} is the daily individual transition rate from I to R, and $\gamma_{IR} = (1-p_a)(1-p_H)/N_s + p_a/N_a$,
- γ_{IH} is the daily individual transition rate from I to H, and $\gamma_{IH} = (1-p_a)p_H(1-p_U)/N_{IH}$,
- γ_{IU} is the daily individual transition rate from I to U, and $\gamma_{IU} = (1-p_a)p_H p_U/N_{IH}$,
- γ_{HR} is the daily individual transition rate from H to R, and $\gamma_{HR} = (1-p_{HD})/N_{HR}$,
- γ_{HD} is the daily individual transition rate from H to D, and $\gamma_{HD} = p_{HD}/N_{HD}$,
- γ_{HU} is the daily individual transition rate from H to U, and $\gamma_{HU} = p_{HU}/N_{HU}$,
- γ_{UR} is the daily individual transition rate from U to R, and $\gamma_{UR} = (1-p_{UD})/N_{UR}$,
- γ_{UD} is the daily individual transition rate from U to D, and $\gamma_{UD} = p_{UD}/N_{UD}$,

with

- p_a: the probability of having light symptoms or no symptoms for the infected individuals; p_H: the probability of needing hospitalization for mild or severely ill people; p_U: the probability of needing intensive care for mild or severely ill people; p_{HU}: the probability of needing intensive care under hospitalization without intensive care; p_{HD}: the probability of death under hospitalization without intensive care; p_{UD}: the probability of death under intensive care;
- N_a: the number of days it takes for an asymptomatic case to recover; N_s: the number of days it takes for a symptomatic case to recover without hospitalization; N_{IH}: the number of days a severely symptomatic case requires until hospitalization; N_{HD}: the number of days before death in the event of hospitalization; N_{HU}: the number of days required for a hospitalized case until intensive care is provided; N_{UD}: the number of days before death in the event of intensive care; N_{HR}: the number of days it takes for a hospitalized case to recover; N_{UR}: the number of days it takes for a case under intensive care to recover.

The infection transmission rate $\beta(t)$ is the rate of the pandemic transmission from an undetected infected person to susceptible individuals at time instant t. As in [MW20], to combine the

complex effects of lockdown strategy, a time-dependent exponentially decreasing function can be used to model the transmission rate $\beta(t)$,

$$\beta(t) = \beta_0 \exp(-\mu(t-\kappa)_+) = \begin{cases} \beta_0 & 0 \le t \le \kappa, \\ \beta_0 \exp(-\mu(t-\kappa)) & t > \kappa, \end{cases} \tag{6.16}$$

with constant parameters β_0, μ and κ. Note that $\beta(t)$ is constant during the initial stage of implementing effective lockdown strategies such as social distance, quarantine, healthcare, and mask worn. The transmission rate exponentially decreases at rate μ after these lockdown strategies take effect. The transmission rate $\beta(t)$ can be illustrated in Figure 6.2. As one of the most

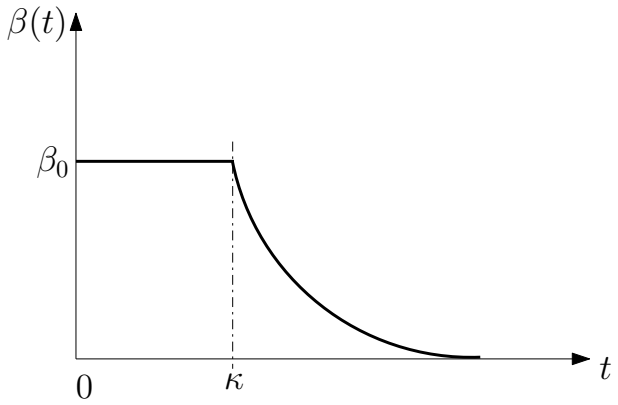

Figure 6.2: Transmission rate β before and during lockdown.

critical epidemiological parameters, the basic reproductive ratio R_0 defines the average number of secondary cases an average primary case produces in a susceptible population (see [KR08]). As for the model in [Cha+20], for the considered model in this chapter, only the I^- individuals transmit the disease to the susceptible individuals during the early phase of the outbreak. If $R_0 < 1$ (i.e., $\dot{I}^-(t) < 0$), the infection "dies out" over time; inversely, if $R_0 > 1$ (i.e., $\dot{I}^-(t) > 0$), the initial number of susceptible individuals exceeds the critical threshold to allow the pandemic to spread. Thus the initial basic reproductive rate is

$$R_0 = \frac{\beta_0 S(t_0)}{\lambda_1^{(4)} + \gamma_{IR} + \gamma_{IH} + \gamma_{IU}}. \tag{6.17}$$

When the transmission rate $\beta(t)$ and the number of susceptible people $S(t)$ evolve as time goes by, a dynamic reproductive rate that depends on time is introduced and known as effective reproduction number $R(t)$ in [Til92]. In this model, it is defined as, for $t \ge 0$,

$$R(t) = \frac{\beta(t) S(t)}{\lambda_1^{(4)} + \gamma_{IR} + \gamma_{IH} + \gamma_{IU}}. \tag{6.18}$$

Similarly, when $R(t) < 1$, the number of secondary cases infected by a primary undetected infected case on the day t, dies out over time, leading to a delay in the number of infected individuals. But when $R(t) > 1$, the number of undetected infected individuals grows over time. Therefore, by the control of the transmission rate $\beta(t)$ that can constrain $R(t)$ to be less than 1, the number of infected individuals grows slowly to ease the pressure on medical resources. When $S(t)$ is below a threshold, the epidemic goes to extinction (see e.g., [PB19]). The required level of vaccination to eradicate the infection is also obtained from the effective reproduction number.

The compartmental model introduced in Figure 6.1 exhibits a large number of unknown parameters (20 if we consider $\lambda_2^{(4)} = 0$). The uncertainty of these parameters can not be neglected.

As an example, until the end of this section, let us propagate uncertainty at the scale of the region *Auvergne-Rhône-Alpes*. The vector of unknown parameters is:

$$p = (p_a, p_H, p_U, p_{HD}, p_{UD}, N_a, N_s, N_{IH}, N_{HD}, N_{UD}, N_{HR}, N_{UR}, R_0, t_0, \mu, \kappa, \lambda_1^{(4)}, p_{HU}, N_{HU}, I_0^-)^\top. \tag{6.19}$$

We take into account the uncertainties on these parameters by considering that each parameter is uniformly distributed with bounds consistent with typical reported values (see, e.g., [Cha+20] and references therein). Lower and upper bounds for each parameter are reported in Table 6.1 hereafter.

parameters	p_a	p_H	p_U	p_{HD}	p_{UD}	N_a	N_s	N_{IH}	N_{HD}	N_{UD}
lower bounds	0.5	0.15	0.15	0.15	0.2	5	8	8	15	8
upper bounds	0.9	0.2	0.2	0.25	0.3	12	15	12	20	12
parameters	N_{HR}	N_{UR}	R_0	t_0	μ	κ	$\lambda_1^{(4)}$	p_{HU}	N_{HU}	I_0^-
lower bounds	15	15	2.5	2020-02-06	0.03	20	1e-4	0.001	1	1
upper bounds	25	20	4.5	2020-02-12	0.1	50	1e-3	0.01	10	100

Table 6.1: Uncertainty bounds for all model parameters.

The parameter sampling approach is based on the generation of a low-discrepancy sequence of 5000 points on the unit hypercube $[0,1]^{20}$. Low-discrepancy sequences have the property of uniformly and regularly filling the unit hypercube, without the clustering issues encountered by Monte Carlo samples. Sobol' sequences [Sob67] are among the best low-discrepancy sequences with solid theoretical properties and good numerical performance when dimension increases.

Figure 6.3 shows that the prior uncertainty is pretty high since for example the difference between the 75 % and the 25 % quantiles for the number of people in hospital is more than 50000 at the end of the lockdown period. On images 6.4 and 6.5 we propagate the parameter uncertainty on the maximum number of people in intensive care units, the date at which this maximum value is attained, and the total number of reported cases. Note that the total number of reported cases is obtained from the daily number of reported cases, DR, which is driven by the following equation:

$$\dot{DR}(t) = (\lambda_1^{(4)} + \gamma_{IH} + \gamma_{IU})I^-(t) - DR(t).$$

The maximum number of people in intensive care is particularly important as it provides information on the capacities the intensive care units should have to face the sanitary crisis. We show for each of these three scalar quantities of interest the boxplot which visualizes five summary statistics (the median, two hinges, and two whiskers) and all outlying points individually. The lower and upper hinges correspond to the first and third quartiles (the 25th and 75th percentiles). The upper whisker extends from the hinge to the largest value no further than 1.5 * IQR from the hinge (where IQR is the inter-quartile range or distance between the first and third quartiles). The lower whisker extends from the hinge to the smallest value at most 1.5 * IQR of the hinge. Data beyond the end of the whiskers are called "outlying" points and are plotted individually. We see for example on these boxplots that the median for the maximum number of people in intensive care is more than 8000 with the IQR greater than 20000.

Given the importance of uncertainties propagated from the model parameters to the quantities of interest (e.g., the number of infected people at hospitals), it appears necessary to calibrate the model. Our calibration procedure is described in the next section.

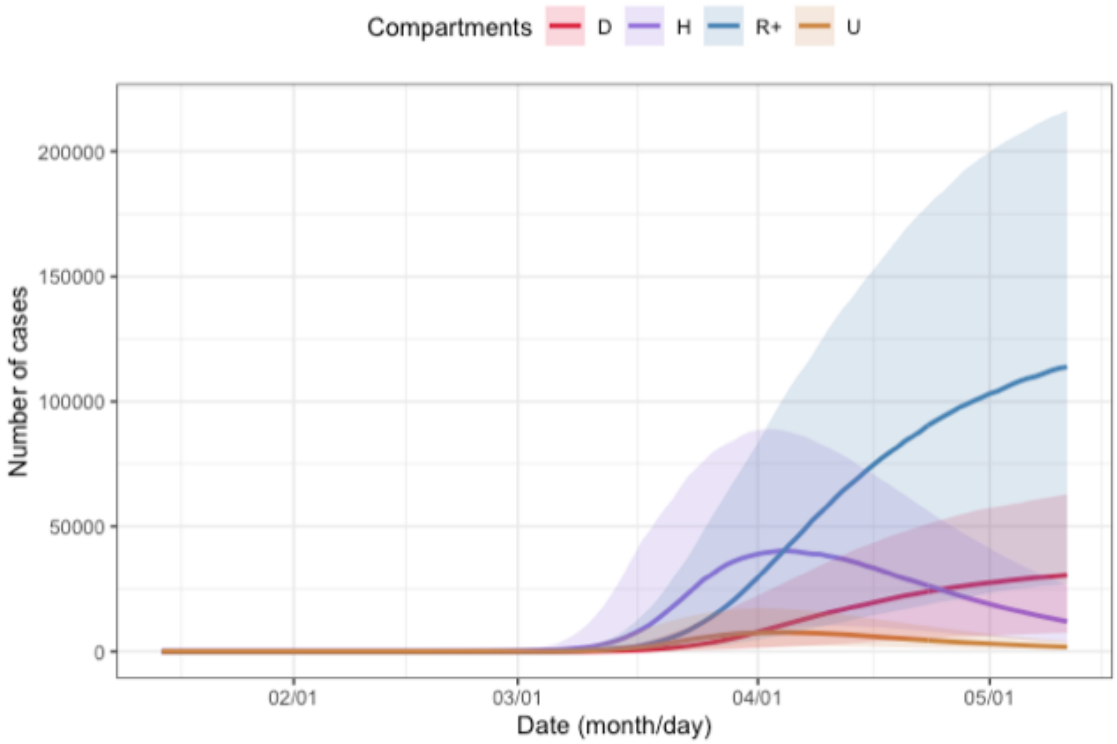

Figure 6.3: Prior uncertainty quantification for compartments D (in red), H (in purple), R^+ (in blue) and U (in orange) for the region *Auvergne-Rhône-Alpes*. The bold lines are the pointwise medians of each functional output, whereas the colored surface is the range between the pointwise first and third quartiles.

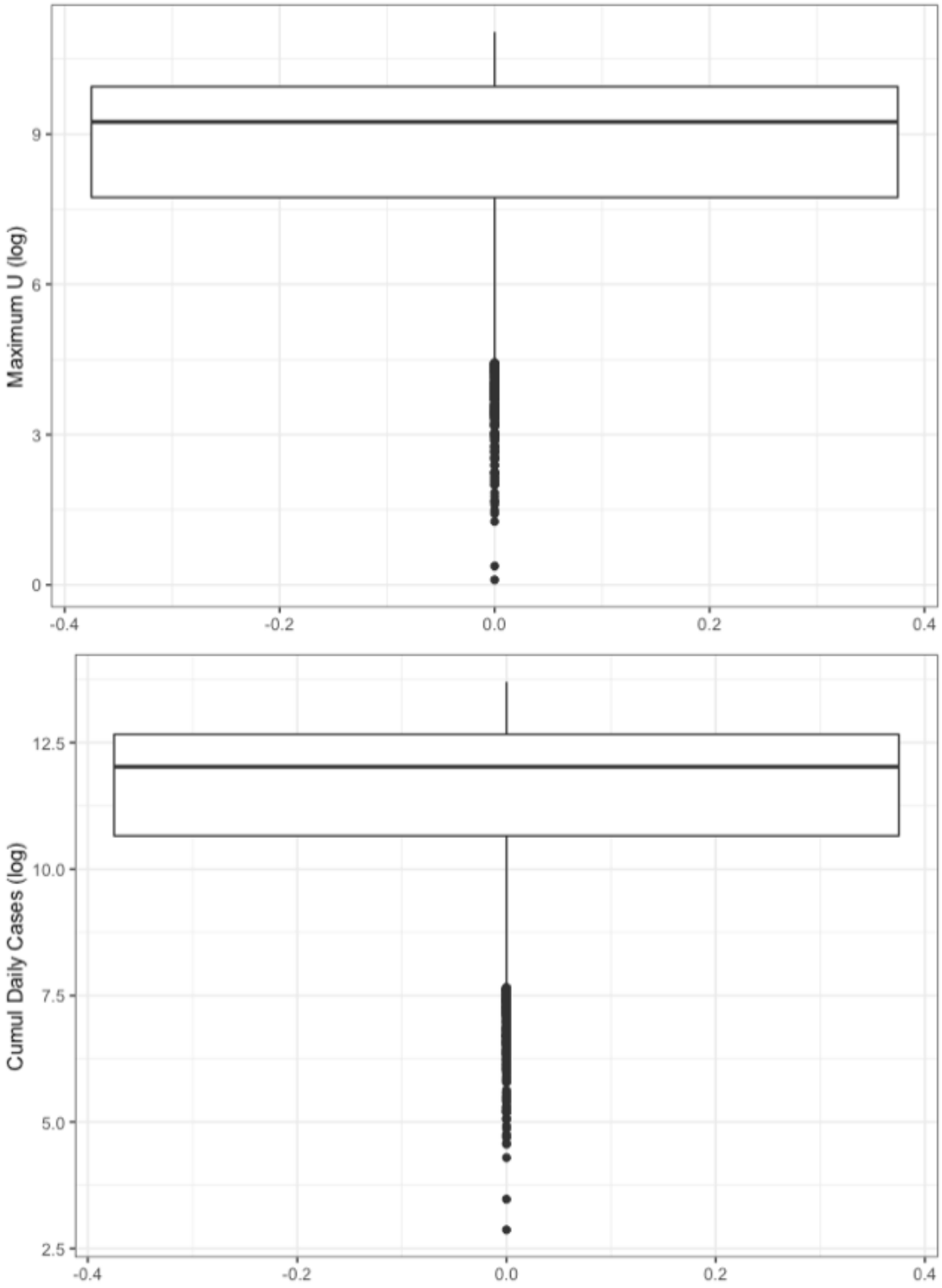

Figure 6.4: Prior uncertainty quantification for maximum value of U (top), and total number of reported cases (bottom) for the region *Auvergne-Rhône-Alpes*.

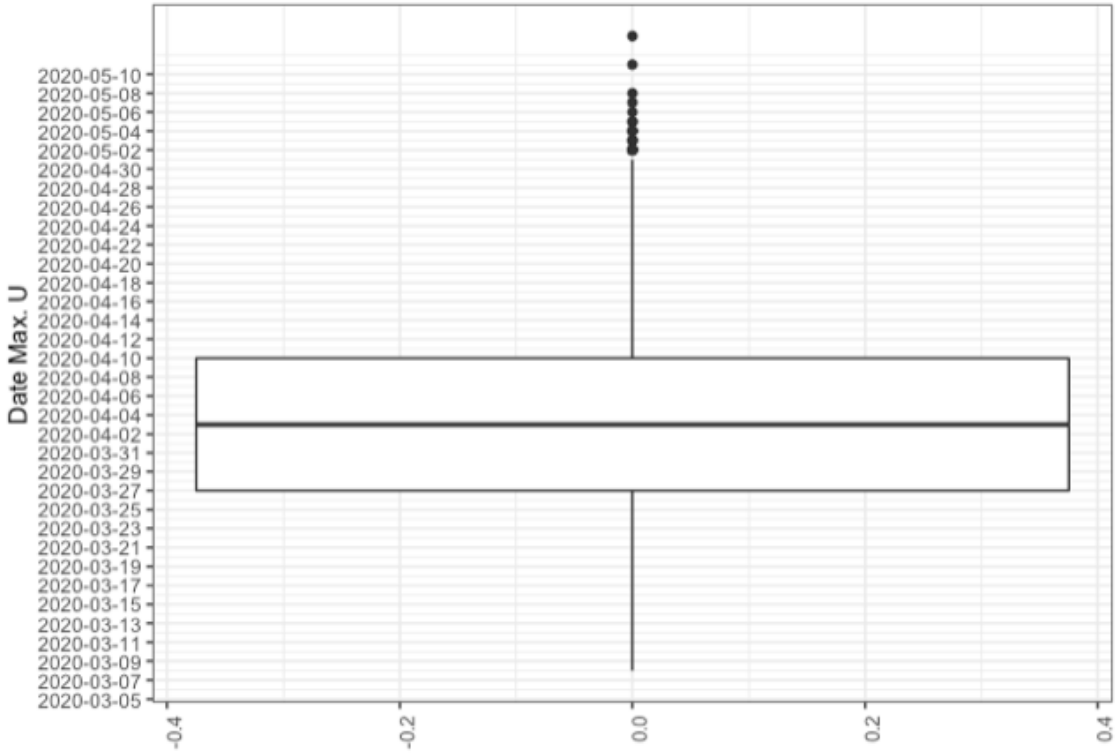

Figure 6.5: Prior uncertainty quantification for the day where the maximum value of U is reached for the region *Auvergne-Rhône-Alpes*.

6.2 Parameter identification

In this section, regional scales of France are considered and all age classes are summed to calibrate the parameters of the pandemic model (6.5)-(6.12) during confinement on the basis of data about the pandemic in France. Since all regions are not connected during the lockdown, it is sufficient to identify separately all unknown parameters for each region. From the calibration of the model, we can observe the effects of lockdown strategies on the unknown variables, in particular for infected undetected populations and recovered undetected populations. The following weighted least square cost function is minimized for parameters optimization:

$$J(p) = \sum_{i=1}^{n} \frac{\left(Z(p,t_i) - Z_{meas}(t_i)\right)^2}{Z_{meas}(t_i)}$$

where p is a vector which consists of calibrated parameters; $Z_{meas}(t_i)$ is the measured values of the corresponding observed state vector $Z(p,t_i)$ at time t_i, $i = 1,\dots,n$, with n the number of days considered for calibration. This optimization problem is solved using the Levenberg-Marquardt algorithm (see [Mor78]). Since it is a local algorithm, we adopt, as in [Vei+20, Chapter 6], a multi-start approach where the initial values are obtained from a Latin Hypercube Sampling (LHS). LHS was introduced in [MBC00] as space-filling designs on the unit hypercube. The LHS is built on the unit hypercube $[0,1]^{20}$ and then rescaled with the upper and lower bounds given in Table 6.1. The unknown parameter vector p defined in (6.19) is calibrated on daily data for H, U, D, and R^+ on the lockdown period 2020-03-18 to 2020-05-11, for each region, from two data sources: the first one is a public and governmental data source [Gou20] and the second one is a dedicated national platform with a privileged access [Min20].

The time step is chosen as ten percent of one day for the numerical discretization. A general solver "scipy.integrate.ode" on Python for ordinary differential equations is used to compute H, U, D or R^+ for each region for all time until the end of lockdown. The results of the calibration are given in Tables 6.2 to 6.5. The results of parameter calibration for the 13 regions in France are shown in images 6.6 and 6.7.

RegionsParameters	p_a	p_H	p_U	p_{HD}	p_{UD}	N_a	N_s
Île-de-France	0.9	0.15	0.2	0.20	0.3	12.0	13.104
Centre-Val de Loire	0.9	0.2	0.2	0.21	0.3	9.674	8.0
Bourgogne-Franche-Comté	0.83	0.18	0.2	0.25	0.3	6.423	8.576
Normandie	0.9	0.2	0.2	0.25	0.3	6.527	15.0
Hauts-de-France	0.9	0.15	0.2	0.244	0.3	12.0	15.0
Grand Est	0.9	0.2	0.2	0.25	0.3	12.0	14.551
Pays de la Loire	0.9	0.189	0.2	0.193	0.3	7.608	9.191
Bretagne	0.9	0.2	0.2	0.151	0.3	12.0	8.153
Nouvelle-Aquitaine	0.9	0.150	0.2	0.15	0.3	6.883	15.0
Occitanie	0.9	0.15	0.2	0.15	0.3	6.803	9.767
Auvergne-Rhône-Alpes	0.9	0.2	0.2	0.176	0.3	7.820	15.0
Provence-Alpes-Côte d'Azur	0.852	0.192	0.192	0.15	0.2	9.446	15.0
Corse	0.9	0.15	0.179	0.222	0.3	6.433	13.62

Table 6.2: Optimal values of parameters p_a, p_H, p_U, p_{HD}, p_{UD}, N_a, N_s for each region.

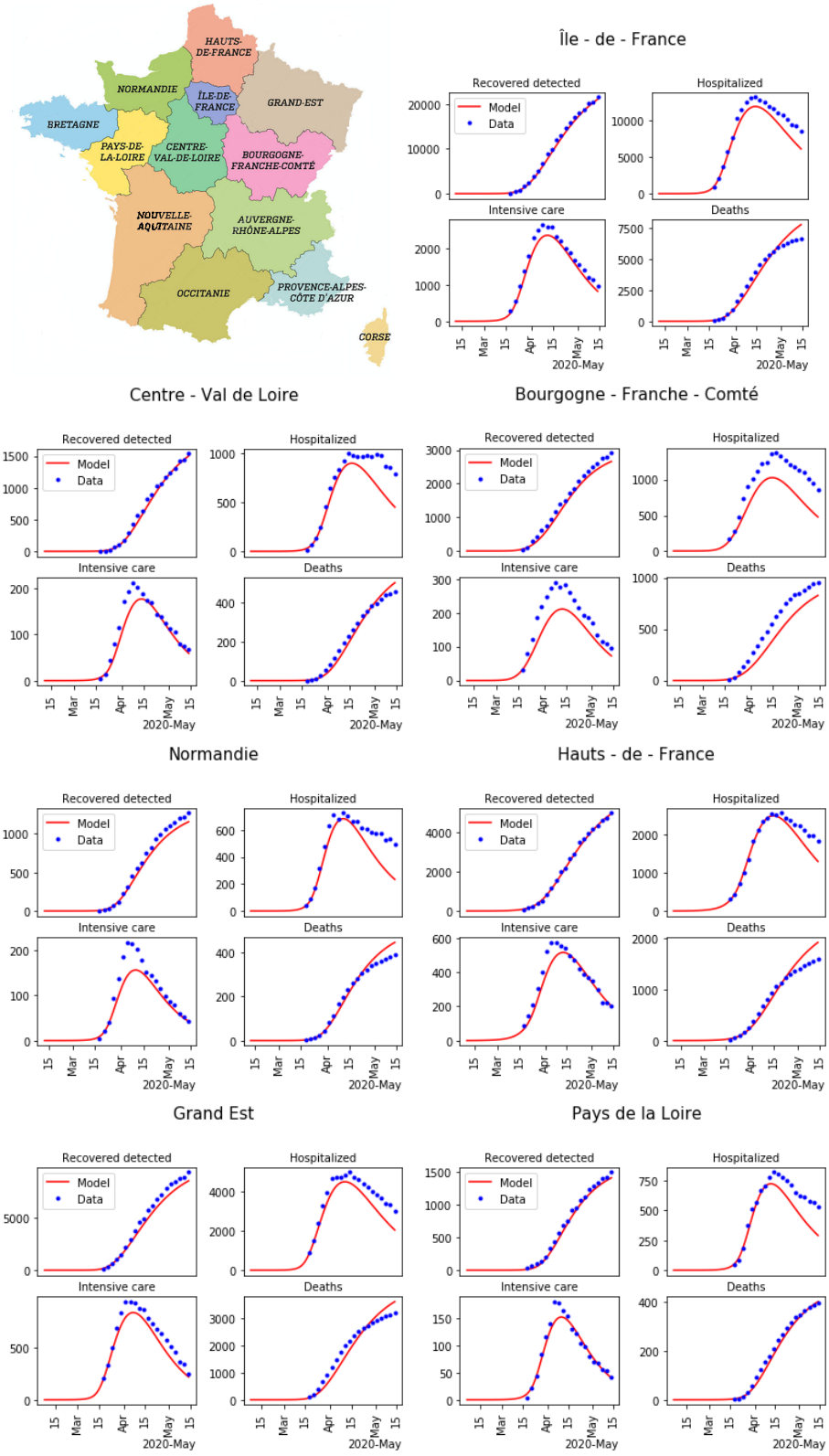

Figure 6.6: Minimap of regions in France, and result of the parameters calibration for the first 7 regions among 13.

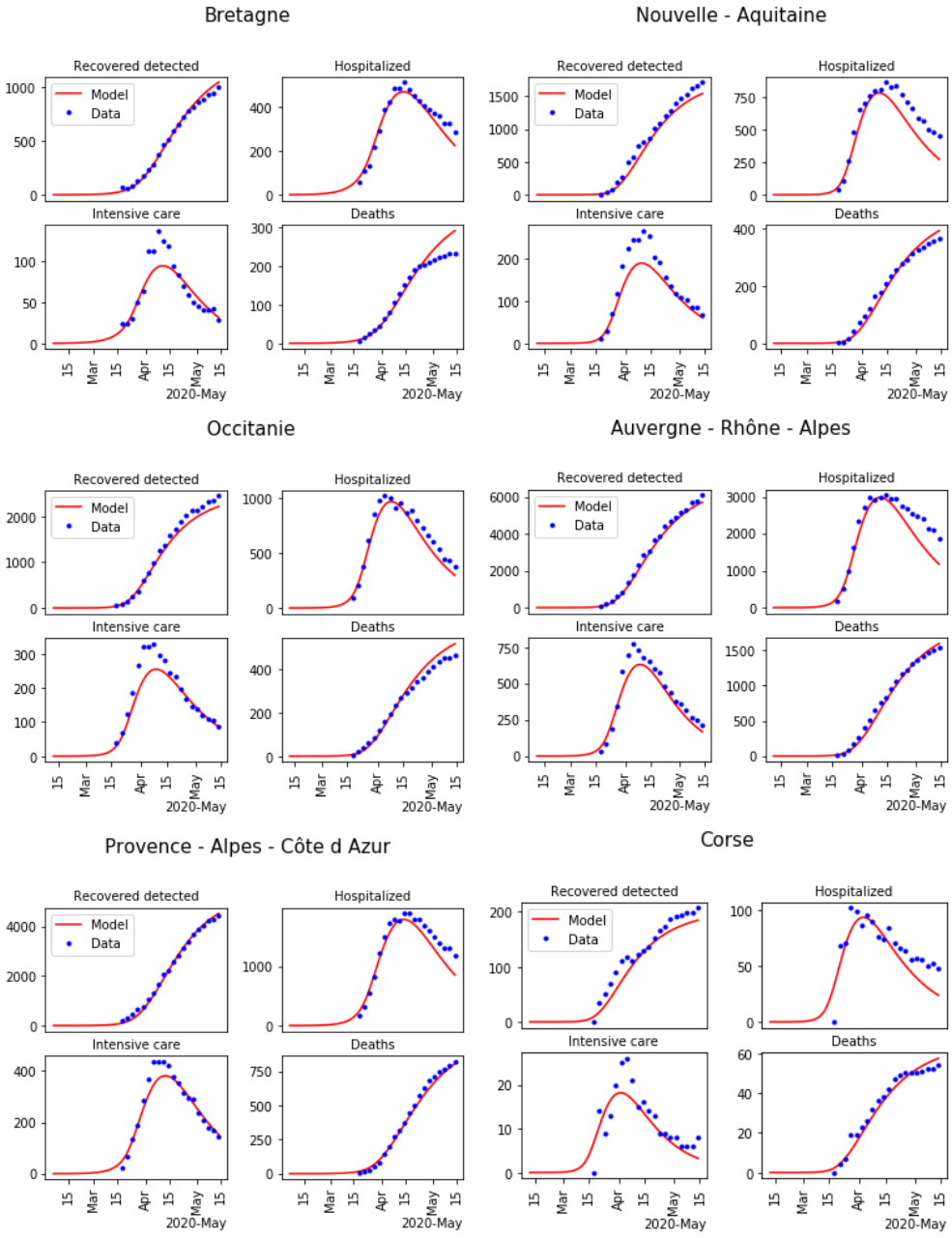

Figure 6.7: Result of parameters calibration for the last 6 regions among 13.

RegionsParameters	N_{IH}	N_{HD}	N_{UD}	N_{HR}	N_{UR}	μ
Île-de-France	12.0	20.0	9.724	25.0	20.0	0.10
Centre-Val de Loire	12.0	20.0	12.0	25.0	15.0	0.1
Bourgogne-Franche-Comté	12.0	20.0	8.391	25.0	20.0	0.043
Normandie	12.0	20.0	12.0	23.027	20.0	0.1
Hauts-de-France	12.0	20.0	9.303	24.331	20.0	0.1
Grand Est	11.221	20.0	8.0	25.0	20.0	0.0997
Pays de la Loire	12.0	20.0	12.0	25.0	20.0	0.1
Bretagne	12.0	15.225	12.0	25.0	15.096	0.1
Nouvelle-Aquitaine	12.0	20.0	12.0	25.0	20.0	0.1
Occitanie	12.0	20.0	12.0	25.0	20.0	0.1
Auvergne-Rhône-Alpes	12.0	20.0	12.0	25.00	20.0	0.1
Provence-Alpes-Côte d'Azur	8.867	20.0	12.0	25.0	20.0	0.084
Corse	12.0	20.0	12.0	25.0	20.0	0.1

Table 6.3: Optimal values of parameters N_{IH}, N_{HD}, N_{UD}, N_{HR}, N_{UR}, μ for each region.

RegionsParameters	κ	$\lambda_1^{(4)}$	p_{HU}	N_{HU}
Île-de-France	35.759	0.0001	0.001	3.071
Centre-Val de Loire	40.141	0.0001	0.01	10.0
Bourgogne-Franche-Comté	25.360	0.001	0.00291	1.564
Normandie	37.718	0.000152	0.01	10.0
Hauts-de-France	40.928	0.000193	0.01	10.0
Grand Est	33.745	0.000261	0.0011	4.588
Pays de la Loire	43.524	0.000296	0.001	8.917
Bretagne	44.838	0.000259	0.01	10.0
Nouvelle-Aquitaine	36.702	0.000194	0.0064	2.277
Occitanie	36.056	0.000330	0.01	2.094
Auvergne-Rhône-Alpes	37.142	0.000247	0.001	3.238
Provence-Alpes-Côte d'Azur	42.813	0.001	0.01	10.0
Corse	29.198	0.000271	0.01	10.0

Table 6.4: Optimal values of parameters κ, $\lambda_1^{(4)}$, p_{HU}, N_{HU} for each region.

6.3 Network simulation

In order to characterize the dynamics of the pandemic transmission processes during the confinement, the epidemiological model (6.5)-(6.12) was described in the previous section. We now consider the government action of unlocking down after confinement, there is a pandemic transmission effect between each region in France. The following pandemic network model of N regions

RegionsParameters	I_0^-	t_0	R_0
Île-de-France	30.454	11/02/2020	4.120
Centre-Val de Loire	1.025	11/02/2020	3.347
Bourgogne-Franche-Comté	1.0	11/02/2020	3.008
Normandie	1.131	12/02/2020	2.774
Hauts-de-France	200.0	10/02/2020	2.883
Grand Est	3.508	08/02/2020	4.5
Pays de la Loire	1.022	06/02/2020	2.772
Bretagne	50.582	06/02/2020	2.5
Nouvelle-Aquitaine	1.282	11/02/2020	2.950
Occitanie	14.708	12/02/2020	2.548
Auvergne-Rhône-Alpes	15.620	11/02/2020	2.884
Provence-Alpes-Côte d'Azur	25.299	06/02/2020	2.583
Corse	1.0	12/02/2020	2.859

Table 6.5: Optimal values of initial conditions I_0^-, start time of infection t_0 and basic reproduction rate R_0.

is introduced, for $i = 1, ..., N$

$$\dot{S}_i(t) = -\beta_i(t) I_i^-(t) S_i(t) + \sum_{k \in C_i} \sigma(i,k,t) \left(\frac{L_{ki}}{N_k} S_k(t) - \frac{L_{ik}}{N_i} S_i(t) \right), \tag{6.20}$$

$$\dot{I}_i^-(t) = \beta_i(t) I_i^-(t) S_i(t) - \lambda_1^{(4i)} I_i^-(t) - (\gamma_{IR}^i + \gamma_{IH}^i + \gamma_{IU}^i) I_i^-(t) + \sum_{k \in C_i} \sigma(i,k,t) \left(\frac{L_{ki}}{N_k} I_k^-(t) - \frac{L_{ik}}{N_i} I_i^-(t) \right), \tag{6.21}$$

$$\dot{I}_i^+(t) = \lambda_1^{(4i)} I_i^-(t) - (\gamma_{IR}^i + \gamma_{IH}^i + \gamma_{IU}^i) I_i^+(t), \tag{6.22}$$

$$\dot{R}_i^-(t) = \gamma_{IR}^i I_i^-(t) - \lambda_2^{(4i)} R_i^-(t) + \sum_{k \in C_i} \sigma(i,k,t) \left(\frac{L_{ki}}{N_k} R_k^-(t) - \frac{L_{ik}}{N_i} R_i^-(t) \right), \tag{6.23}$$

$$\dot{R}_i^+(t) = \gamma_{IR}^i I_i^+(t) + \lambda_2^{(4i)} R_i^-(t) + \gamma_{HR}^i H_i(t) + \gamma_{UR}^i U_i(t), \tag{6.24}$$

$$\dot{H}_i(t) = \gamma_{IH}^i (I_i^-(t) + I_i^+(t)) - (\gamma_{HR}^i + \gamma_{HU}^i + \gamma_{HD}^i) H_i(t), \tag{6.25}$$

$$\dot{U}_i(t) = \gamma_{IU}^i (I_i^-(t) + I_i^+(t)) + \gamma_{HU}^i H_i(t) - (\gamma_{UR}^i + \gamma_{UD}^i) U_i(t), \tag{6.26}$$

$$\dot{D}_i(t) = \gamma_{UD}^i U_i(t) + \gamma_{HD}^i H_i(t), \tag{6.27}$$

where

- the transmission rate $t \mapsto \beta_i(t)$ of region i is a continuous function depending on the scenario (lockdown or no-lockdown), depending on the time t;
- L_{ik} is the number of individuals moving from region i to region k for a given time length T_{ik} depending on the pair (i,k);
- the function $\sigma(i,k,t)$ is a weighting function that determines the mobility between the region i and the region k at time t. It is assumed to be time-periodic with the period T_{ik}, satisfies $\int_0^{T_{ik}} \sigma(i,k,t)\mathrm{d}t = 0$, and takes value in the interval $[-1,1]$;
- N_k is the population of region k; the other parameters $\lambda_1^{(4i)}$, γ_{IR}^i... depend on the location i;
- C_i is the set of all regions that have a pandemic transmission with region i.

As the fast periodic switching policy in [Bin+20], we consider the inverse of the (same) exponential function of infection transmission rate $\beta(t)$ in (6.16) to denote $\beta_i(t)$. Even though the end of confinement, the social strategies still go on, so a continuous function $\beta(t)$ is used for the whole transmission process of COVID-19 from the start date of infection,

$$\beta(t) = \begin{cases} \beta_0 \exp(-\mu(t-\kappa)_+), \text{ during lockdown,} \\ (\beta_0 \exp(-\mu(t_{end}-\kappa)_+) - \beta_0) \exp(-\mu(t-t_{end}-\kappa)_+) + \beta_0, \end{cases} \tag{6.28}$$

after lockdown, with the end time of lockdown t_{end}.
The transmission rate $\beta(t)$ for the whole transmission process is illustrated in Figure 6.8. For the

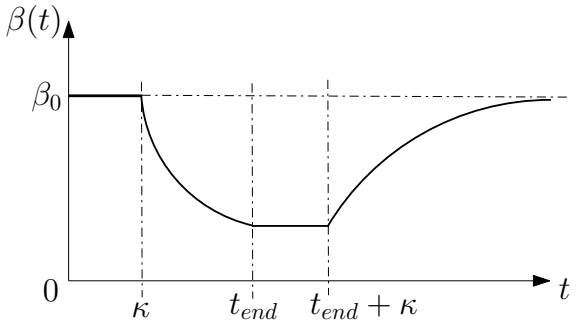

Figure 6.8: Transmission rate β for network model.

mobility analysis after lockdown, we compute the mobility matrix $\{\frac{L_{ki}}{N_k}\}_{N\times N}$ using data of the displacement of population in France as measured by the *Institut national de la statistique et des études économiques* (INSEE). To be more specific, the professional displacements and the scholar displacements are given for each French city in [INS20] for some age classes. This information allows us to compute, for each $k = 1, \ldots, N$, $i = 1, \ldots, N$, $\frac{L_{ki}}{N_k}$ as the fraction of people (with respect to the total population in region k) travelling from the region k to the region i. For the numerical simulation, we assume that the mobility matrix is computed for a time length of one day (that is $T_{ik} = 1$ day) for any pair of regions (i, k). The components of the matrix $\{\frac{L_{ki}}{N_k}\}_{N\times N}$ are shown in Tables 6.6-6.8.

Region kRegion i	Île-de-France	Centre-Val de Loire	Bourgogne-Franche-Comté	Normandie
Île-de-France	0.000e+00	3.662e-04	1.870e-04	3.828e-04
Centre-Val de Loire	5.485e-03	0.000e+00	8.279e-04	5.642e-04
Bourgogne-Franche-Comté	1.136e-03	4.346e-04	0.000e+00	5.651e-05
Normandie	2.803e-03	6.993e-04	5.574e-05	0.000e+00
Hauts-de-France	4.077e-03	6.803e-05	8.013e-05	5.169e-04
Grand Est	7.146e-04	5.116e-05	5.833e-04	6.038e-05
Pays de la Loire	7.411e-04	6.476e-04	5.488e-05	8.895e-04
Bretagne	6.099e-04	1.103e-04	4.689e-05	4.358e-04
Nouvelle-Aquitaine	6.153e-04	3.345e-04	6.910e-05	7.362e-05
Occitanie	4.616e-04	5.165e-05	7.992e-05	5.219e-05
Auvergne-Rhône-Alpes	4.855e-04	1.066e-04	8.104e-04	5.503e-05
Provence-Alpes-Côte d'Azur	5.062e-04	4.511e-05	8.287e-05	5.736e-05
Corse	8.718e-04	1.388e-04	1.388e-04	9.041e-05

Table 6.6: First part of components of mobility matrix $\{\frac{L_{ki}}{N_k}\}_{N\times N}$.

For the numerical simulation, we choose 1 hour as the time step. As far as the function σ is concerned, for any regions i and k, $\sigma(i, k, t)$ is constant and negative between time t =7am and

Region kRegion i	Hauts-de-France	Grand Est	Pays de la Loire	Bretagne	Nouvelle-Aquitaine
Île-de-France	7.848e-04	3.485e-04	2.200e-04	1.412e-04	2.667e-04
Centre-Val de Loire	1.475e-04	1.452e-04	7.035e-04	1.668e-04	7.710e-04
Bourgogne-Franche-Comté	1.020e-04	1.203e-03	6.397e-05	5.295e-05	1.091e-04
Normandie	8.391e-04	1.043e-04	6.113e-04	4.062e-04	1.193e-04
Hauts-de-France	0.000e+00	6.536e-04	6.719e-05	7.274e-05	8.853e-05
Grand Est	3.738e-04	0.000e+00	7.719e-05	7.086e-05	8.116e-05
Pays de la Loire	1.112e-04	8.988e-05	0.000e+00	1.470e-03	1.013e-03
Bretagne	1.175e-04	9.190e-05	1.661e-03	0.000e+00	1.835e-04
Nouvelle-Aquitaine	1.229e-04	8.998e-05	6.295e-04	9.172e-05	0.000e+00
Occitanie	1.169e-04	9.261e-05	7.412e-05	6.760e-05	1.044e-03
Auvergne-Rhône-Alpes	1.262e-04	1.512e-04	6.770e-05	6.426e-05	2.210e-04
Provence-Alpes-Côte d'Azur	1.212e-04	1.117e-04	5.164e-05	6.124e-05	1.312e-04
Corse	1.970e-04	1.647e-04	6.781e-05	1.292e-04	4.036e-04

Table 6.7: Second part of components of mobility matrix $\{\frac{L_{ki}}{N_k}\}_{N\times N}$.

Region kRegion i	Occitanie	Auvergne-Rhône-Alpes	Provence-Alpes-Côte d'Azur	Corse
Île-de-France	2.133e-04	3.019e-04	1.429e-04	1.001e-05
Centre-Val de Loire	1.209e-04	3.582e-04	6.160e-05	2.747e-06
Bourgogne-Franche-Comté	1.009e-04	1.918e-03	1.084e-04	3.198e-06
Normandie	8.647e-05	1.681e-04	6.719e-05	2.712e-06
Hauts-de-France	8.618e-05	1.409e-04	5.090e-05	1.008e-06
Grand Est	7.556e-05	1.791e-04	1.106e-04	1.808e-06
Pays de la Loire	9.884e-05	2.159e-04	5.404e-05	2.520e-06
Bretagne	1.097e-04	1.638e-04	6.189e-05	6.252e-06
Nouvelle-Aquitaine	9.997e-04	3.356e-04	9.190e-05	4.873e-06
Occitanie	0.000e+00	6.060e-04	1.626e-03	7.430e-06
Auvergne-Rhône-Alpes	3.787e-04	0.000e+00	4.293e-04	6.202e-06
Provence-Alpes-Côte d'Azur	1.115e-03	8.193e-04	0.000e+00	2.613e-05
Corse	5.199e-04	3.487e-04	1.698e-03	0.000e+00

Table 6.8: Third part of components of mobility matrix $\{\frac{L_{ki}}{N_k}\}_{N\times N}$.

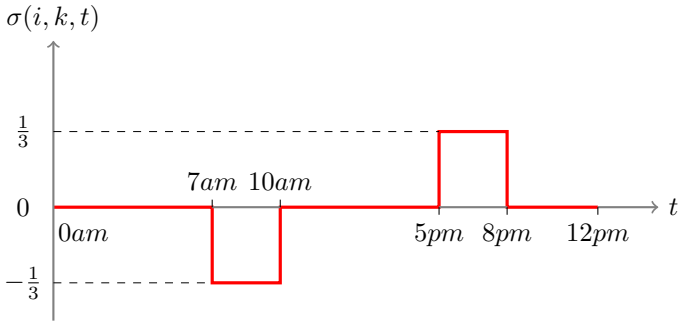

Figure 6.9: Weighting function $\sigma(i,k,.)$ for mobility matrix, for any pair of regions (i,k).

t =10am and $\sigma(i,k,t)$ is constant and positive between t =5pm and t =8pm, zero otherwise and satisfies $\int_{day}\sigma(i,k,t)dt=0$. See Figure 6.9 for the discretized version of the function $t\mapsto\sigma(i,k,t)$. Physically, it corresponds to constant traffic of people in the morning from region i to region k and constant traffic of people back in the afternoon. The simulation results of the considered network model for 13 regions in France are shown in images 6.10 and 6.11, all parameters and the values of all states at the starting date of lockdown have been identified during the lockdown, and the end date of confinement is 11th of May in France. Note that the end of the simulation horizon on images 6.10 and 6.11 is the beginning of August, thus the calibrated parameters appear to fit very well to the data during 2.5 months, which is very positive.

6.4 Network of cities

In this section, we use the parameter identification method developed in Section 6.2 to simulate another network of areas. Instead of considering the network of the 13 metropolitan regions as in Section 6.3, we consider the network of all French cities. There are around 36.000 cities in France, and INSEE measures the displacement of people between each couple of cities [INS20]. To simulate the transport effect on the pandemic dynamics, we follow the same approach as in Section 6.3. To be more specific, we use the same model as (6.20)-(6.27) but instead of considering $N=13$ regions, we consider $N=36.000$ cities:

$$\dot{S}_i(t)=-\beta_i(t)I_i^-(t)S_i(t)+\sum_{k\in C_i}\sigma(i,k,t)\left(\frac{L_{ki}}{N_k}S_k(t)-\frac{L_{ik}}{N_i}S_i(t)\right), \tag{6.29}$$

$$\begin{aligned}\dot{I}_i^-(t)=&\beta_i(t)I_i^-(t)S_i(t)-\lambda_1^{(4i)}I_i^-(t)-(\gamma_{IR}^i+\gamma_{IH}^i+\gamma_{IU}^i)I_i^-(t)\\&+\sum_{k\in C_i}\sigma(i,k,t)\left(\frac{L_{ki}}{N_k}I_k^-(t)-\frac{L_{ik}}{N_i}I_i^-(t)\right),\end{aligned} \tag{6.30}$$

$$\dot{I}_i^+(t)=\lambda_1^{(4i)}I_i^-(t)-(\gamma_{IR}^i+\gamma_{IH}^i+\gamma_{IU}^i)I_i^+(t), \tag{6.31}$$

$$\dot{R}_i^-(t)=\gamma_{IR}^iI_i^-(t)-\lambda_2^{(4i)}R_i^-(t)+\sum_{k\in C_i}\sigma(i,k,t)\left(\frac{L_{ki}}{N_k}R_k^-(t)-\frac{L_{ik}}{N_i}R_i^-(t)\right), \tag{6.32}$$

$$\dot{R}_i^+(t)=\gamma_{IR}^iI_i^+(t)+\lambda_2^{(4i)}R_i^-(t)+\gamma_{HR}^iH_i(t)+\gamma_{UR}^iU_i(t), \tag{6.33}$$

$$\dot{H}_i(t)=\gamma_{IH}^i(I_i^-(t)+I_i^+(t))-(\gamma_{HR}^i+\gamma_{HU}^i+\gamma_{HD}^i)H_i(t), \tag{6.34}$$

$$\dot{U}_i(t)=\gamma_{IU}^i(I_i^-(t)+I_i^+(t))+\gamma_{HU}^iH_i(t)-(\gamma_{UR}^i+\gamma_{UD}^i)U_i(t), \tag{6.35}$$

$$\dot{D}_i(t)=\gamma_{UD}^iU_i(t)+\gamma_{HD}^iH_i(t),\ i=1,...,N, \tag{6.36}$$

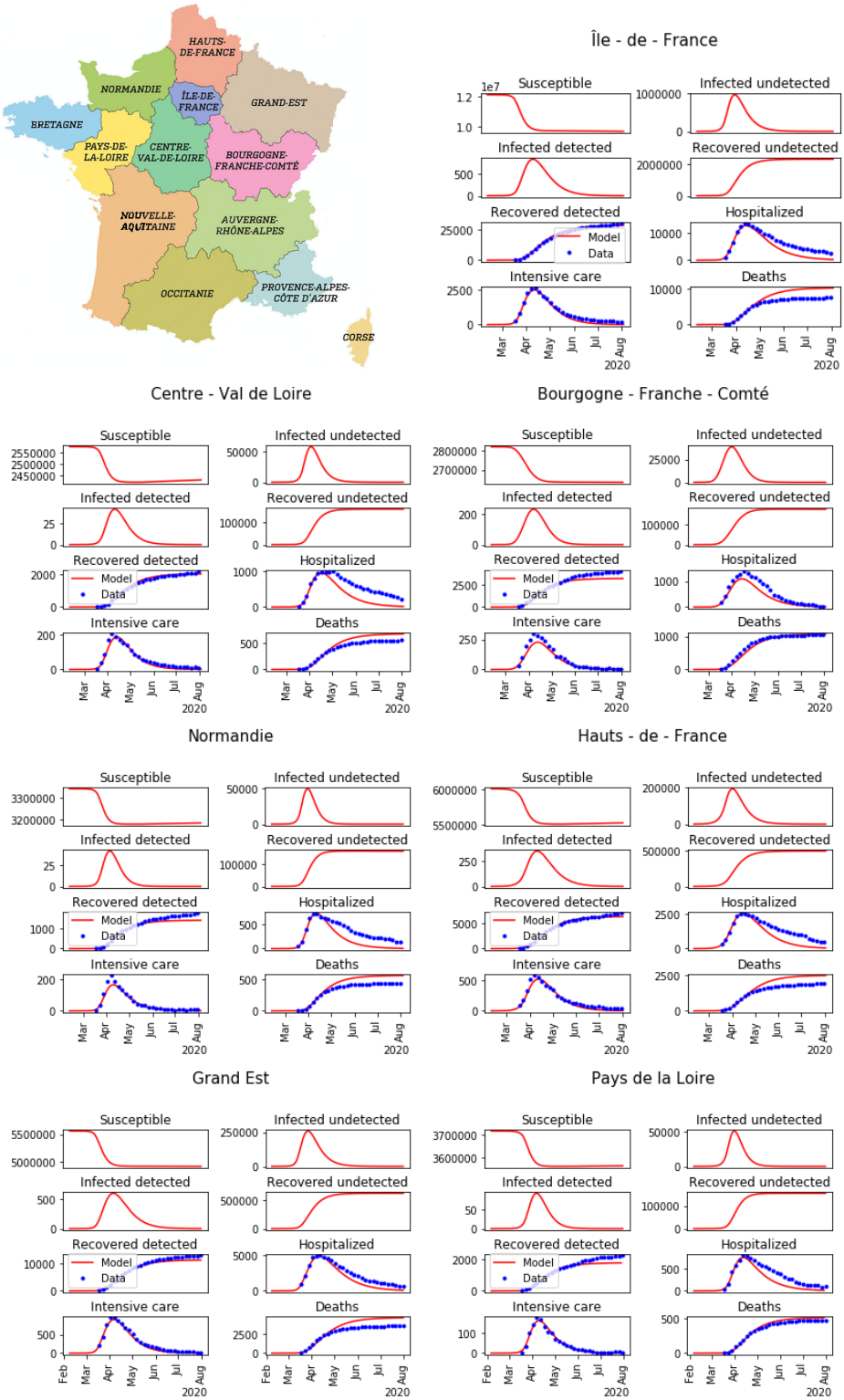

Figure 6.10: Minimap of regions in France, and simulation of pandemic network model for first 7 regions among 13.

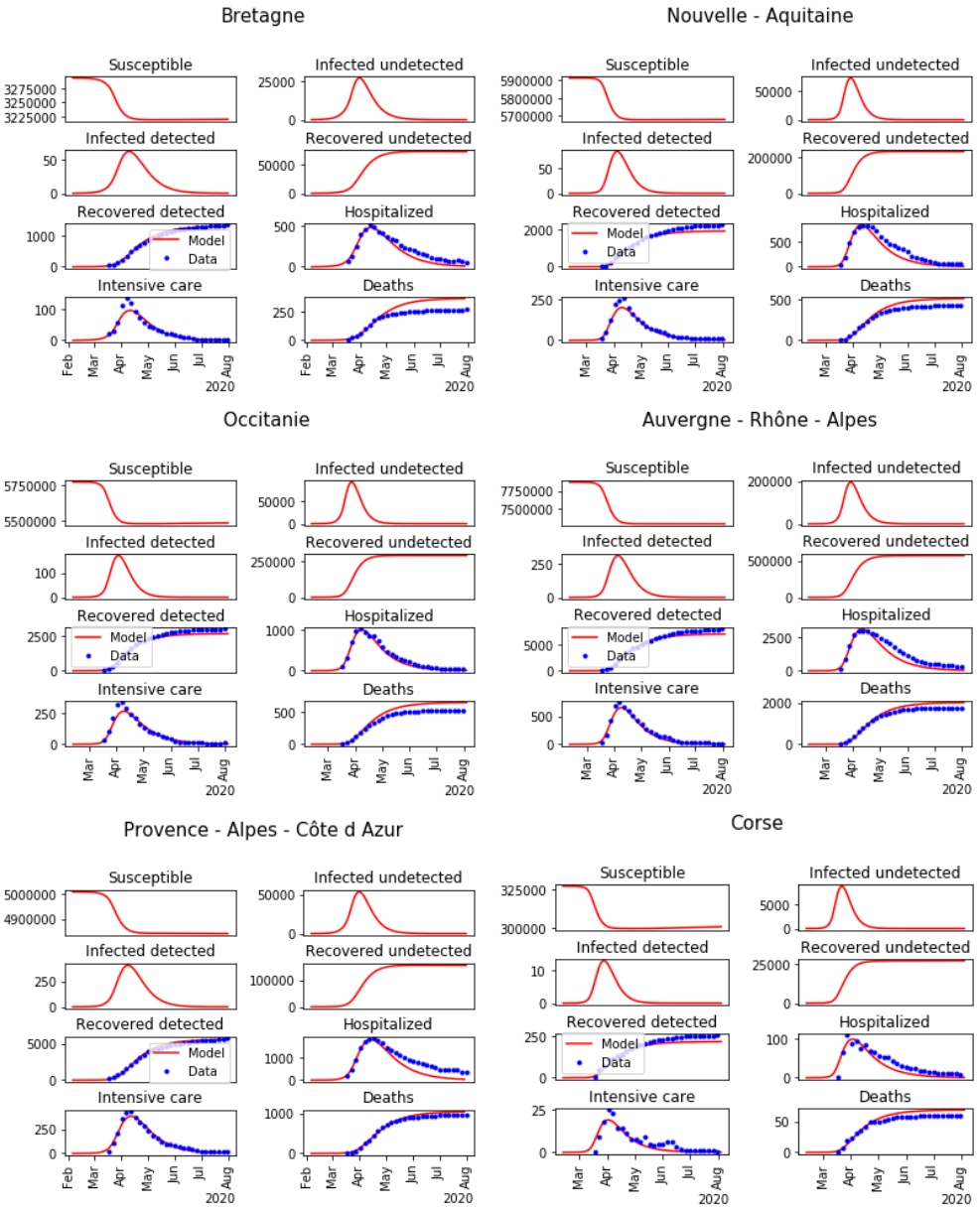

Figure 6.11: Simulation of pandemic network model for the last 6 regions among 13.

where L_{ki} is the number of individuals moving from city k to the city i and is derived from the real data of INSEE, and C_i is the set of all cities that have a pandemic transmission with city i. All the other parameters are chosen as the ones of the region to which each city belongs.

To simulate this system of $8 * 36.000$ differential equations, we now specify initial conditions. To simplify, the epidemic start date of each city is taken as the same as the epidemic start date of the region to which it belongs, and the initial condition for the undetected infected individuals I_0^- for the capital of each region is one of the regions, while it is set to 0 for all other cities in the region. It is equivalent to saying that the pandemic dynamics start at the capital of each region. The population of each French city is used as the initial condition for the susceptible individuals.

The transport effect between cities is seen on images 6.12-6.14.

In these images, we observe the spatial evolution of the pandemics between 2020-03-17 and 2020-08-01. At an early date, the results are impacted by the initial conditions. During the lockdown, the pandemic is just located in the regional capitals because no infected people can go out of the capitals (compare the left and right parts of Figure 6.12 with the left part of Figure 6.13) and recall that the end of the lockdown in France in the 11th of May. Then the effect of transport between cities is seen after lockdown when other cities than capitals are affected see Figure 6.13 (right) and Figure 6.14. Using Figure 6.13 (right) and Figure 6.14 allows to conclude that the number of undetected infected are decreasing until the 1st of August. Note that we did not model the wearing of cloth face coverings in public settings, which could be included in the modeling of the transmission rate $\beta(t)$.

6.5 Discussion and a new integro-differential model

In this section, the general form of an integrodifferential model capable of integrating different age classes and areas is introduced to discuss the transport effect of COVID-19 in France after the lockdown. By "areas" we mean a given geographical scale as the set of 13 Metropolitan regions (as considered in Section 6.3), or the set or all 101 French departments, or all cities (as considered in Section 6.4), or other geographical areas. For each age class $a \in ages$ in area $x \in areas$, we consider the following integrodifferential equations, for any time $t \geq 0$ after confinement,

$$\begin{aligned}\partial_t X(a,x,t) =& f_a(X(.,x,t)) + \int_{areas} \sigma(a,x,y,t)\Big(\Lambda_{in}(a,x,y,t)X(a,y,t) \\ &- \Lambda_{out}(a,x,y,t)X(a,x,t)\Big)\,\mathrm{d}y + F_{ext}(a,x,t),\end{aligned} \tag{6.37}$$

with

- $ages$, the set of different age classes of the population, depending on the age scale under study. As an example, we can consider all scholar age classes, or elderly ages, or a mix of such age classes as the set

$$ages = \{-15,\ 15-44,\ 44-64,\ 65-74,\ 75-\}\ ;$$

- $areas$, the set of different areas of the population under study, depending on the considered geographical scale. As an example, considering all metropolitan regions, as considered in

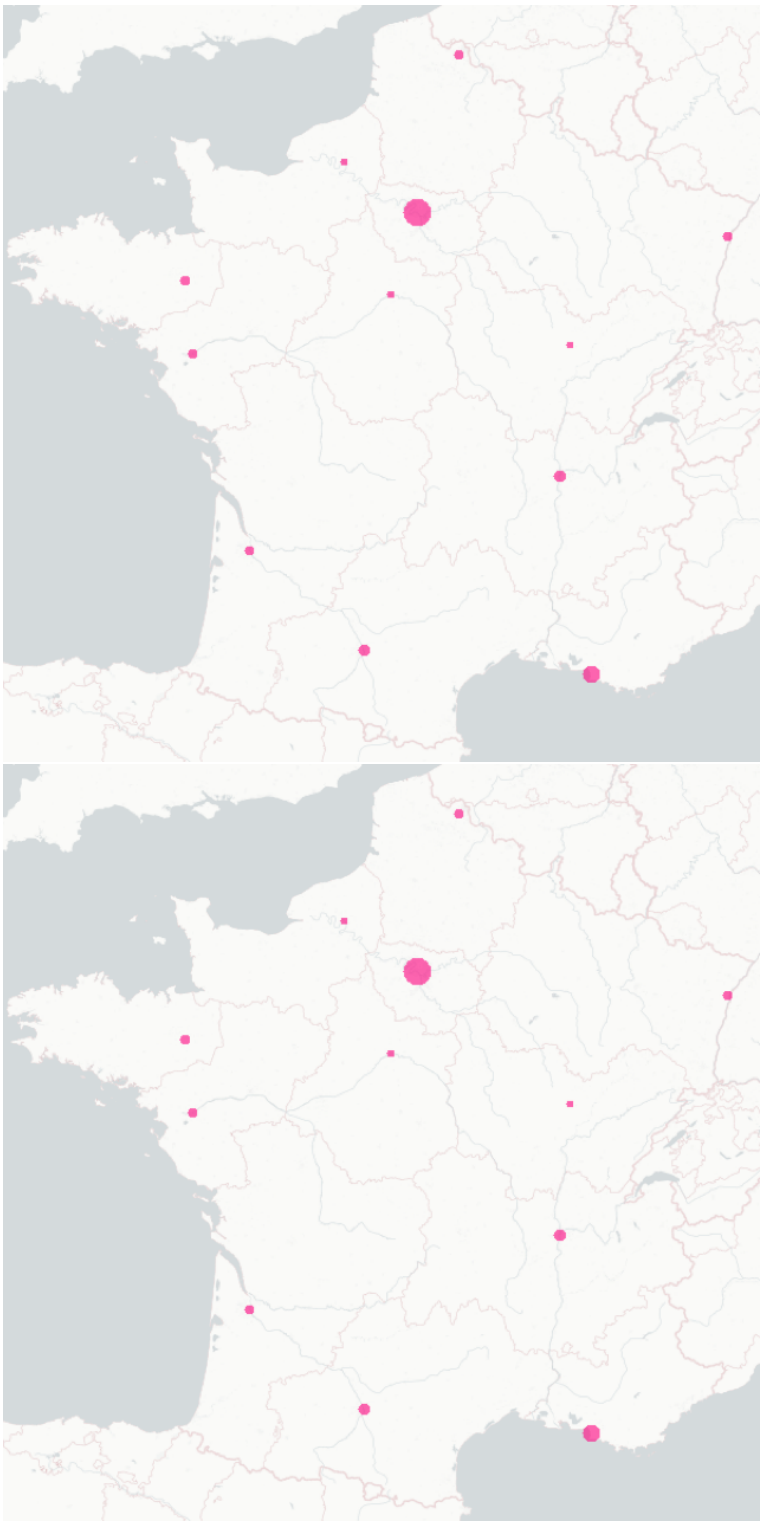

Figure 6.12: The maps of the transport effect between cities in France (undetected infected plus detected infected from 0% (blue) to 2% (magenta) of the population for each commune): the date for the map on the top is 2020-03-17 (start date of the lockdown in France) and the one for the map on the bottom is 2020-04-01.

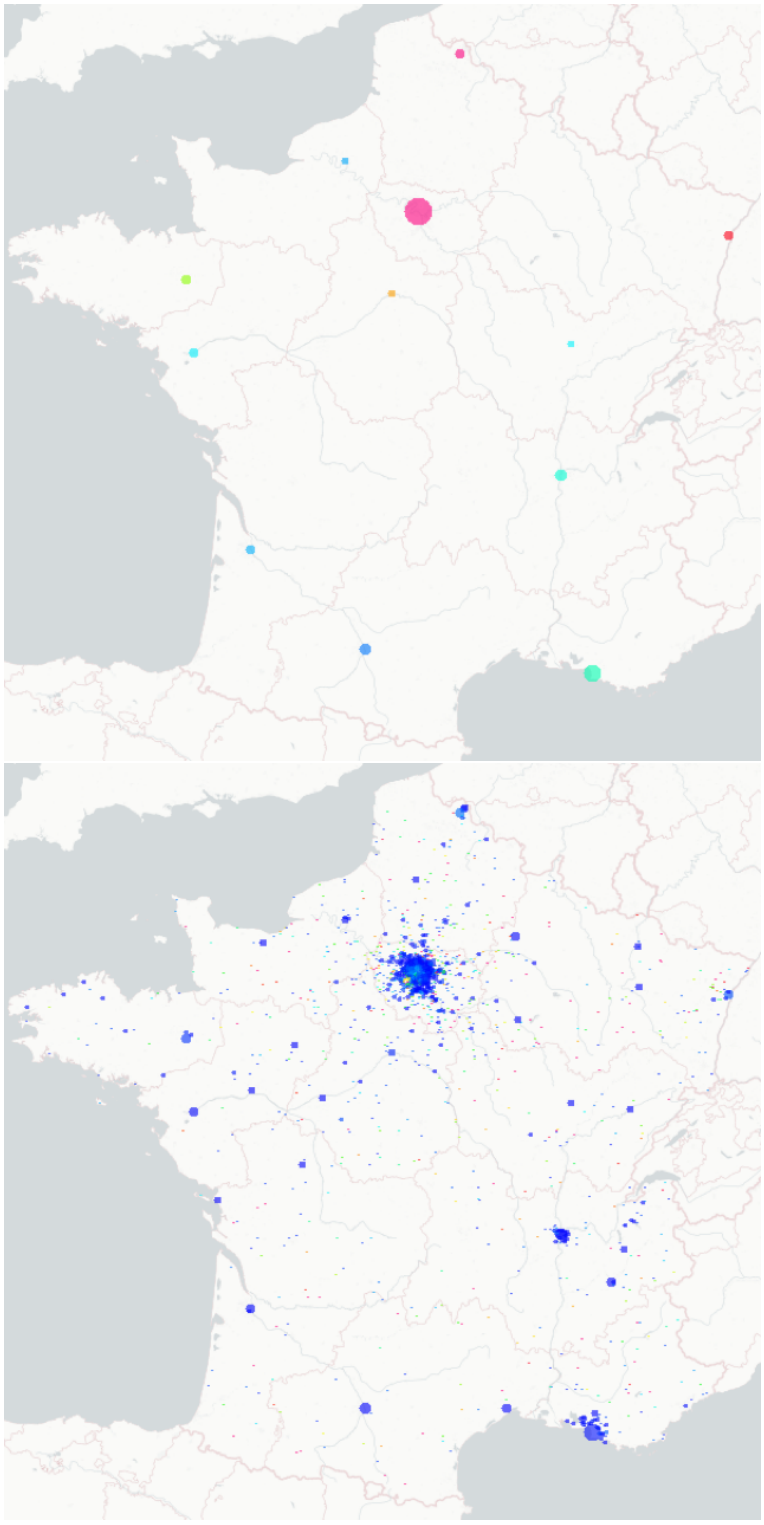

Figure 6.13: The maps of the transport effect between cities in France (undetected infected plus detected infected from 0% (blue) to 2% (magenta) of the population for each commune): the date for the map on the left is 2020-05-01 and the one for the map on the right is 2020-06-01.

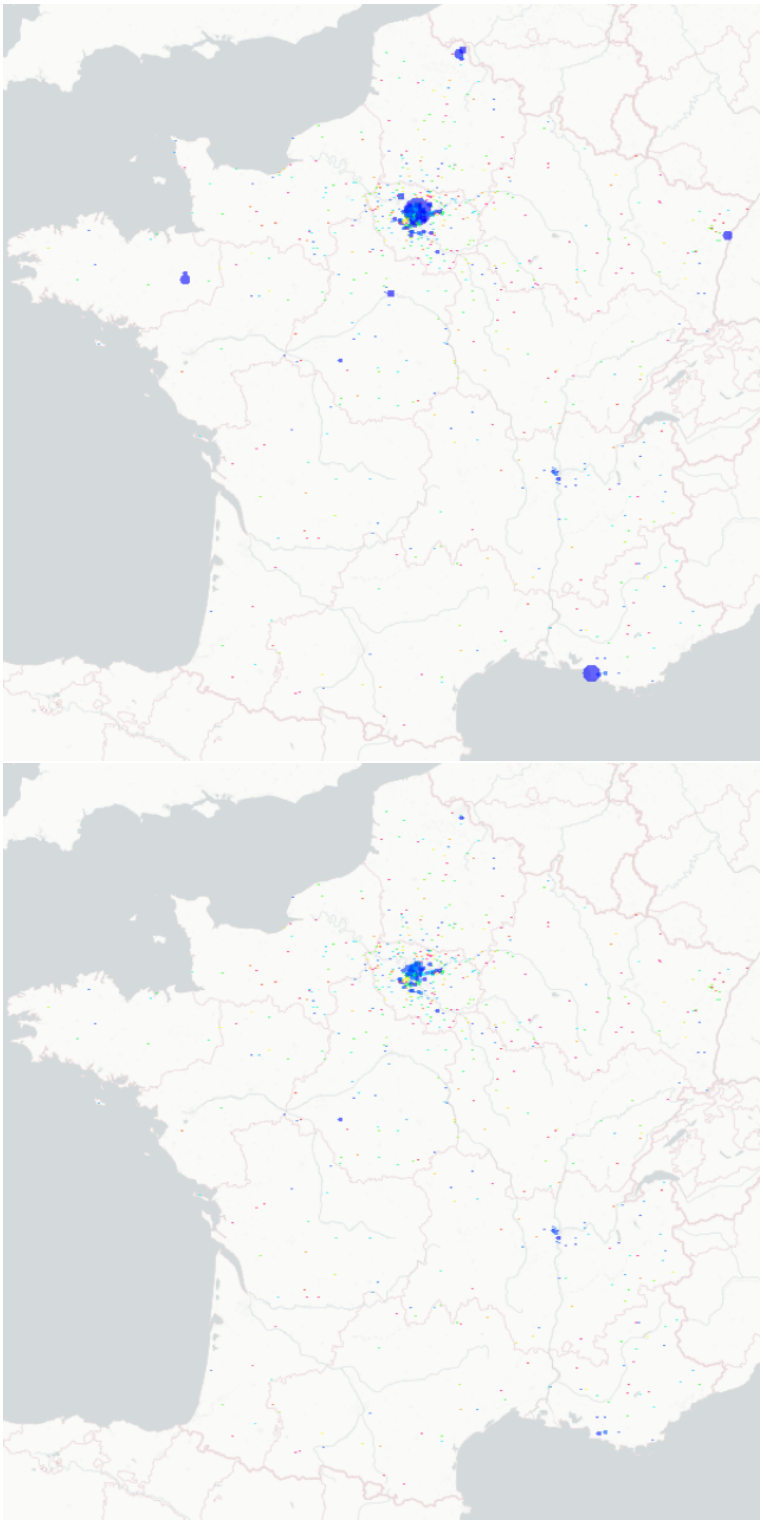

Figure 6.14: The maps of the transport effect between cities in France(undetected infected plus detected infected from 0% (blue) to 2% (magenta) of the population for each commune): the date for the map on the left is 2020-07-01 and the one for the map on the right is 2020-08-01.

Section 6.3, yields the set

$$\begin{aligned} areas = \{&\text{Île - de - France, Centre-Val de Loire, Bourgogne - Franche - Comté,} \\ &\text{Normandie, Hauts - de - France, Grand Est, Pays de la Loire,} \\ &\text{Bretagne, Nouvelle - Aquitaine, Occitanie, Auvergne - Rhône - Alpes,} \\ &\text{Corse, Provence - Alpes - Côte d'Azur}\}, \end{aligned}$$

As another example, considering all French departments give a set of 101 areas, or considering the geographical scale of French cities yields a set of around 36.000 areas, as considered in Section 6.4 and so on... We can even consider the set of countries to model the international transport effect when international activities become more frequent.

- $X(a,x,t) \in \mathbb{R}^8$ is the 8-vector consisting of compartments of the age class a, in the area x, at time t;

- For all age class a, $f_a(X(.,x,t))$ is the pandemic transmission dynamics for age class a from all other age classes in the area x at time t. Without considering the age effect, it is given by the right-hand side of systems (6.5)-(6.12). Inspired by the contact matrix approach developed in e.g. [KR08, Chapter 3, Page 76], by considering multiple age classes, the transmission term is the following integral

$$\int_{ages} \beta_{a,b,x}(t) I^-(b,x,t)\,\mathrm{d}b\; S(a,x,t)$$

instead of

$$\beta(t) I^-(t) S(t)\ ,$$

where $\beta_{a,b,x}(t)$ is the contact function between age classes a and b, in the area x, and at time t. Therefore the function f_a is given by

$$f_a(X(.,x,t)) = \begin{pmatrix} -\int_{ages} \beta_{a,b,x}(t) I^-(b,x,t)\,\mathrm{d}b\; S(a,x,t), \\ \int_{ages} \beta_{a,b,x}(t) I^-(b,x,t)\,\mathrm{d}b\; S(a,x,t) - \lambda_1^{(4)} I^-(a,x,t) - (\gamma_{IR}+\gamma_{IH}+\gamma_{IU}) I^-(a,x,t), \\ \lambda_1^{(4)} I^-(a,x,t) - (\gamma_{IR}+\gamma_{IH}+\gamma_{IU}) I^+(a,x,t), \\ \gamma_{IR} I^-(a,x,t) - \lambda_2^{(4)} R^-(a,x,t), \\ \gamma_{IR} I^+(a,x,t) + \lambda_2^{(4)} R^-(a,x,t) + \gamma_{HR} H(a,x,t) + \gamma_{UR} U(a,x,t), \\ \gamma_{IH}(I^-(a,x,t) + I^+(a,x,t) - (\gamma_{HR}+\gamma_{HU}+\gamma_{HD}) H(a,x,t), \\ \gamma_{IU}(I^-(a,x,t) + I^+(a,x,t) + \gamma_{HU} H(a,x,t) - (\gamma_{UR}+\gamma_{UD}) U(a,x,t), \\ \gamma_{UD} U(a,x,t) + \gamma_{HD} H(a,x,t) \end{pmatrix}^\top$$

where all parameters depend on the age class a and the area x;

- $\Lambda_{in}(a,x,y,t) \in \mathbb{R}$ is the density of people coming (in) area x from area $y \in areas$ at time t, for age class a;

- $\Lambda_{out}(a,x,y,t) \in \mathbb{R}$ is the density of people going to (out) area $y \in areas$ from area x at time t, for age class a;

- $F_{ext}(a,x,t) \in \mathbb{R}^8$ is the external flux coming into location x at time t in the age class a. As an example for the simulations of Section 6.3 (where the metropolitan regions are considered) and of Section 6.4 (where all French cities are considered), it is 0 because the boundary of France is close (at the time of the simulation);

- $\sigma(a,x,y,t)$ is a weighting function that determines the mobility between area x and area y, at time time t for the age class a. It stands for a (lockdown or no-lockdown) function for the age class a, between the areas x and y at time t. As an example, before the 11th of May, it was forbidden to travel for more than 100km in France. Such a policy could depend on the age classes and on the areas, e.g., to control so-called "clusters" of COVID-19;
- $\int_{areas} \sigma(a,x,y,t)\Lambda_{in}(a,x,y,t)X(a,y,t)\,\mathrm{d}y$ provides the total number of people coming into area x from all the other areas;
- $\int_{areas} \sigma(a,x,y,t)\Lambda_{out}(a,x,y,t)\,\mathrm{d}y\,X(a,x,t)$ provides the total number of people coming from area x into any of the other areas.

Equation (6.37) describes the network dynamics of the COVID-19 pandemic after lockdown and the transport effect on different age classes on the basis of the regional pandemic transmission dynamics during the lockdown. The interest of this model is that it could be adapted to any geographical scale, and to all age classes. From a control point of view, the most important term is $\sigma(a,x,y,t)$ which defines the lockdown policy that defines the mobility between areas x and y at time t for the age class a. Many control problems could be studied for this model, as optimal control to reduce the pandemic effect, or to minimize mortality in particular. It is of great importance for the mobility dynamics of the pandemic.

Beyond that, inspired by advection-diffusion modeling of population dynamics (as considered in [FM07]), it is natural to model the displacement inside a given area by a diffusion term (see [Cra80]). The corresponding model is formulated as follows:

$$\begin{aligned}\partial_t X(a,x,t) =& f_a(X(.,x,t)) + d(a,x,t)\partial_{xx}X(a,x,t) + \int_{areas} \sigma(a,x,y,t)\Big(\Lambda_{in}(a,x,y,t)X(a,y,t)\\ &- \Lambda_{out}(a,x,y,t)X(a,x,t)\Big)\,\mathrm{d}y + F_{ext}(a,x,t),\end{aligned} \tag{6.38}$$

where the diffusion coefficient $d(a,x,t)$ is a function that depends on age class a, areas x and time t.

This 2nd order partial differential equation predicts, for age class a in the area x, how diffusion and displacement cause the number of individuals in the different compartments, especially undetected infectives and deaths. As long as one susceptible person is infected after directly or indirectly contacting disease carriers in the area x, diffusion takes place. When the number of infectious individuals in a local area is low compared to the surrounding areas, the pandemic will diffuse from the surroundings, so the number of infections in this area will increase. Conversely, the pandemic will diffuse and the number of infections will increase in the surrounding areas.

Finally, gender differentiation or other properties may be taken into account to characterize types of populations and to study the optimal lockdown control of pandemic dynamics based on our previous work. It is worth stressing that, in the long run, optimal lockdown strategies should consider the balance between the lower number of deaths and minimum healthcare and social costs.

6.6 Conclusion

In this chapter, we investigated an extended model of the classical SIRD pandemic model to characterize the regional transmission of COVID-19 after the lockdown in France. Incorporating

the time delays arising from incubation, testing, and the complex effects of government measures, an exponential function of the transmission rate β was presented for the regional model. By fitting the regional model to the real data, the optimal parameters of this regional model for each region in France were derived. Based on the previous results of the extended model, we introduced and simulated a network model of pandemic transmission between regions after confinement in France while considering age classes. Regarding the transmission rate β for the network model, we selected a continuous function related to the reciprocal function of β during lockdown to contribute to the transport effect after lockdown. By using the same model and method, we simulated the pandemic network for all cities in France to visualize the transport effects of the pandemic between cities. Considering age classes, we discussed an integrodifferential equation for modeling the network of infectious diseases in the discussion part.

In future works, we will formulate and study optimal control problems in order to balance the induced sanitary and economic costs. The lockdown strategies implemented in France should be evaluated and compared to the proposed optimal strategies.

Chapter 7

Conclusion and perspectives

The analysis of stability and rejection of disturbances for homogeneous and heterogeneous hyperbolic PDEs traffic flow systems has been addressed in this thesis. The motivation is to optimally solve the traffic congestion problem with the high traffic demand at the left inlet and a bottleneck in the downstream boundary of the considered road segment. Inspired by the research of traffic flow systems, by using the optimization method to fit the extended regional ODEs model and network model to the real data, parameters of pandemic models are identified, and then the pandemic network for all cities in France is simulated to visualize the transport effects of the pandemic between cities.

For homogeneous traffic flow systems, this research addressed the problem of seeking the optimal tuning PI boundary feedback controller and designing an observer-based output feedback control law for the linearized ARZ system. The conditions for finite-gain L^2 stability and the computation of the L^2 gain were given in Chapter 2. Based on these conditions, we formulated and solved an optimization problem to derive the optimal tuning PI controller. Moreover, numerical simulation emphasizes the interest of this optimal tuning controller for the nonlinear model. In Chapter 3, a full-state feedback controller was designed to stabilize the linearized ARZ model. And designing an exponentially convergent observer with proper injection gains, an output feedback controller, and the iISS of a closed-loop system were achieved by only measuring the upstream inlet vehicles' velocity.

For heterogeneous traffic flow systems, the robust control problem was studied to stabilize the multi-type linearized AR traffic flow system in Chapter 4. A controller was designed by using backstepping and the existence of an optimal tuning controller was validated by solving the optimization problem. Then, in Chapter 5, applying the control law which was designed for the linearized system to the quasi-linear system to solve the problem of boundary stabilization by actuation at the inlet boundary of the considered road segment.

In Chapter 6, an extended model of the classical SIRD pandemic model is studied to characterize the regional transmission of COVID-19 after the lockdown in France. Incorporating the time delays arising from incubation, testing, and the complex effects of government measures and fitting the regional model to the real data, the parameters of the regional model are identified for each region in France. Based on the previous results of the extended model, we introduced and simulated a network model of pandemic transmission between regions after confinement in France while considering age classes. By using the same model and method, we simulated the pandemic network for all cities in France to visualize the transport effects of the pandemic between cities. Considering age classes, we discussed an integrodifferential equation for modeling the network of infectious diseases in the discussion part.

The main challenges in the future are:

- optimization problems of traffic flow systems with respect to other control objectives such

as the minimum fuel consumption, CO_2 emissions, total travel time and the maximum throughput, driving comfort;

- studying the class of nonlinear traffic flow systems with L^2 disturbance or other disturbance measurement methods to maximize the disturbance rejection capacity, generalizing what is done in Chapter 2;
- the extension of the optimization problem to the network of roads with consecutive bottlenecks;
- introducing some new technologies, such as the event-triggered communication technique (working with Nicolas Espitia and Ying Tang on a joint paper of robust event-triggered control for the ARZ traffic flow system by using small-gain method).

Bibliography

[AA18] Henrik Anfinsen and Ole Morten Aamo. "Adaptive control of linear 2×2 hyperbolic systems". In: *Automatica* 87 (2018), pp. 69–82 (cit. on p. 6).

[AA19] Henrik Anfinsen and Ole Morten Aamo. *Adaptive Control of Hyperbolic PDEs*. Communications and Control Engineering. Springer, 2019 (cit. on p. 41).

[AB22] Jean Auriol and Delphine Bresch Pietri. "Robust state-feedback stabilization of an underactuated network of interconnected $n + m$ hyperbolic PDE systems". In: *Automatica* 136.110040 (2022) (cit. on p. 5).

[ACL05] Kiam Heong Ang, Gregory Chong, and Yun Li. "PID control system analysis, design, and technology". In: *IEEE transactions on control systems technology* 13.4 (2005), pp. 559–576 (cit. on p. 5).

[AD08] V Thamizh Arasan and G Dhivya. "Measuring heterogeneous traffic density". In: *Proceedings of International Conference on Sustainable Urban Transport and Environment, World Academy of Science, Engineering and technology, Bangkok*. Vol. 36. Citeseer. 2008, p. 342 (cit. on p. 5).

[AR00] A. Aw and M. Rascle. "Resurrection of "second order" models of traffic flow". In: *SIAM Journal on Applied Mathematics* 60.3 (2000), pp. 916–938 (cit. on p. 3).

[Aur20] Jean Auriol. "Output feedback stabilization of an underactuated cascade network of interconnected linear PDE systems using a backstepping approach". In: *Automatica* 117 (2020), p. 108964 (cit. on p. 6).

[Bay+21] Alexandre Bayen, Jean-Michel Coron, Nicola De Nitti, Alexander Keimer, and Lukas Pflug. "Boundary controllability and asymptotic stabilization of a nonlocal traffic flow model". In: *Vietnam Journal of Mathematics* 49.3 (2021), pp. 957–985 (cit. on p. 4).

[BC11] Georges Bastin and Jean-Michel Coron. "On boundary feedback stabilization of non-uniform linear 2×2 hyperbolic systems over a bounded interval". In: *Systems & Control Letters* 60 (2011), pp. 900–906 (cit. on p. 53).

[BC17] Georges Bastin and Jean-Michel Coron. "A quadratic Lyapunov function for hyperbolic density–velocity systems with nonuniform steady states". In: *Systems & Control Letters* 104 (2017), pp. 66–71 (cit. on p. 49).

[BCC12] Fred Brauer and Carlos Castillo-Chavez. *Mathematical Models in Population Biology and Epidemiology*. Vol. 2. Springer, 2012 (cit. on p. 77).

[BCH21] Georges Bastin, Jean-Michel Coron, and Amaury Hayat. "Input-to-State Stability in sup norms for hyperbolic systems with boundary disturbances". In: *Nonlinear Analysis* 208 (2021) (cit. on p. 6).

[BD+35] Greenshields BD, Bibbins JR, Channing WS, and Miller HH. "A study of traffic capacity". In: *Highway Research Board Proceedings* 1935 (1935) (cit. on pp. 3, 14, 48).

[BGC03] Sylvie Benzoni-Gavage and Rinaldo M. Colombo. "An n-populations model for traffic flow". In: *European Journal of Applied Mathematics* 14.5 (2003), 587–612 (cit. on p. 5).

[BHM20] David W Berger, Kyle F Herkenhoff, and Simon Mongey. *An SEIR Infectious Disease Model with Testing and Conditional Quarantine*. Tech. rep. 26901. National Bureau of Economic Research, 2020 (cit. on p. 7).

[Bin+20] M. Bin, P. Cheung, E. Crisostomi, P. Ferraro, H. Lhachemi, R. Murray-Smith, C. Myant, T. Parisini, R. Shorten, S. Stein, and L. Stone. "On Fast Multi-Shot COVID-19 Interventions for Post Lock-Down Mitigation". In: arXiv:2003.09930 (2020) (cit. on p. 91).

[Bla80] Leland Blank. *Statistical Procedures for Engineering, Management, and Science*. McGraw-Hill College (June 1, 1980), 1980 (cit. on p. 2).

[BLV19] Nikolaos Bekiaris-Liberis and Rafael Vazquez. "Nonlinear bilateral output-feedback control for a class of viscous Hamilton-Jacobi PDEs". In: *Automatica* 101 (2019), pp. 223–231 (cit. on p. 6).

[BYK21] Mark Burkhardt, Huan Yu, and Miroslav Krstic. "Stop-and-go suppression in two-class congested traffic". In: *Automatica* 125 (2021), p. 109381 (cit. on pp. 6, 48, 51, 52).

[Cav05] Roger W. Caves. *Encyclopedia of the City*. Routledge, 2005 (cit. on p. 1).

[Cha+20] Arthur Charpentier, Romuald Elie, Mathieu Laurière, and Viet Chi Tran. "COVID-19 pandemic control: balancing detection policy and lockdown intervention under ICU sustainability". In: (May 13, 2020). arXiv: `2005.06526v3 [q-bio.PE]` (cit. on pp. 78, 81, 82).

[Cor+13] Jean-Michel Coron, Rafael Vazquez, Miroslav Krstic, and Georges Bastin. "Local Exponential H^2 Stabilization of a 2×2 Quasilinear Hyperbolic System Using Backstepping". In: *SIAM Journal on Control and Optimization* 51.3 (2013), pp. 2005–2035 (cit. on pp. 6, 28, 33, 34, 36, 63, 67, 69, 71, 74, 75).

[Cra80] J. Crank. *The Mathematics of diffusion*. Oxford University Press, 1980 (cit. on p. 101).

[Dar90] May Adolf Darlington. *Traffic flow fundamentals*. 1990 (cit. on p. 1).

[DBC12] Ababacar Diagne, Georges Bastin, and Jean-Michel Coron. "Lyapunov exponential stability of 1-D linear hyperbolic systems of balance laws". In: *Automatica* 48 (2012), pp. 109–114 (cit. on p. 5).

[Deu17a] Joachim Deutscher. "Backstepping Design of Robust State Feedback Regulators for Linear 2×2 Hyperbolic Systems". In: *IEEE Transactions on Automatic Control* 62.10 (2017), pp. 5240–5247 (cit. on p. 6).

[Deu17b] Joachim Deutscher. "Finite-time output regulation for linear 2×2 hyperbolic systems using backstepping". In: *Automatica* 75 (2017), pp. 54–62 (cit. on p. 6).

[DEY00] Angeli D., Sontag E.D., and Wang Y. "A characterization of integral input-to-state stability". In: *IEEE Transactions on Automatic Control* 45.6 (2000), pp. 1082–1097 (cit. on p. 30).

[Ele14] Lily Elefteriadou. *An Introduction to Traffic Flow Theory*. Springer, 2014 (cit. on pp. 2, 3).

[FHSA93] Liquor Federated Hotel and Catering Association of South Africa. *Hotelier & Caterer: Official Magazine of FEDHASA*. Ramsay Son & Parker, 1993 (cit. on p. 1).

[FLH04] Haijun Fang, Zongli Lin, and Tingshu Hu. "Analysis of linear systems in the presence of actuator saturation and $\mathcal{L}2$-disturbances". In: *Automatica* 40 (2004), pp. 1229–1238 (cit. on p. 4).

[FM07] B. Faugeras and O. Maury. "Modeling fish population movements: from an individual-based representation to an advection-diffusion equation". In: *Journal of Theoretical Biology* 247.4 (2007), pp. 837–848 (cit. on p. 101).

[Fra20] FranceTvInfo. *Coronavirus : 450 personnes en quatorzaine après des cas de Covid-19 déclarés dans une école de Lyon*. `https://www.francetvinfo.fr/sante/maladie/coronavirus/coronavirus-450-personnes-en-quatorzaine-apres-des-cas-dans-une-ecole-de-lyon_4036889.html`. 2020, accessed July 9, 2020 (cit. on p. 7).

[FS13] Shimao Fan and Benjamin Seibold. "Data-Fitted First-Order Traffic Models and Their Second-Order Generalizations: Comparison by Trajectory and Sensor Data". In: *Transportation Research Record* 2391.1 (2013), pp. 32–43 (cit. on p. 14).

[FW15] Shimao Fan and Daniel B. Work. "A Heterogeneous Multi-class Traffic Flow Model with Creeping". In: *SIAM Journal on Applied Mathematics* 75.2 (2015), pp. 813–835 (cit. on p. 4).

[Gar+20] M. Garavello, P. Goatin, T. Liard, and B. Piccoli. "A multiscale model for traffic regulation via autonomous vehicles". In: *J. Differential Equations* 7.269 (2020), pp. 6088–6124 (cit. on p. 5).

[GK07] A. K. Gupta and V. K. Katiyar. "A new multi-class continuum model for traffic flow". In: *Transportmetrica* 3.1 (2007), pp. 73–85 (cit. on p. 4).

[Goa+21] Paola Goatin, Chiara Daini, Maria Laura Delle Monache, and Antonella Ferrara. "Interacting moving bottlenecks in traffic flow". working paper or preprint. Dec. 2021 (cit. on p. 1).

[Gos+20] Katelyn Gostic, Ana CR Gomez, Riley O Mummah, Adam J Kucharski, and James O Lloyd-Smith. "Estimated effectiveness of symptom and risk screening to prevent the spread of COVID-19". In: *eLife* 9 (2020). Ed. by Eduardo Franco, Neil M Ferguson, and James M McCaw, e55570 (cit. on p. 6).

[Gou20] Gouvernement français. *Info coronavirus covid 19*. `https://www.gouvernement.fr/info-coronavirus/carte-et-donnees`. 2020, accessed July 9, 2020 (cit. on p. 86).

[Gua+20] Lina Guan, Christophe Prieur, Liguo Zhang, Clémentine Prieur, Didier Georges, and Pascal Bellemain. "Transport effect of COVID-19 pandemic in France". In: *Annual Reviews in Control* 50 (2020), pp. 394–408 (cit. on p. 77).

[GZP20] Lina Guan, Liguo Zhang, and Christophe Prieur. "Optimal PI controller rejecting disturbance for ARZ traffic model". In: 59^{th} *Conference on Decision and Control (CDC)*. 2020, pp. 5665–5670 (cit. on p. 13).

[GZP21a] Lina Guan, Liguo Zhang, and Christophe Prieur. *Optimal Boundary ISS Controller for Heterogeneous and Congested Traffic*. Submitted for publication, Dec. 2021 (cit. on p. 47).

[GZP21b] Lina Guan, Liguo Zhang, and Christophe Prieur. "Optimal observer-based output feedback controller for traffic congestion with bottleneck". In: *International Journal of Robust and Nonlinear Control* 31 (15 2021), pp. 7087–7106 (cit. on p. 25).

[GZP22] Lina Guan, Liguo Zhang, and Christophe Prieur. *Stabilization of Heterogeneous Quasilinear Traffic Flow System with Disturbances*. Submitted for publication, 2022 (cit. on p. 65).

[HLM02a] Tingshu Hu, Zongli Lin, and Chen Ben M. "An analysis and design method for linear systems subject to actuator saturation and disturbance". In: *Automatica* 38.2 (2002), pp. 351–359 (cit. on p. 4).

[HLM02b] Tingshu Hu, Zongli Lin, and Chen Ben M. "Analysis and design for discrete-time linear systems subject to actuator saturation". In: *Systems & Control Letters* 45.2 (2002), pp. 97–112 (cit. on p. 4).

[Hu+16] Long Hu, Florent Di Meglio, Rafael Vazquez, and Miroslav Krstic. "Control of Homodirectional and General Heterodirectional Linear Coupled Hyperbolic PDEs". In: *IEEE Transactions on Automatic Control* 61.11 (2016), pp. 3301–3314 (cit. on pp. 6, 56).

[INS20] INSEE. *Mobilités professionnelles et scolaires en France*. `https://www.insee.fr/fr/information/2383243` and `https://www.insee.fr/fr/information/2383297`. 2020, accessed July 9, 2020 (cit. on pp. 91, 93).

[JW04] Rui Jiang and QingSong Wu. "Extended Speed Gradient Model for Mixed Traffic". In: *Transportation Research Record* 1883.1 (2004), pp. 78–84 (cit. on p. 5).

[KG02] Hassan K Khalil and Jessy W Grizzle. *Nonlinear systems*. Vol. 3. Prentice hall Upper Saddle River, NJ, 2002 (cit. on pp. 2, 17).

[KG18] Z.H. Khan and T.A. Gulliver. "A macroscopic traffic model for traffic flow harmonization". In: *European Transport Research Review* 10 (2018), p. 30 (cit. on p. 3).

[KMZ21] Christoph Kawan, Andrii Mironchenko, and Majid Zamani. *A Lyapunov-based ISS small-gain theorem for infinite networks of nonlinear systems*. 2021 (cit. on p. 5).

[KR08] Matt J. Keeling and Pejman Rohani. *Modeling infectious diseases in humans and animals*. Princeton University Press, 2008 (cit. on pp. 81, 100).

[Krs08] Miroslav Krstic. *Boundary control of PDEs: A course on backstepping design*. Philadelphia, PA, USA: Society for Industrial and Applied Mathematics, 2008 (cit. on p. 6).

[KS08] Miroslav Krstic and Andrey Smyshlyaev. "Backstepping boundary control for first-order hyperbolic PDEs and application to systems with actuator and sensor delays". In: *Systems & Control Letters* 57.9 (2008), pp. 750–758 (cit. on p. 6).

[Kuc+20] Adam J Kucharski, Timothy W Russell, Charlie Diamond, Yang Liu, John Edmunds, Sebastian Funk, and Rosalind M Eggo. "Early dynamics of transmission and control of COVID-19: a mathematical modelling study". In: *The Lancet Infectious Diseases* 20 (5 2020), pp. 553–558 (cit. on p. 6).

[LB+20] Nicolas Laurent-Brouty, Alexander Keimer, Paola Goatin, and Alexandre Bayen. "A macroscopic traffic flow model with finite buffers on networks: Well-posedness by means of Hamilton-Jacobi equations". In: *Communications in Mathematical Sciences* 18.6 (2020), pp. 1569–1604 (cit. on p. 4).

[LBCG20] Nicolas Laurent-Brouty, Guillaume Costeseque, and Paola Goatin. "A macroscopic traffic flow model accounting for bounded acceleration". In: *SIAM Journal on Applied Mathematics* (2020) (cit. on p. 4).

[Liu+21] Tong Liu, Leilei Cui, Bo Pang, and ZhongPing Jiang. "Data-driven adaptive optimal control of mixed-traffic connected vehicles in a ring road". In: 60^{th} *IEEE Conference on Decision and Control (CDC)*. Austin, USA, 2021, pp. 77–82 (cit. on p. 5).

[LL18] Yuanlong Li and Zongli Lin. *Stability and Performance of Control Systems with Actuator Saturation*. Birkhauser Basel, 2018 (cit. on p. 4).

[LW55] M. J. Lighthill and G. B. Whitham. "On kinematic waves II. A theory of traffic flow on long crowded roads". In: *Proceedings of the Royal Society A: Mathematical, Physical and Engineering Sciences* 229.1178 (1955), pp. 317–345 (cit. on p. 3).

[MAC12] Treiber M., Kesting A., and Thiemann C. *Traffic Flow Dynamics: Data, Models and Simulation*. Springer Berlin Heidelberg, 2012 (cit. on pp. 1, 15, 26, 27).

[MBC00] Michael D McKay, Richard J Beckman, and William J Conover. "A comparison of three methods for selecting values of input variables in the analysis of output from a computer code". In: *Technometrics* 42.1 (2000), pp. 55–61 (cit. on p. 86).

[MI15a] Andrii Mironchenko and Hiroshi Ito. "Construction of Lyapunov Functions for Interconnected Parabolic Systems: An iISS Approach". In: *SIAM Journal on Control and Optimization* 53.6 (2015), pp. 3364–3382 (cit. on p. 5).

[MI15b] Andrii Mironchenko and Hiroshi Ito. "Construction of Lyapunov Functions for Interconnected Parabolic Systems: An iISS Approach". In: *SIAM Journal on Control and Optimization* 53.6 (2015), pp. 3364–3382. eprint: `https://doi.org/10.1137/14097269X` (cit. on p. 30).

[Min20] Ministère des solidarités et de la santé. *Plateforme COVID-19*. `https://covid-19.sante.gouv.fr/login?to=/ressources`. 2020, accessed July 9, 2020 (cit. on p. 86).

[MJ20] Irene Martínez and WenLong Jin. "Optimal location problem for variable speed limit application areas". In: *Transportation Research Part B: Methodological* 138 (2020), pp. 221–246 (cit. on p. 1).

[MM22] A M Ishtiaque Mahbub and Andreas A. Malikopoulos. "A platoon formation framework in a mixed traffic environment". In: *IEEE Control Systems Letters* 6 (2022), pp. 1370–1375 (cit. on p. 5).

[Mol+19] Stéphane Mollier, Maria Laura Delle Monache, Carlos Canudas de Wit, and Benjamin Seibold. "Two-dimensional macroscopic model for large scale traffic networks". In: *Transportation Research Part B: Methodological* 122 (2019), pp. 309–326 (cit. on p. 4).

[Mor78] Jorge J Moré. "The Levenberg-Marquardt algorithm: implementation and theory". In: *Numerical analysis*. Springer, 1978, pp. 105–116 (cit. on p. 86).

[MP20] Andrii Mironchenko and Christophe Prieur. "Input-to-state stability of infinite-dimensional systems: recent results and open questions". In: *SIAM Review* 62.3 (2020), pp. 529–614 (cit. on pp. 4, 9).

[MR06] Ch. Mallikarjuna and K. Ramachandra Rao. "Area occupancy characteristics of heterogeneous traffic". In: *Transportmetrica* 2.3 (2006), pp. 223–236 (cit. on p. 5).

[MR17] Ranju Mohan and Gitakrishnan Ramadurai. "Heterogeneous traffic flow modelling using second-order macroscopic continuum model". In: *Physics Letters A* 381.3 (2017), pp. 115–123 (cit. on pp. 4, 48).

[MR21] Ranju Mohan and Gitakrishnan Ramadurai. "Multi-class traffic flow model based on three dimensional flow–concentration surface". In: *Physica A: Statistical Mechanics and Its Applications* 577.126060 (2021) (cit. on p. 5).

[MW20] Pierre Magal and Glenn Webb. "Predicting the Number of Reported and Unreported Cases for the COVID-19 Epidemic in South Korea, Italy, France and Germany". In: *SSRN* (2020) (cit. on p. 80).

[NL07] Dong Ngoduy and Ronghui Liu. "Multiclass first-order simulation model to explain nonlinear traffic phenomena". In: *Physica A: Statistical Mechanics and Its Applications* 385 (2007), pp. 667–682 (cit. on p. 4).

[Pay71] H. J. Payne. "Models of Freeway Traffic and Control". In: *Mathematical Models of Public Systems* 1 (1971), pp. 51–61 (cit. on p. 3).

[PB19] Etienne Pardoux and Tom Britton. *Stochastic Epidemic Models with Inference*. Springer, 2019 (cit. on p. 81).

[PG06] Benedetto Piccoli and Mauro Garavello. *Traffic flow on networks*. Vol. 1. American institute of mathematical sciences, 2006 (cit. on pp. 15, 27, 53).

[Pra+20] Mélanie Prague, Linda Wittkop, Quentin Clairon, Dan Dutartre, Rodolphe Thiébaut, and Boris Pierre Hejblum. "Population modeling of early COVID-19 epidemic dynamics in French regions and estimation of the lockdown impact on infection rate". In: *medRXiv* (2020) (cit. on p. 7).

[Ric56] Paul I. Richards. "Shock waves on the highway". In: *Operations Research* 4.1 (1956), pp. 42–51 (cit. on p. 3).

[Roq+20] Lionel Roques, Etienne K. Klein, Julien J. Papaix, Antoine Sar, and Samuel Soubeyrand. "Effect of a one-month lockdown on the epidemic dynamics of COVID-19 in France". 2020 (cit. on p. 7).

[SCK10] Andrey Smyshlyaev, Eduardo Cerpa, and Miroslav Krstic. "Boundary Stabilization of a 1-D Wave Equation with In-Domain Antidamping". In: *SIAM Journal on Control and Optimization* 48.6 (2010), pp. 4014–4031 (cit. on p. 6).

[SM+08] Valérie dos Santos Martins, Georges Bastin, Jean-Michel Coron, and B. d'Andréa Novel. "Boundary control with integral action for hyperbolic systems of conservation laws: Stability and experiments". In: *Automatica* 44 (2008), pp. 1310–1318 (cit. on p. 5).

[Sob67] Il'ya Meerovich Sobol'. "On the distribution of points in a cube and the approximate evaluation of integrals". In: *Zhurnal Vychislitel'noi Matematiki i Matematicheskoi Fiziki* 7.4 (1967), pp. 784–802 (cit. on p. 82).

[Son08] Eduardo Sontag. "Input to State Stability: Basic Concepts and Results". In: *Lecture Notes in Mathematics* (2008), pp. 163–220 (cit. on p. 5).

[Son89] Eduardo Sontag. "Smooth stabilization implies coprime factorization". In: *IEEE Transactions on Automatic Control* 34 (1989), pp. 435–443 (cit. on p. 5).

[Tan+09] Tieqiao Tang, Haijun Huang, Shougen Zhao, and Huayan Shang. "A new dynamic model for heterogeneous traffic flow". In: *Physics Letters A* 373.29 (2009), pp. 2461–2466 (cit. on p. 4).

[Tar+11] Sophie Tarbouriech, Germain Garcia, João Manoel Gomes da Silva Jr., and Isabelle Queinnec. *Stability and Stabilization of Linear Systems with Saturating Actuators*. Springer, 2011 (cit. on p. 4).

[TAX18] Ngoc-Tu Trinh, Vincent Andrieu, and Cheng-Zhong Xu. "Output regulation for a cascaded network of 2×2 hyperbolic systems with PI controller". In: *Automatica* 91 (2018), pp. 270–278 (cit. on p. 5).

[Tay+21] Andrew J. Taylor, Victor D. Dorobantu, Sarah Dean, Benjamin Recht, Yisong Yue, and Aaron D. Ames. "Towards robust data-driven control synthesis for nonlinear systems with actuation uncertainty". In: 60^{th} *IEEE Conference on Decision and Control (CDC)*. Austin, USA, 2021, pp. 6469–6476 (cit. on p. 5).

[TCL21] Liudmila Tumash, Carlos Canudas de Wit, and Maria Laura Delle Monache. "Boundary Control for Multi-Directional Traffic on Urban Networks". In: *hal-03182546v2* (2021) (cit. on p. 5).

[Til92] H. E. Tillett. "Infectious Diseases of Humans: Dynamics and Control. R. M. Anderson, R. M. May, Pp. 757. Oxford University Press, 1991". In: *Epidemiology and Infection* 108.1 (1992), pp. 211–211 (cit. on p. 81).

[TJ+20] Alexandre Terrand-Jeanne, Vincent Andrieu, Melaz Tayakout-Fayolle, and Valérie dos Santos Martins. "Regulation of Inhomogeneous Drilling Model With a P-I Controller". In: *IEEE Transactions on Automatic Control* 65.1 (2020), pp. 58–71 (cit. on p. 5).

[TK12] M. Treiber and A. Kesting. *Traffic Flow Dynamics: Data, Models and Simulation*. Springer, 2012 (cit. on p. 1).

[TPSJ05] Sophie Tarbouriech, Christophe Prieur, and João Manoel Gomes da Silva Jr. "$\mathcal{L}2$ performance design problem for systems presenting nested saturations". In: 44^{th} *Conference on Decision and Control (CDC)*. Seville, Spain. Seville, Spain, 2005, pp. 5000–5005 (cit. on p. 16).

[Vaz+19] Rafael Vazquez, Miroslav Krstic, Jing Zhang, and Jie Qi. "Stabilization of a 2-D reaction-diffusion equation with a coupled PDE evolving on its boundary". In: 58^{th} *Conference on Decision and Control (CDC)*. IEEE. 2019, pp. 2169–2174 (cit. on p. 6).

[Vei+20] Sébastien Da Veiga, Fabrice Gamboa, Bertrand Iooss, and Clémentine Prieur. *Basics and trends in sensitivity analysis. Theory and practice in R*. SIAM, 2020 (cit. on pp. 79, 86).

[VK19] Rafael Vazquez and Miroslav Krstic. "Boundary control and estimation of reaction-diffusion equations on the sphere under revolution symmetry conditions". In: *International Journal of Control* 92.1 (2019), pp. 2–11 (cit. on p. 6).

[VKB12] Rafael Vazquez, Jean-Michel Coronand Miroslav Krstic, and Georges Bastin. "Collocated output-feedback stabilization of a 2×2 quasilinear hyperbolic system using backstepping". In: *2012 American Control Conference (ACC)*. 2012, pp. 2202–2207 (cit. on p. 6).

[VKC11] Rafael Vazquez, Miroslav Krstic, and Jean-Michel Coron. "Backstepping boundary stabilization and state estimation of a 2×2 linear hyperbolic system". In: *IEEE Conference on Decision and Control and European Control Conference*. Orlando, FL, 2011, pp. 4937–4942 (cit. on pp. 6, 28, 34).

[Whi99] Gerald Beresford Whitham. *Linear and nonlinear waves*. Pure and Applied Mathematics: A Wiley Series of Texts, Monographs and Tracts. Wiley-Interscience, 1999. Online–Ressource (PDF–Dateien: XVI, 636 S.) (Cit. on p. 3).

[YK19a] Huan Yu and Miroslav Krstic. "Traffic congestion control for Aw-Rascle-Zhang model". In: *Automatica* 100 (2019), pp. 38–51 (cit. on p. 6).

[YK19b] Huan Yu and Miroslav Krstic. "Traffic congestion control for Aw-Rascle-Zhang model". In: *Automatica* 100 (2019), pp. 38–51 (cit. on p. 6).

[Yu+20] Huan Yu, Qijian Gan, Alexandre Bayen, and Miroslav Krstic. "PDE Traffic Observer Validated on Freeway Data". In: *IEEE Transactions on Control Systems Technology* 29 (3 2020) (cit. on p. 6).

[Zen+21] Junwei Zeng, Yongsheng Qian, Ziwen Lu, Fan Yin, Leipeng Zhu, Yongzhi Zhang, and Dejie Xu. "Expressway traffic flow under the combined bottleneck of accident and on-ramp in framework of Kerner's three-phase traffic theory". In: *Physica A: Statistical Mechanics and its Applications* 574 (2021), p. 125918 (cit. on p. 1).

[Zha02] H. M. Zhang. "A non-equilibrium traffic model devoid of gas-like behavior". In: *Transportation Research Part B* 36.3 (2002), pp. 275–290 (cit. on p. 3).

[Zha+06] Peng Zhang, Ruxun Liu, S. C. Wong, and Shiqiang Dai. "Hyperbolicity and kinematic waves of a class of multi-population partial differential equations". In: *European Journal of Applied Mathematics* 17 (2006), pp. 171–200 (cit. on p. 51).

[ZP17] Liguo Zhang and Christophe Prieur. "Necessary and sufficient conditions on the exponential stability of positive hyperbolic systems". In: *IEEE Transactions on Automatic Control* 62.7 (2017), pp. 3610–3617 (cit. on p. 5).

[ZPQ19] Liguo Zhang, Christophe Prieur, and Junfei Qiao. "PI boundary control of linear hyperbolic balance laws with stabilization of ARZ traffic flow models". In: *Systems & Control Letters* 123 (2019), pp. 85–91 (cit. on pp. 5, 39).

Résumé — Dans mes recherches, le contrôle optimal tuning du trafic des régimes de congestion est étudié pour rejeter les perturbations et stabiliser le trafic. La perturbation s'applique à la limite du modèle de flux de trafic. Afin d'analyser et de concevoir le contrôleur PI optimal tuning pour le modèle Aw-Rascle-Zhang linéarisé, le gain L_2 est calculé pour estimer le rejet de perturbation. L'estimation d'une borne supérieure du gain L_2, de la perturbation à la sortie contrôlée, peut être formulée comme un problème d'optimisation avec des inégalités matricielles linéaires pour calculer des conditions traitables numériquement. Un contrôle de rétroaction de sortie optimal tuning basé sur un observateur est conçu pour la répartition du trafic afin de dissoudre la congestion du trafic à l'aide de la méthode de retour en arrière et de l'optimisation. Le modèle Aw-Rascle-Zhang linéarisé est pris en compte avec les conditions aux limites constituées d'une frontière à densité constante et d'une chute de vitesse à l'entrée amont d'un goulot d'étranglement, et d'une frontière à perturbation d'afflux (forte demande de trafic) à l'entrée du tronçon routier considéré. A propos d'une loi de contrôle aux frontières optimale pour un modèle de trafic Aw-Rascle (AR) hétérogène de classe N, après linéarisation des équations du modèle autour des états stationnaires en fonction de la variable spatiale et en utilisant la méthode de backstepping, un contrôleur mis en œuvre par une mesure de rampe à la limite d'entrée est conçue pour rejeter les perturbations afin de stabiliser le système de trafic hétérodirectionnel. La stabilité entrée-état intégrale H^2 d'un système de trafic multi-type décrit par des équations aux dérivées partielles hyperboliques quasi-linéaires du premier ordre est obtenue en boucle fermée avec un contrôleur de frontière à la frontière d'entrée de la section de route considérée. En utilisant la transformation de retour en arrière, la stabilité intégrale entrée-état du système quasi-linéaire est dérivée en mappant le système quasi-linéaire transformé en un système cible stable entrée-état intégral pour lequel une fonction de Lyapunov stricte est construite.

Mots clés : Modèle de trafic, Congestion du trafic, Perturbations, Backstepping, Contrôleur optimal tuning.

Abstract — In my research, optimal tuning traffic control of congestion regimes is investigated to reject the disturbances and stabilize the traffic. The disturbance applies at the boundary of the traffic flow model. To analyze and design the optimal tuning PI controller for the linearized Aw-Rascle-Zhang model, the L_2 gain is computed to estimate the disturbance rejection. The estimation of an upper bound of the L_2 gain, from the disturbance to the controlled output, can be formulated as an optimization problem with linear matrix inequalities to compute numerically tractable conditions. An optimal tuning observer-based output feedback control is designed for traffic breakdown to dissolve traffic congestion using the backstepping method and optimization. The linearized Aw-Rascle-Zhang model is taken into account with the boundary conditions consisting of a boundary with a constant density and a speed drop at the upstream inlet of a bottleneck, and a boundary with a disturbance of inflow (high traffic demand) at the inlet of the road segment under consideration. About an optimal tuning boundary control law for a heterogeneous N-class Aw-Rascle (AR) traffic model, after linearizing the model equations around the equilibrium depending on the spacial variable and using the backstepping method, a controller implemented by a ramp metering at the inlet boundary is designed for rejecting the disturbances to stabilize the hetero-directional traffic system. The H^2 integral input-to-state stability of a multi-type traffic system described by first-order quasi-linear hyperbolic partial differential equations is obtained

in a closed loop with a boundary controller at the inlet boundary of the considered road section. Making use of the backstepping transformation, the integral input-to-state stability of the quasi-linear system is derived by mapping the transformed quasi-linear system into an integral input-to-state stable target system for which a strict Lyapunov function is constructed.

Keywords: Traffic model, Traffic congestion, Distubances, Backstepping, Optimal tuning controller.

GIPSA-lab Grenoble Images Parole Signal Automatique, UMR 5216 CNRS-Grenoble
INP-Université Grenoble Alpes 11 rue des Mathématiques Grenoble Campus BP46 F-38402
SAINT MARTIN D'HERES Cedex
Grenoble